Synthesis and Catalytic Potential of Rare Earth Heterobimetallic Complexes

August 2015

Thesis submitted in accordance with the requirements of The University of Liverpool for the degree of Doctor in Philosophy by Christopher David Thomas.

Acknowledgements

I always anticipated writing an acknowledgements section, however now that I'm here I realise that there are far more people to thank than room to mention them.

First thank yous go to my supervisors Helen Aspinall and Nick Greeves for giving me the opportunity to work on some very interesting chemistry. Likewise I must thank the EPSRC for my funding and use of the National Mass Spectrometry Centre, without which I would have been in serious difficulty.

Next I would like to thank the various masters students I've had the privilege of mentoring over the years: Ed Eden, Frances Potjewyd, Amanada Catherall, Stephanie Moore, Danielle Mehta, Connor Black, Ellie Singleton and Tolly Robinson. I will always be so proud of each of you.

Particular special thanks go to: Jen Smith for all the chemicals, Mike Beaumont for the NMR and hiking, Iain Aldous and Gaia Neri who were always up for a pint when I needed to vent, Mike Craven for the pub quizzes, Mike Davidson for climbing and for being crazier than me, Casper Kuntzman-Olsen for the home brewing, Bob Smith for being far more inappropriate than me and Faye Hern who was never afraid to tell me to shut up. Each and every one of you has made my time far more enjoyable and brighter, I will miss all of you more than words can say…especially at lunch time.

The people of the 4th floor lab both past and present deserve a mention, there are far too many of you to mention by name but working up there would have been far duller without you.

I am indebted to various members of technical staff here at Liverpool: Dr Craig Robertson for XRD analysis, Moya McCarron for MS analysis and Jean Ellis for CHN. Thank yous are also owed to Charles Clavering, Gordon Bostock and Richard Dewson for keeping my battered equipment running. Thanks too to Paul Cross, who manufactured what must amount to a small hills worth of specialist glassware for me.

Finally to all the members of the department both past and present that I've not mentioned by name; each and every one of you makes the department what it is and I will miss you all.

List of Abbreviations

Binol 1,1'-Bi-2-naphthol

BOX Bis (oxazoline)

DCM Dichloromethane

Ln Rare earth metal

PHOX Phosphinooxazoline

PyBOX 2,6Bis[2oxazolinyl]pyridine

Silylamide $[N(SiMe3)2]^-$

THF Tetrahydrofuran

NMR-Nuclear Magnetic Resonance

TLC Thin Layer Chromatography

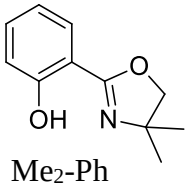 Me_2-Ph	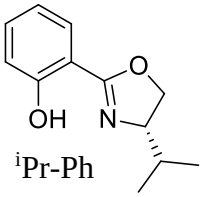 ^{i}Pr-Ph	
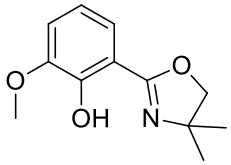 Me_2-MeOPh	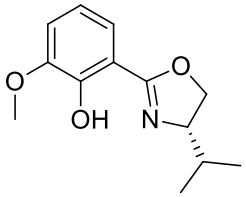 ^{i}Pr-MeOPh	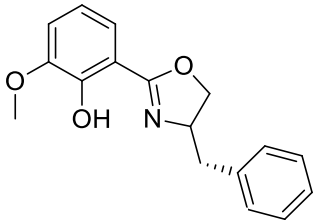 $PhCH_2$-MeOPh
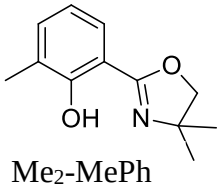 Me_2-MePh	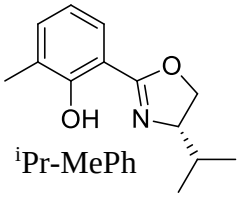 ^{i}Pr-MePh	
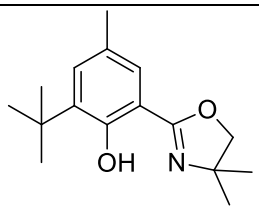 Me_2-^{t}BuPh	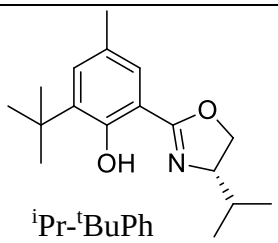 ^{i}Pr-^{t}BuPh	

Contents

Abstract

A novel route to chiral and achiral 2-aryloxazolyl compounds, building upon work already extant in the group has allowed for the development of an alternative route to oxazoline ligands. This route allows for the previous ease of scalability and high yields whilst vastly reducing reaction times and improving the purification procedure. This new method is significantly gentler using ambient conditions throughout much of the procedure and is therefore synthetically much simpler. The total reaction time has also been reduced allowing for the production of cleaner materials, faster and in analogous yields. These ligands possess many characteristics that would make them ideal for catalysis especially with high oxidation state metals.

We have demonstrated the effective anhydrous self-assembly of several heterobimetallic complexes using these ligands with Ln^{3+} and alkali metals (M) such as lithium or sodium of the general formula $M_x[Ln(L)_{x+3}]$. These have been fully characterised and their catalytic potential demonstrated with the nitroaldol reaction. It is hoped that through this initial study into the catalytic potential of these complexes we can gain insight into the catalytic pathway which will lead to further optimisation of these catalysts.

Oxazoline Ligands

This chapter will discuss the history and general background information of oxazoline ligands, starting with an initial discussion of asymmetric catalysis and expanding into the application of oxazoline to this field. Ligands employing the oxazoline motif will be discussed, including PHOX, BOX and PYBOX ligands. 2-oxazolylphenols and their limited literature examples will be discussed before the existing synthetic routes to these ligands are evaluated. Finally a discussion of the research conducted within this study will be provided.

1. Ligand Introduction

1.1 Asymmetric catalysis

Chiral compounds, most often as single enantiomers are a fundamentally key component of several major industries including, but not limited to, pharmaceuticals, agricultural chemicals, flavours, fragrances and materials. As such there is a high demand for large amounts of enantiomerically pure chemicals; historically this has meant resolution of a racemic sample of the two enantiomers, which has the obvious drawback of a maximum yield of only 50%. Alternatively chemical transformation of a racemic stockpile could be carried out (i.e. kinetic resolution); however these reactions require stoichiometric quantities of a suitable precursor.

Asymmetric catalysis offers a significant improvement of these older methods; being able to generate far greater yields by the fact that the chiral catalyst is continually regenerated throughout the course of the reaction. Enzymes already fulfil this role in nature and Schiff base catalysis is a key example of trying to directly emulate the structure of these enzymes in an attempt to achieve similar catalytic activities.

Asymmetric catalysis relies on the chiral catalyst being regenerated in the course of the reaction. This allows for relatively small amounts of catalyst to be used in each reaction. This fact lends itself well to large scale industrial chemistry, meaning that even relatively difficult to make catalysts can often be used on sufficient scale to be economically viable.

Most asymmetric catalysts are metal complexes with organic ligands sterically controlling the outcome of a metal assisted process to favour production of one enantiomer. There are a limited range of catalytically active metals available so the main focus has fallen on developing ligands to give higher yields, higher enantiomeric excesses (ees) and doing this more efficiently and cleanly (i.e. fewer if any by-products).[1,2,3]

Oxazolines (Fig 1.1) have been known and used since the 1880s, with the first synthesis by Rudolf Andreasch in 1884 and further clarification of the structure provided by Sigmund Gabriel in 1889.[4,5] However it wasn't until Brunner et al in the 1980s that oxazolines began to see use in asymmetric catalysis.[6] At present ligands containing chiral oxazolines rings are one of the most common structural features in the field. [7,8]

The particular interest in these ligands derives from the relative ease of their synthesis, when compared with other more complex ligand types. Synthesis is often achieved via chiral amino alcohols (which when derived from amino acids represent a cheap and variable chiral feedstock, available in both enantiomers).[9] Additionally their wide range of structural forms and the ability of their complexes to catalyse a versatile range of catalytic reactions further add to their attraction.[8,10]

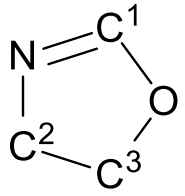

Figure 1.1: Simple oxazoline ring structure

Oxazoline (Fig. 1.1) has several structural and electronic properties which make it an excellent ligating species.[8] The imine is a good hard donor as it is poorly basic, the oxazoline ring is non-aromatic and this leaves the nitrogen lone pairs free for coordination.[11] Oxazoline is thermally stable and resistant to bases, radicals, and weak acids as well as being fairly resistant to hydrolysis and oxidation; thus it can be expected to remain stable in a wide range of reaction conditions.[12]

Furthermore oxazoline ligands are a potentially diverse class of ligand: chirality can be introduced into the oxazoline ring, and due to the use of amino alcohols during the synthesis

this places the chiral centre close to the metal, facilitating effective transfer of chiral information to the catalytically active site.[13,14]

Further steric and electronic properties can be tuned *via* choice of substituents at the C2 position (Fig 1.1). By increasing or decreasing the steric bulk, the ligand can be made to favour branched or linear metal-substrate intermediates.[11] This can be done through careful choice of the amino alcohol.[11,15,16]

1.2 Development of oxazolines as ligands for asymmetric catalysis

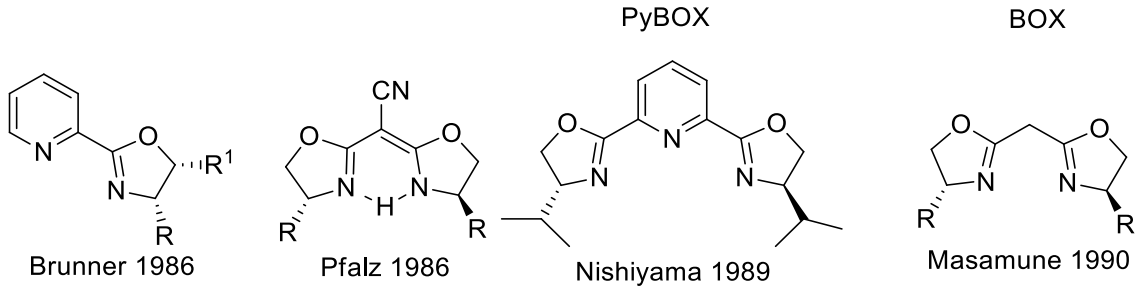

Figure 1.2: Early oxazoline containing ligands

As stated earlier, oxazolines have been known since the late 1800s, but it wasn't until the work of H. Brunner et al. in 1986 in the monophenylation of diols that oxazolines began to see use as ligands in asymmetric catalysis (Fig. 1.3).[17]

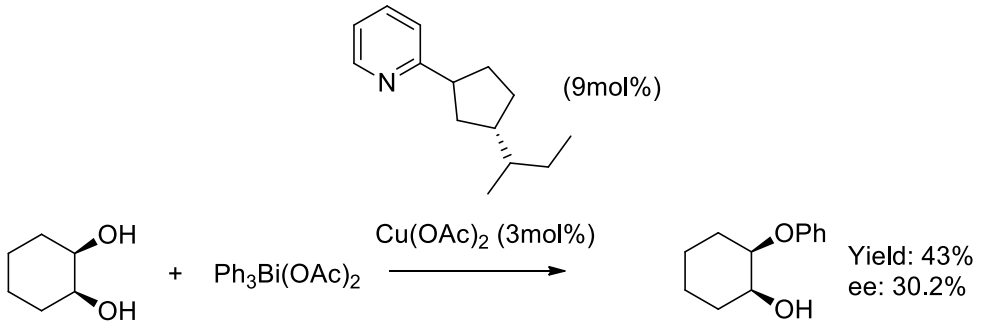

Figure 1.3: Monophenylation of diols by Brunner[17]

Figure 1.3 shows the optimised conditions for the reaction. The yields from the various ligands used remained fairly consistent (ranging from 43-35%). However it was found that changing the identity of the chiral unit shown above could drastically affect the ee, with a methyl group producing 14% ee (yield 38%).

At the same time Pfalz et al. published work on the use of C_2-symmetric semicorrin ligands for enantioselective carbenoid cyclopropanations, with their ligands bearing strong structural similarities to those of Brunner et al. (Fig. 1.2).[6]

The work of Brunner led to Nishiyama et al. developing the pyridine bis(oxazoline) or PyBOX ligands in 1989 for use in the hydrosilylation of ketones, at which they performed exceptionally in the presence of silver salts. With $AgBF_4$ (2 mol%) in the presence of the catalyst shown in figure 1.4 ee's of 98% were achieved (Yield: 91%) (Fig. 1.4).[18,19]

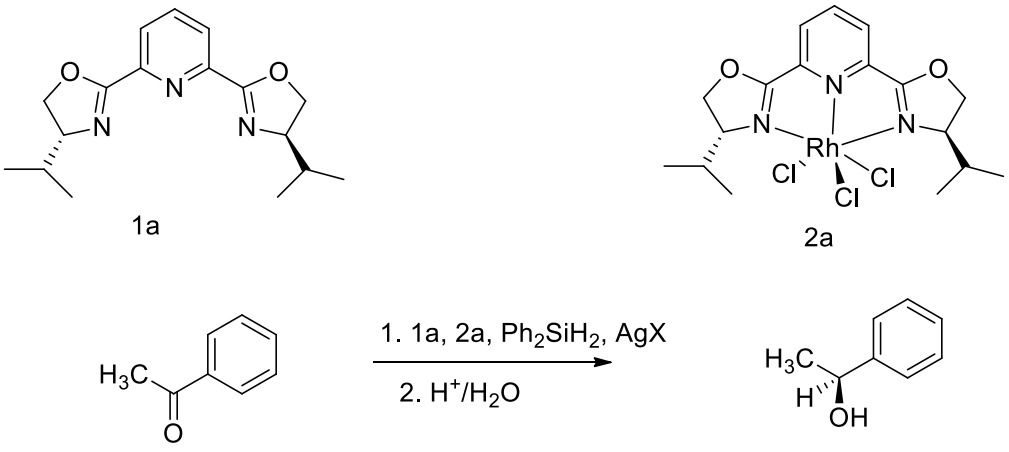

Figure 1.4: Hydrosilylation of ketones using Rh(PyBOX)[18]

In 1990 Masamune et al. synthesised the first BOX bis(oxazoline) ligands and demonstrated their effectiveness in copper catalysed cyclopropanation reactions of olefins and styrenes.[20]

The low catalytic loadings and the ease of synthesis prompted much interest in the field, the first review article arrived in 1996. Today a significant number of bis(oxazolines) exist; structurally the field is still dominated by the BOX and PYBOX motifs but there is an emerging group of alternative structures.[21,22,23,24,25,26]

1.3 Phosphinooxazolines (PHOX)

PHOX ligands are another class of oxazoline ligand that have found recent widespread use in asymmetric catalysis (Fig. 1.5). The use of these ligands can be attributed both to the ease and versatility of their synthesis, which is conducted in a distinct modular fashion, and their high degree of effectiveness. [27]

Figure 1.5: PHOX ligands, free ligand and co-ordinated

Their initial investigation was conducted to exploit asymmetry in the electronic environment experienced by substrates when binding to the metal centre thereby providing a higher degree of regioselectivity. This effect would not be seen in symmetric ligands such as PYBOX and BOX ligands. A good example of a reaction where this is usefully exploited is the transition-metal catalysed allylic alkylation via symmetric allyl complexes (Fig. 1.6 and Fig. 1.7).[27,28]

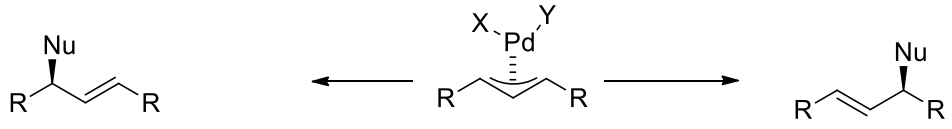

Figure 1.6: Allylic alkylation reaction

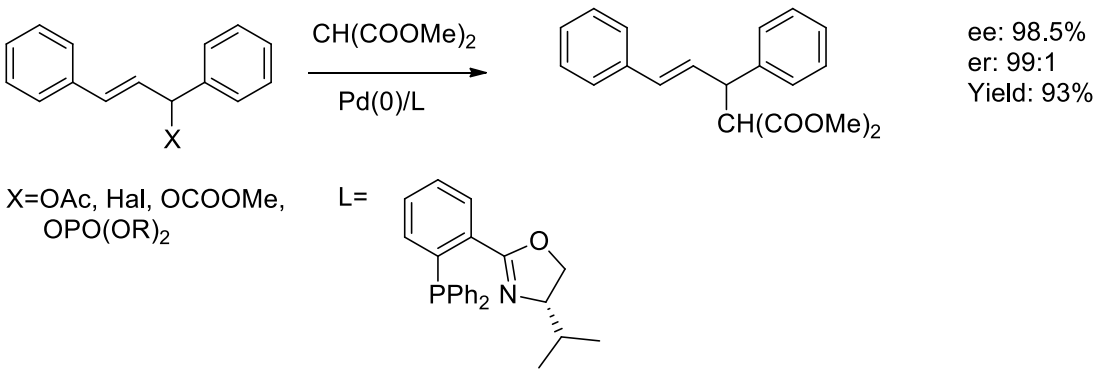

Figure 1.7: Palladium catalysed allylic alkylation investigated by Pfalz using PHOX ligands.[27]

Furthermore the two donor atoms have different donor affinities for the metal centre; as such one donor will be more labile than the other at any given time. This property known as hemilability has been found to significantly increase the activity of catalysts. A co-ordinatively saturated complex will be able to rearrange to allow the binding of reagents to the metal centre.[29] This can be done with the ligand still remaining partially bound and as such able to influence the regio- and stereo-chemistry of the reaction. This effect will also allow for efficient removal of product from the catalyst centre due to re-coordination of the labile section of the ligand.

1.4 2-Oxazolylphenol ligands and their analogues

2-Oxazolylphenols are a class of ligand structurally related to the PHOX ligands discussed earlier, and with similar hemilability.[30] However, they are far less prevalent in the literature, and this is thought to be due to the relative difficulty of their synthesis. They were first identified as a ligand in iron binding mycobactin in 1955.[31,32] These ligands however were not employed in asymmetric catalysis until the work of Bolm et al. in 1995, when they were employed in the copper catalysed Baeyer-Villiger oxidation of cyclic ketones to produce lactones (Fig. 1.8).[15]

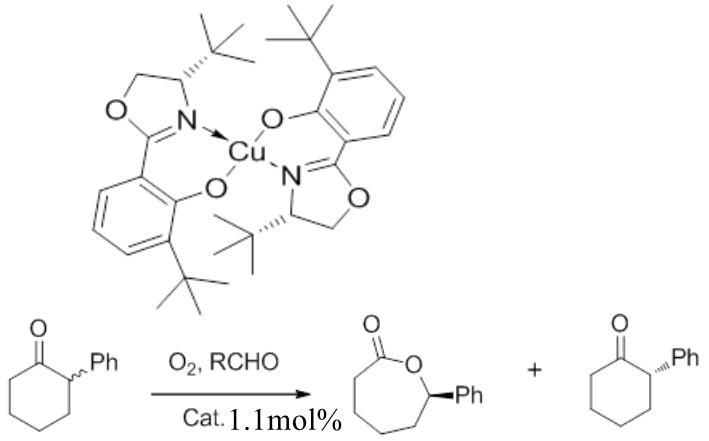

Figure 1.8: asymmetric Baeyer-Villiger oxidation of cyclic ketones by Bolm et al.[15]

Since this first demonstration of these ligands in asymmetric catalysis few other examples have been produced, although these examples have demonstrated the versatility of this class of ligands with examples in: oxidations, Mukaiyama reactions, allylations, hydrocyanations and Diels-Alder reactions.[33,34,35,36,37] This stands in stark contrast to the earlier PYBOX and BOX ligands which saw rapid development and extensive review articles published within a few years of their initial discovery. [8]

2-Oxazolylphenol ligands have a number of characteristics that favour their deployment in asymmetric catalysis: phenols are readily available, inexpensively, in a variety of forms and with a number of different substituents. Their chemistry is fairly well understood and transformations on these structures have been carried out extensively.[11,38] The phenols lend themselves naturally towards modular synthesis and design of ligands, with the para position (Fig. 1.9 (R^2)) being most suited to electronic and solubility improving groups leaving the ortho position (Fig. 1.9 (R^1)) free for steric or secondary binding groups. Additionally the positioning of the oxazoline moiety ortho to the phenolic OH seems to reduce the risk of hydrolysis significantly, making these ligands more stable than the PHOX ligands.[14,23,39]

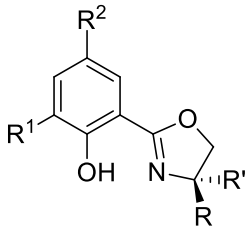

Figure 1.9: 2-oxazolylphenol ligand

The ability of the phenolic moiety to be deprotonated allows these ligands to counter a cationic charge, something often encountered when binding higher oxidation state transition metals, rare earths or alkaline earth metals, i.e. hard Lewis acids. This is a key advantage over PHOX and BOX ligands which are unable to support these sorts of systems. These harder Lewis acidic systems could have massive potential in catalysis and the 2-oxazolylphenols should allow exploration of this area.

2-Oxazolylphenols have a number of advantages over other ligands based around oxazolines, therefore why are they not more widely employed in the field? Simply this seems to be due to a matter of their synthesis. Existing routes to oxazolines appear to be unsuitable for use with the phenol moiety, either due to simply not being compatible or due to their use of dangerous or expensive reagents.

1.5 Discussion of previous synthetic routes

As stated in section 1.1 the oxazoline moiety can be found widely in chemistry. One of the primary reasons is the range of reactions potentially capable of producing them, as exemplified in a paper by Gomez et al. (Fig. 1.10). Often, however, these are incompatible with electron donating groups such as phenols.

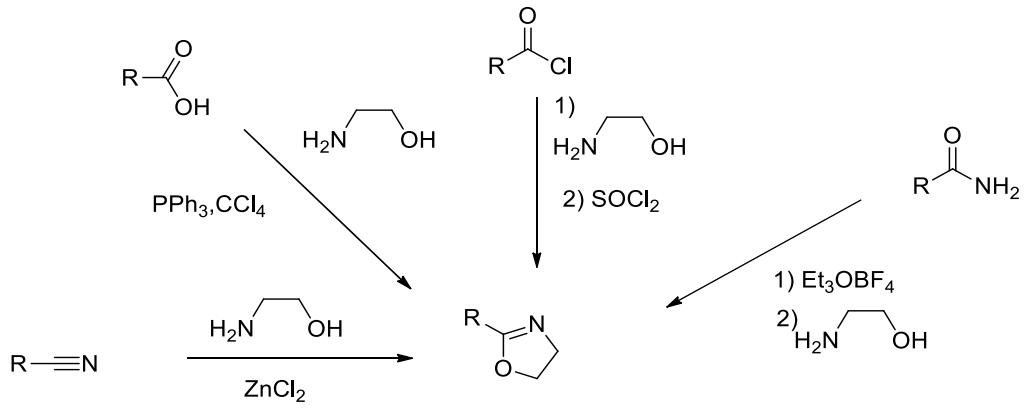

Figure 1.10: Diagram showing the variety of starting material for oxazoline synthesis stated by Gomez et al. (1990)[11]

Currently the synthesis of oxazolines is dominated by a number of 'standard' reactions which use common reagents and conditions generally amenable to lab preparation. Synthesis from nitriles in the presence of $ZnCl_2$ has long been considered the most straightforward method for oxazoline synthesis. What follows is a brief overview of the more common methods of synthesis.

1.6 Appel reaction

The Appel reaction is the conversion of alcohols into alkyl chlorides using triphenylphosphine and carbon tetrachloride. The reaction is credited to and named after Rolf Appel although it had been described earlier. It has been found to also be effective on carboxylic acids converting them into oxaxolines, thiazolines and oxazines. The use of the Appel reaction (Fig. 1.11) has a number of drawbacks, specifically the production of phosphine oxides in large quantities, which becomes a particular problem when scale up is considered. Furthermore the banning of carbon tetrachloride under the Montreal protocol severely limits the use of this reaction. [40]

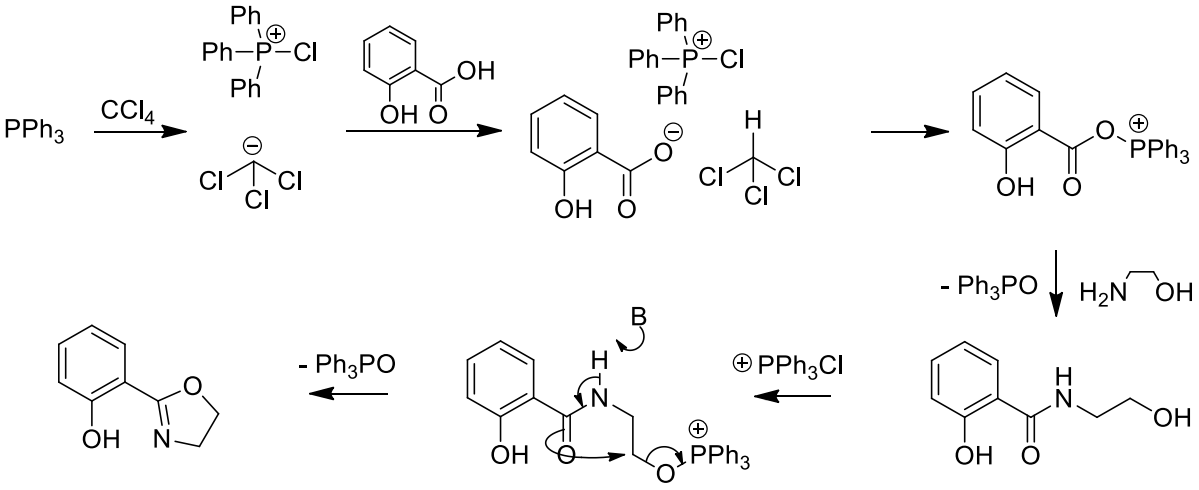

Figure 1.11: The Appell reaction[40]

Previous work conducted by others in the group effectively demonstrated the inconvenience of this route as the phosphine oxide is soluble in the organic solvent and all attempts at removal (including flash column chromatography) proved unsuccessful.[41] Switching to using reagents which produced more convenient side by-products led to significant reductions in yield.

1.7 Thionyl Chloride Reaction

Another reaction trialled by the group was the thionyl chloride catalysed reaction of acid chlorides with amino alcohols (Fig. 1.12).

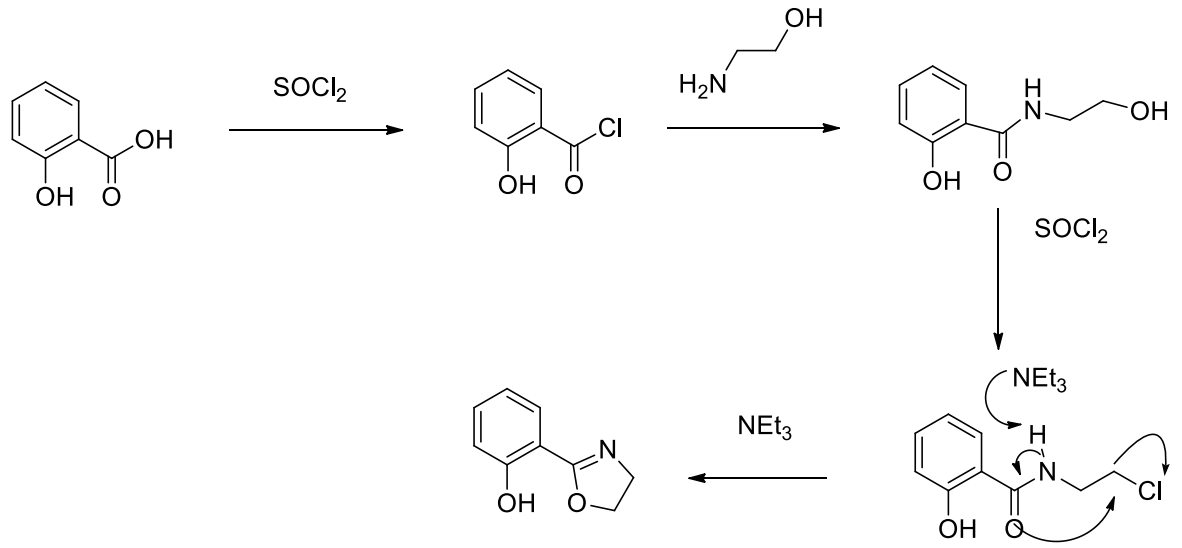

Figure 1.12: Thionyl chloride mediated oxazoline formation[42]

This was considered the most obvious alternative to the Appell reaction as the by-products (HCl and SO_2) are gaseous, avoiding isolation problems. However this also failed to work even after purification of the thionyl chloride via distillation. It was discovered that the oxazoline ring can undergo a ring opening reaction especially in the presence of trace water, however it was found that this occurred under anhydrous conditions also. It was later determined that hydrogen bonding between the phenolic OH and the oxazoline N led to sufficient activation of the ring system to allow ring opening to occur (Fig. 1.13).

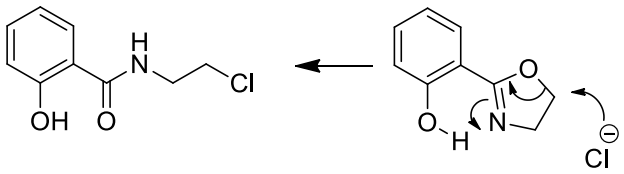

Figure 1.13: Ring cleavage mechanism[42]

1.8 Witte-Seeliger Conditions

The synthesis used by the group previously involves reaction of nitriles with amino alcohols; this is conducted under anhydrous conditions at elevated temperatures (130°C). There a few

major drawbacks with the original synthesis; few phenolic nitriles are commercially available and synthesis of the nitrile starting materials was previously conducted under synthetically inconvenient conditions, i.e use of CuCN as a reagent which has high levels of toxicity and problems with isolation, including coordination of product to residual Cu.[43]

A convenient alternative was found from Chill et al (2010) in which the aldehyde is heated at 100°C with hydroxylamine hydrogen chloride for 6 hours using DMSO as the solvent (Fig. 1.14).

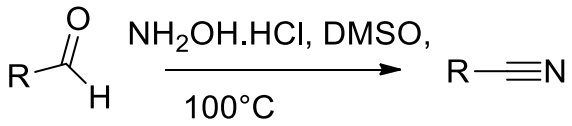

Figure 1.14: Nitrile synthesis developed by Chill et al (2010)[44,45]

Cyclisations were then performed via the synthesis originally reported by Witte and Seeliger, in which the nitrile is heated with a slight excess of the amino alcohol in the presence of a catalytic amount of $ZnCl_2$.[43] This is conducted at high temperatures (130°C) and as such the reactions use chlorobenzene as the solvent under anhydrous conditions (Fig. 1.15).

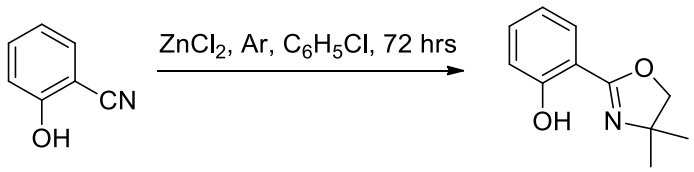

Figure 1.15: Cyclisation reaction employed by Aspinall et al. (2011)[45,46]

Although this synthesis has proven to be successful and represents a significant improvement on pre-existing routes, it does require flash column chromatography at each stage of the synthesis in order to obtain products of sufficient purity. Furthermore the reaction requires the use of unusual solvents at elevated temperatures under anhydrous conditions for long periods of time (up to 72hrs in the case of the final cyclisation stage). The yields of products, although

good, were lower than had originally been hoped for and finally the route was not able to synthesise the bis(oxazoline) (Fig.1.16) which was a molecule of interest.

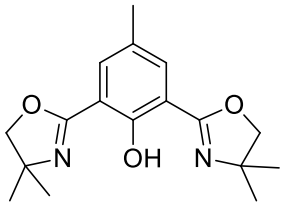

Figure 1.16: Bis(oxazoline) identified as a molecule of interest by Aspinall et al. (2011)

Due to our failure to synthesise the bis-oxazoline via the pre-existing method and variants thereof (i.e. substituting catalyst, changing catalyst loading etc.) we began investigating other approaches. This eventually led us to a paper by Bode et al. (2003) in which they detail the synthesis of isoxazoles from the corresponding oxime (yields between 35-83%) (Fig.1.17).[47,48]

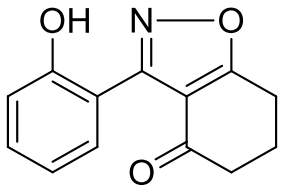

Figure 1.17: Example of the Isoxazoles synthesised by Bode et al.[47,48]

1.9 Isoxazole synthesis of Bode et al.

The process begins with initial chlorination of the oxime at the "imine" carbon followed by reaction with the "addition species" in the presence of base (Fig.1.18). In the case of Bode this was an enolate or more accurately a cyclic diketone which was made into an enolate by *in situ* reaction with base (in our case this would be an amino alcohol).

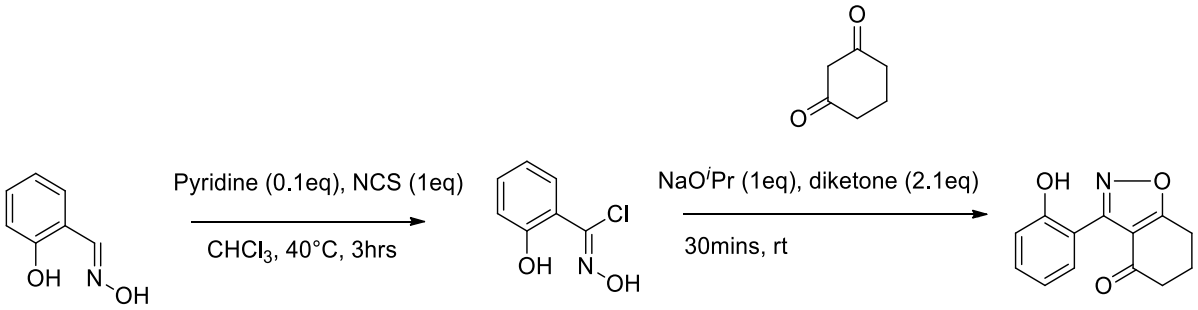

Figure 1.18: Full synthesis used by Bode et al. (2003)[47]

Purification of the final isoxazole was carried out by column chromatography. In comparison to the methods described earlier it was believed that this reaction showed the most promise, in making the ligand synthesis more convenient and higher yielding.

1.10 Research aims

The aim of this initial body of research is to further develop a practical synthetic route to 2-oxazolylphenol ligands, with specific attention placed on the isolation of the bis-oxazoline ligand. This method should ideally be able to match and expand upon the range of ligands produced under the previous synthesis. The method should also utilise both inexpensive starting materials and easily achievable reactions and isolation conditions, which in combination should allow scale-up to multi-gram reactions.

2. Results and Discussion of Ligand Synthesis

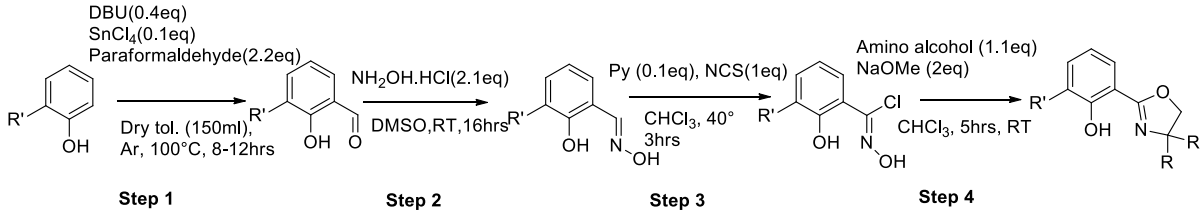

Figure 2.1: Overall synthetic plan used in this study

Figure 2.1 shows a generalised overall view of the synthesis deployed in this study, due to ready availability of the aldehyde starting materials it was possible to skip step 1when R= OMe or H. Each of the steps shown above will be discussed in detail below, however generally all of the steps in figure 2.1 were reasonably facile, with the most synthetically difficult steps being the forymlation step (step 1) and the chlorination step (step 3).

2.1 Formylation Reactions

Formylation of compounds 3 and 5 to produce the corresponding mono-formylated phenols 4 and 6 was conducted using a modification of the Casiraghi reaction (Fig. 2.2).[49]

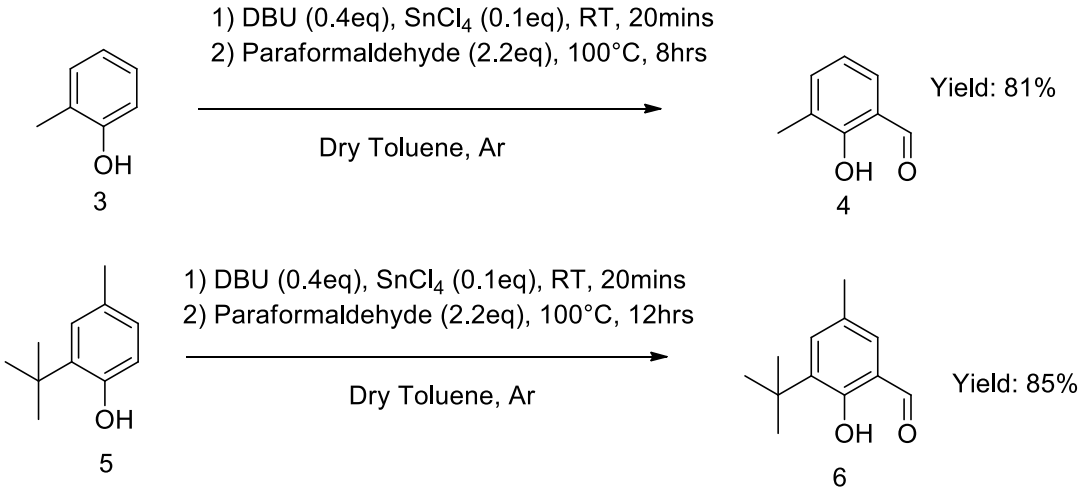

Figure 2.2: Formylation of compound 3 and 4 using modified Casiraghi conditions

The reaction proceeded as for previous literature examples in the case of 4 with production of a significant amount of a resin like substance. However, 6 was produced cleanly by the reaction

and product was yielded as yellow crystals straight from the work up. This was unexpected and previous reactions undertaken by the group had indicated that column chromatography was required to yield products of analytical purity. In the case of 6 yields were higher than had been previously stated (85%). However in the case of 4, although it was determined that the crude product was of sufficient purity to be used in later stages, there was a large amount of tar like residue which had been previously reported.[50] The identity of this solid was determined to be a phenol-formaldehyde resin akin to Bakelite, and was thought to be a result of an uncontrolled reaction between paraformaldehyde and phenol.

Formylation of napth-2-ol (7) was conducted using the Reimer-Tiemann synthesis (Fig. 2.3). This yielded formylated compound 8 as yellow solid without further purification.[51] Typically this procedure presents poor regioselectivity when reacting on phenols, however when using napth-2-ol only a single aldehyde was isolated.

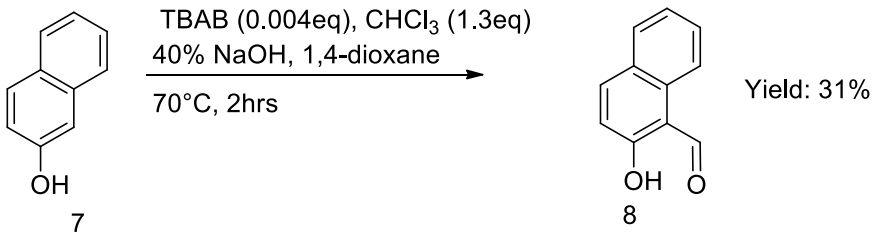

Figure 2.3: Formylation of napth-2-ol

The diformyl compound was synthesised *via* the Duff reaction, which uses hexamethylenetetramine as the formyl source (Fig 2.4).This reaction (unlike the above mentioned Reimer-Tiemann) is not regioselective and as such the starting material had to be para-substituted.

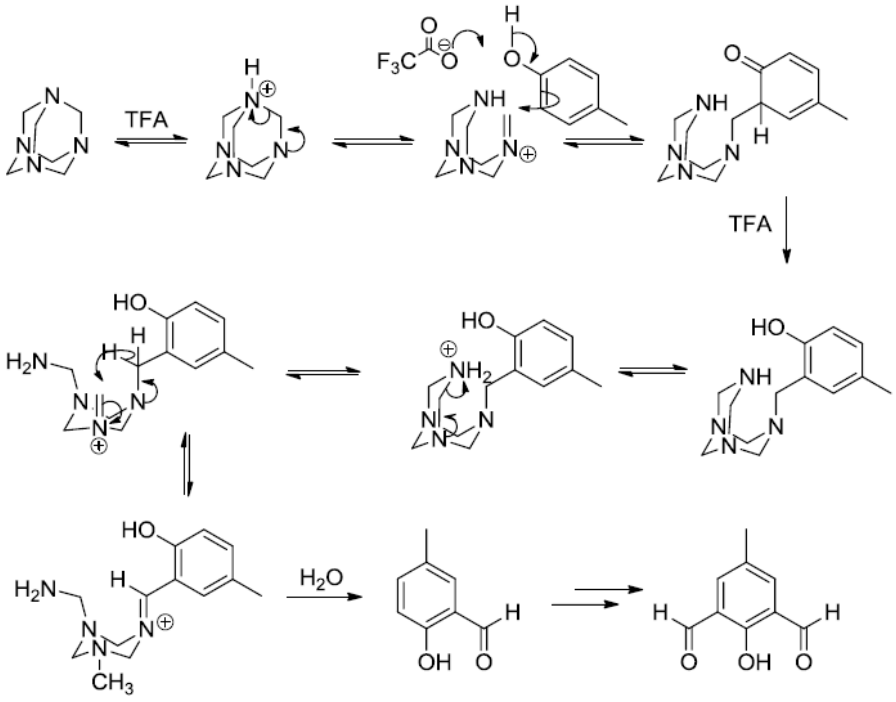

Figure 2.4: Formylation to the diformyl using the Duff reaction[52]

2.2 Oxime formation

During work previously conducted by the group to produce nitriles for use in the Witte-Seeliger oxazoline synthesis, it was found that the reaction proceeded via an aldoxime intermediate (Fig. 2.5).[44,45]

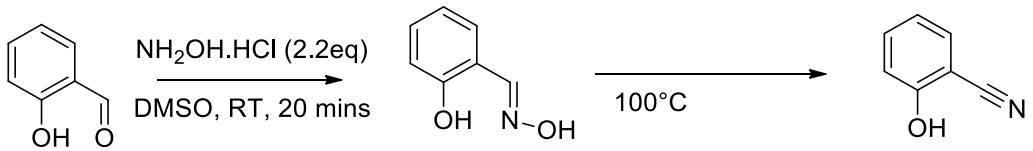

Figure 2.5: Nitrile synthesis[44]

Stopping the reaction after the initial stage (i.e. without heating) yielded the oxime and increasing the reaction time to 6 hours yielded product in high yields (95-65%) depending on the starting aldehyde (Table 2.1).

Table 2.1: Isolated yields of Aldoximes

A	Yields
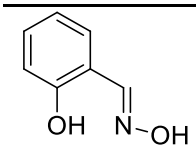	91%
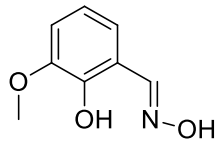	74%
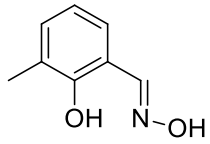	78%
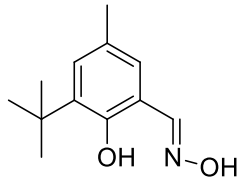	80%
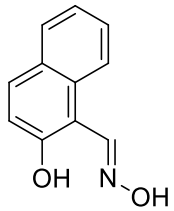	95%
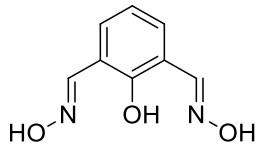	65%

This reaction proceeded cleanly for all starting materials without any further purification required (example shown in Fig. 2.6) and the product oximes are of sufficient stability to be synthesised on a large scale and stored almost indefinitely.

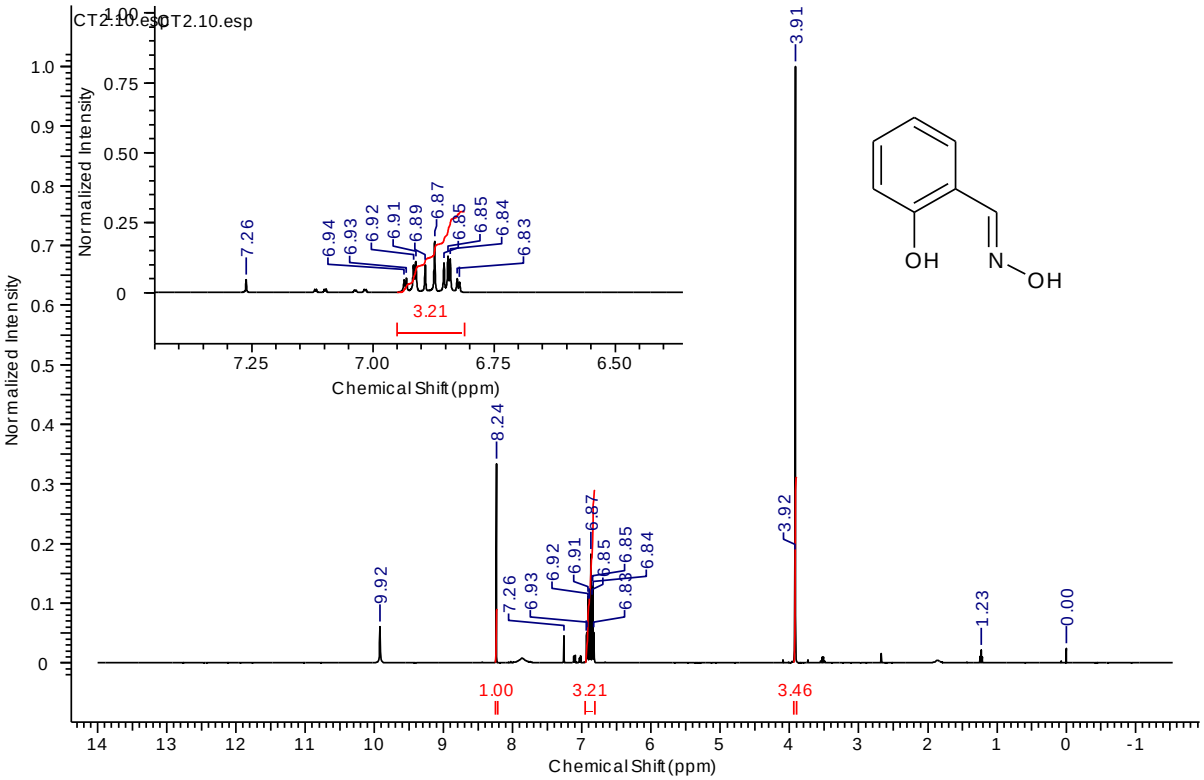

Figure 2.6: ^{1}H NMR (400MHz, $CDCl_3$, 15-25C) spectrum of 2A demonstrating "clean" nature of "crude" products

A reaction mechanism has been proposed for the synthesis of the oxime intermediate (Fig. 2.7):

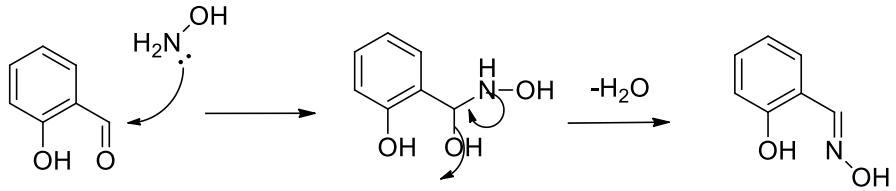

Figure 2.7: Proposed mechanism for oxime formation

It should be noted in the case of compound 3A due to it being “telescoped” through from the formylation step without purification there was a significant amount of baseline impurities present in the NMR spectrum. Taking into account peak shifting due to oxime formation the impurities found were identified as those already present in the aldehyde going into the oxime

synthesis. This indicates that oxime formation *via* this method is a robust process, insensitive to small amounts of impurity.

2.3 Chlorination of oximes

Nitrile oxides are well documented highly reactive intermediates.[53,54] Due to their high reactivity they must be generated *in situ*; they can be generated in a number of ways, however one of the most convenient is *via* chlorination of oximes.[55] The chlorination of the oximes was based on the work of Bode et al. (2003) (Fig. 2.8)**.**The reactions were successful yielding product in 98-84% yield (Table 2.2).[56]

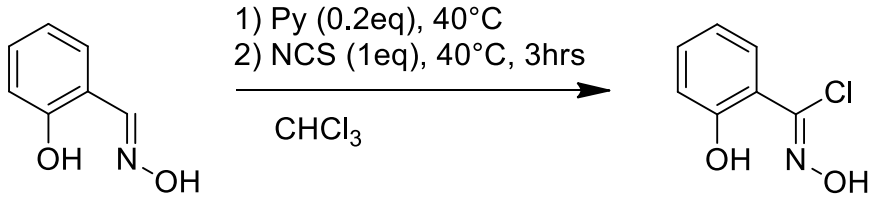

Figure 2.8: Chlorination of oximes, adapted from Bode et al. [48]

Table 2.2: Crude yields of Chloro-oximes

B	Crude Yield
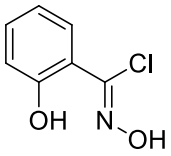	84%
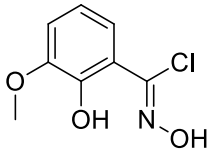	98%
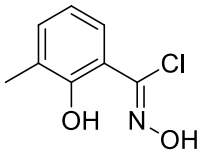	85%
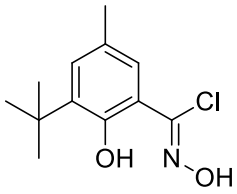	86%
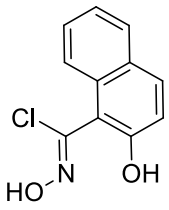	91%

The chlorinated product was isolated directly from the work-up without any further purification and was initially considered to be pure enough for further reactions (Fig. 2.9). However upon closer investigation we discovered that a small amount of ring chlorination was occurring along with chlorination of the oxime. This was found to occur for all chlorinations with selective chlorination of the napthol oximes (**5A**) being particularly unpredictable. There were additional, although small peaks, in the ^{1}H NMR spectra of chlorinated samples that didn't

correspond to either unreacted oxime or chlorinated oxime. Mass spectrometry of chlorinated samples showed mass peaks at 35.5 and 37.5 mass units higher than the mass ion in all cases.

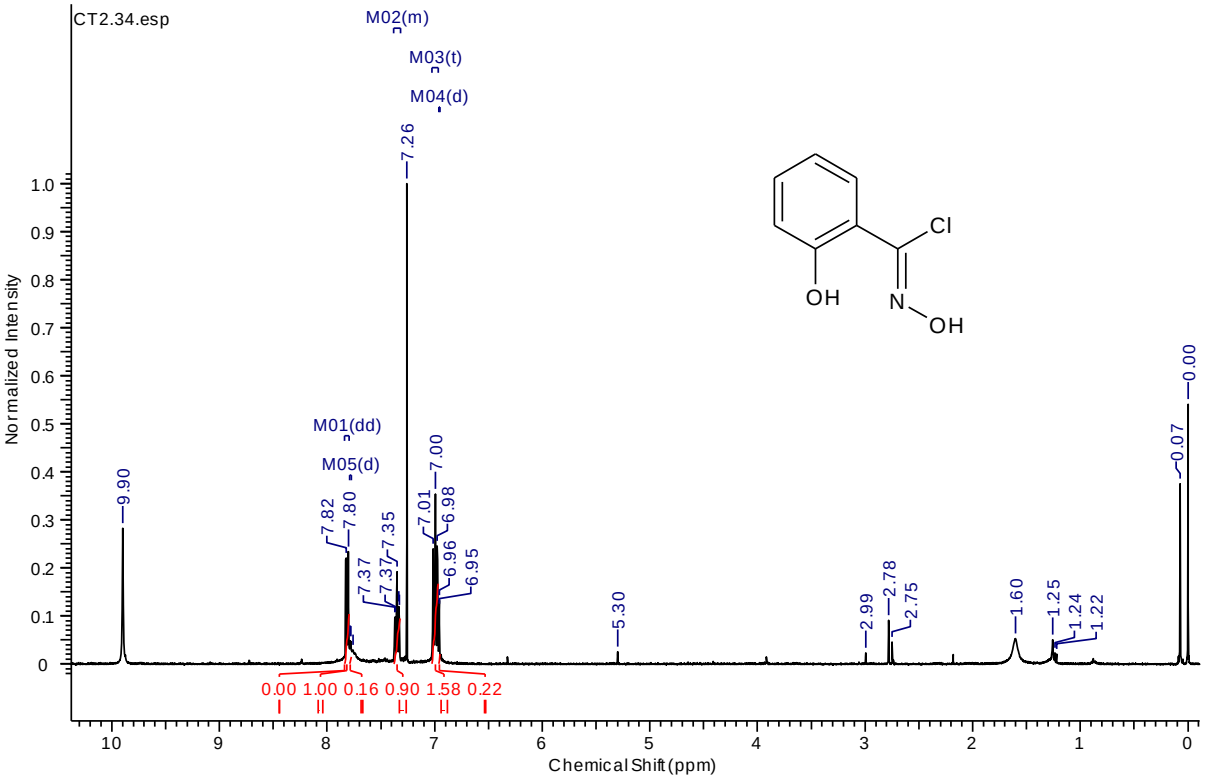

Figure 2.9: ^{1}H NMR (400MHz, $CDCl_3$, 15-25C) spectrum of (1A)

The amount of "overchlorination" varied according to the exact structure of the ligand, with particularly electron rich ring systems such as (**2A**) and (**5A**) showing the most and relatively electron deficient systems such as (**1A**) and (**4A**) chlorinating relatively cleanly. Chlorination of the ring in addition to chlorination of the oxime led to incomplete conversion and actual yields for this process are probably lower than actually stated. It was determined by ^{1}H NMR spectroscopy that "overchlorination" made up approximately 10% of the sample. Due to the equivalents of chlorinating agent used it could also be assumed that unreacted oxime makes up at least another 10%, this was backed up by the presence of the oxime (H-C=N) proton in the ^{1}H NMR spectrum of chlorinated compounds.

Pyridine was shown to be crucial to the reaction with no reaction occurring with triethylamine and an uncontrolled reaction occurring when no base was used. A reaction mechanism was proposed (Fig. 2.11).[57]

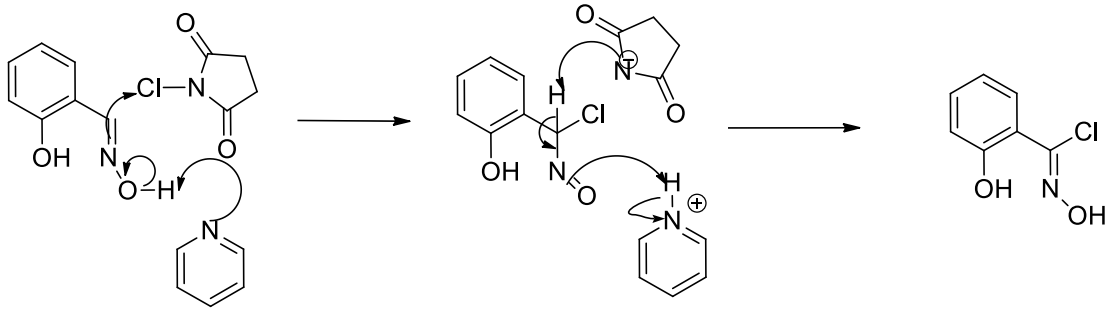

Figure 2.11: Proposed reaction mechanism for the chlorination step

Due to the problems associated with the chlorination step a number of different attempts were made to improve the system. These included using different chlorinating agents such as sodium hypochlorite, use of oxone and HCl in DMF and one attempt at a chlorination using acidified silica gel. [58–60] Unfortunately all of these failed to improve the situation, giving analogous or worse results and more often than not leading to complicated or unpleasant work up conditions.

Although continued production of overchlorinated oxime would drop final isolated yields by approximately 20% the reaction could be completed in 3hrs and the impurities produced were not thought to interfere with the cyclisation step and as such overchlorination of the ring was not considered a major issue.

2.4 Cyclisations from chlorinated oximes

The cyclisation step was the main focus of our investigations (due to the apparent effectiveness of the chlorination step). From previous experience with oxazoline ring formation the first cyclisation attempts were conducted anhydrously. As such initial reactions conducted using

this method utilised dry triethylamine as the base (Fig. 2.12), despite the paper stating the use of isopropoxide[48]

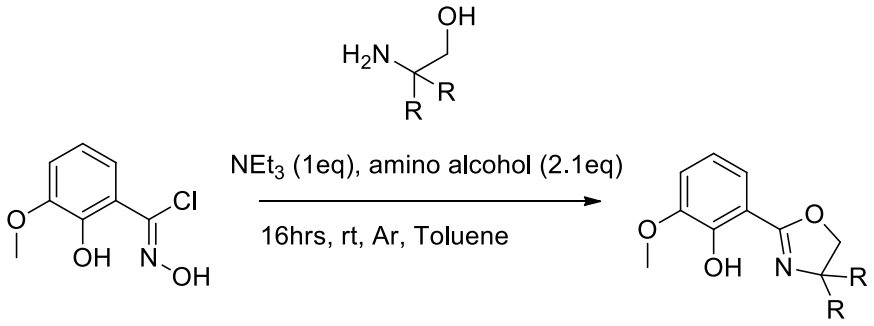

Figure 2.12: First cyclisation attempt

The first cyclisation attempt was conducted at room temperature under argon using triethylamine as the base and toluene as the solvent (both dry). There were solubility issues with this reaction as the chlorinated oxime never fully dissolved. The reaction was left to stir vigorously overnight giving a crude yield of 55% which was purified by column chromatography to yield product in 26%. The reaction was repeated using chloroform as the reaction solvent; this increased the crude yield to 62% (40% after column chromatography). It is worth noting that the work up for these reactions was not clean and that separation between the aqueous and organic phases was not straightforward. This was believed to be due to the triethylamine being partially soluble in both phases.

Previous work by Bode et al. has identified nitrile oxides as a reactive intermediate in the cyclisation employed during their synthesis of isoxazoles (Fig. 2.13). The reaction mixture has been observed to be basic upon completion which would imply production of water and ammonia, if the reaction mechanism is correctly understood (Fig.2.14), this led us to believe the reaction should be tolerant to atmospheric moisture.

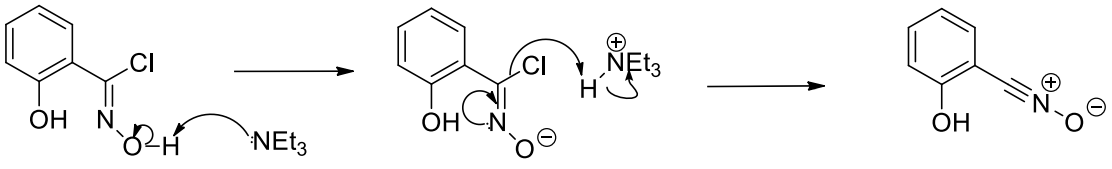

Figure 2.13: Proposed mechanism for the formation of the nitrile oxide intermediate[48,54,61]

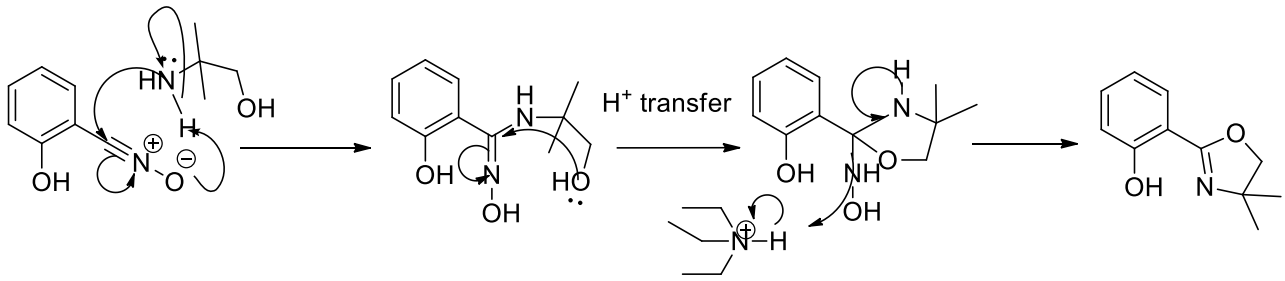

Figure 2.14: Proposed cyclisation mechanism[54]

Further reactions were conducted using different bases, sodium methoxide, potassium tertiary butoxide and potassium carbonate (Table 2.3). These reactions were conducted under argon using chloroform as the solvent and left stirring at room temperature for 5hrs (Fig. 2.15). Interesting to note is that the ^{1}H NMR spectrum of this reaction is quite clean with only minor impurities (Fig. 2.16), regardless of the base.

Table 2.3: Base Study conducted on reaction shown in (Fig. 24)

Base	Crude Yields
NEt_3	60%
NaOMe	88%
KO^tBu	86%
K_2CO_3	61%

As can be seen from Table 2.3 NaOMe provided the highest crude yields and was used routinely.

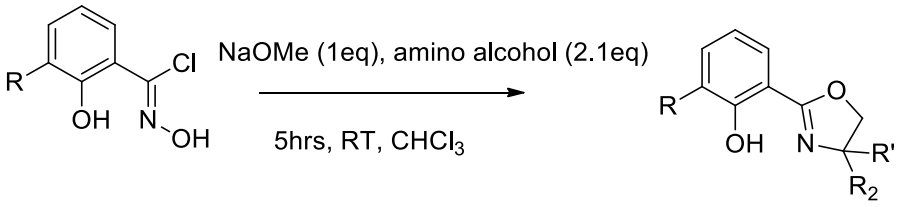

Figure 2.15: Optimised reaction conditions

Table 2.4: Final ligands synthesised via the chloro oxime route

C	Yield	D	Yield	E	Yield
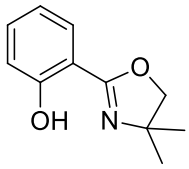	54%	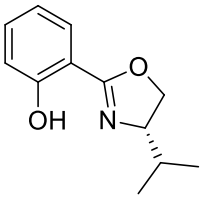	28%		
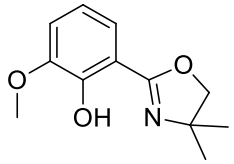	45%	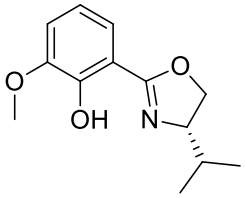	27%	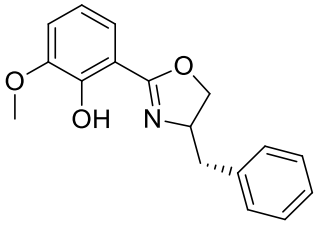	29%
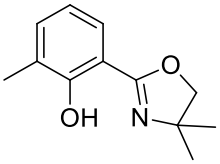	21%	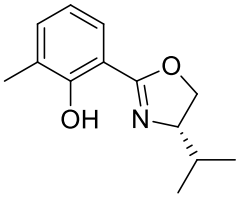	20%		
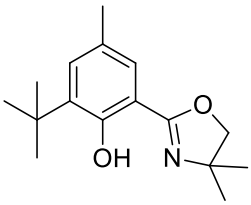	10%	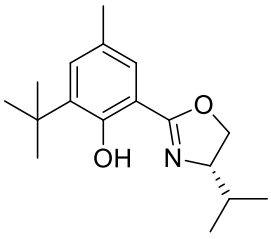	7%		

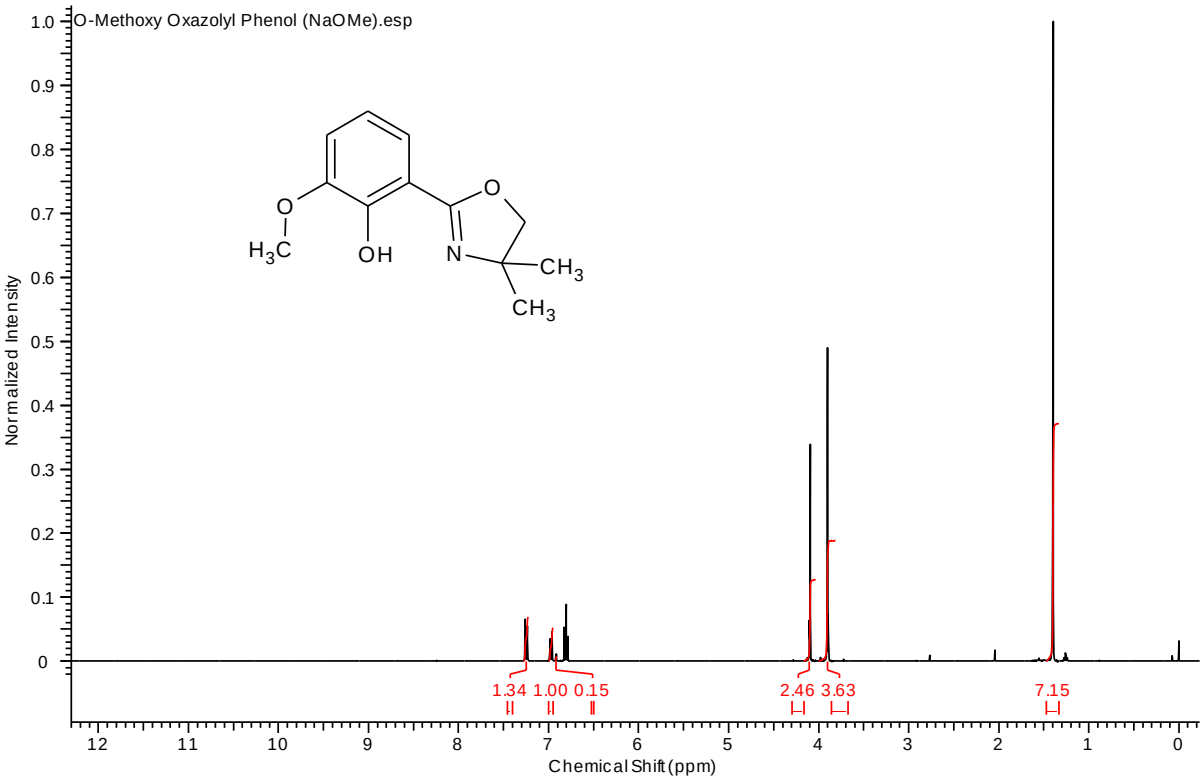

Figure 2.16: Example ^{1}H-NMR spectrum (400MHz, $CDCl_3$, 15-25C) of the final cyclisation product 2C

From (Fig. 2.16) it can be seen that the crude products of the cyclisation reaction are very clean, with only small amounts of baseline impurity present. Upon closer inspection, this seemed to be unreacted oxime carried through from the chlorination stage, with this there was some "overchlorinated" oxime. These impurities were identified by comparison of ^{1}H NMR spectra and presence of a peak in the MS spectra which corresponded to cyclised product plus chlorine with the characteristic isotopic splitting pattern of chlorine.

It was found that the reaction was tolerant to atmospheric moisture with no noticeable drop in yield and all reactions were conducted under non-anhydrous conditions.

Removal of the unreacted oxime was achieved by addition of a NaOH wash which effectively removed the oxime into the aqueous phase. However it was found that the crude products still contained impurities. Triturating with hexane yielded product of analytical purity although this

did result in a significant drop in yield. Upon examination of the residue it was found to be largely unreacted amino alcohol and “overchlorinated” product. However ultimately it was decided that column chromatography would yield the best results allowing the removal of all remaining impurities whilst maximising yields.

2.5 Conclusion

In conclusion we have demonstrated the successful synthesis of oxazolyl ligands from chlorooximes. Although the reaction is still unable to synthesise the bis-oxazoline the synthesis still has several advantages over existing methods as it avoids the use of any toxic or hazardous materials. The chlorination of the oximes proved to be a sticking point that was difficult to move past, although oxime formation and the eventual cyclisation steps proceeded with little trouble, in good yield and had easy purification methods.

Rare Earth Complexes

This chapter will discuss the general background of rare earth elements and their complexes, with a focus on the complexes of rare earths with 2-oxazolylphenols. This will then lead to a discussion of the research conducted in this study.

All crystal structure data obtained in this study were resolved by Dr Craig Robertson at the University of Liverpool.

3. Introduction to Lanthanide complexes

3.1 The lanthanide elements

The lanthanide elements consist of the 15 elements from lanthanum (La) to lutetium (Lu) corresponding with the filling of the 4f orbitals. In older literature known as the lanthanons, IUPAC have more recently redefined the series as the lanthanoids and together with the the chemically similar scandium (Sc) and yttrium (Y) they make up the rare earth elements (Fig. 3.1).[62] The term rare earth is a misnomer as several of the elements have relatively high natural abundances in the earth's crust. For example neodymium is far more abundant (~35,000 times) than gold, and even thulium (the rarest of the lanthanides) is more abundant than iodine.

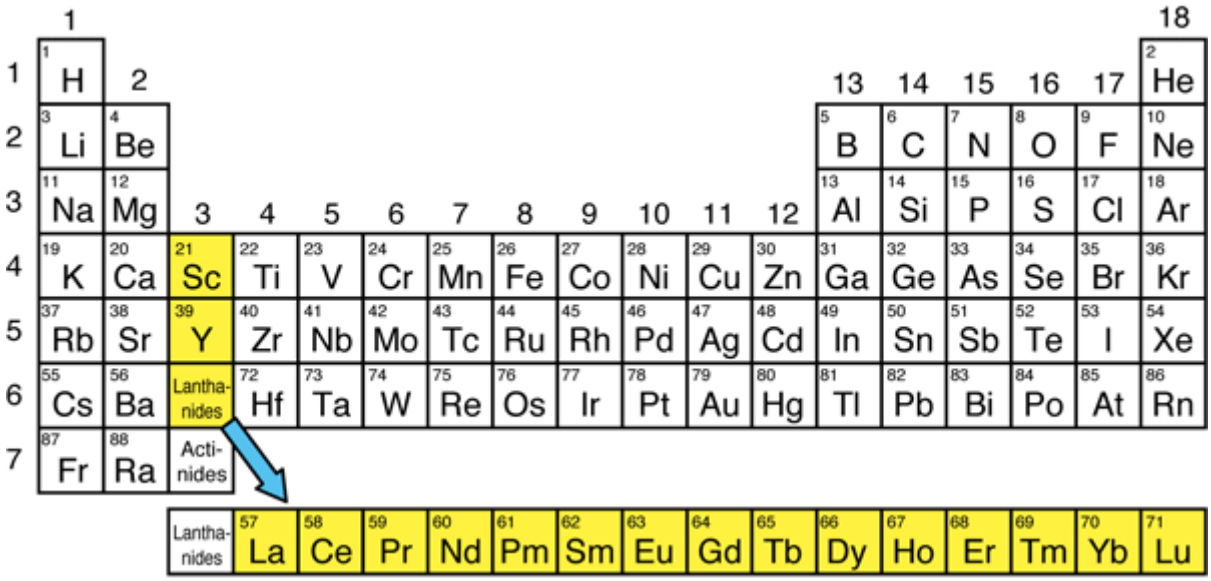

Figure 3.1: Rare earth elements (yellow)

The 4f electrons have a high probability of being found close to the nucleus and are thus strongly affected by nuclear charge.[63] So as nuclear charge increases across the period the ionic radius reduces leading to a phenomenon known as the lanthanide contraction. The low probability of the 4f electrons being found at the outer regions of the atom or ion permits little overlap between the lanthanide orbitals and any binding ligands. Thus lanthanide complexes

typically have little to no covalent character and are not influenced by orbital geometries or ligand field effects (Fig. 3.2).[64] This lack of orbital interaction also means that metal complexes are relatively insensitive to variation of the metal centre; this fact enables broad trends in chemistry and reactivity to be made. Complexes are held together by electrostatic interactions, meaning that ligand-ligand interactions dominate. Consequently, rare earth complexes tend to be fluxional with irregular geometries.[65]

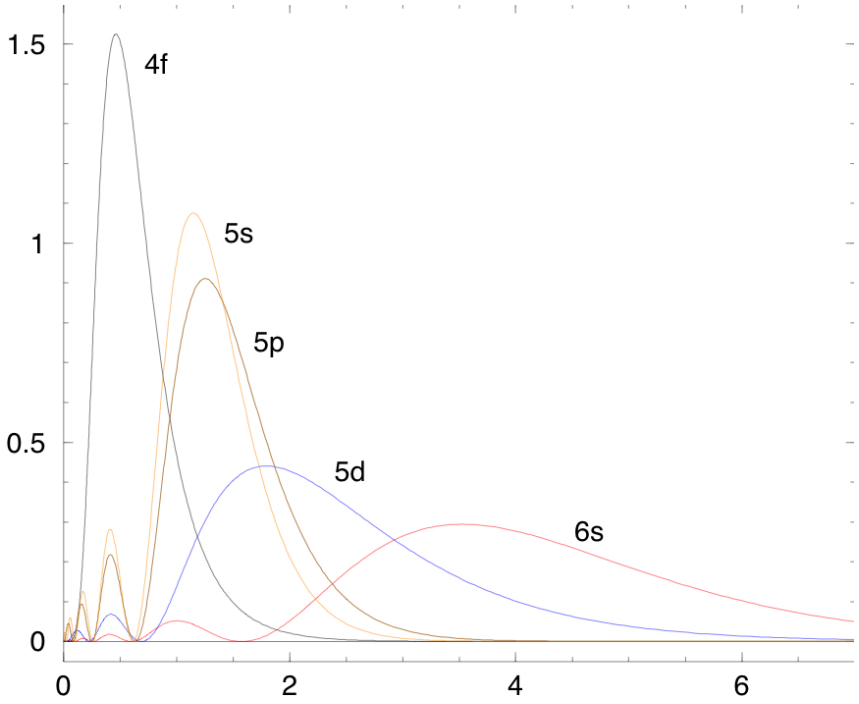

Figure 3.2: Radial distribution function plot for [Lu] (y-axis=radial distribution function, x-axis=distance from nucleus) [66]

Many of these features make lanthanides effective catalysts.[66] Hard Lewis acids make good catalysts as they're able to polarize bonds upon co-ordination and thus alter the electrophilicity of molecules.[67] The large ionic radii coupled with labile electrostatic bonding allows for bulky substrate binding and for rapid product dissociation, respectively.[68] In turn this results in high turnover rates, allowing for high yields to be achieved even with relatively low catalyst loadings.[69,70]

3.2 Development of rare earths complexes as asymmetric catalysts

The rare earths' catalytic development has its roots in their use as NMR shift reagents. Due to the Pauli Exclusion Principle, lanthanides can contain a large number of unpaired electrons (up to 7) causing many of them to be powerfully paramagnetic. This factor coupled with the strong Lewis acidity associated with lanthanides generally means that lanthanides make effective NMR shift reagents.[71]

The most popular NMR shift reagents generally contain europium due to its relative lack of line broadening, which can often be an issue for other lanthanides, especially when used in high concentrations.[72]

Many of the properties that make rare earth complexes effective NMR shift reagents are similar to those that make for good Lewis acid catalysts.[73] Indeed one of the most popular shift reagents, $Eu(FOD)_3$, has been used in the cyclocondensation of dienes with aliphatic and aromatic aldehydes to yield dihydropyrans, with high endo selectivity. This was demonstrated by Danishevsky in 1983 when he reported the use of $Eu(FOD)_3$ for the Diels-Alder reaction of aldehydes with siloxydienes (Fig. 3.3). [74]

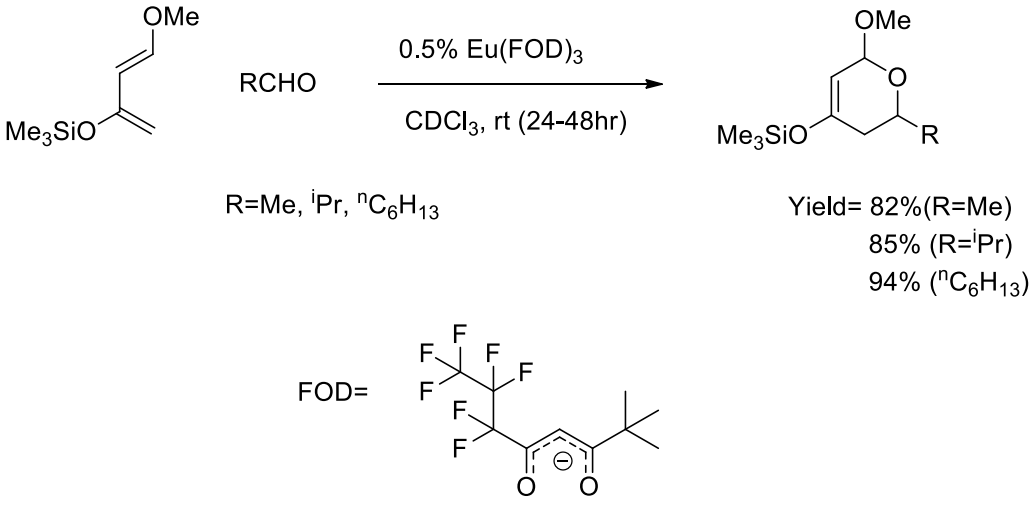

Figure 3.3: Diels-Alder reaction demonstrated by Danishevsky using $Eu(FOD)_3$

Danishevsky et al. also demonstrated the asymmetric catalytic potential of these complexes when they employed europium (3) tris [3-(heptafluoropropylhydroxymethylene)-(+)-camphorate], $Eu(hfc)_3$, with ee's of 58% with molar loadings of only 1% (Fig. 3.4).[75]

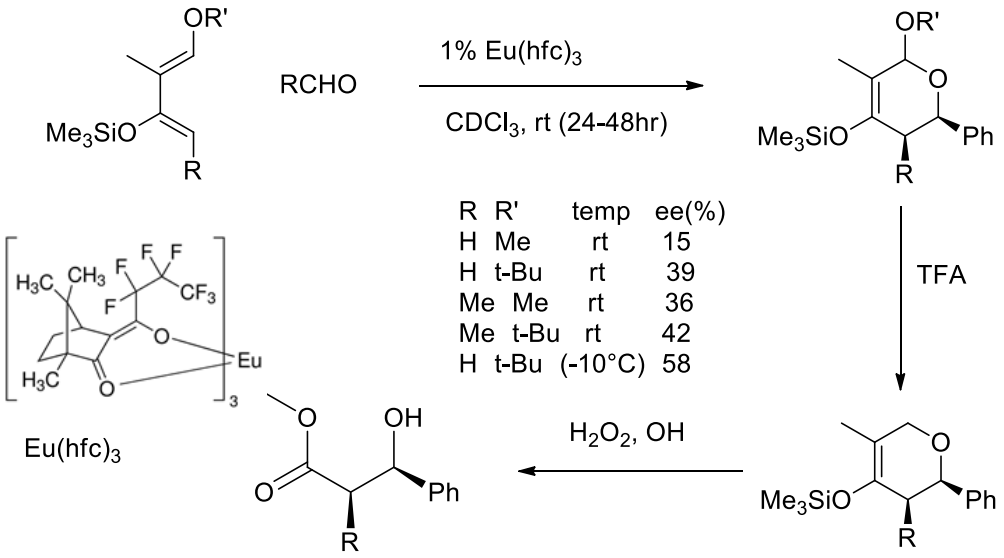

Figure 3.4: One of the first examples of a lanthanide asymmetric catalyst[75]

This initiated some interest in the use of these complexes as asymmetric catalysts for Diels-Alder,[76] Mukaiyama aldol[77] and Michael addition reactions[78]. However significant research was not conducted until complexes more specifically designed for asymmetric synthesis were produced. The first example was produced by Shibasaki et al. in 1992, where they used a chiral lanthanum tri binaphtholate complex to catalyse an asymmetric nitrolaldol (Henry) reaction in good yield and ee (Fig. 3.5).[79]

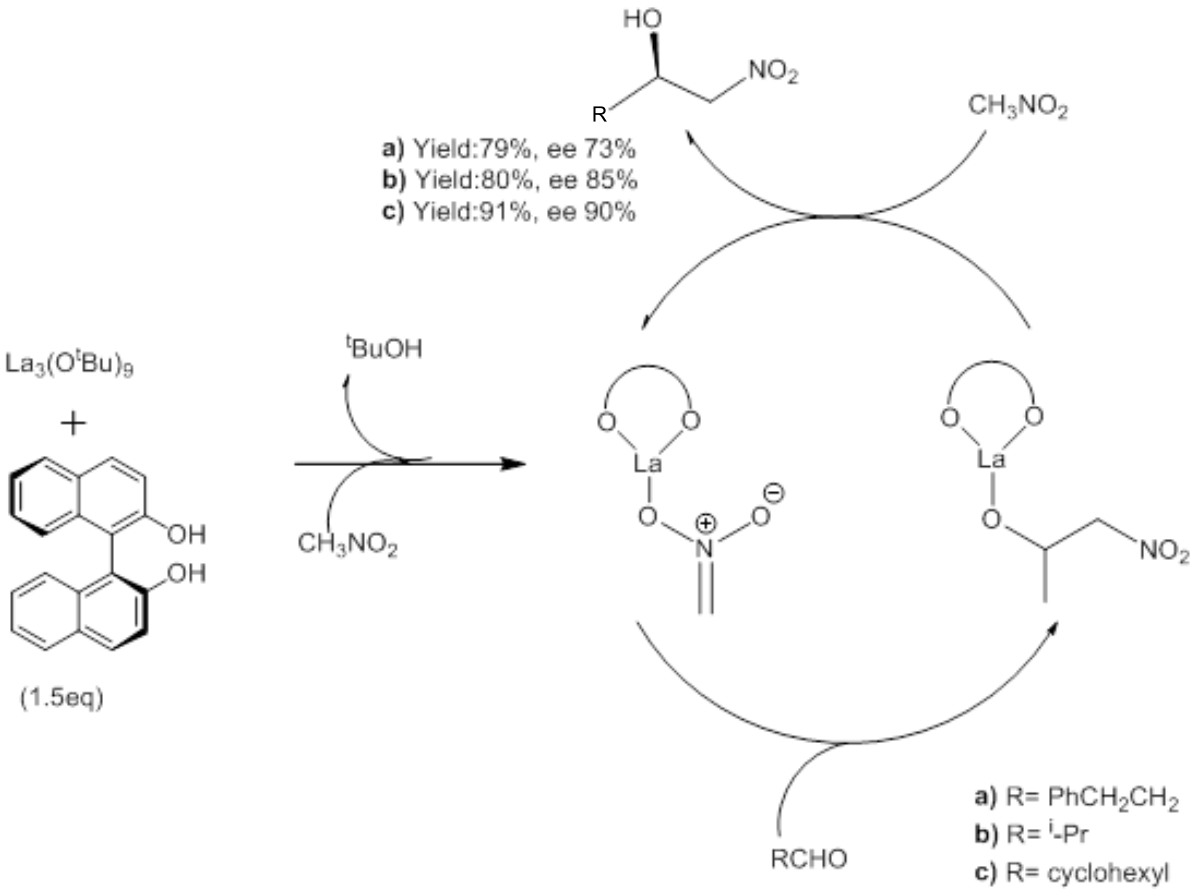

Figure 3.5 Asymmetric Nitroaldol reaction[79]

Further developments by the Shibasaki group led to optimisation of these catalysts, with the elucidation of a standard formula for these complexes as $(Ln(BINOL)_3(M)_3)$ (M=alkali metal e.g. Li, Na etc.) and a crystal structure coming shortly after.[80,81] These catalysts would prove to be very effective not just for nitroaldol reactions but for a range of systems including hydrophosphorylation,[82] Michael[83] and Diels-Alder[84] reactions. The effectiveness and versatility of these catalysts can be attributed to their ability to act both as Brønsted bases and Lewis acids through the metal alkoxides and lanthanide ion, respectively. It was found the effectiveness of these catalysts was highly dependent on the combination of rare earth and alkali metal, with the nitroaldol reaction responding best when Ln=Eu and when M=Li, whereas the Michael reaction responded best for Ln=La and M=Na (Fig. 3.6).[81,85]

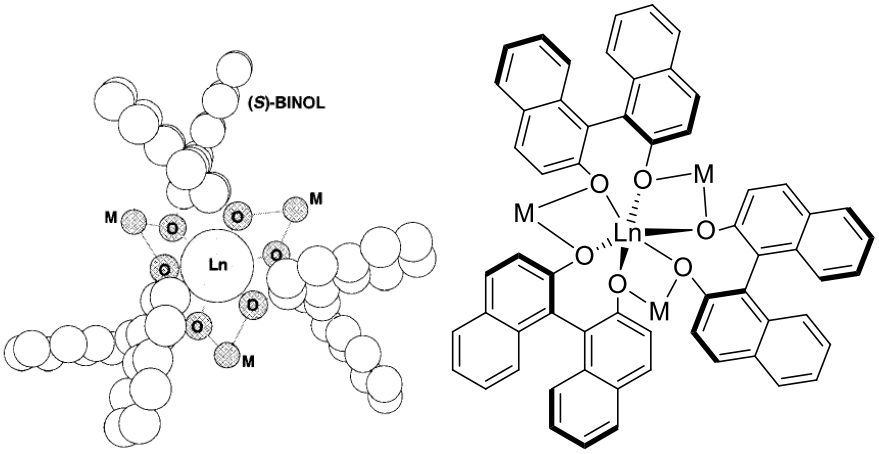

Figure 3.6: Representation of the crystal structure of $[Ln(BINOL)_3(M)_3]$[1,86]

The effectiveness of these catalysts, coupled with their ease of modification generated great interest leading to a wide range of new rare-earth catalysts.[84,86,87]

3.3 Asymmetric catalysts involving rare earth elements with oxazoline ligands

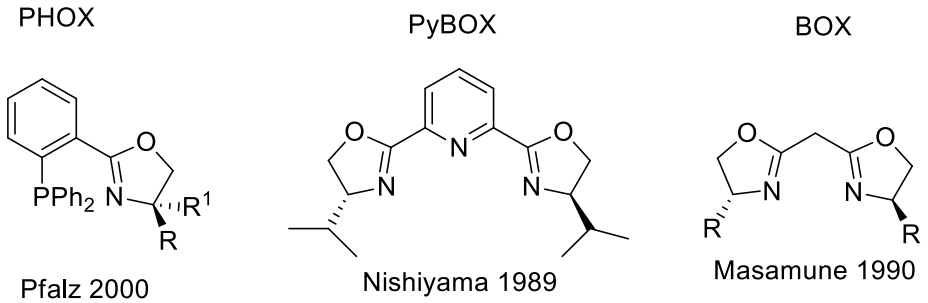

Figure 3.7: Oxazoline ligands used in asymmetric catalysis[19,20,27]

Despite the effectiveness of both rare earths and oxazolines in asymmetric catalysis there are relatively few examples of their use in combination. Strikingly complexes involving BOX and PHOX ligands have never been isolated (Fig. 3.7). However an example of PYBOX ligated $Yb(OTf)_3$ complexes were the first to demonstrate enantioselectivity with rare earth complexes

containing oxazolines ligands.[88] This was conducted by Jørgenson et al. (1997) who demonstrated the effectiveness of an uncharacterised $Yb(OTf)_3$ PYBOX catalyst in the 1,3-dipolar cycloaddition of nitrones with alkenes (Fig. 3.8).[88] These catalysts proved more active than BINOL ligands, which gave a racemic product, but less active than $Ln(OTf)_3$ complexes.

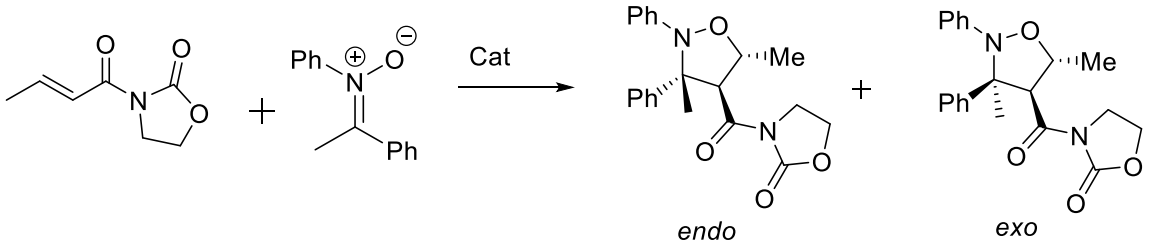

Figure 3.8: 1,3-dipolar cycloaddition of nitrones with alkenes.[88]

Examples of heteroleptic complexes of PYBOX and a lanthanide have been found to be useful for cyanohydrin formation[69] and hetero Diels-Alder reactions,[89] achieving good yields and ee's in each case. X-ray crystal structure data would later show that the structure of these complexes takes the form: $[Ln(PYBOX)(OTf)_3]$.[69,90] This structure data led to a greater understanding of the catalytic potential of these complexes leading to their use in more asymmetric reactions including Strecker hydrocyanations,[91] Michael additions[83] and Mukaiyama-aldol reactions.[33] As a result, these complexes have arguably been one of the most successful uses of rare earth complexes incorporating oxazoline ligands in asymmetric catalysis.

There are relatively few examples of rare earth complexes containing more than one oxazoline ligand. BOX, PHOX and PYBOX ligands are all charge neutral making them unable to satisfy the +3 charge of the metal ion. BOX (bis(oxazolines)) ligands, however, can be deprotonated to give anionic bis(oxazolinato) ligands, these were first used as ligands in rare earth complexes by Anwander et al. in 1999 (Fig. 3.9). The synthesis was based on the common silylamide route, using bis (silylamide) as both a ligand and an in-situ base. This allowed the production of both the mono- and Bis (bis(oxazolinato)) complexes however the tris-complex could not form, even when very large lanthanide ions were used.[26]

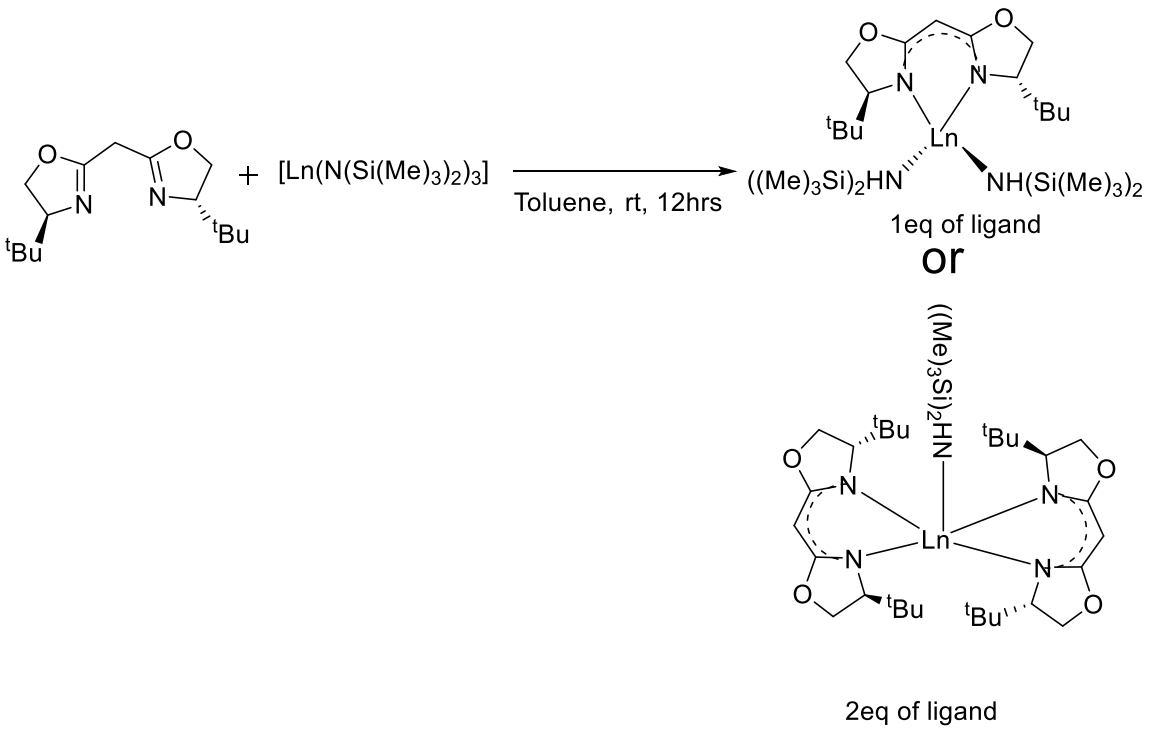

Figure 3.9: Formation of Bis (oxazolinato) complexes by Anwander et al.[92,26]

Complexes incorporating Bis (oxazolinato) ligands were found to be effective for enantioselective intramolecular hydroamination and cyclisation in 2003, as well as ring-opening polymerisation in 2006, but no other example have been reported since.[93,94] This is most likely due to the poor stability of these complexes. The anionic charge on the BOX ligand, although stabilised by delocalisation and co-ordination to the rare earth centre, is still a carbanion and as such will be prone to protonation and electrophilic addition, limiting the processes and solvents these complexes may be used in.[92]

A related class of oxazolines ligands which have also shown promise in rare earth catalyst formation are the trisoxazoline (TRISOX or TOX) ligands.[95] Despite being neutral they are able to form stable complexes with high oxidation state metals, such as rare earths, through the chelate effect. There are two general synthetic strategies for TRISOX ligands; the first is the direct method where three oxazolines are made in one step. This enables production to take relatively few steps, but does prevent production of heterochiral TRISOX ligands with different

oxazoline subunits. The second method is to construct three oxazoline rings in a modular fashion. In this strategy a bisoxazoline framework is first synthesised containing an oxazoline precursor which then can either be directly transformed into the third oxazoline or directly coupled to a preformed oxazoline. Although this method is indirect, requiring several steps, it does allow synthesis of TRISOX ligands using different oxazoline subunits, which in turn allows for synthesis of both hetero- and homochiral ligands (Fig. 3.10).[95]

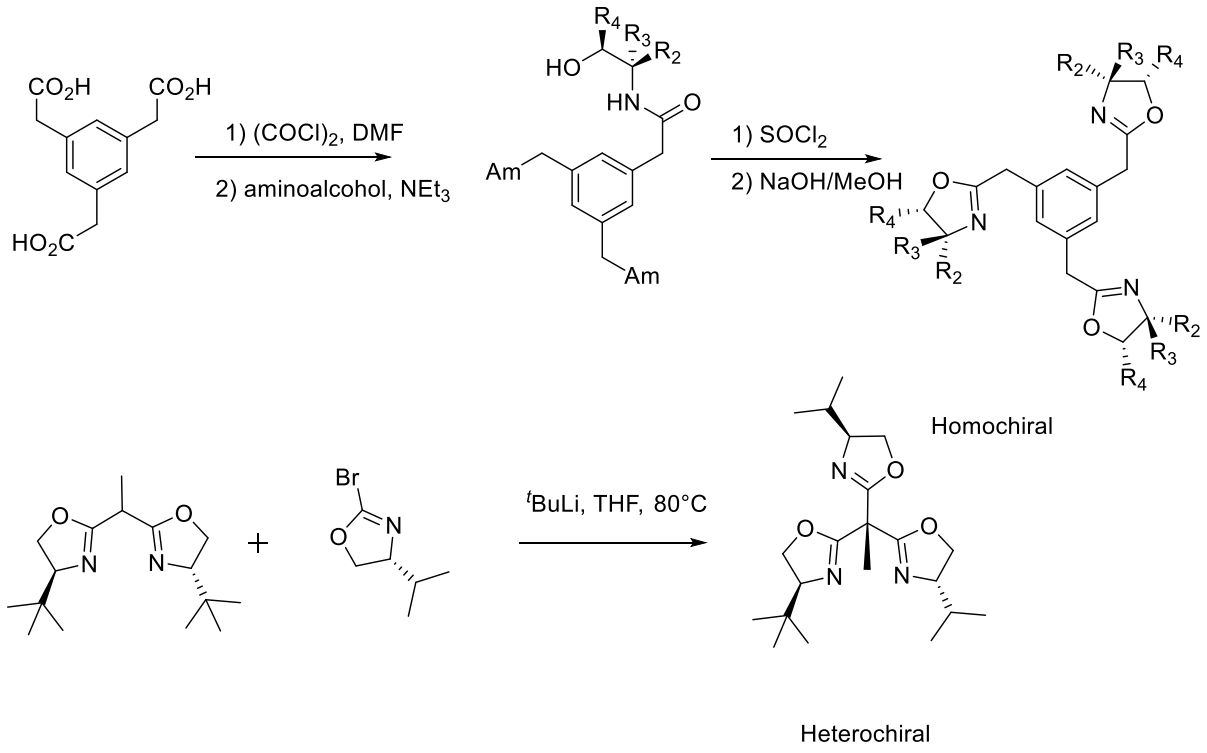

Figure 3.10: Routes to trisoxazoline ligands[95,96]

Complexes of trisoxazoline ligands with rare earths have proven to be successful in the synthesis of poly (α-alkenes), giving high tacticity and catalytic activity.[97–100] One structurally similar example is that of the tris (oxazolinyl)borate ligand which uniquely for TRISOX ligands binds as the anion to yttrium, these complexes were found to be useful in hydroamination reactions.[101]

3.4 Rare earth complexes with 2-oxazolylphenols

To date there are limited examples of rare earth complexes with 2-oxazolylphenol ligands, totalling only three papers.[102,103,104] The earliest of the three papers by Hubert-Pfalzgraf et al. investigated using these complexes in metal organic chemical vapour deposition (MOCVD) with a view to generating thin films of cerium (IV) oxide.[102] Berg et al. conducted a structural study of these complexes, providing the only detailed structural analysis to date.[103] Shibasaki et al. most recently investigated heteroleptic lanthanum complexes with 2-oxazolylphenols and their use in *anti*-selective Mannich reactions.[104]

Hubert-Pfalzgraf et al. investigated two tetrakis 2-oxazolylphenol cerium complexes and their applications for liquid injection MOCVD (Fig. 3.11). [102] Both complexes were noticeably less volatile than other cerium precursors despite having similar molecular weights. This is most likely due to π-π stacking between the phenyl substituents. TGA-GC/MS and mass spectrometry (EI) were used to investigate the decomposition pathways of the two complexes. It was interesting to note the stark differences between the two complexes despite their structural similarities. Ultimately it was concluded that complex 2, Ce (^{i}PrHoxaz)$_4$, was suitable as a potential precursor for CeO_2 deposition under an inert atmosphere. Complex 1, Ce (Me_2oxaz)$_4$ was unsuitable as a precursor in non-oxidative conditions. The difference between the two complexes decomposition pathways is largely due to sterics.

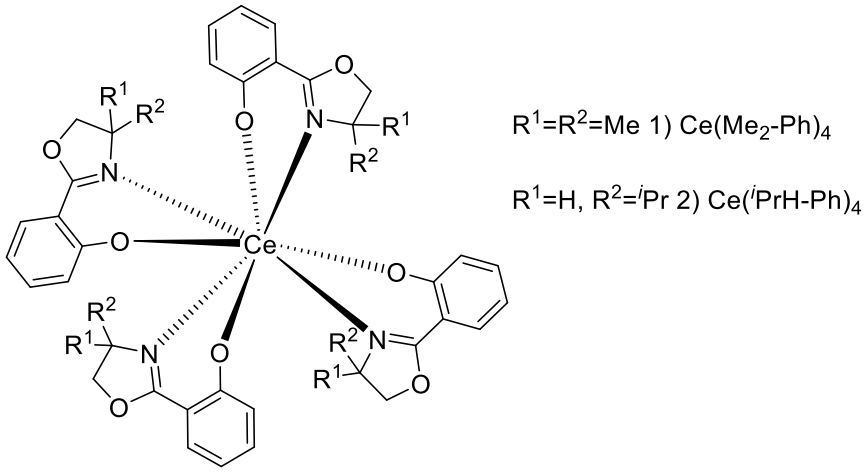

Figure 3.11: Proposed structure of cerium tetrakis oxazolylphenolate complexes[102]

Berg et al. synthesised tris allox complexes with a range of lanthanides with the general formula $Ln(Allox)_3$ (Ln=La, Ce, Sm, Er, Y).[103] These complexes were well characterized by ^1H NMR spectroscopy in solution and single crystal XRD in the solid state for the Ce and Er complexes. The purpose of the study was to understand the structural changes of the tris(oxazoline-phenoxide) complexes both in the solid state and in solution. The addition of the allyl substituents was primarily incorporated to see whether coordination of the tethered alkene can occur, but also to provide additional steric bulk.

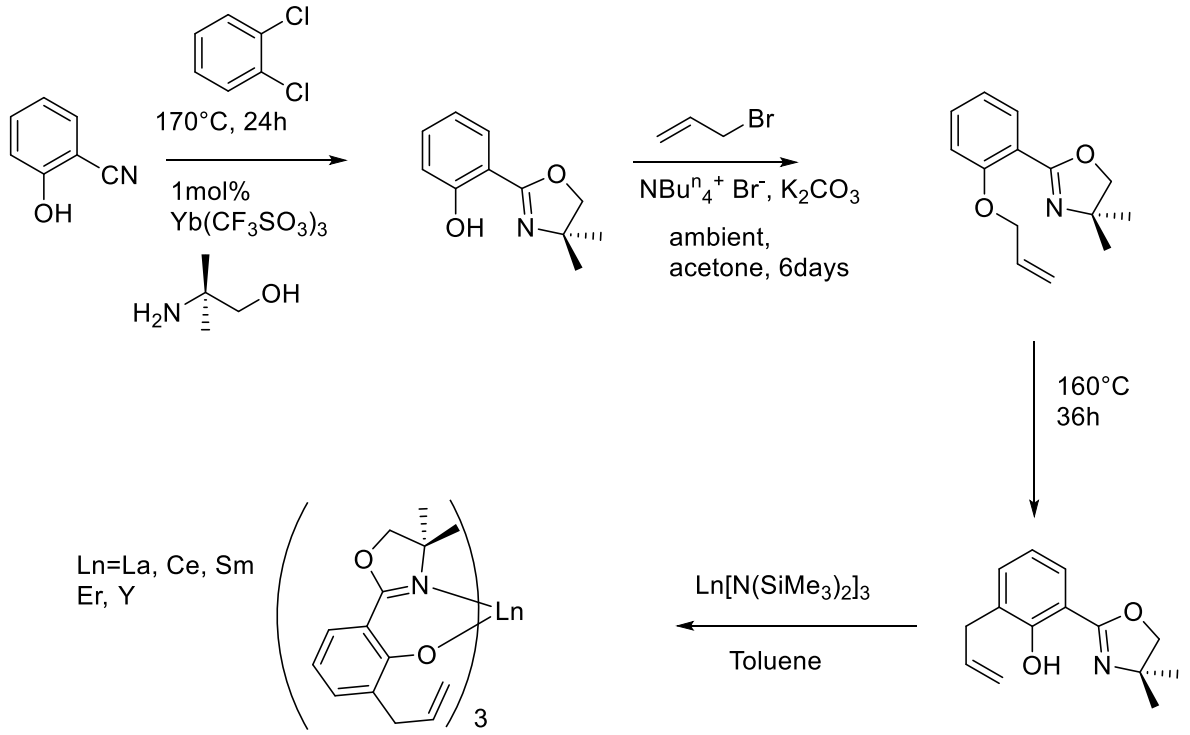

Figure 3.12: Synthesis of oxazolylphenolate complexes by Berg et al. [103]

Crystal structures for the cerium and erbium complexes were obtained and they were very similar to each other. Both demonstrated distorted octahedral coordination geometry, with a mer arrangement of the three coordinating allox ligands. This showed the allyl groups to be non-coordinating, as the closest contact between the metal and the terminal or internal alkene carbons was 4Å.

Solution ^{1}H NMR spectra of the complexes in d_8-toluene showed a set of 9 resonances consistent with an average C_{3v} symmetry. Berg et al. noted that Ln(Allox)$_3$ complexes can exist in two different geometries, facial and meridional (Fig. 3.13), and that the differing symmetries between these two forms could be distinguished by ^{1}H NMR spectroscopy. The facial form would be C_3 symmetric and as such corresponding chemical shifts on the ligands would be equivalent leading to a total of 12 chemical shifts. The meridional form would have C_1 symmetry rendering all corresponding chemical shifts to be inequivalent and giving 36 chemical shifts. As such, 9 chemical shifts would indicate a facial geometry for the complexes;

however crystal structure data strongly indicated meridional complexes. This strongly implies the two geometries are interconverting and the chemical shifts are being thermally averaged in the ^{1}H NMR spectra.

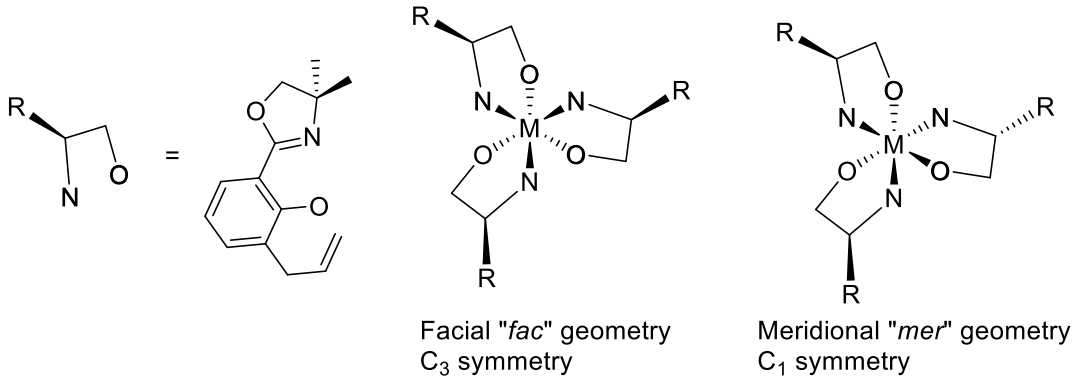

Figure 3.13: Facial (*fac)* and Meridional (*mer*) isomers

Berg et al. attribute this fluxionality to the Bailar (trigonal) or Ray-Dutt (rhombic) twists.[105] The Bailar twist cannot interconvert between *mer* and *fac* isomers, but it can scramble between sites of the same geometry (for example *fac*-Δ and *fac*-Λ) (Fig. 3.14 and Fig. 3.15). Ray-Dutt twists can interconvert between all four isomers (*mer*-Δ, *mer*-Λ, *fac*- Δ and *fac*- Λ) (Fig. 3.16).[103]

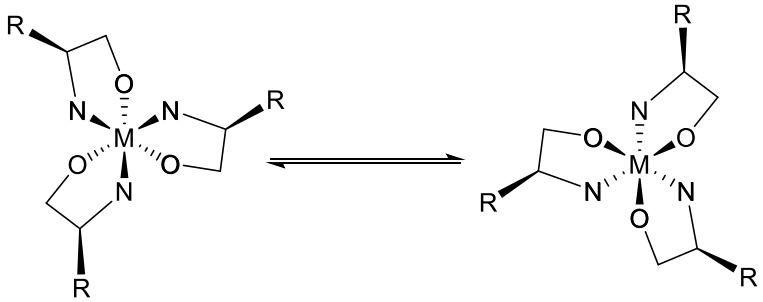

Figure 3.14: Bailar twist interconversion of *fac*-Δ (on the left) to *fac*-Λ (on the right)

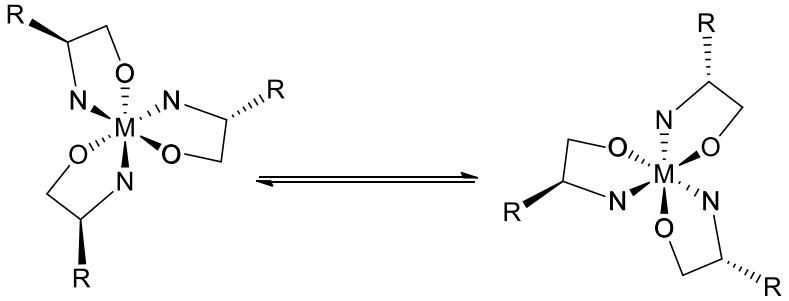

Figure 3.15: Bailar twist interconversion of *mer*-Λ (on the left) to *mer*-Δ (on the right)

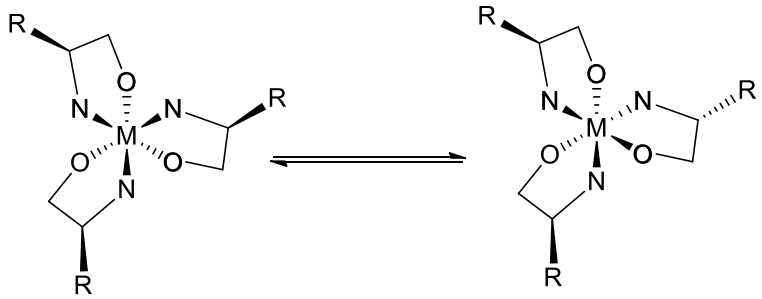

Figure 3.16: Ray-Dutt twist interconversion of *fac*-Δ (on the left) to *mer*-Λ (on the right)

Berg et al. notes that it is not possible to distinguish between these two processes as the *fac* isomer isn't visible at low temperatures. Consequently, it is not possible to rule out that these complexes may be just fluxional *mer* complexes showing thermal averaging in ^{1}H NMR. However taking into account the work of other groups and the highly fluxional nature of rare earth co-ordination, they believe it is highly likely that both processes are occurring simultaneously.[105]

It should be noted that as the allox ligand is achiral its *mer*-Δ and *mer*-Λ complexes (as well as *fac*-Δ and *fac*-Λ complexes) are enantiomers of each other and therefore indistinguishable by ^{1}H NMR spectroscopy. By comparison the chiral ligands used in this study will have Δ and Λ forms of the two geometries that will be diastereisomers of each other; hence all forms (*mer*-Δ, *mer*-Λ, *fac*-Δ, *fac*-Λ) are inequivalent, resulting in very complicated NMR spectra.

Shibasaki et al. have thus far been the only group to investigate the catalytic potential of rare earth complexes of 2-oxazolylphenols.[104] The anti-selective Mannich-type reaction between

N-substituted imines and trichloromethyl ketone (an ester donor equivalent) was effectively catalysed by a heteroleptic lanthanum complex in good yield and ee (Fig. 3.17).

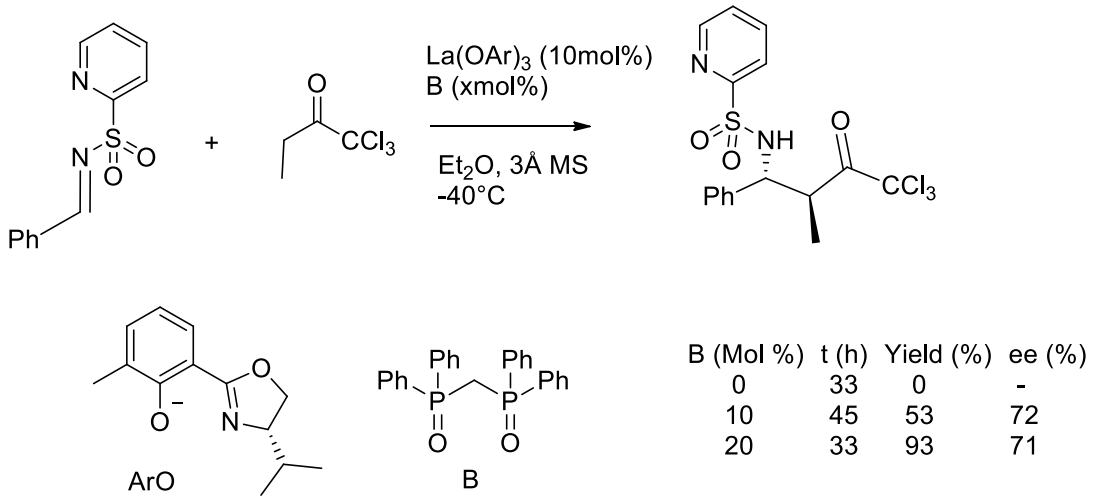

B (Mol %)	t (h)	Yield (%)	ee (%)
0	33	0	-
10	45	53	72
20	33	93	71

Figure 3.17: Anti-selective direct catalysed Mannich type reaction[104]

The process is notable due to its use of a Lewis base to catalyse a Brønsted base catalysed process. The catalyst was formed in situ and as such the active form of the catalyst was not characterised; however probable transition states were proposed (Fig. 3.18). This model strongly favours the formation of the less sterically hindered intermediate, resulting in *anti*-selectivity.

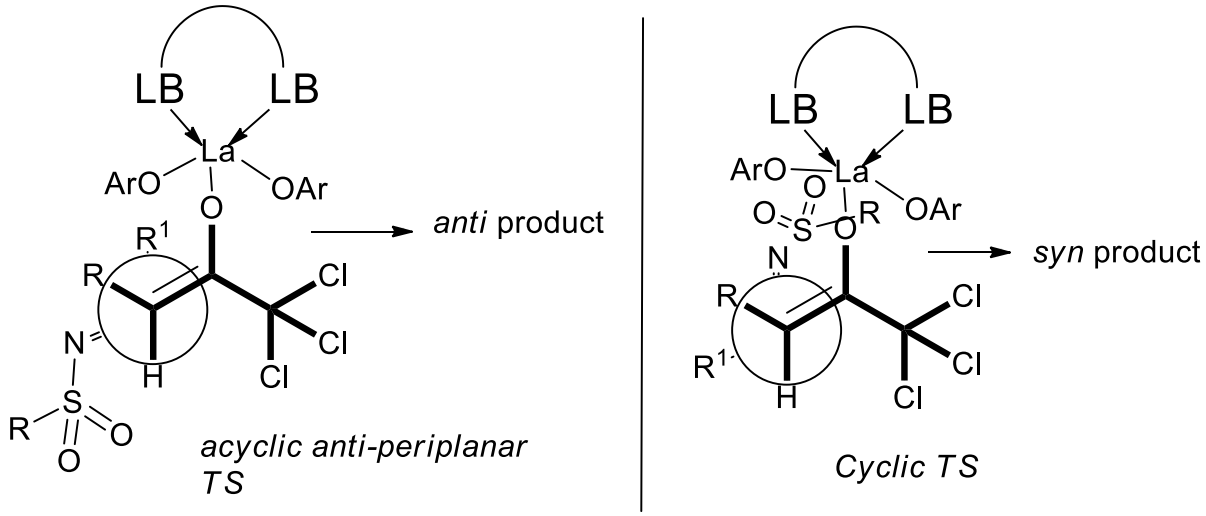

Figure 3.18: Transition state (TS) models proposed by Shibasaki et al. (2008)[104]

3.5 Research Aims

Despite the great success shown individually by rare earths and oxazoline ligands in asymmetric catalysis, there are only limited examples of their use together.

The aim of this research is to establish a simple and reliable synthesis to produce 2-oxazolylphenol complexes with rare earths. Once a range of complexes have been synthesised and characterized, they will be assessed for their catalytic potential. The hope is that through this research we can achieve an understanding of the catalytic potential of these complexes and how the underlying structure of the complexes affects the activity and enantioselectivity of the catalysts.

4. Results and Discussion of Rare Earth Complexes

4.1 Overview of synthetic routes to rare earth complexes

Rare earth alkoxide complexes, of the type synthesised in this study, often demonstrate moisture sensitivity. Generally this is due to a combination of factors, but most crucially the ease of protonation of the ligand combined with the thermodynamic stability of the rare earth hydroxide. Additionally the insolubility of the rare earth hydroxides in most solvents pushes the equilibrium (Fig. 4.1) over to the right. This effect, given sufficient time, causes the complexes to degrade significantly in wet solutions.

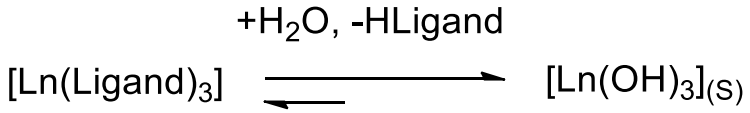

Figure 4.1: Hydrolysis of a rare earth complex

Rare earth alkoxide or aryloxide complexes are generally synthesised by one of two routes. The first is a metathesis reaction between a rare earth halide and an alkali metal salt of the ligand. The second is an acid base reaction between a pro-ligand and a rare earth metal complex with Brønsted basic ligands. There are a number of ligands suitable for this purpose including: alkyls, alkoxides, dialkylamides and silylamides, the last of which was our precursor of choice due to extensive group experience with their handling and synthesis (Fig. 4.2).

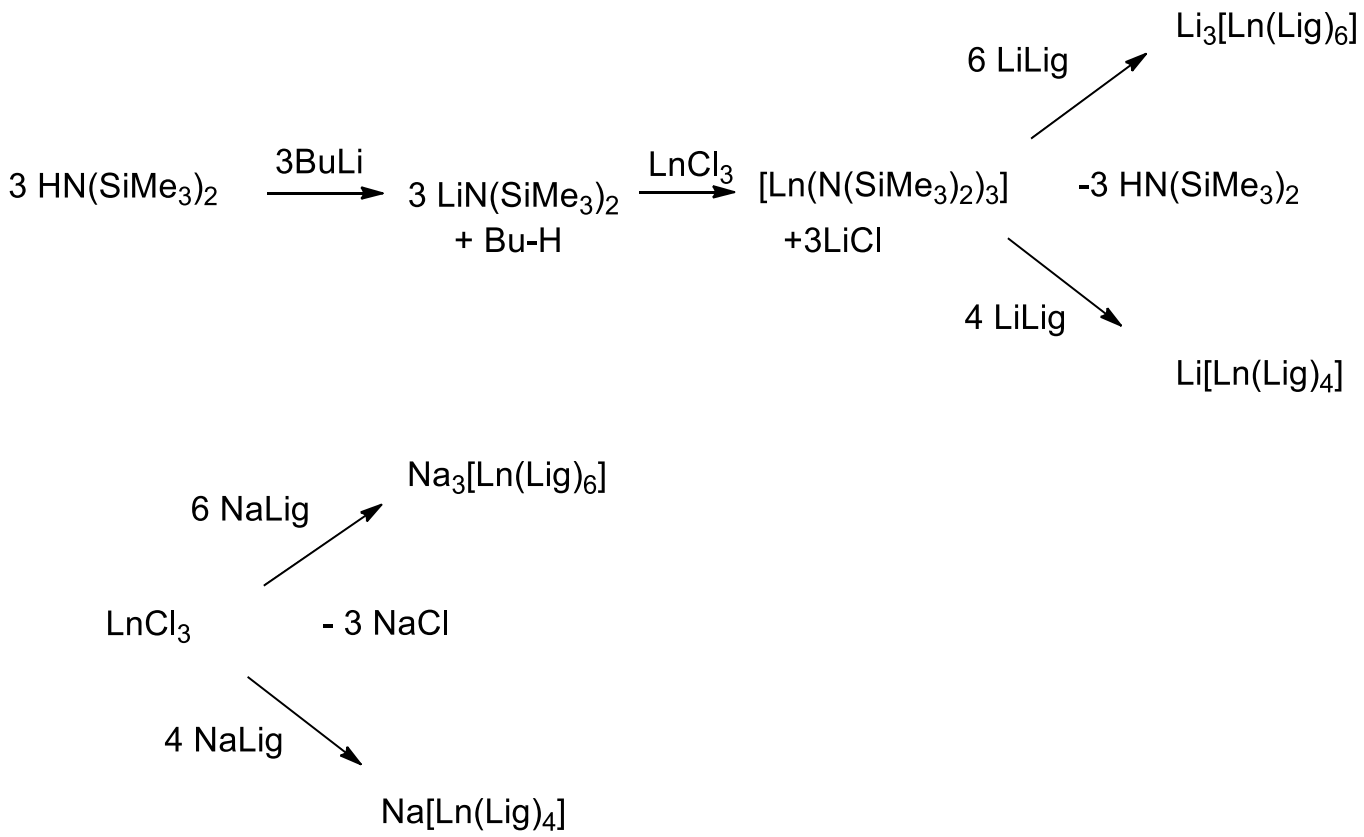

Figure 4.2: The silylamide route[106] (top) and the salt metathesis route (bottom)

Both processes require access to anhydrous rare earth chlorides which, although commercially available, are expensive. This led to us synthesising them from the rare earth oxides (Fig. 4.3). Details of this process are provided in the experimental section. [107]

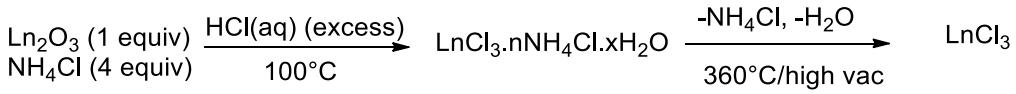

Figure 4.3: Production of anhydrous rare earth chlorides with sublimation of NH_4Cl

Unfortunately we found that rare earth chlorides produced in this manner seemed to be unreactive in all further reactions, and as such an alternative method was sought.

Production of the rare earth chlorides began *via* heating the rare earth oxides in concentrated HCl. The hydrated rare earth chloride was then refluxed in trimethylorthoformate under argon (Fig.4.4); this was then reduced to dryness in *vacuo*.

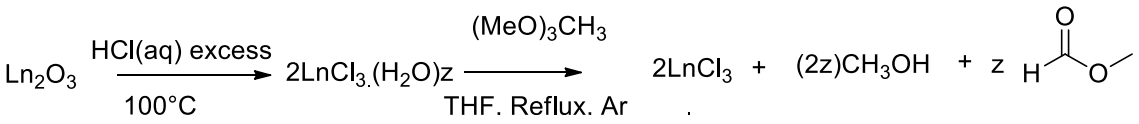

Figure 4.4: Trimethylorthoformate dehydration of rare earth chlorides[108,109]

The dehydration was performed *in situ* and the alkali metal-ligand salt added as a solution in THF (Fig. 4.5).[108] The methyl formate produced has been known to decompose further into formic acid under sufficiently aqueous conditions in the presence of Lewis acids.[109]

Figure 4.5: Synthetic procedure for complexes made from trimethylorthoformate dehydration of rare earth chlorides

The above procedure produced a semi-crystalline white solid after removal of the solvent and recrystallization produced several crystals of X-ray quality. Complexes isolated *via* this method formed partially hydrolysed tri yttrium clusters as can be seen from figure 4.6. The yttrium atoms are linked by oxygen bridges and each of the yttrium centres are ligated by two oxazolylphenol ligands (Me_2-Ph). One sodium ion is also incorporated into the cluster.

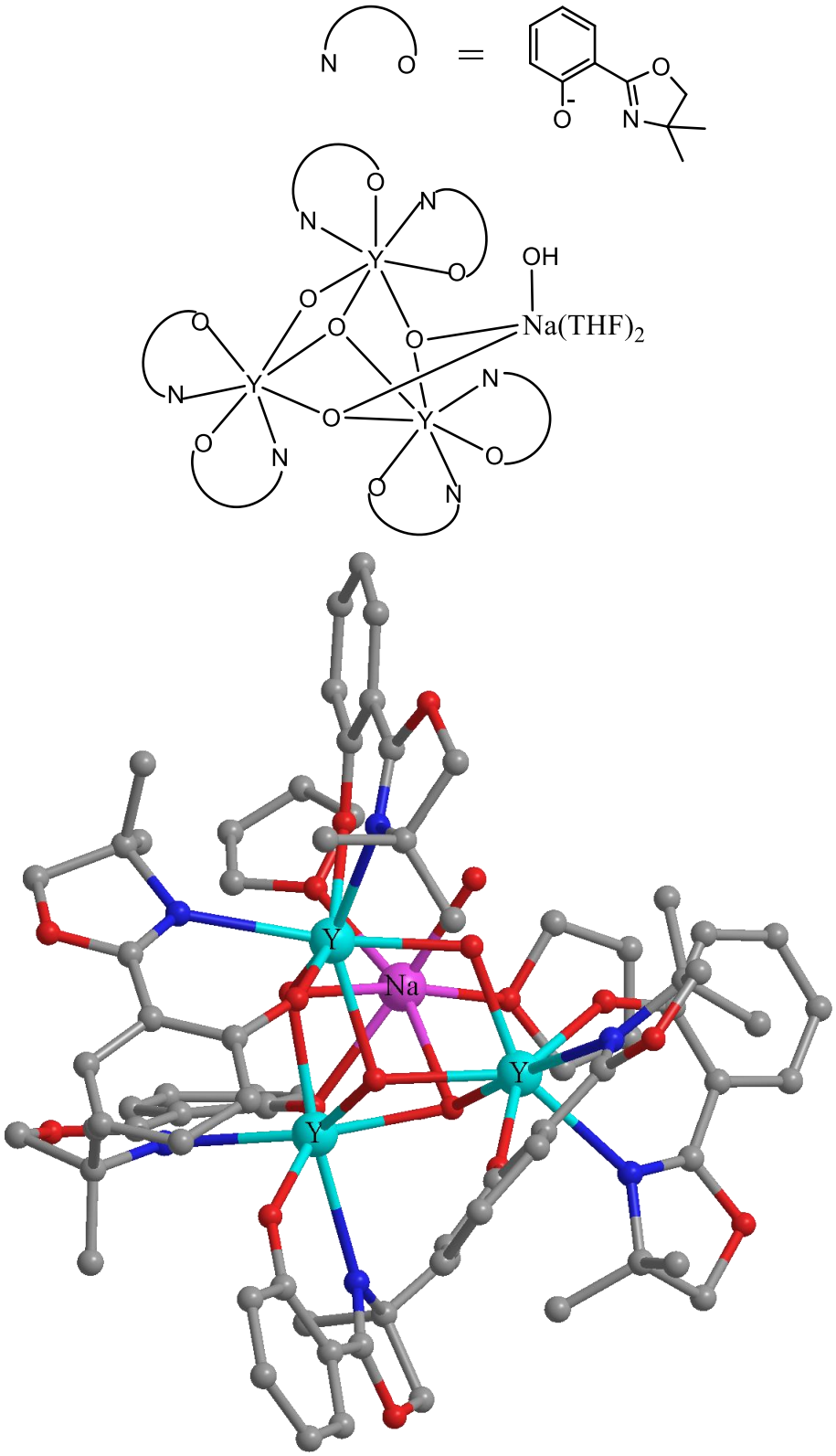

Figure 4.6: Partially hydrolysed tri-yttrium cluster isolated from the trimethylorthoformate dehydration method.

Although the formation of this cluster was interesting, it was not the heterobimetallic complex we were attempting to synthesise and so a new method was found. This process relied on the use of lanthanum nitrate tetraglyme ($Ln(NO_3)_3$(Tetraglyme)), which had previously been prepared by the group as starting materials for the synthesis of rare earth alkoxide and aryloxide complexes.[110] The synthesis of these starting materials is relatively simple and when Ln is lanthanum the product can be precipitated in high yield and purity (Fig. 4.7).[111] Only lanthanum nitrate tetraglyme was produced in this study.

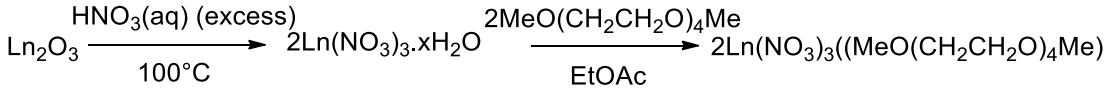

Figure 4.7: Preparation of lanthanum nitrate tetraglyme.[112]

Isolation of this complex as a white solid was followed by reaction with the sodium salt of the ligand (Fig. 4.8).

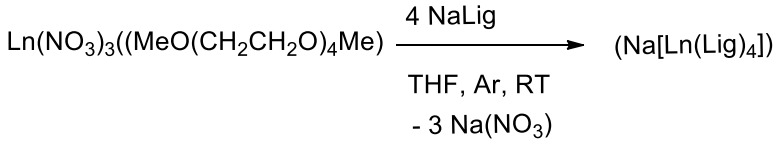

Figure 4.8: Synthesis of rare earth hetreobimetallic complexes from rare earth nitrate tetraglyme.

The complex synthesised in the above process was isolated as a white semi-crystalline solid, however crystal structure data showed that instead of forming the heterobimetallic complexes as intended an ion pair had formed with the tetraglyme coordinated to the sodium centre. The lanthanum formed a negatively charged eight co-ordinate complex with four ligands (Fig. 4.9).[113]

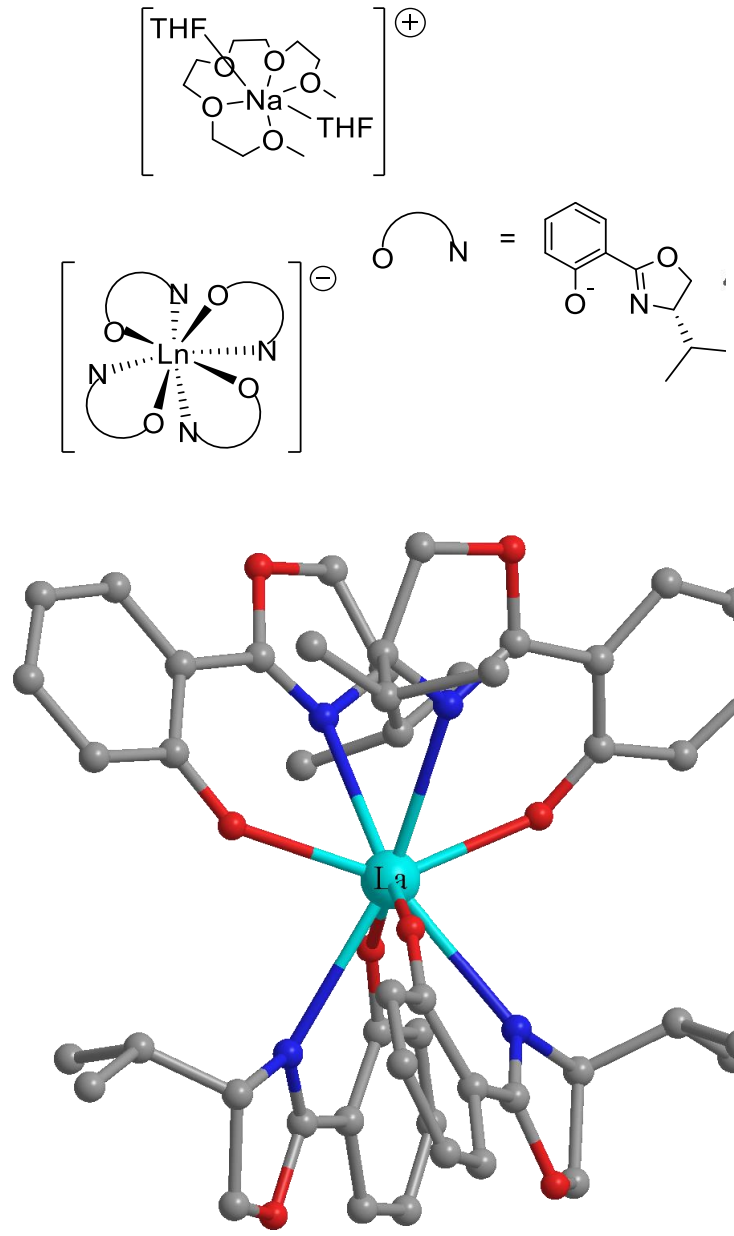

Figure 4.9: Ion pair complexes with the Na complex omitted for clarity

Synthesis of the hetereobimetallic complexes from the rare earth nitrate tetraglyme adducts was not possible. We then turned to thionyl chloride ($SOCl_2$) (Fig. 4.10) as a method of producing anhydrous rare earth chlorides. Initial production of the rare earth chlorides still proceeded via heating of the rare earth oxides in HCl. This was followed by refluxing the hydrated rare earth chloride in thionyl chloride for 24-48 hours.

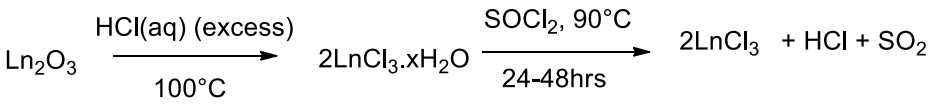

Figure 4.10: Dehydration of rare earth chlorides using thionyl chloride

This was followed by removal of thionyl chloride *in vacuo* to yield the dehydrated lanthanide chloride. Two rare earths were elected for study: yttrium and europium. Yttrium is diamagnetic and should give relatively simple ^{1}H NMR spectra. Yttrium is also relatively inexpensive and so was thought to be a sensible starting point. Europium is somewhat more expensive, however it causes shifts in the NMR spectra of its complexes and so it was hoped this could prove interesting. Furthermore europium (III) has a larger ionic radius than yttrium (III) and it was thought would make for an interesting study into the effects of ionic radius on structure and catalytic activity of any complexes formed. Additionally good crystal structure data were available for complexes produced previously by other members of the group for both yttrium and europium.[41,114]

4.2 Discussion of Crystal Structure Data Previously Obtained in the Group

Complexes of 2-oxazolylphenol ligands have been relatively poorly explored in the literature for reasons mentioned extensively in chapters 1 and 3.

In contrast to this, these complexes have been studied in depth by the Aspinall group for many years. This has led to the accumulation of a great deal of knowledge about the structure of these complexes. In particular several crystal structures have been isolated over the years, elucidating the structure of these complexes with different combinations of rare earth/alkali metal and ligand.

All complexes discussed in this section have been synthesised using the processes outlined in figure 4.2.

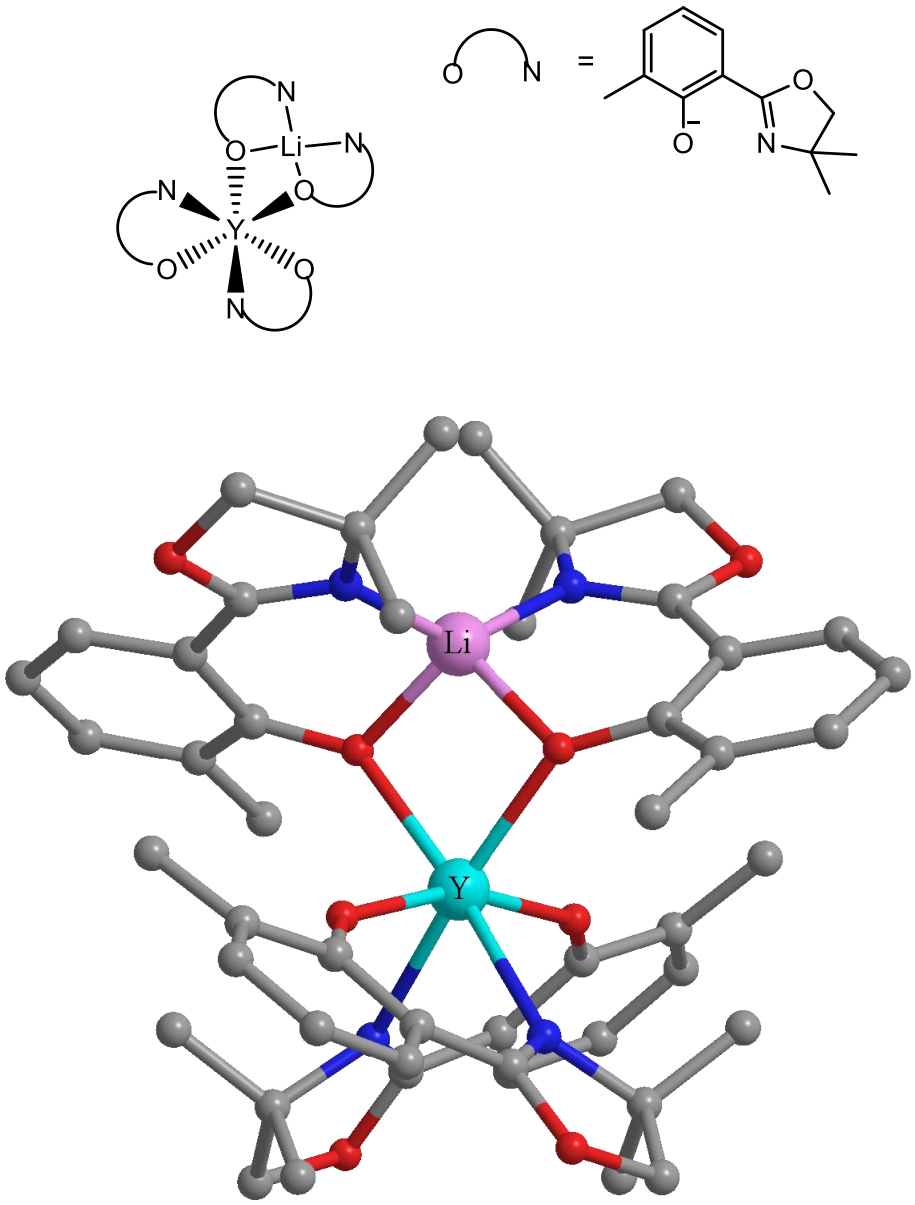

Figure 4.11: Crystal structure for Li[Y(Me$_2$-Me-Ph)$_4$] produced by Matt Hobbs[114]

Figure 4.11 shows the crystal structure of a six co-ordinate yttrium complex with lithium.

What is of interest is the binding environment with the yttrium centre, with two distinct ligand binding modes: the first shows co-ordination of both the imine nitrogen and phenolic oxygen donor groups to the yttrium without the presence of lithium; the second shows the lithium ion held in a chelate ring between two phenolic oxygens and two imine nitrogens; the oxazoline oxygens show no signs of co-ordinating in the complex.

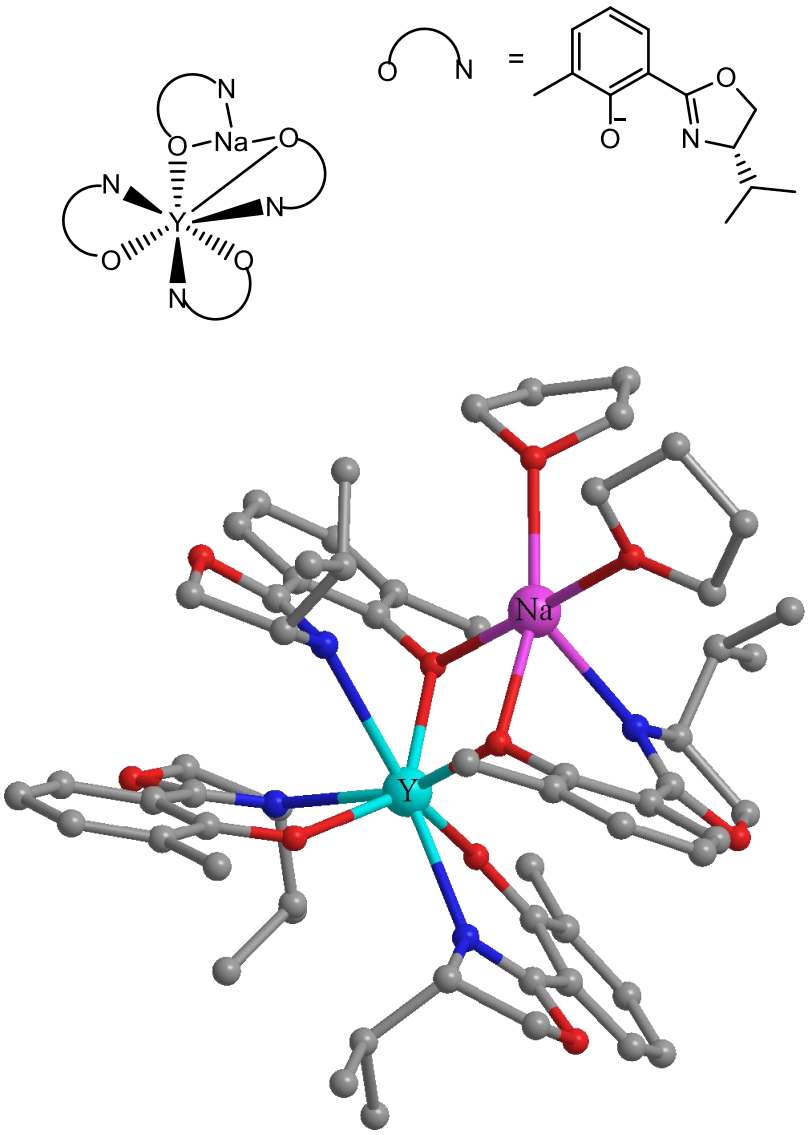

Figure 4.12: Crystal structure of Na[Y(^{i}Pr-Me-Ph)$_4$] isolated by Oliver Beckingham[41]

The structure shown above in figure 4.12 makes use of a different ligand and uses sodium as opposed to lithium as the alkali metal. Na[Y(^{i}Pr-Me-Ph)$_4$] is structurally different from Li[Y(Me$_2$-Me-Ph)$_4$]. The yttrium centre is seven coordinate in the sodium/yttrium complex compared with a six coordinate yttrium centre in the lithium/yttrium complex. This gives rise to three ligand binding modes. The first shows ligand coordinated to only the yttrium centre. The second shows ligand binding to both yttrium and sodium through the phenolate oxygen and to sodium through the imine nitrogen. The third mode has binding to both yttrium and

sodium through the phenolate oxygen. In the third mode we see additional binding to yttrium through the imine nitrogen.

Overall Li[Y(Me_2-Me-Ph)$_4$] and Na[Y(^{i}Pr-Me-Ph)$_4$] have very similar structure; however, the binding modes of the ligands are different. This is most likely due to the presence of sodium in place of the lithium as the structure of the ligands is largely unchanged.

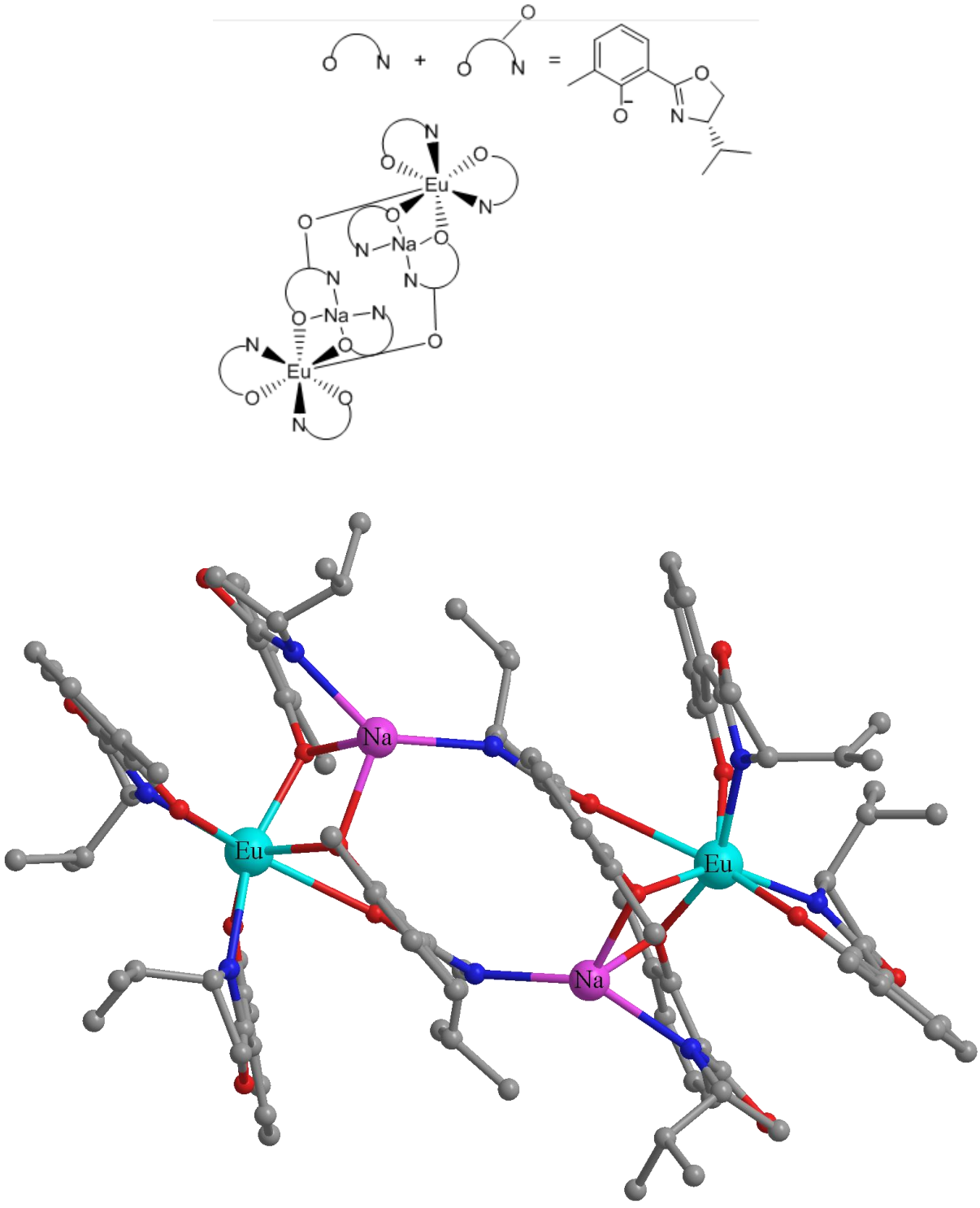

Figure 4.13: Crystal structure of Na[Eu(^{i}Pr-Me-Ph)$_4$] isolated by Oliver Beckingham[41]

Figure 4.13 shows the structure of Na[Eu(^{i}Pr-Me-Ph)$_4$]. Comparing against the structure shown in figure 4.12 changing the rare earth centre from yttrium to europium has resulted in a dimer, with the oxazoline oxygen of one monomer binding to the europium centre of the other. This

is not surprising due to the ionic radius of europium (III) (108.7pm) being larger than that of yttrium (III) (104pm).

From these structures a number of general structural trends can be identified: firstly changing the alkali metal centre seems to have little effect on the overall structure of the complex (comparing Fig. 4.11 with Fig. 4.12). However, the inclusion of sodium instead of lithium has changed the ligand binding modes. Secondly, changing the rare earth centre can have a marked effect on the structure of the complex e.g. forming a dimer when the larger europium (III) centre was used but forming a monomer when the yttrium centred complex was produced.

4.3 Discussion of M[Ln(Ligand)$_4$] Complexes

What follows is an extension to the work mentioned above. Analogies will be made, and using the underlying patterns outlined above, structural similarities inferred. The sodium/yttrium complexes were produced *via* the salt metathesis route (Fig. 4.14).

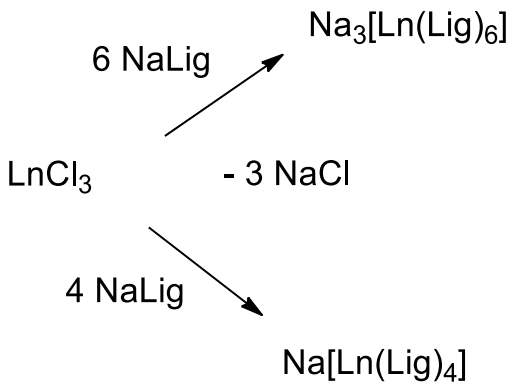

Figure 4.14: Salt metathesis route

Various attempts at formation of X-ray quality crystals were made for these complexes. It was hoped that data could be obtained that would be representative of both the lithium and sodium rare earth complexes. Unfortunately, it proved difficult to obtain crystals of sufficient quality

to obtain a crystal structure for the M[Ln(Ligand)$_4$] complexes. What follows is an account of the data obtained for each of the complexes.

4.3.1 Discussion of Data for Complex with the Proposed formula Na[Y(^{i}Pr-MePh)$_4$]

The crystal structure of this complex was previously determined within the research group. From this solid state structure we would expect the ^{1}H NMR spectrum to consist of four sets of resonances in the ratio of 1:1:1:1 as each of the ligands are inequivalent (Fig. 4.15).

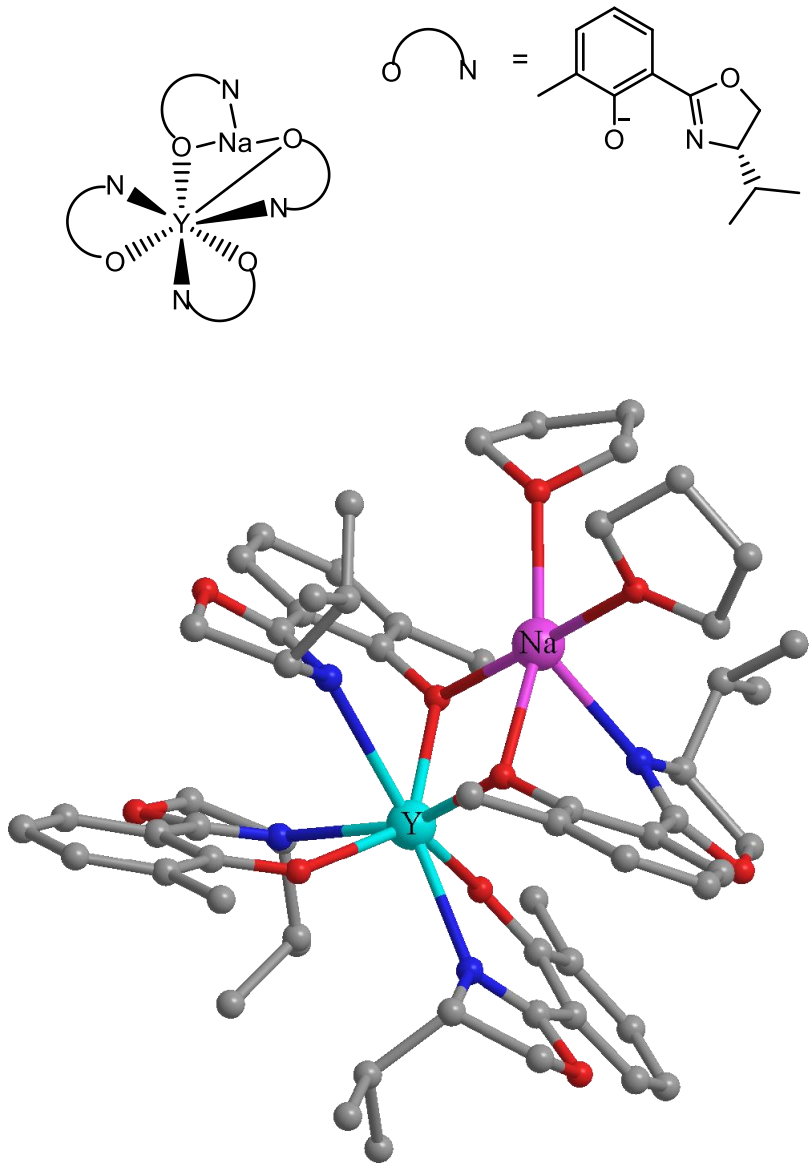

Figure 4.15: Crystal structure of the Na[Y(^{i}Pr-Me-Ph)$_4$] isolated by Oliver Beckingham[41]

At room temperature we get a spectrum that shows an integration pattern of 2:1 with signs of broadening, especially in the oxazoline ring region (4.25-3.75ppm) (Fig. 4.16). The broadening is caused by thermal averaging of different diastereoisomers at room temperature as such variable temperature NMR was performed in an effort to reduce interconversion between the diastereoisomers . This produced a much more defined spectrum with 3 distinct sets of resonances in the ratio of 2:1:1 (Fig. 4.17-4.19). Although figure 4.20 does show a peak where

we would normally expect the phenolic OH to occur (12ppm), there are no other peaks corresponding to free ligand in the ^{1}H NMR of the complex. So the third set of resonances is not caused by the existence of free ligand in the sample.

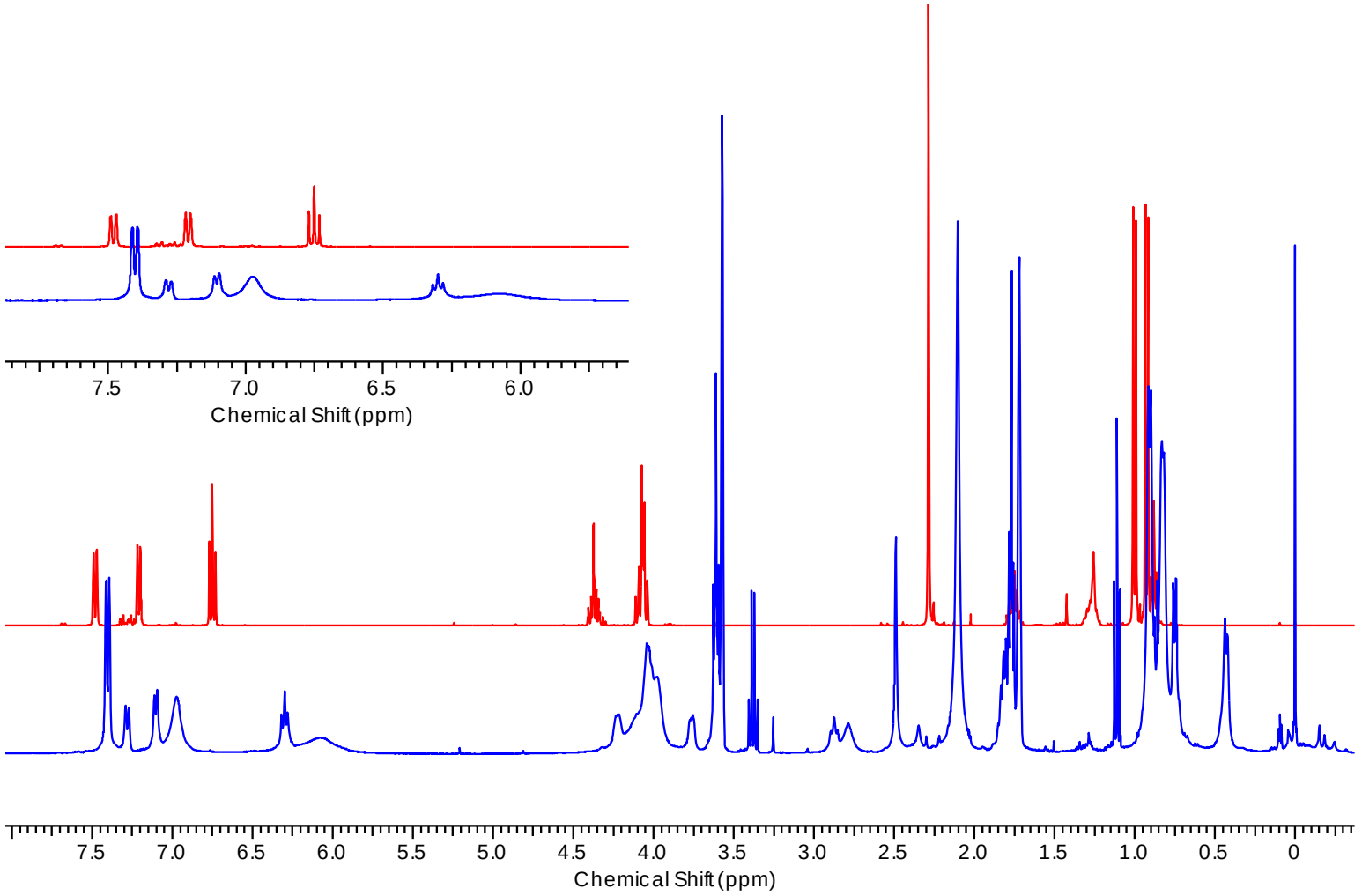

Figure 4.16: Comparison of ^{1}H NMR spectra of H-^{i}Pr-MePh (red, top) with Na[Y(^{i}Pr-MePh)$_4$] (blue, bottom) at room temperature in THF.

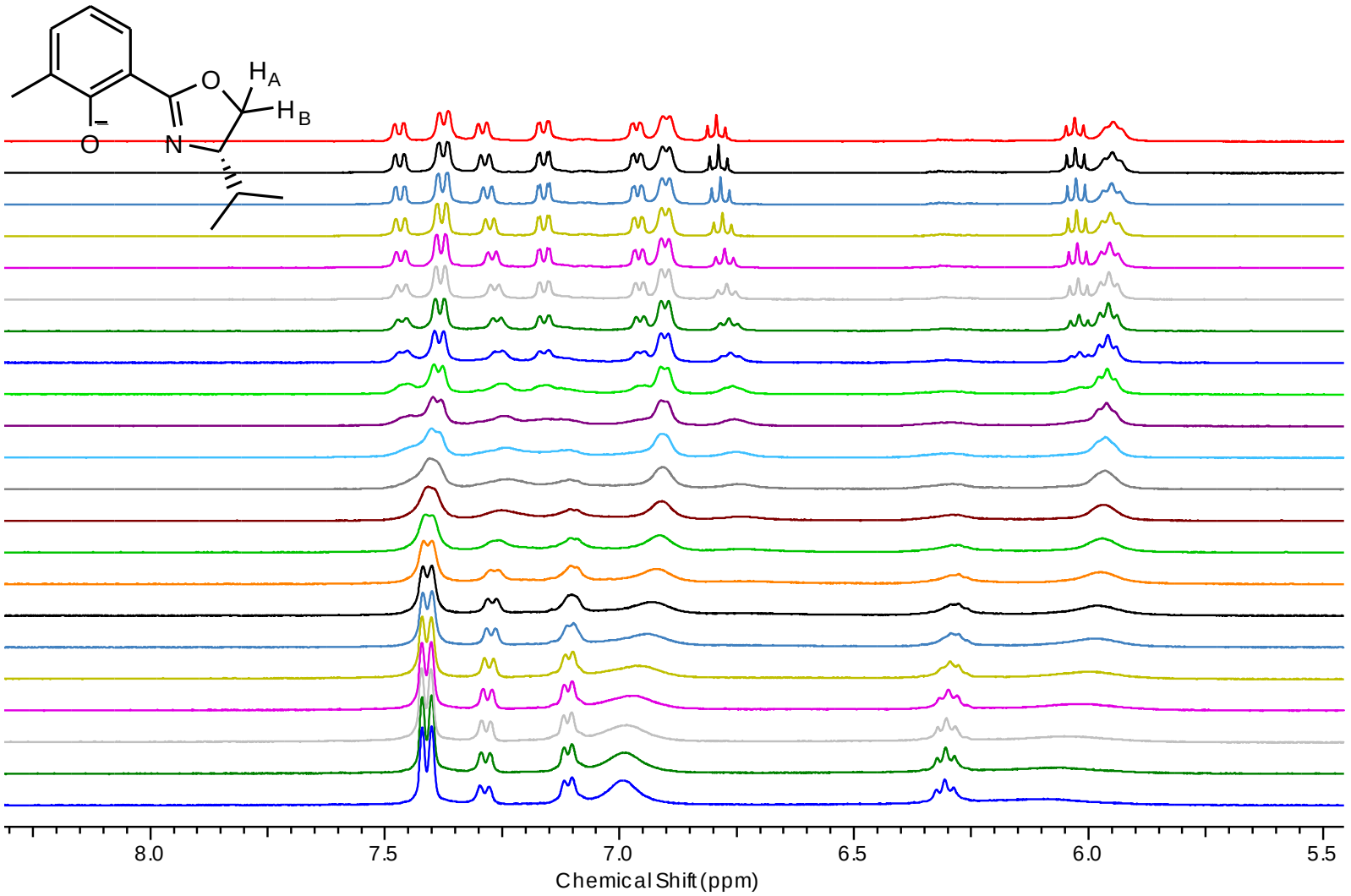

Figure 4.17: VT ^{1}H NMR data for the aromatic region of Na[Y(^{i}Pr-MePh)$_4$] showing the full range of temperatures explored from -80°C (red, top) to room temperature (blue, bottom) in 5°C increments

Figure 4.17 shows the effect of decreasing temperature on the aromatic protons of Na[Y(^{i}Pr-Ph)$_4$]. Decreasing the temperature has slowed the thermal averaging processes that lead to the simplistic spectrum at room temperature. The doublet of doublets at 7.4ppm has split into two doublets, whereas the broad peak at 7ppm has been split into two doublets. The pseudo triplet at 6.3ppm looks to have split into 3 triplets, with the shift at 6ppm being particularly broad.

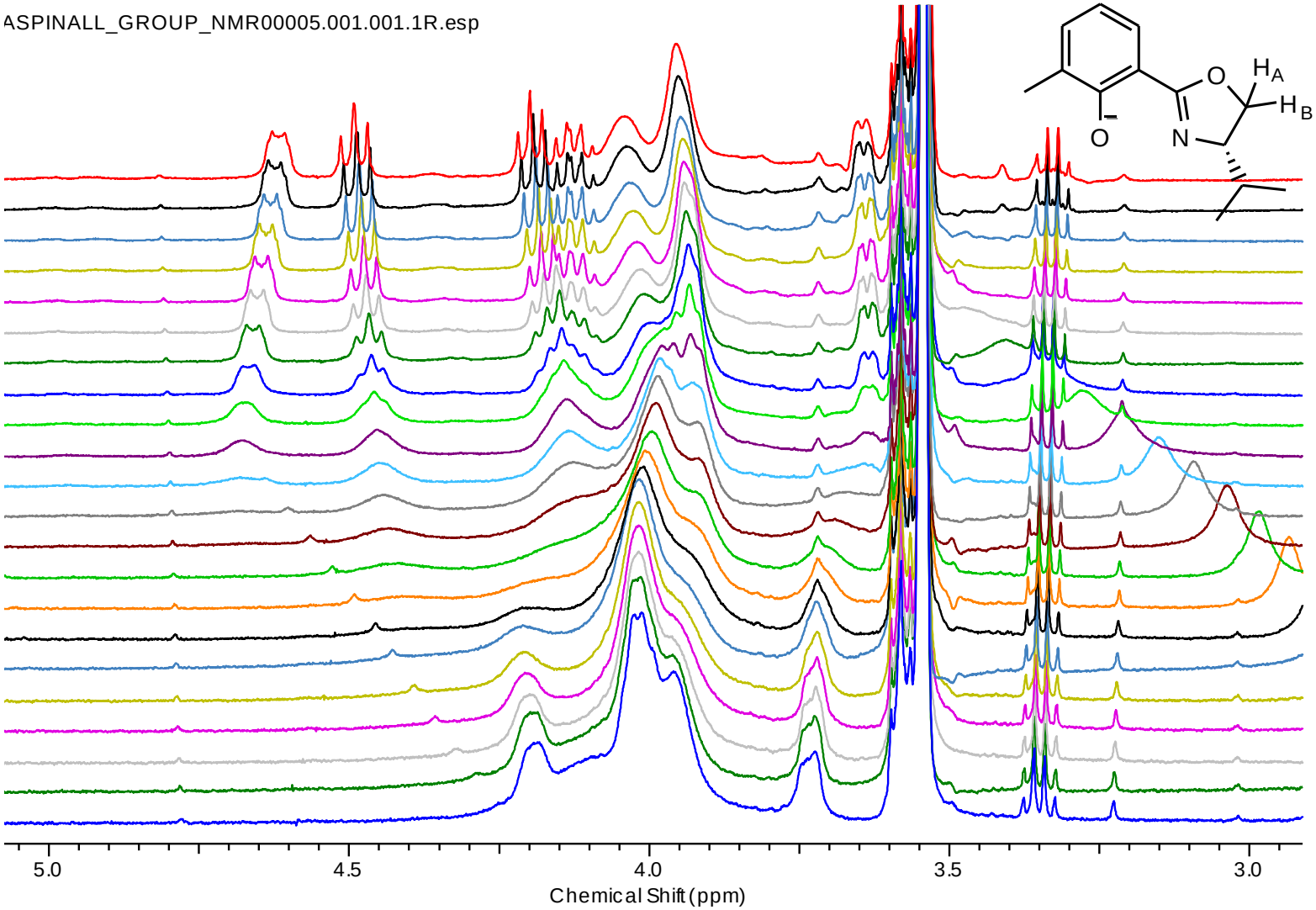

Figure 4.18: Expansion of the ^{1}H NMR spectrum of Na[Y(^{i}Pr-Me-Ph)$_4$] showing the "oxazoline ring" indicated by protons H_A and H_B region

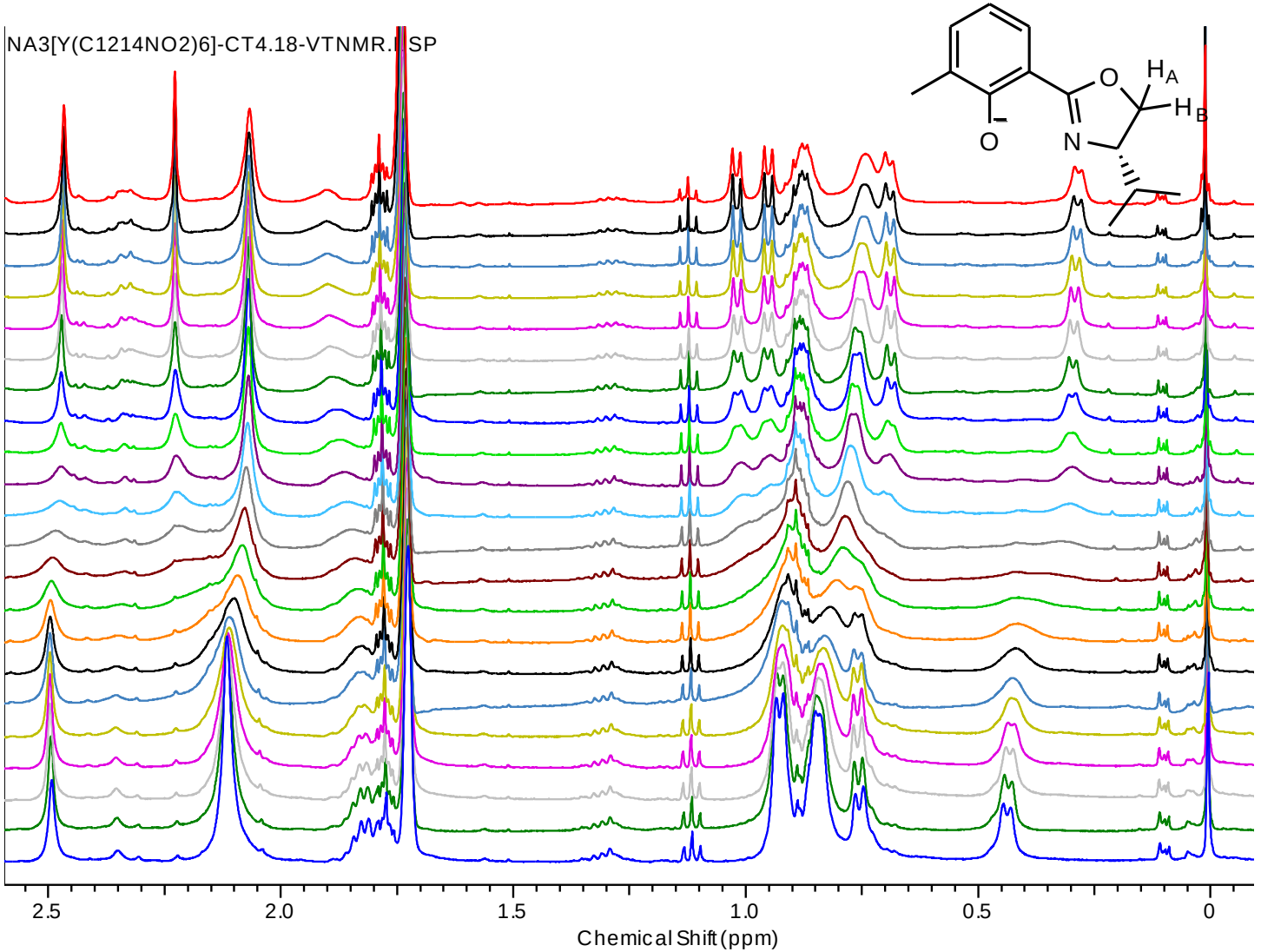

Figure 4.19: ^{1}H NMR data for the methyl and isopropyl regions of Na[Y(^{i}Pr-MePh)$_4$] showing the full range of temperatures explored from -80°C (red, top) to room temperature (blue, bottom) in 5°C increments

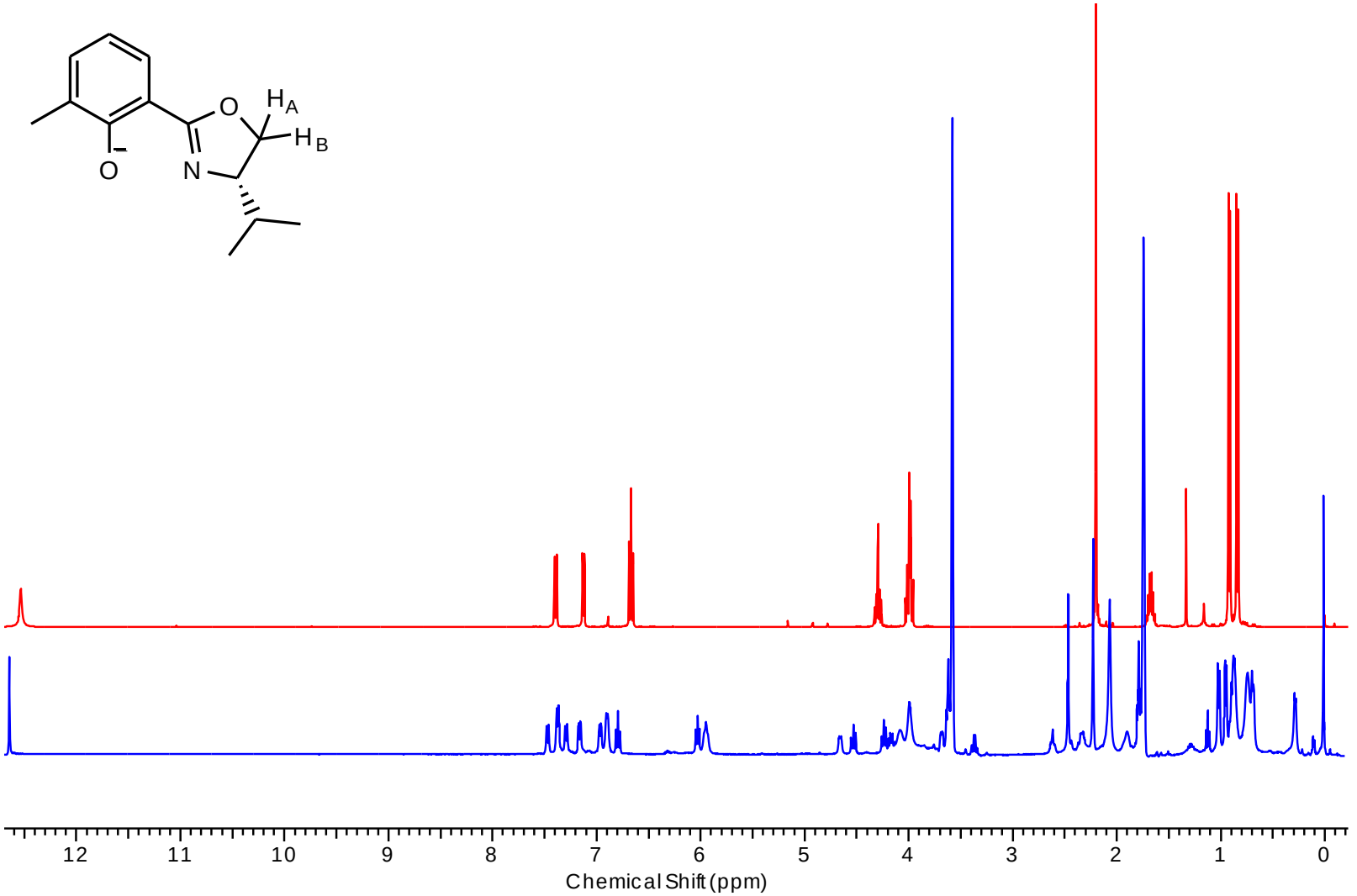

Figure 4.20: Comparison of ^{1}H NMR spectra of H-^{i}Pr-MePh (red, top) with Na[Y(^{i}Pr-MePh)$_4$] (blue, bottom) at -80°C in THF.

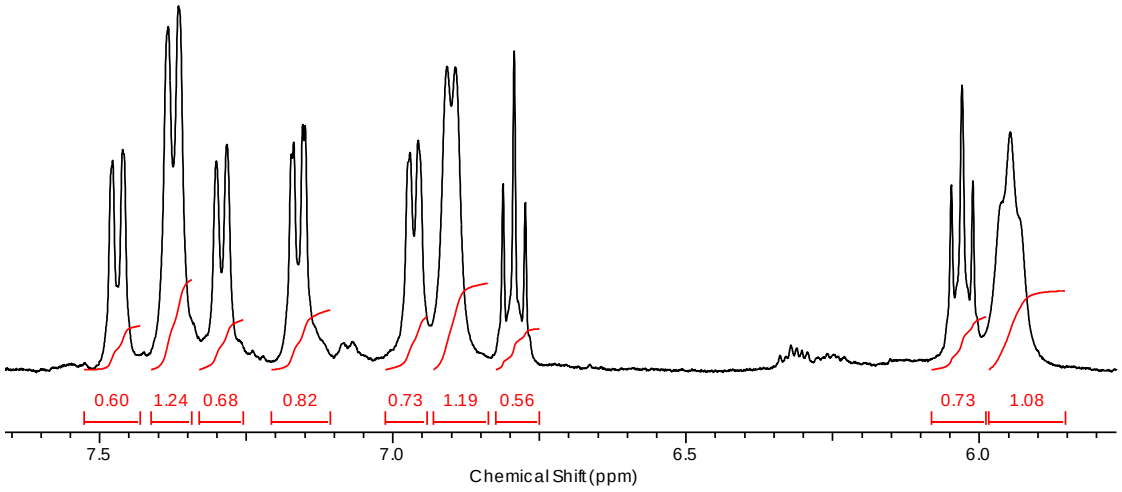

Figure 4.21: ^{1}H NMR expansion of the aromatic region for Na[Y(^{i}Pr-MePh)$_4$]) at -80°C in THF.

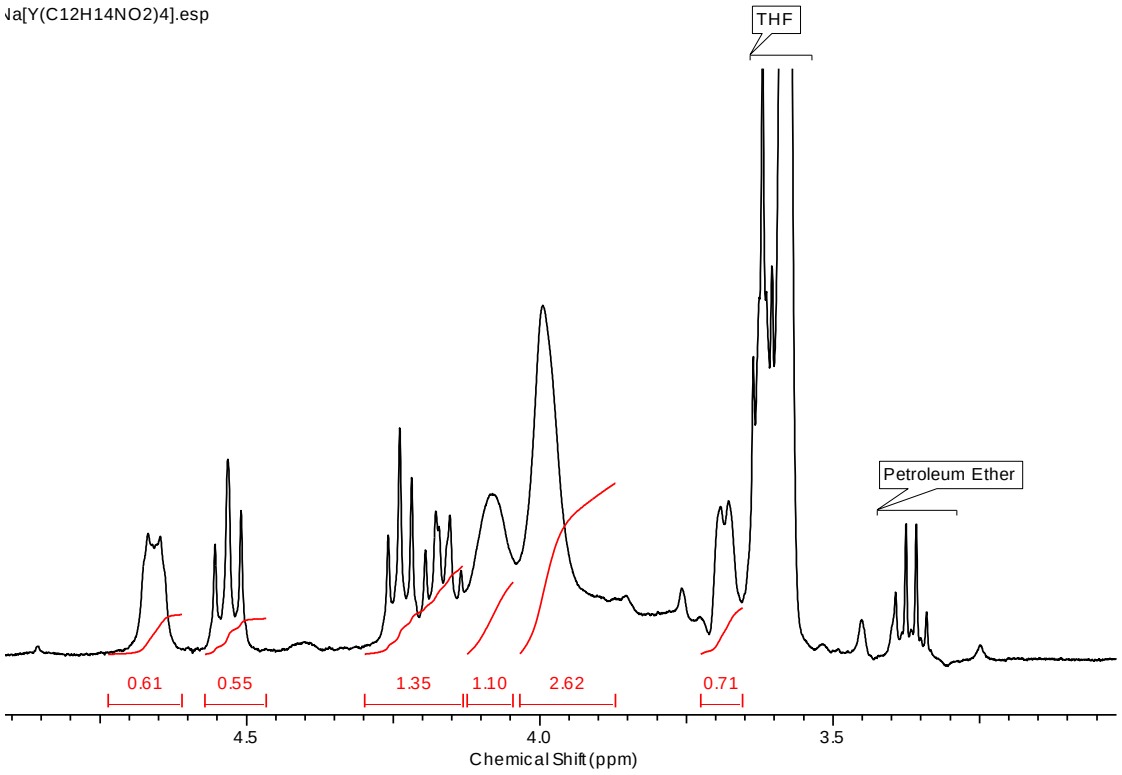

Figure 4.22: ^{1}H NMR expansion of the oxazoline ring region for Na[Y(^{i}Pr-MePh)$_4$]) at -80°C in THF.

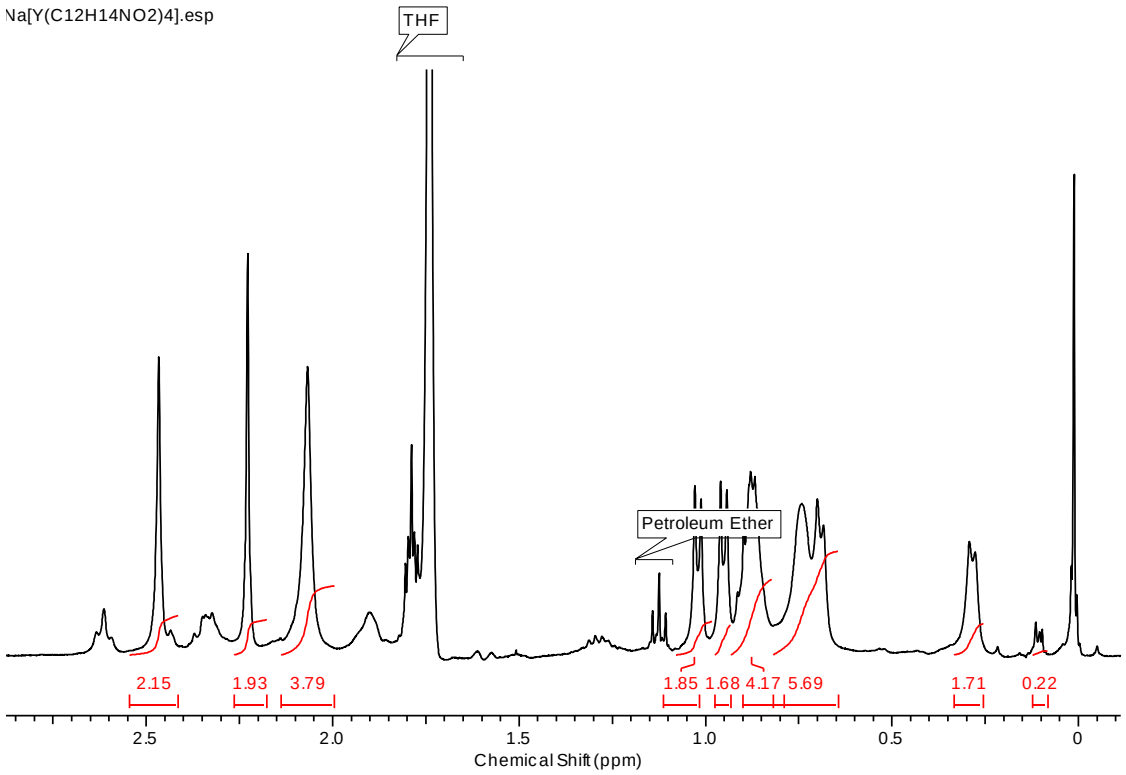

Figure 4.23: ^{1}H NMR expansion of the methyl region (2.5-2.0ppm) and the aliphatic region (1.5-0.5ppm) for Na[Y(^{i}Pr-MePh)$_4$] at -80°C in THF.

As can be seen from the above figures (4.21-4.23) the 1H NMR spectrum for Na[Y(^{i}Pr-MePh)$_4$]) at -80°C yields three sets of resonances with integration in the ratio 1:1:2. From comparison of the ^{1}H NMR spectra of the free ligand ^{i}Pr-MePh-H against Na[Y(^{i}Pr-MePh)$_4$] (Fig. 4.19) a small amount of free ligand is present in the sample (≤10%). From the crystal structure we would expect the ligands to be inequivalent giving four sets of resonances in the ratio 1:1:1:1. As can be seen from figures 4.20-4.22 even at -80°C there is still some significant broadening in those peaks with an integration double that of the others. It is possible that two ligands remain fluxional even at lower temperatures. The ^{1}H NMR spectrum can be interpreted as four different ligand environments existing in solution at the same time with two sets of resonances well separated and two others which are still coalesced at -80°C.

Anhydrous mass spectrometry was performed on this sample. Na[Y(^{i}Pr-MePh$_3$] was found to be the most stable ion for the this complex (Fig. 4.24), however there was another significant peak at 743.2 m/z indicating loss of sodium [Y(^{i}Pr-MePh)$_3$]$^{+}$.

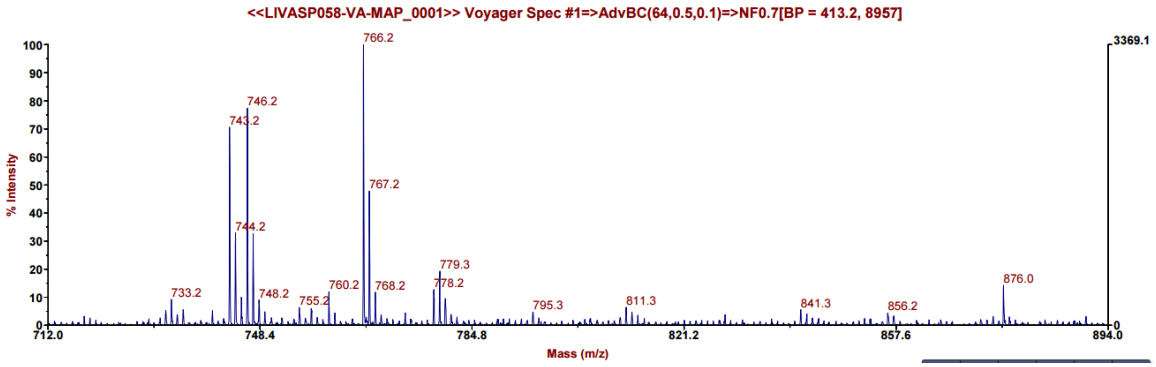

Figure 4.24: Mass Spectrum of Na[Y(^{i}Pr-MePh)$_4$] with the key mass fragment (Na[Y(^{i}Pr-MePh)$_3$]) at 766.2 m/z

Table 4.1: Elemental Analysis results for Na[Y(^{i}Pr-MePh)$_4$]

	Na[Y(^{i}Pr-MePh)$_4$] Calculated	Na[Y(^{i}Pr-MePh)$_4$] Found
Carbon (%)	63.13	62.91
Hydrogen (%)	6.93	6.43
Nitrogen (%)	5.73	5.53
C:N	11.02	11.38

Table 4.1 shows the calculated and found elemental analysis results for the proposed complex Na[Y(^{i}Pr-Me-Ph)$_4$]. As can be seen from the above table the two sets of results bear a close resemblance, deviating by 0.12% in the carbon.

The elemental analysis coupled with the mass spectrometry and the integration pattern of the ^{1}H NMR spectrum strongly indicates the formation of the complex as Na[Y(^{i}Pr-Me-Ph)$_4$].

4.3.2 Discussion of Data for Proposed Complex Na[Y(Me$_2$-Ph)$_4$]

A crystal structure of this complex was not produced either in this study or previously within the group. However we should expect the solid state structure of this complex to be analogous to that of Na[Y(^{i}Pr-MePh)$_4$] (Fig. 4.25).

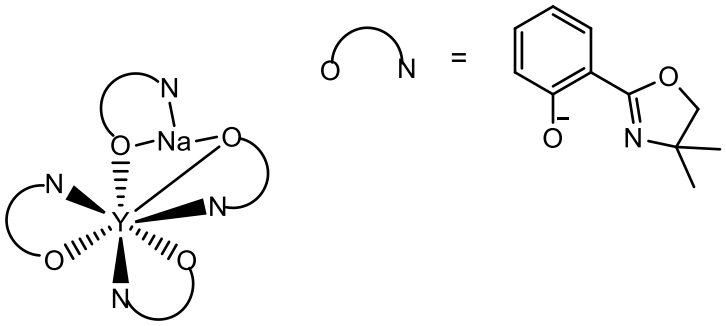

Figure 4.25: Proposed solid state structure of Na[Y(Me$_2$-Ph)$_4$]

The ^{1}H NMR spectrum of the Na[Y(Me$_2$-Ph)$_4$] complex (Fig. 4.26) was particularly straight forward at room temperature, with only a tiny trace of free ligand impurity. There was significant line broadening most likely due to fluxionality between isomers.

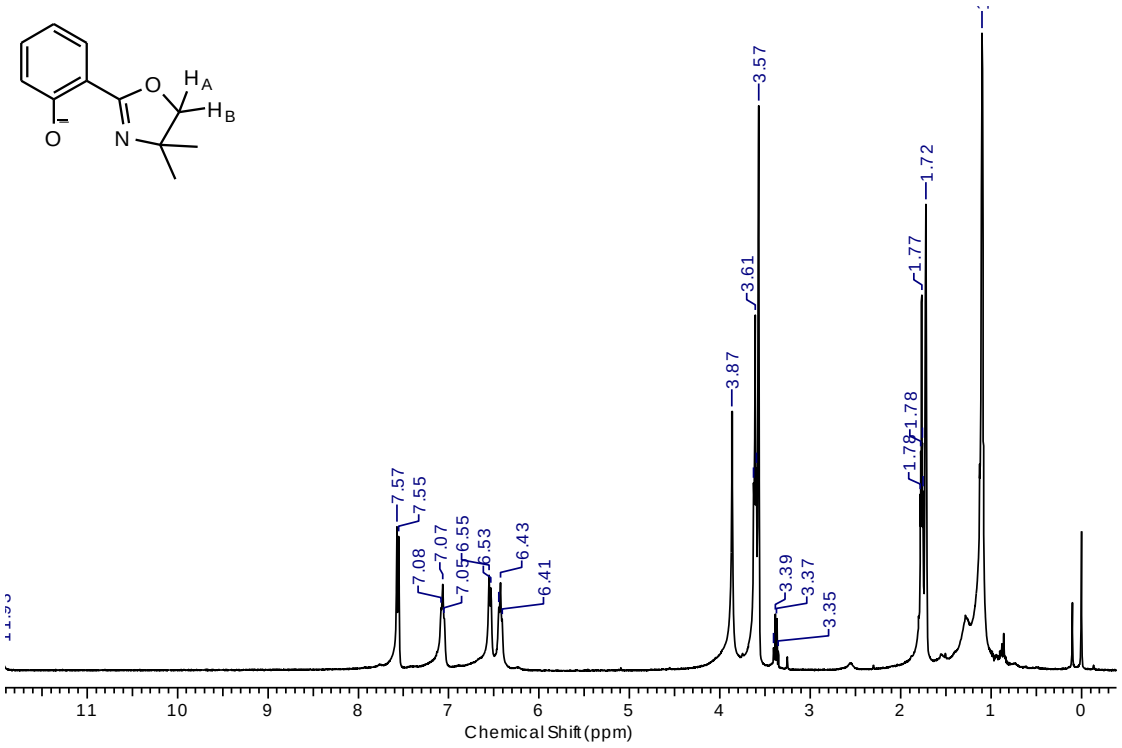

Figure 4.26: ^{1}H NMR spectrum of Na[Y(Me$_2$-Ph)$_4$] at room temperature in *d*-THF

In addition to line broadening a comparison of the ^{1}H NMR spectrum of the complex against the free ligand clearly demonstrates that the chemical shifts of the co-ordinated ligand are different (Fig. 4.27).

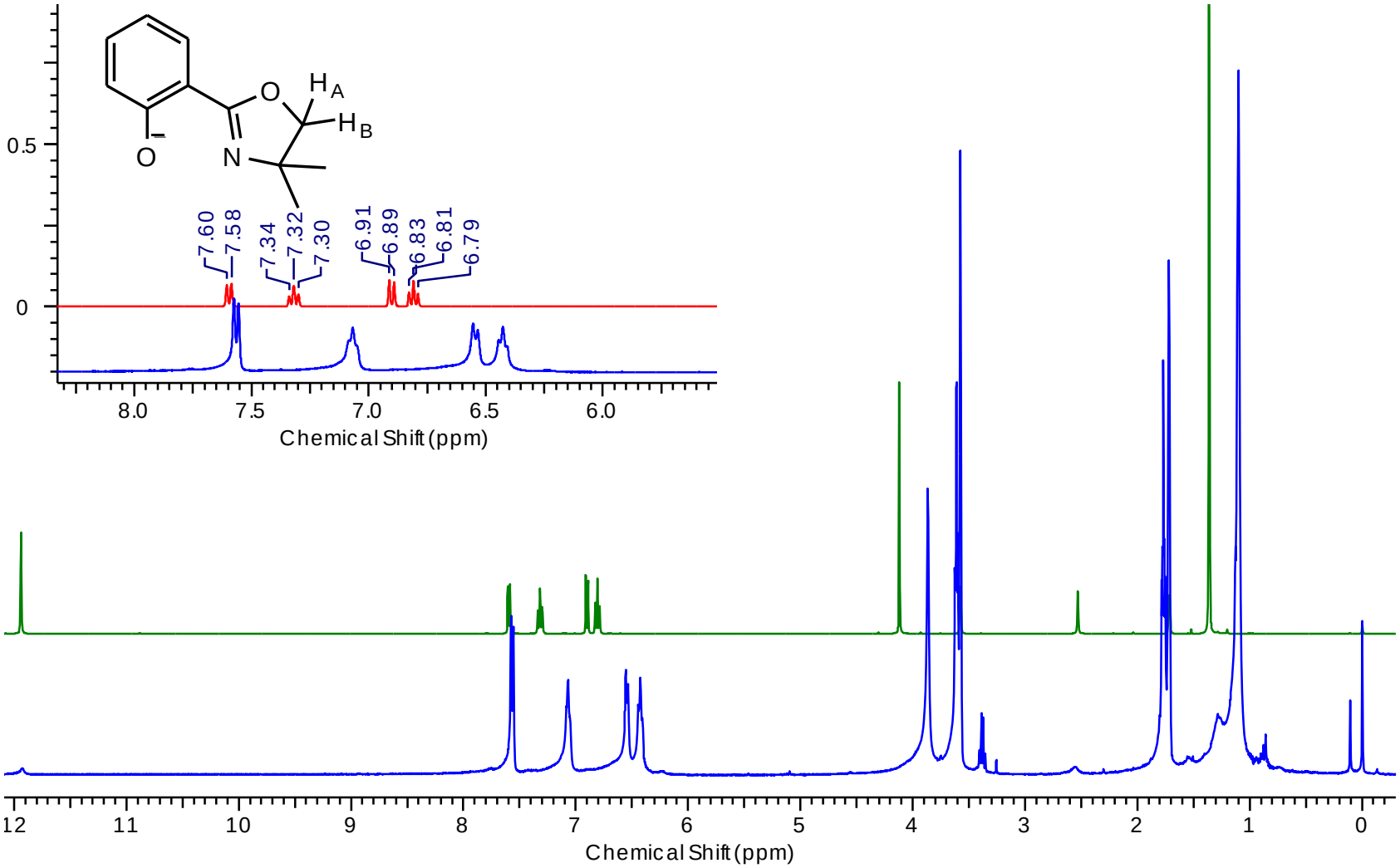

Figure 4.27: Comparison of ^{1}H NMR spectrum of H-Me$_2$-Ph with that of Na[Y(Me$_2$-Ph)$_4$] at room temperature in *d*-THF

Due to the large amount of line broadening seen in this sample it was decided that variable temperature (VT) NMR would allow us to see the distinct resonances of the complex, effectively freezing out the fluxionality of the complex. As can be seen from figures 4.28-4.30 the 4 simple broad resonances at room temperature have separated when cooled, revealing a more complex ^{1}H NMR spectrum.

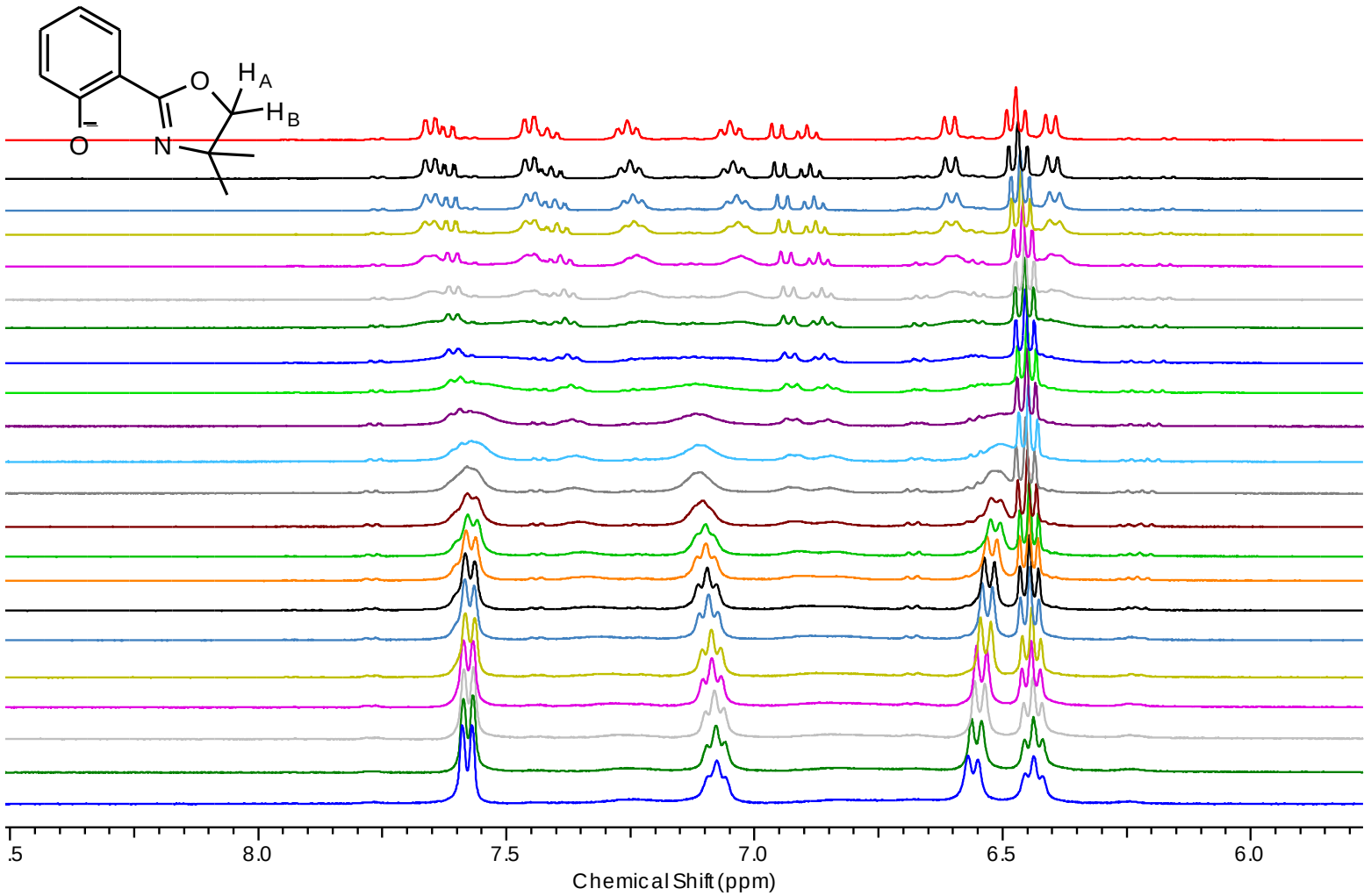

Figure 4.28: VT ^{1}H NMR data for the aromatic region of Na[Y(Me$_2$-Ph)$_4$] showing the full range of temperatures explored from -80°C (red, top) to room temperature (blue, bottom) (in *d*-THF)

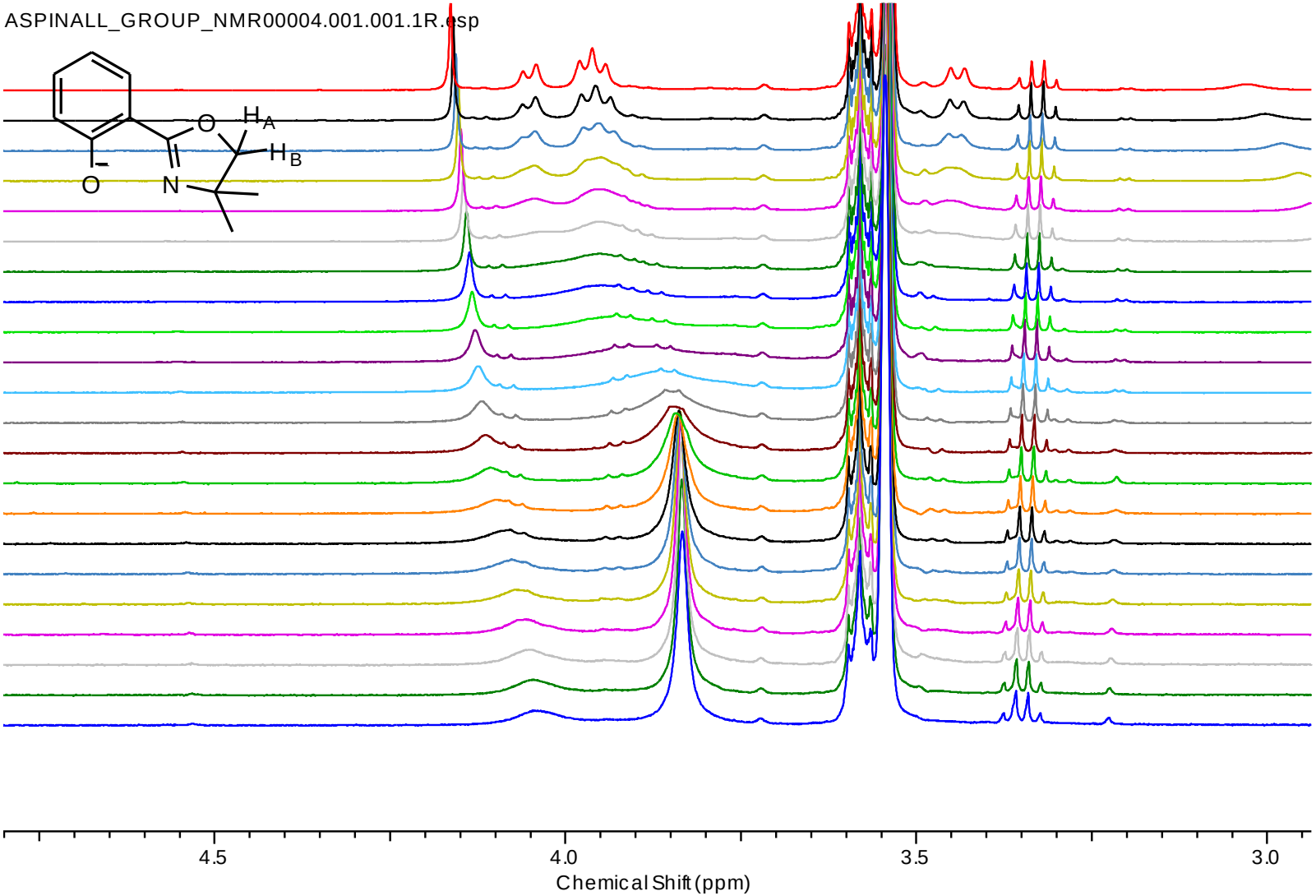

Figure 4.29: VT ^{1}H NMR data for the oxazoline ring region of Na[Y(Me$_2$-Ph)$_4$] showing the full range of temperatures explored from -80°C (red, top) to room temperature (blue, bottom) in *d*-THF

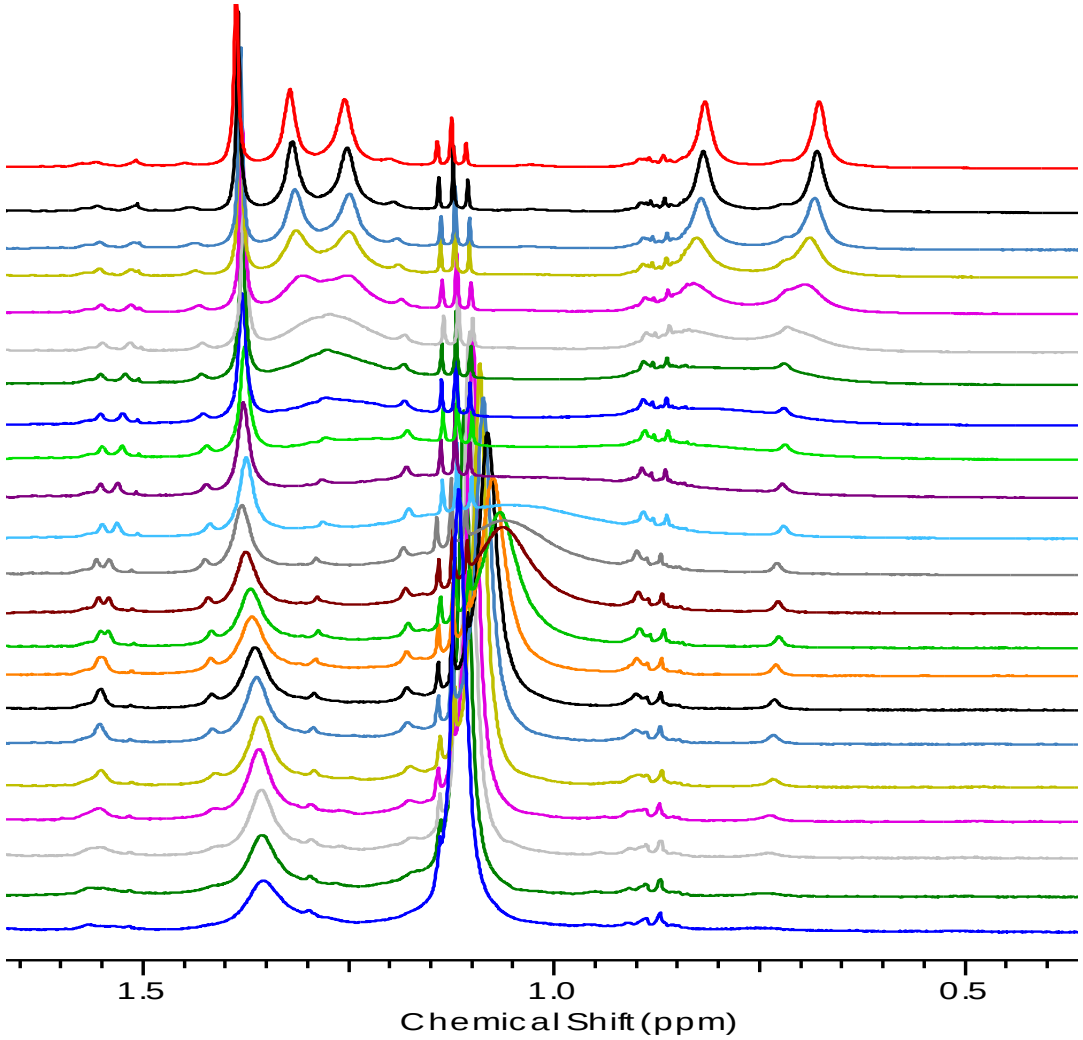

Figure 4.30: VT ^{1}H NMR data of the methyl region of Na[Y(Me$_2$-Ph)$_4$] showing the full range of temperatures explored from -80°C (red, top) to room temperature (blue, bottom) in *d*-THF

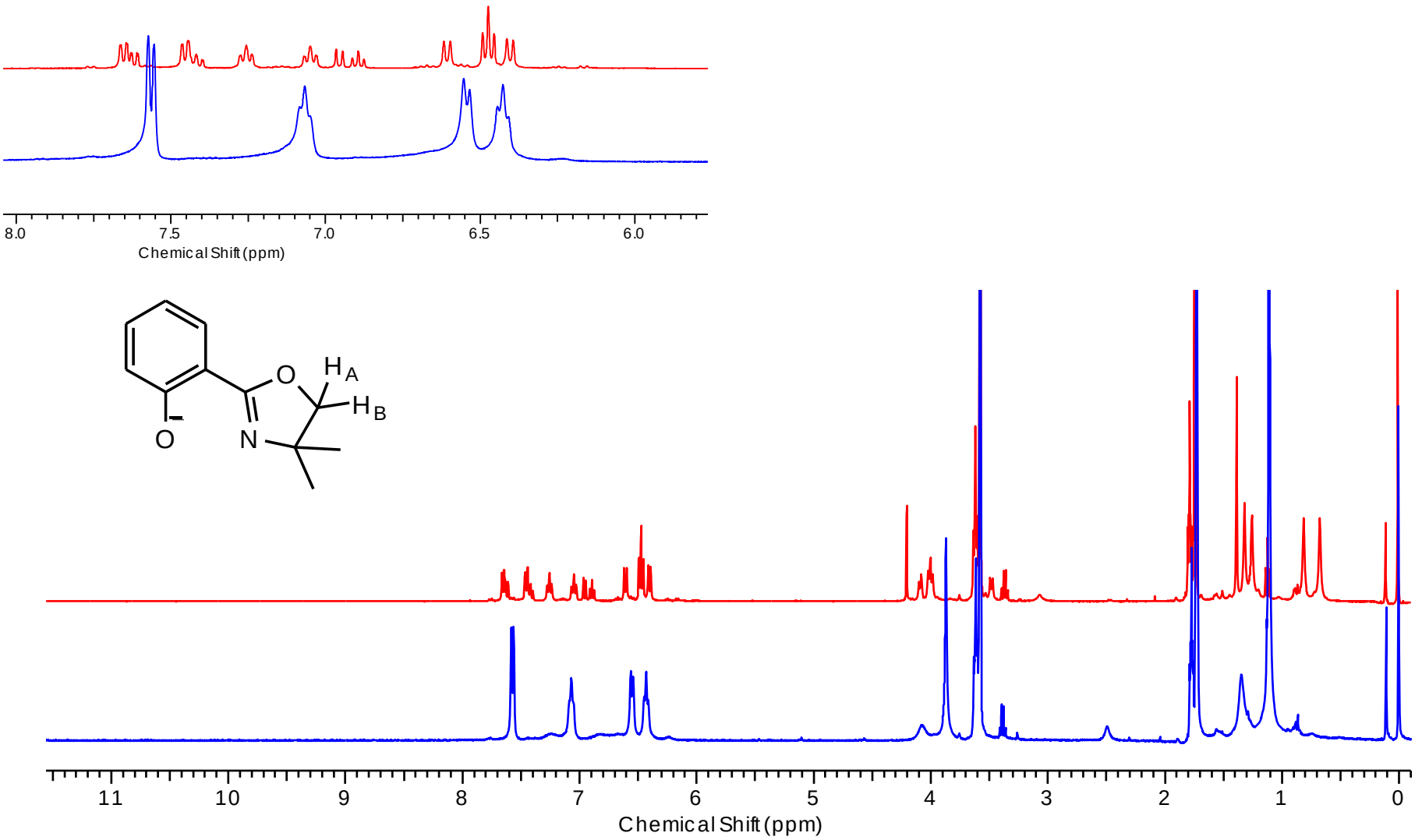

Figure 4.31: Comparison of ^{1}H NMR spectrum of Na[Y(Me$_2$-Ph)$_4$] at 25°C (blue) vs -80°C (red) in *d*-THF, with an expansion of the aromatic region

Figure 4.31 shows the effect of reducing temperature on the ^{1}H NMR spectrum of the Na[Y(Me_2-Ph)$_4$] complex. The blue (bottom) spectrum shows the highly broadened ^{1}H NMR spectrum taken at room temperature (25°C) and the red (top) spectrum shows the ^{1}H NMR spectrum at -80°C clearly demonstrating that the actual structure is far more complicated than that seen at room temperature, with 12 resonances now visible in the aromatic region (Fig. 4.32).

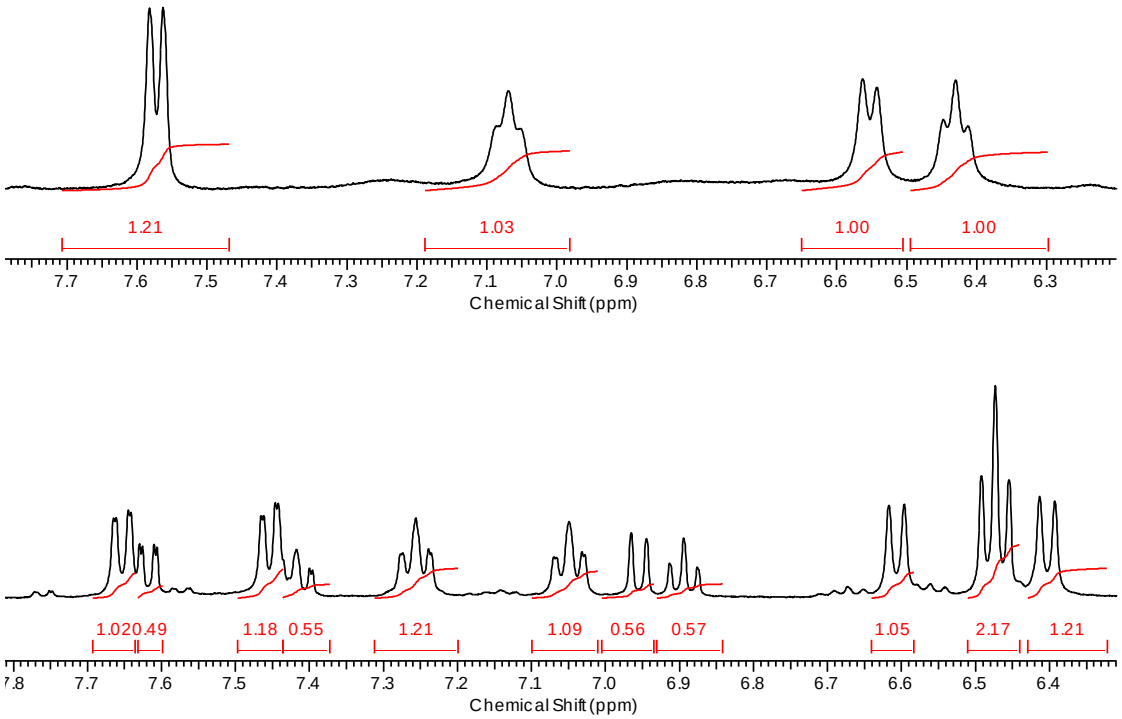

Figure 4.32: Comparison of aromatic region of ^{1}H NMR spectra of Na[Y(Me_2-Ph)$_4$] at room temp. (Top) vs Na[Y(Me_2-Ph)$_4$] at -80°C (Bottom). in *d*-THF

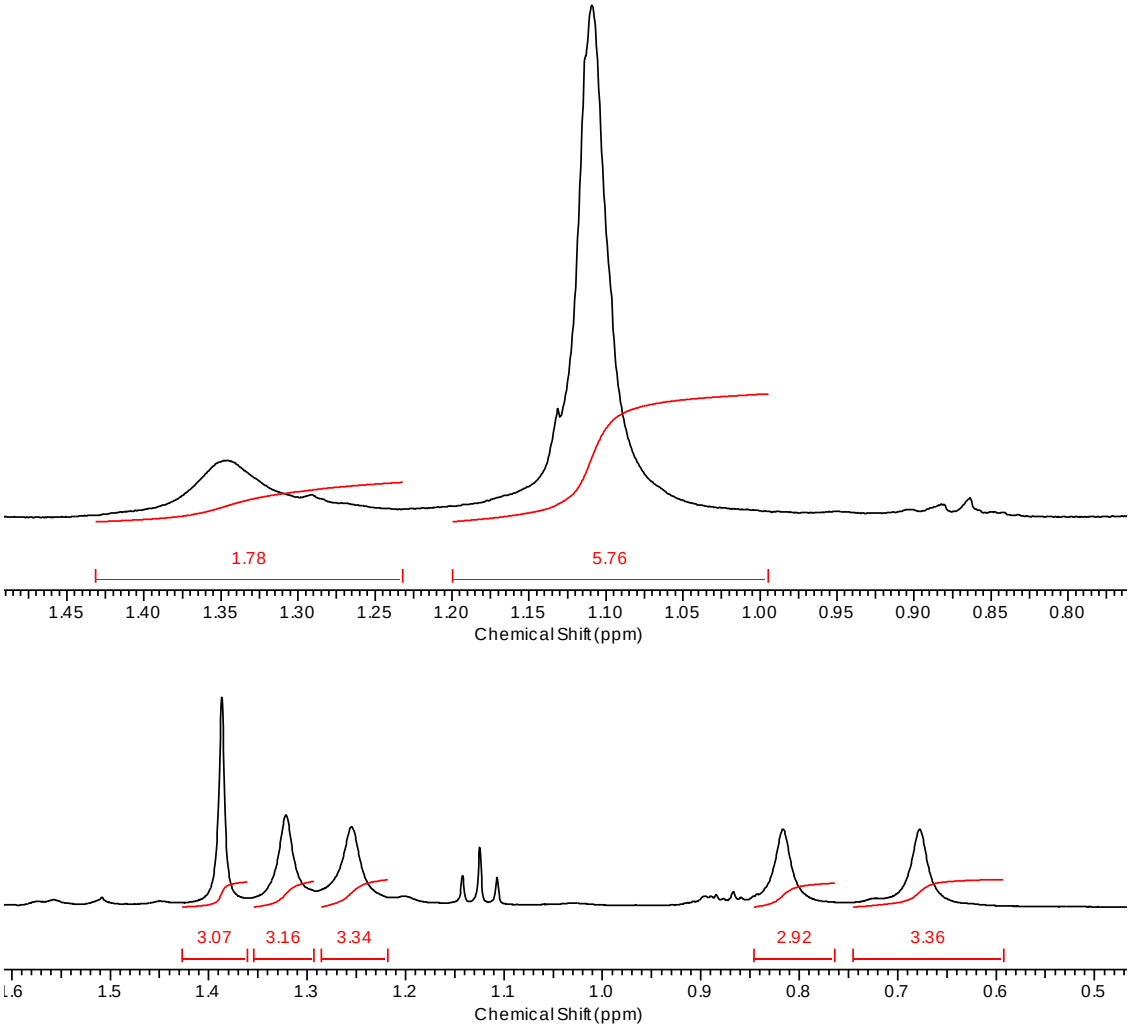

Figure 4.33: Comparison of methyl region of ^{1}H NMR spectra of Na[Y(Me$_2$-Ph)$_4$] at room temp. (Top) vs Na[Y(Me$_2$-Ph)$_4$] at -80°C (Bottom) in *d*-THF.

If we compare the ^{1}H NMR spectra of Na[Y(Me$_2$-Ph)$_4$] at -80°C against Me$_2$-Ph-H at room temperature (Fig. 4.34) we see that there's significant contamination from what looks to be sodium-phenolate. This leaves 2 sets of resonances of equal intensity.

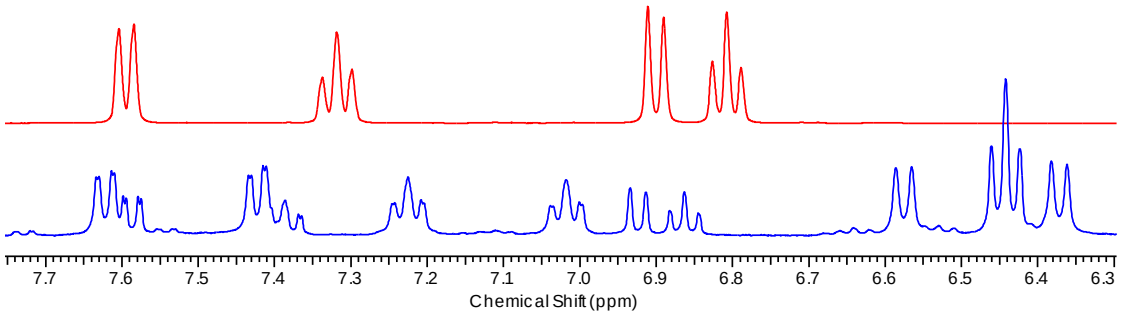

Figure 4.34: Comparison of the aromatic region of the ^{1}H NMR spectrum of H-Me$_2$-Ph (free ligand) (red, top) (room temperature in *d*-THF) with that of Na[Y(Me$_2$-Ph)$_4$] (blue, bottom) at -80°C in *d*-THF.

If the crystal structure of Na[Y(Me$_2$-Ph)$_4$] is analogous to that for Na[Y(^{i}Pr-Me-Ph)$_4$], then we would expect 4 sets of resonances of equal intensity (Fig. 4.35).

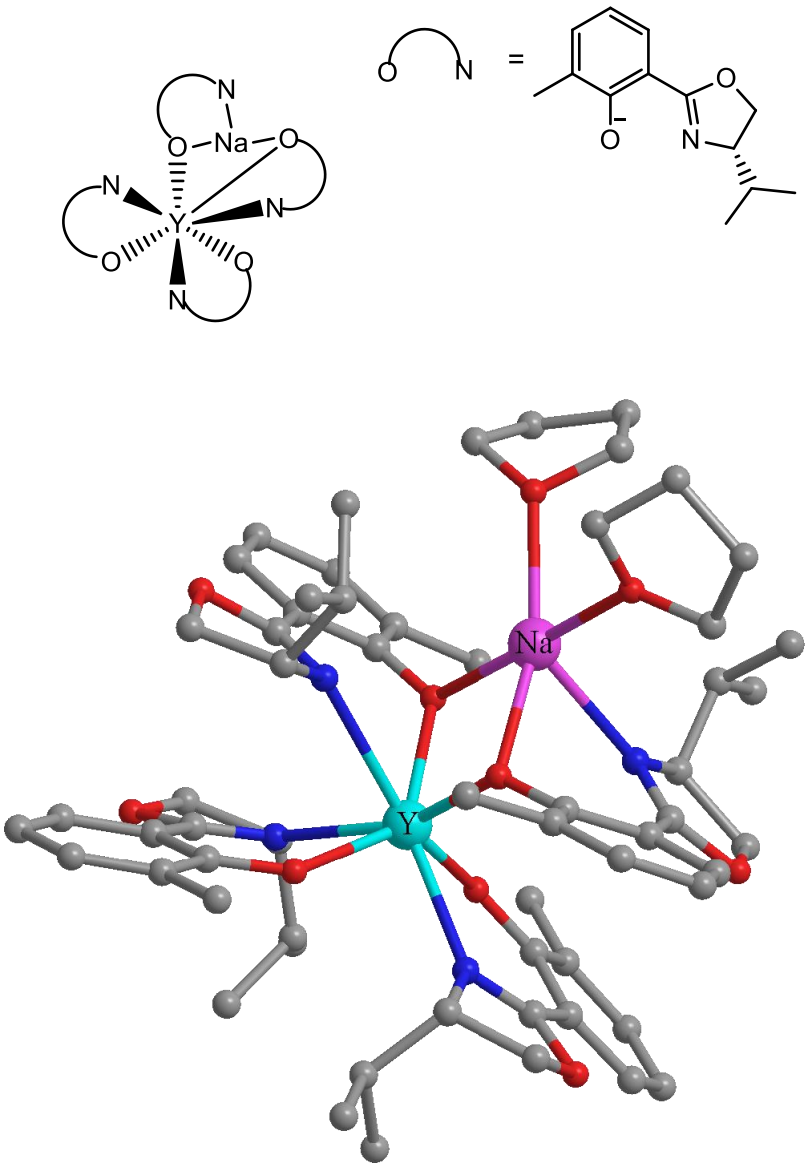

Figure 4.35: Crystal structure of the Na[Y(^{i}Pr-Me-Ph)$_4$] isolated by Oliver Beckingham[41]

However, we don't see 4 sets of resonances we see 2 (Fig. 4.36). It is possible that the complex formed is highly fluxional and we have yet to separate all of the resonances, even at -80°C.

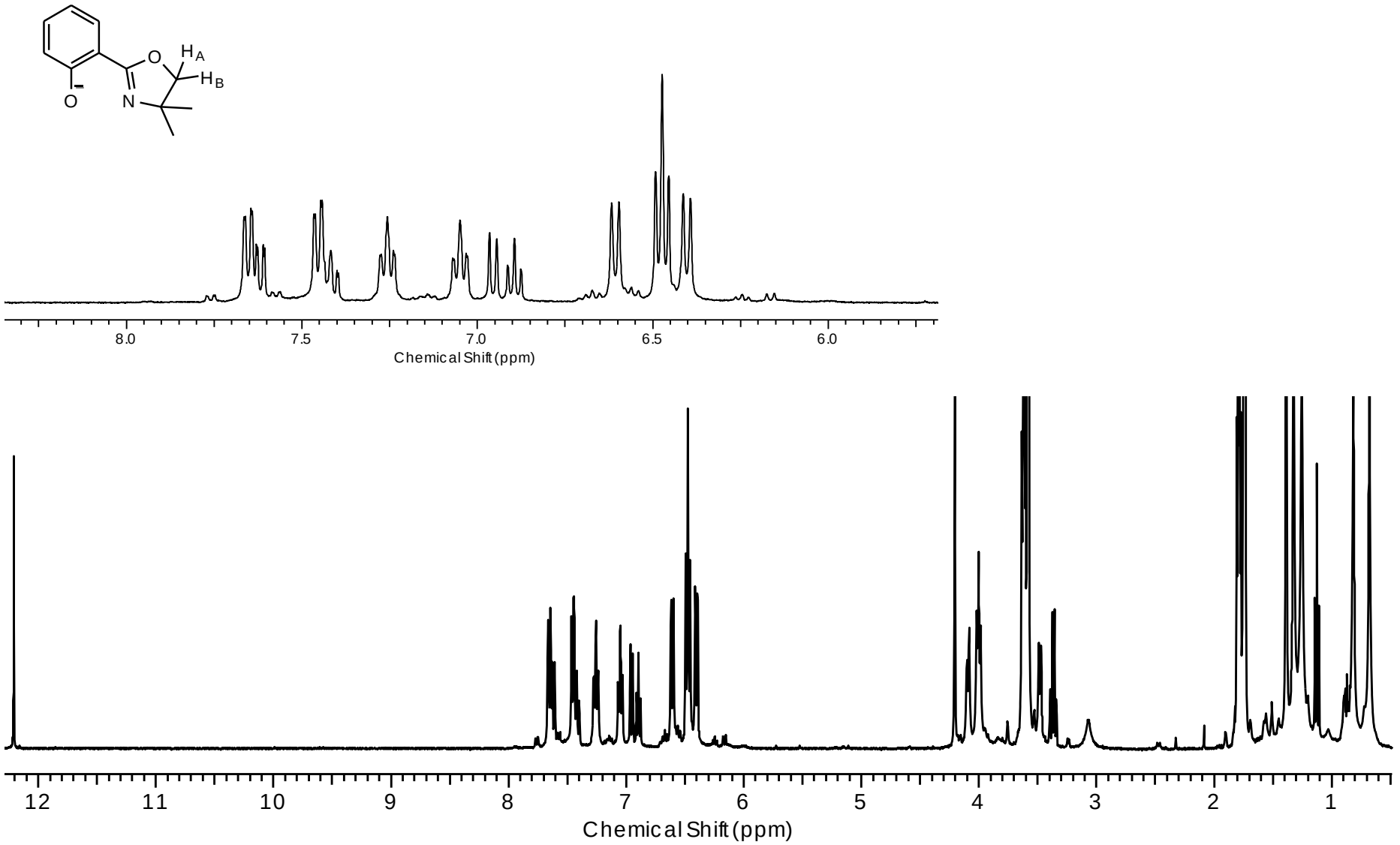
O
N
O
H_A
H_B
8.0
7.5
7.0
6.5
6.0
Chemical Shift (ppm)
12
11
10
9
8
7
6
5
4
3
2
1
Chemical Shift (ppm)

Figure 4.36: ^{1}H NMR spectrum of $Na_3[Y(Me_2\text{-}Ph)_6]$ at -80°C in *d*-THF, with an expansion of the aromatic region

Another possibility is that the binding around the alkali metal in Na[Y(Me_2-Ph)$_4$] is different to that seen in Na[Y(^{i}Pr-MePh)$_4$]. With ligands binding to the alkali metal in the same way as they do in Li[Y(Me_2-Me-Ph)$_4$] (Fig. 4.37). This would produce a complex with a crystallographic C_2 axis and hence would produce 2 sets of resonances of equal intensity.

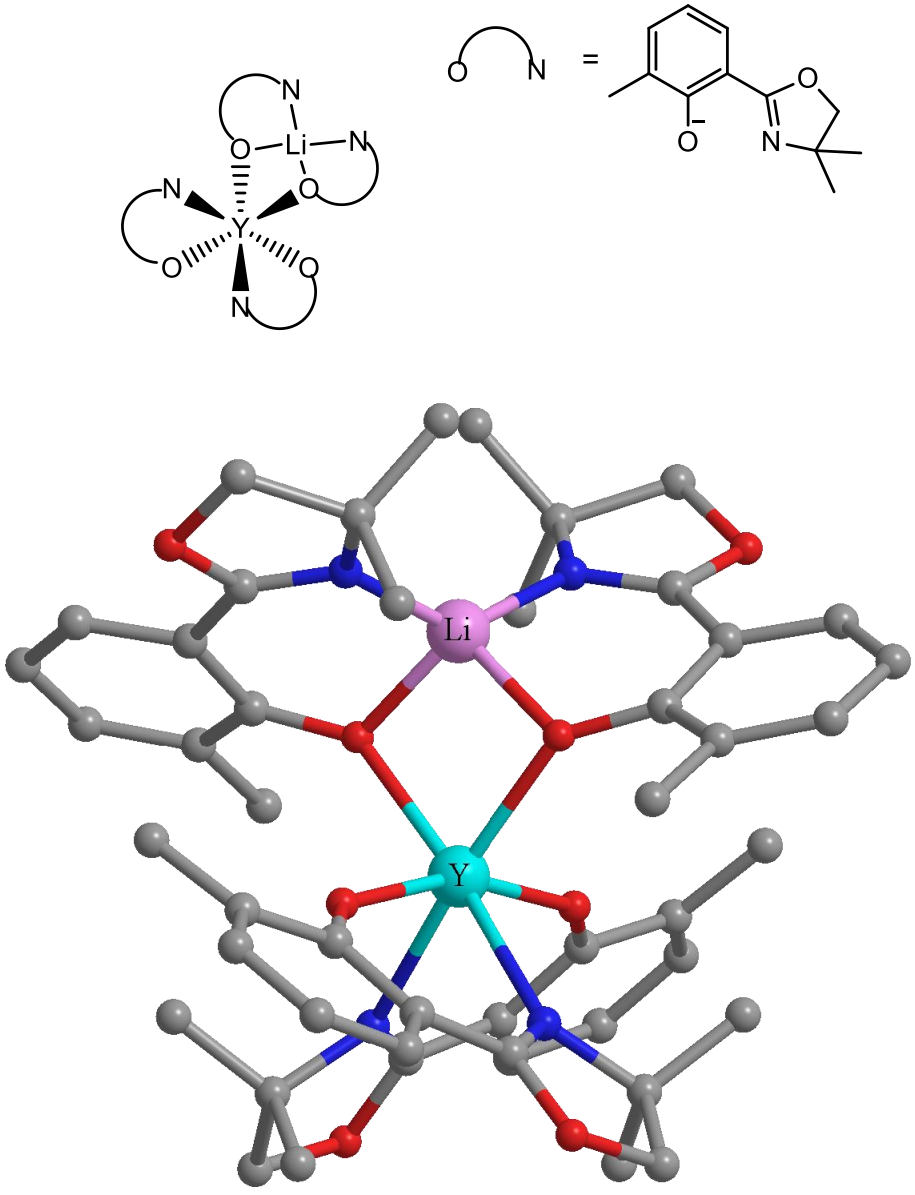

Figure 4.37: Crystal structure for Li[Y(Me_2-Me-Ph)$_4$] produced by Matt Hobbs[114]

It is difficult to determine which of these two possibilities is correct by ^{1}H NMR spectroscopy. But, from the ^{1}H NMR spectra it appears that $Na[Y(Me_2\text{-}Ph)_4]$ formed instead of the intended $Na_3[Y(Me_2\text{-}Ph)_6]$.

Mass spectrometry under anhydrous conditions failed to show molecular ions; however several fragments were identified in MALDI^{+} indicating addition of sodium, with $Na_2[Y(Me_2\text{-}Ph)_4]$ being a particularly stable mass ion (Fig. 4.38).

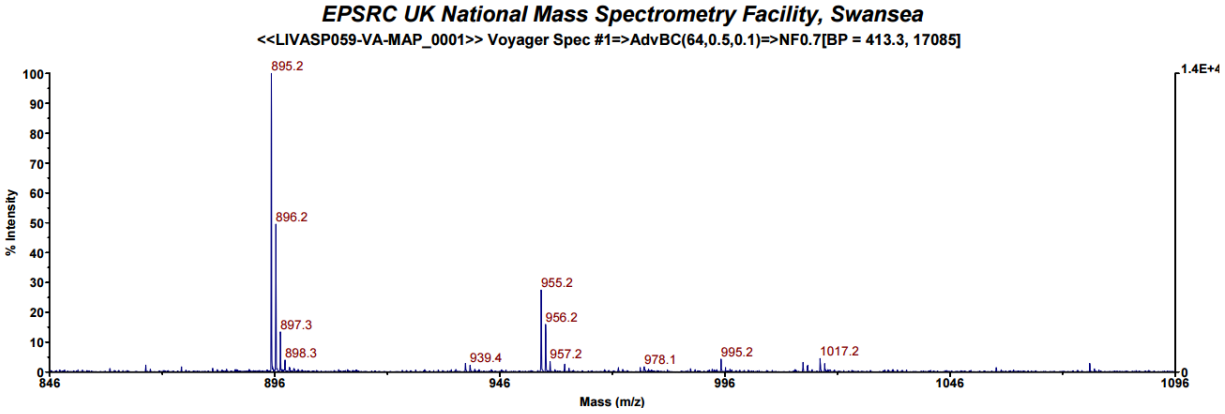

Figure 4.38: Mass Spectrum of $Na[Y(Me_2\text{-}Ph)_4]$ with the key mass fragment ($Na_2[Y(Me_2\text{-}Ph)_4]$) at 895.2 m/z

Table 4.2: Elemental Analysis results for $Na[Y(Me_2\text{-}Ph)_4]$

	$Na[Y(Me_2\text{-}Ph)_4]$ Calculated	$Na[Y(Me_2\text{-}Ph)_4]$ Found
Carbon (%)	60.55	60.78
Hydrogen (%)	5.54	5.55
Nitrogen (%)	6.42	6.42
C:N	9.43	9.46

Table 4.2 shows the anhydrous elemental analysis results for the proposed complex $Na_3[Y(Me_2\text{-}Ph)_6]$. As can be seen from above there is a strong correlation between the

calculated and found values with a deviation of 0.21% in carbon, 0.04% in hydrogen, 0.05% in nitrogen.

The elemental analysis results presented here represent a close match to those expected for the complexes proposed. The C:N ratio is of particular interest as it gives a good indicator of the identity of the organic ligand bound to the complex although it can be affected by residual solvent.

The elemental analysis coupled with the mass spectrometry and the integration pattern of the ^{1}H NMR spectrum strongly indicates the formation of the complex as Na[Y(Me$_2$-Ph)$_4$].

4.4 Discussion of M$_3$[Ln(Ligand)$_6$] Complexes.

What follows is an extension to the work mentioned above. Analogies will be made, and using the underlying patterns outlined above structural similarities inferred. The lithium/rare earth complexes were produced *via* the silylamide route (Fig. 4.39).

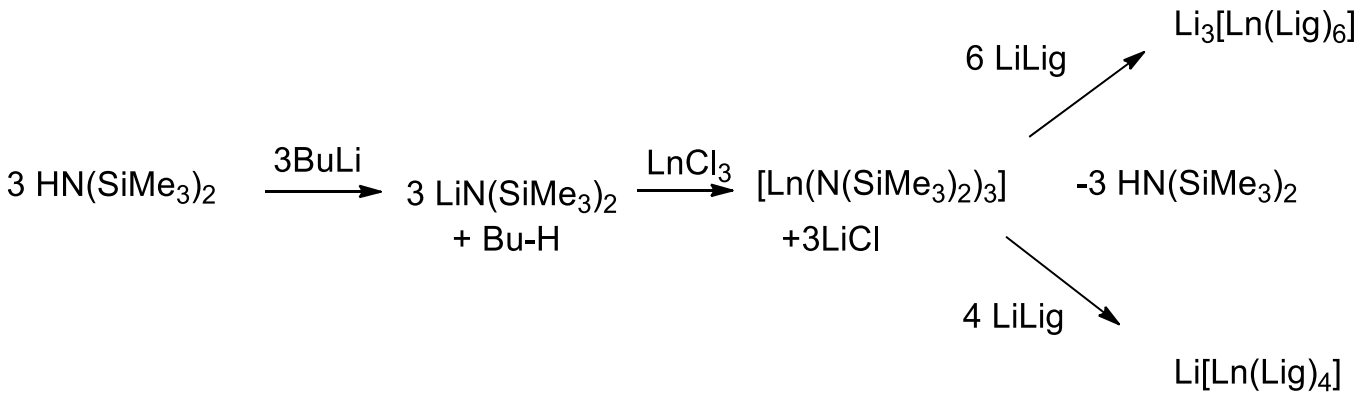

Figure 4.39: The silylamide route

Various attempts at formation of X-ray quality crystals were made for these complexes. It was hoped that data could be obtained that would be representative of both the lithium and sodium rare earth complexes. Crystals of sufficient quality were obtained for both of the lithium yttrium complexes Li$_3$[Y(Me$_2$-Ph)$_6$] and Li$_3$[Y(^{i}Pr-Ph)$_6$]. Unfortunately for the lithium europium

complex $Li_3[Eu(Me_2\text{-}Ph)_6]$ crystals were not obtained . What follows is an account of the data obtained for each of the complexes.

4.4.1 Discussion of Data for Complex with the Proposed formula $Li_3[Y(Me_2\text{-}MePh)_6]$

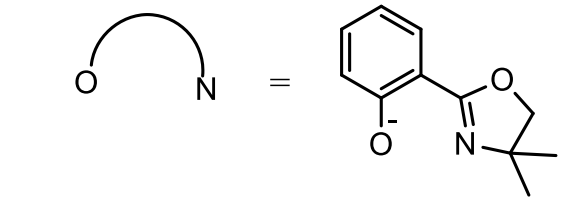

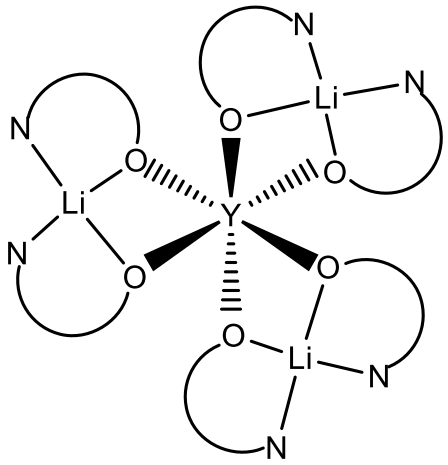

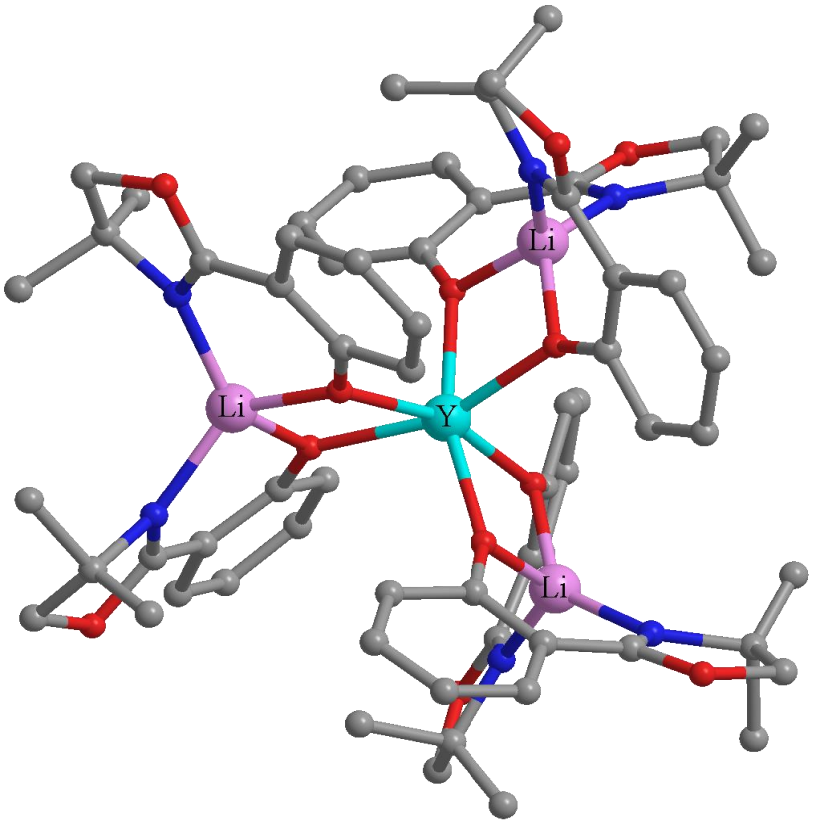

Figure 4.40: Crystal structure of $Li_3[Y(Me_2\text{-}Ph)_6]$ synthesised during the current study

Shown above (Fig. 4.40) is the structure of the yttrium/lithium complex $Li_3[Y(Me_2\text{-}Ph)_6]$ synthesised during this study. From the above diagram it can be seen that the binding motif experienced at the yttrium centre in the $M_3[Ln(Ligand)_6]$ structure is made up of three repeat units (Fig. 4.41).

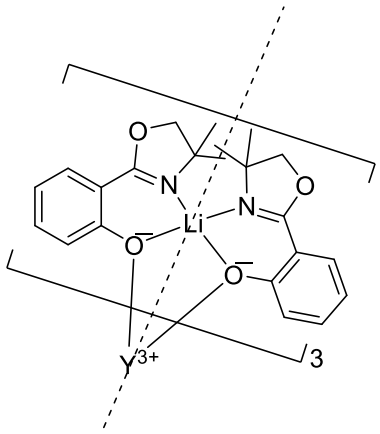

Figure 4.41: The repeat unit used in the synthesis of the $M_3[Ln(Ligand)_6]$ complex $Li_3[Y(Me_2\text{-}Ph)_6]$

From figures 4.40 and 4.41 it can be seen that the complex consists of three $Li(Me_2\text{-}Ph)$ subunits where Y^{3+} is co-ordinated to all six phenolates and each lithium is co-ordinated between two imine and two phenolate moieties forming two six membered chelate rings.

The average bond distance between the yttrium centre and the phenolate oxygens is 2.25Å. Compared against the structurally similar Shibasaki BINOL complexes, which have an average bond length of between 2.42Å (R.E=La) and 2.30Å (R.E.=Eu), this seems like a sensible bond distance given the smaller ionic radius (104pm) of yttrium (III) compared with europium (III) (108ppm) and lanthanum (115ppm).[2] As further comparison, the average Y-O(phenolate) bond distance in the four ligand complex, $Li[Y(Me_2\text{-}Me\text{-}Ph)_4]$ (Figure 4.11), is 2.23Å. It is important to note that in the last comparison only the ligands also bound to the alkali metal have been included in the average. This is because they have the same binding mode as those in the six ligand $Li_3[Y(Me_2\text{-}Ph)_6]$ complex.

Figure 4.41 shows that the Li[Me_2-Ph]$_2$ units have a C_2 symmetry axis running through the lithium centre and that the subunits are helically chiral due to the direction of rotation between the planar Me_2-Ph ligands. The complex also possesses a crystallographic C_2 axis. The helical chirality of the complex is detailed below (table 4.3), with a full description of the complex being Λ-λδδ-Li_3[Y(Me_2-Ph)$_6$] (Fig. 4.42). This is the preferred form in the solid state however in solution rapid thermal exchange processes will cause these isomers (Δ or Λ) to average out with loss of splitting and resulting in peak broadening.

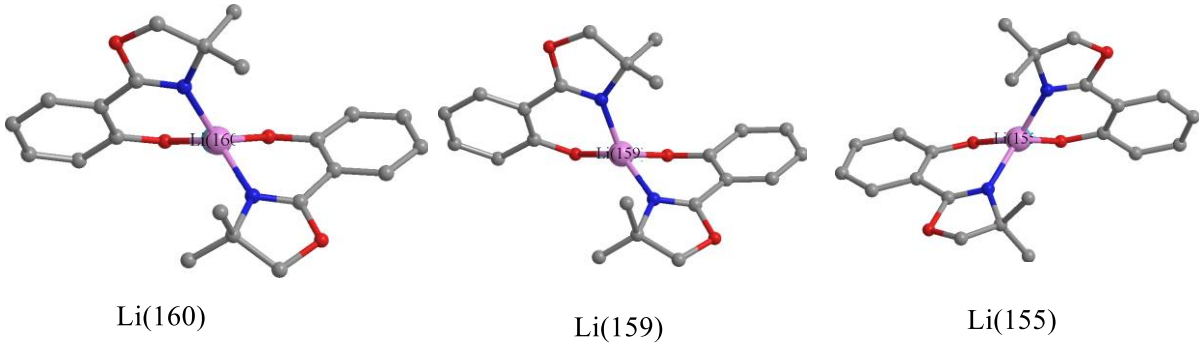

Figure 4.42: Chirality of Li(Me_2-Ph)$_2$ subunits viewed along the lithium-yttrium axis, torsion angles given in the table below (Lithium atom number provided below each subunit)

Table 4.3: Torsion angles and assigned chirality of Li(Me_2-Ph)$_2$ subunits. Angles have been measured from N-C-C-C(O), determining the torsion between the oxazoline unit and the phenol ring (See section 14.1 for crystal structure data tables).

Lithium Number	Torsion Angle (°C)	Chirality
Li(160)	-22.45(9), -20.81(10)	δ
Li(159)	-13.52(8), -24.81(8)	δ
Li(155)	13.82(11), 8.08(13)	λ

From the values in table 4.3, there is not a high degree of symmetry between the subunits present in the complex. The two δ subunits are not symmetrical to each other nor are either of them symmetrical to the λ subunit.

From this we might expect the ^{1}H NMR spectrum to consist of 3 distinct sets of resonances in the ratio of 1:1:1 due to the C_2 axis.

However, as can be seen from figure 4.43-4.45 the ^{1}H NMR spectrum is very complex with a large number of sharp resonances. As mentioned above we might have expected a small number of highly broadened peaks in the ^{1}H NMR spectrum of $Li_3[Y(Me_2\text{-}Ph)_6]$ (Fig. 4.43) due to thermal averaging of a number of different isomers (δδδ, λλλ, λλδ, ααλ). However as can be seen from the below spectrum taken at room temperature we in fact see a highly complex ^{1}H NMR spectrum with a large number of sharp resonances with defined splitting patterns. Much of the complexity will be due to the existence of several different isomers in solution at the same time.

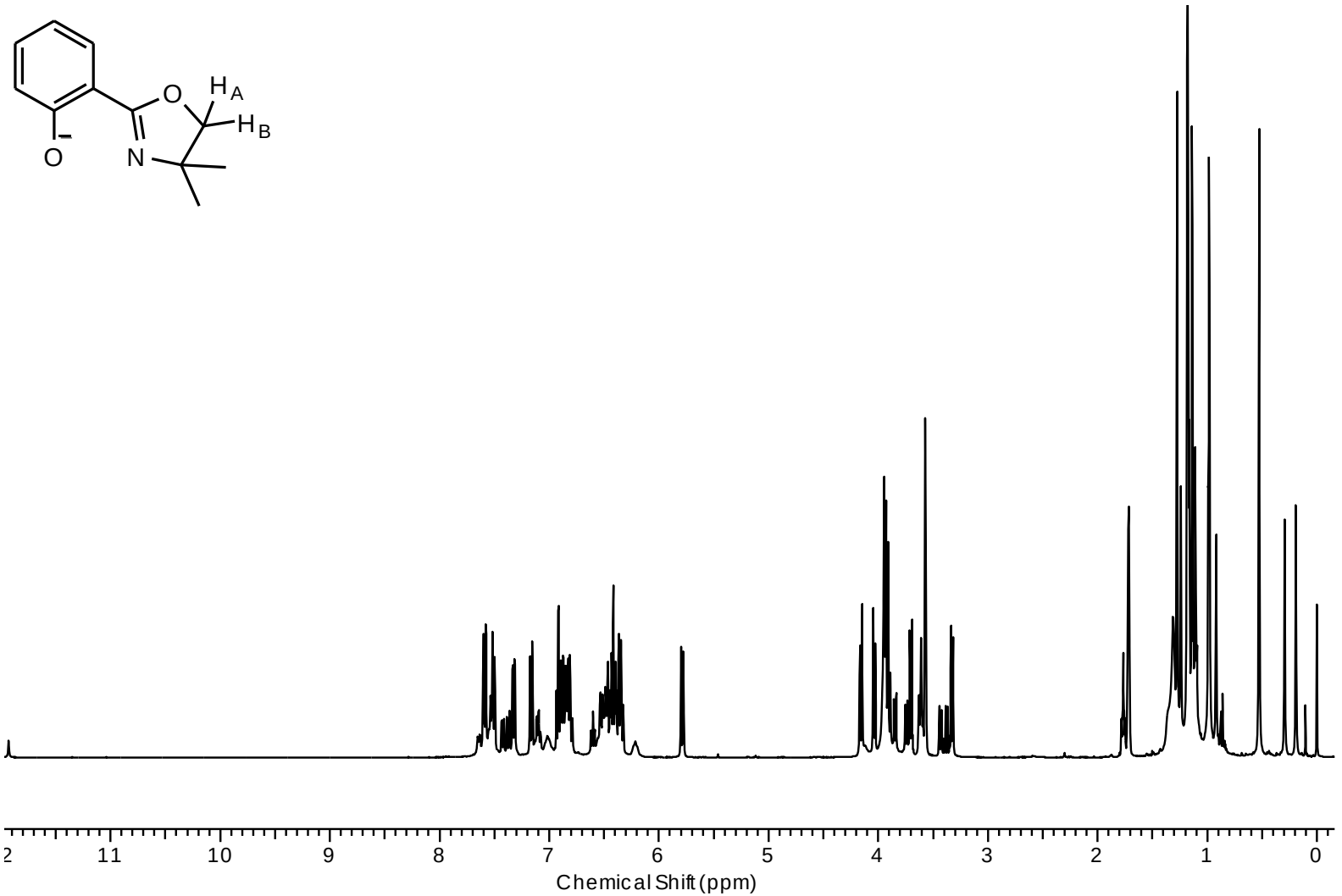

Figure 4.43: ^{1}H NMR spectrum of $Li_3[Y(Me_2\text{-}Ph)_6]$ at room temperature in *d*-THF

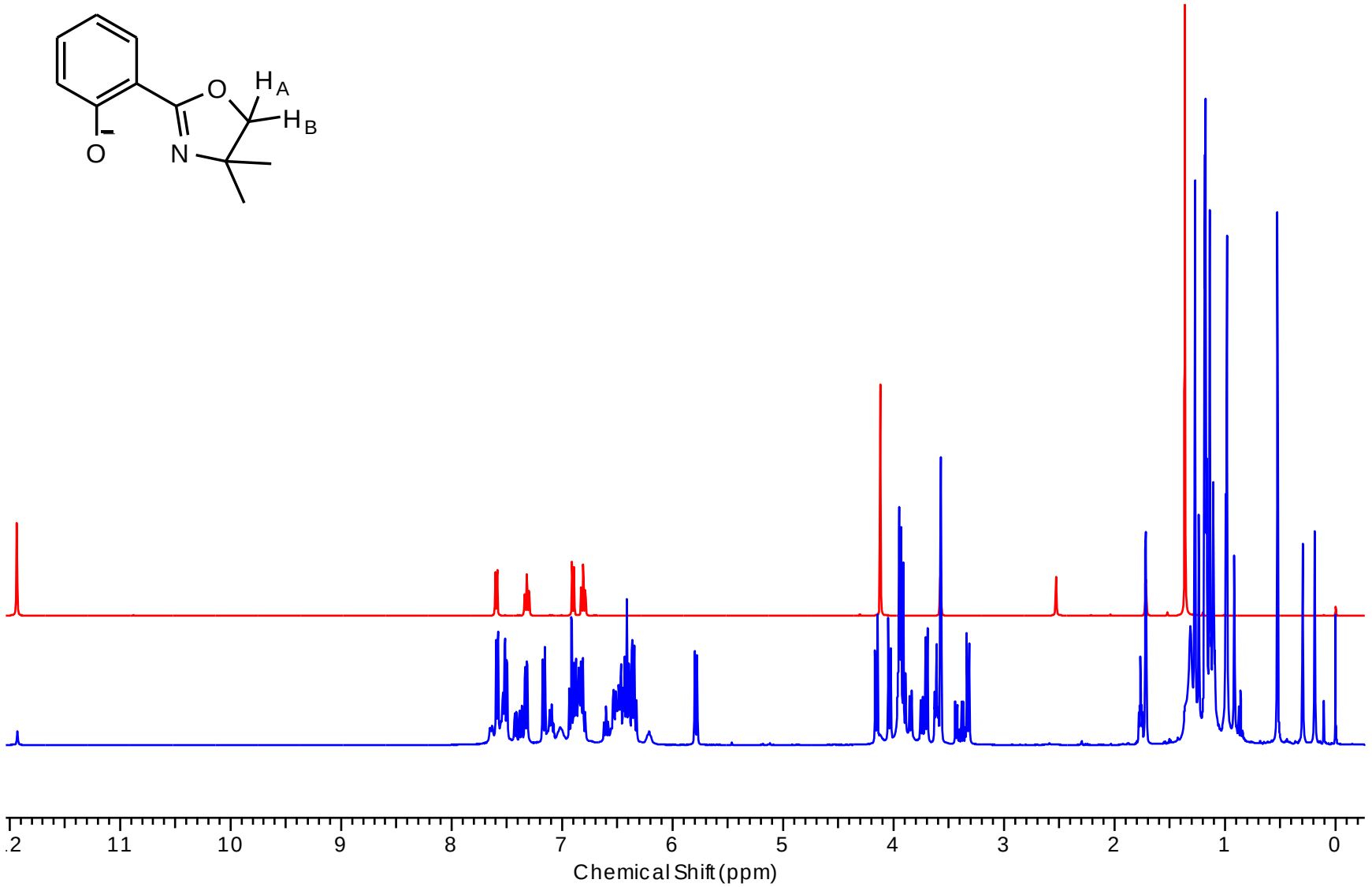

Figure 4.44: ^{1}H NMR spectrum of $Li_3[Y(Me_2\text{-}Ph)_6]$ (blue, bottom) vs free ligand H-Me_2-Ph (red, top) (*d*-THF, room temperature).

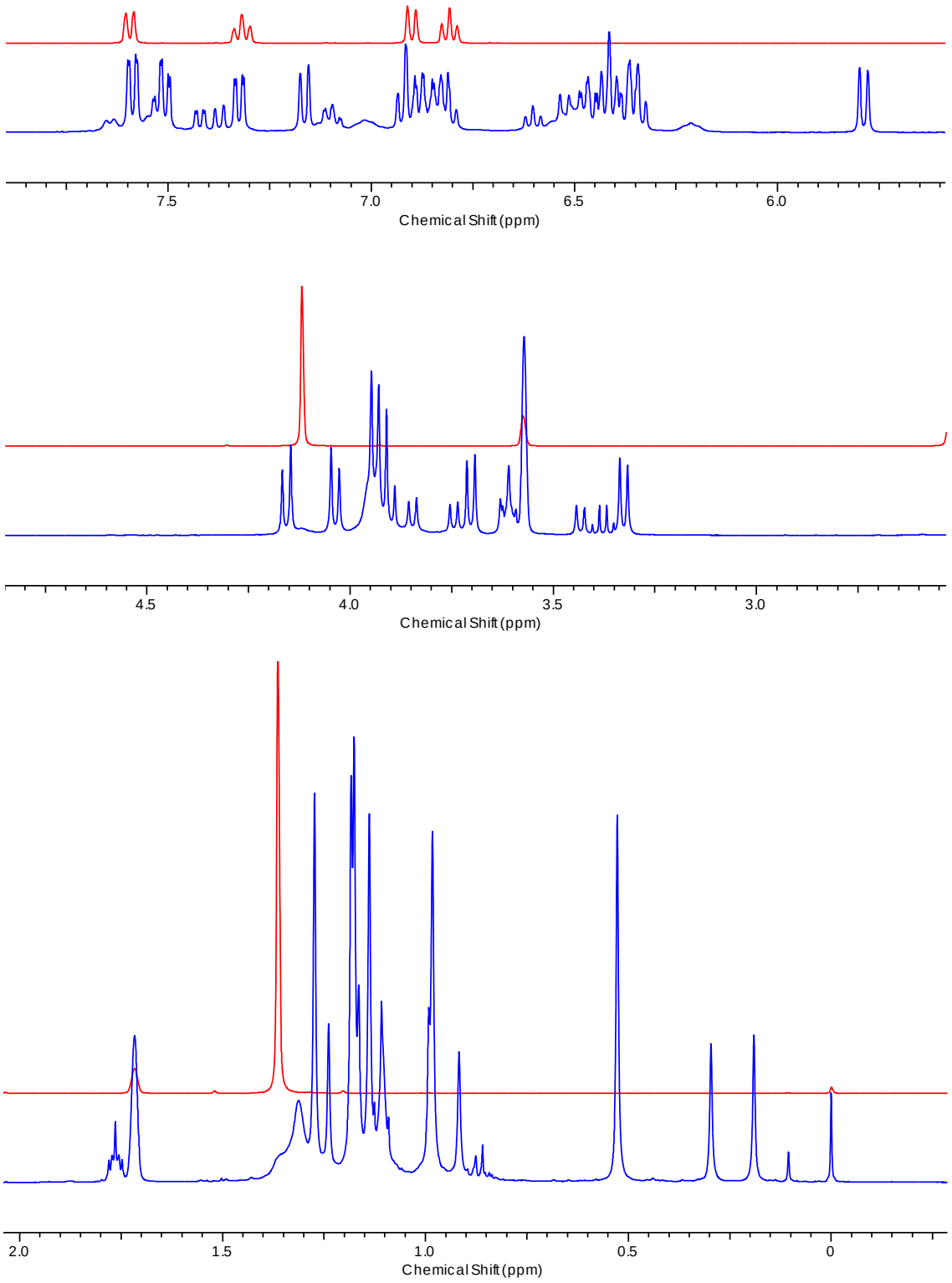

Figure 4.45: A series of diagrams showing the key areas of the ^{1}H NMR spectrum of $Li_3[Y(Me_2\text{-}Ph)_6]$ (blue, bottom) vs free ligand H-Me_2-Ph (red, top) (*d*-THF, room temperature).

As can be seen from figures 4.44 and 4.45 there is very little correlation between the ^{1}H NMR spectrum of the complex and that of the free ligand H-Me$_2$-Ph. There is however a peak at ~12ppm which is associated with free phenolic OH, however integration of the peak indicates free ligand accounts for less than 10% of the sample.

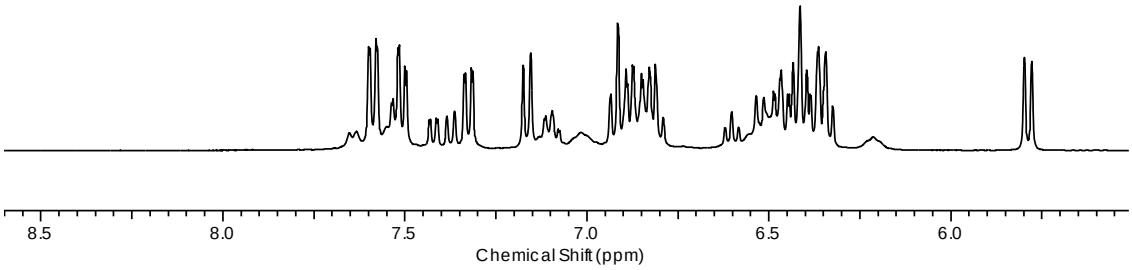

Figure 4.46: Expansion of the aromatic region of the ^{1}H NMR of Li$_3$[Y(Me$_2$-Ph)$_6$] (*d*-THF, room temperature

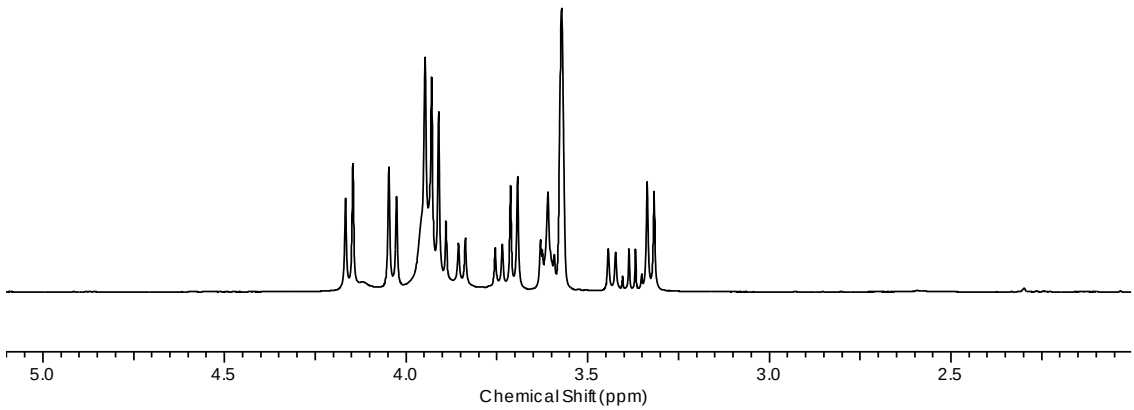

Figure 4.47: Expansion of the oxazoline ring region of the ^{1}H NMR of Li$_3$[Y(Me$_2$-Ph)$_6$] (*d*-THF, room temperature)

Figure 4.47 shows an expansion of the "oxazoline ring" region of the ^{1}H NMR spectrum of Li$_3$[Y(Me$_2$-Ph)$_6$]. The AB system (AB system 1, Fig. 4.48)) at 4.20-4.0ppm indicates the loss of the plane of symmetry in the ligand, which would be expected from formation of the complex. The oxazoline ring protons now experience a different magnetic field and so are no longer equivalent and hence split each other. There appears to be a number of "AB" type systems visible in this region with another present between 3.7-3.35ppm (Fig. 4.48).

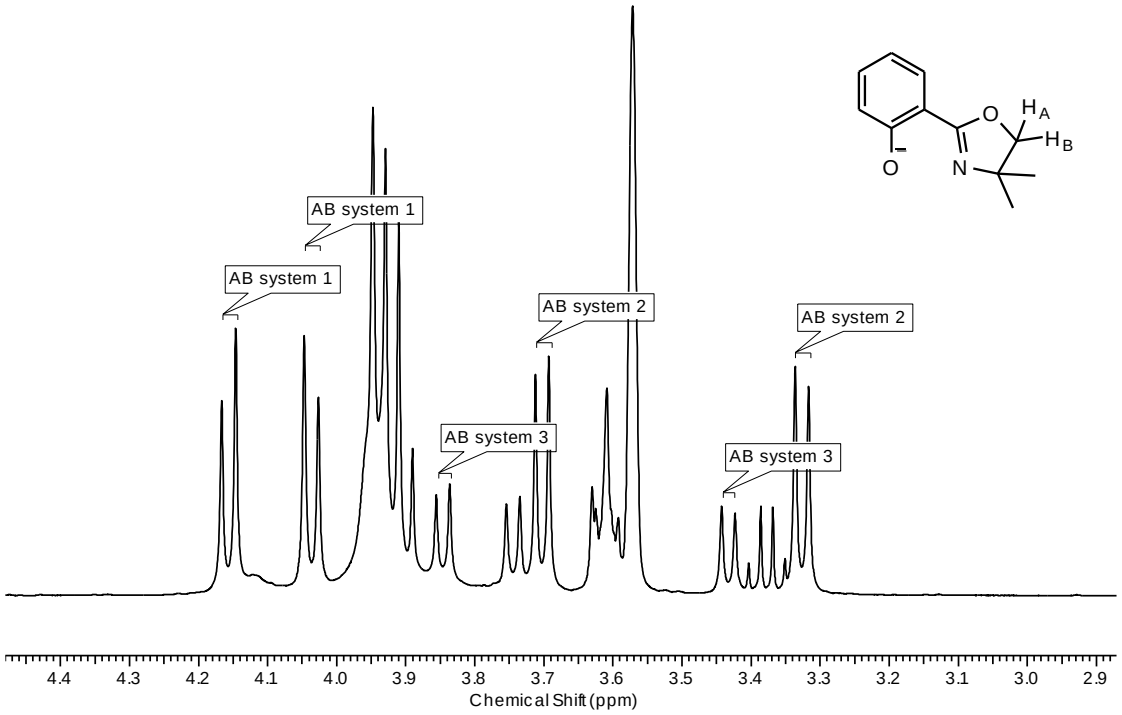

Figure 4.48: Expansion of the oxazoline ring region of the ^{1}H NMR of $Li_3[Y(Me_2\text{-}Ph)_6]$, with AB systems highlighted (*d*-THF, room temperature)

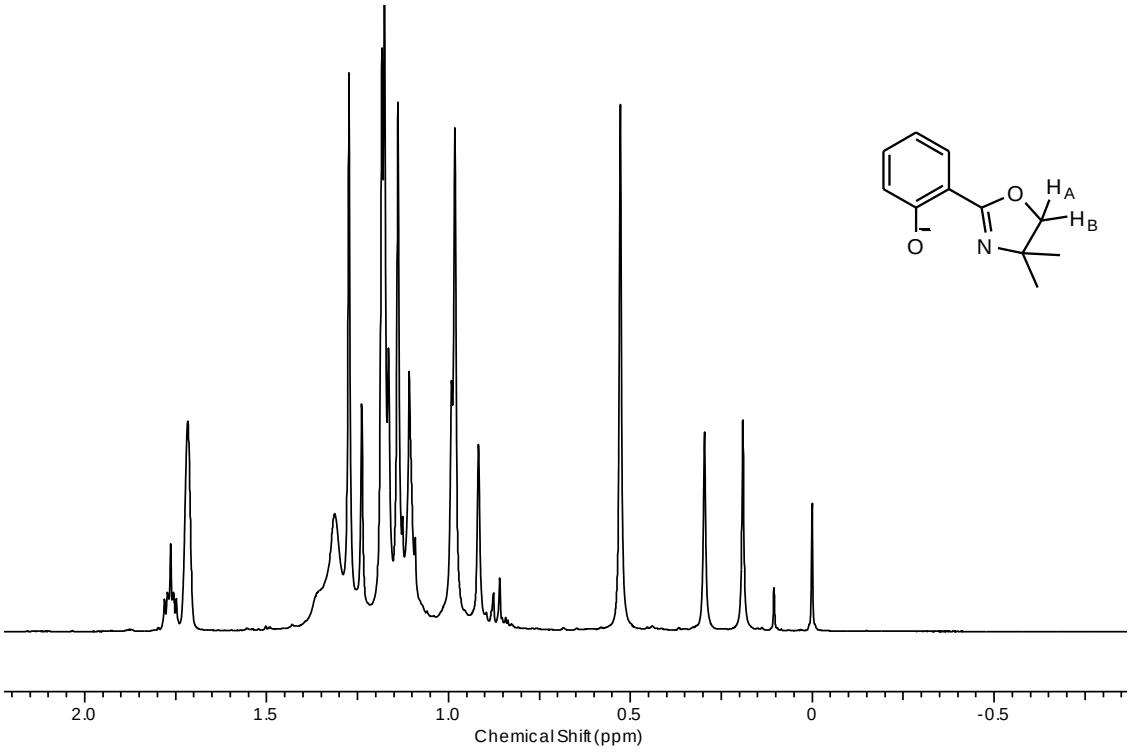

Figure 4.49: Expansion of the methyl region of the ^{1}H NMR of $Li_3[Y(Me_2\text{-}Ph)_6]$ (*d*-THF, room temperature

The aromatic proton at 5.5ppm has been shifted way outside of the aromatic region. This can be ascribed to intramolecular interactions between this aromatic proton and π-systems of adjacent phenol rings. A similar effect has been noted in Ir(III) complexes containing oxazolyl phenolate and cyclometallated pyrazolylphenyl ligands (Fig. 4.49). [115]

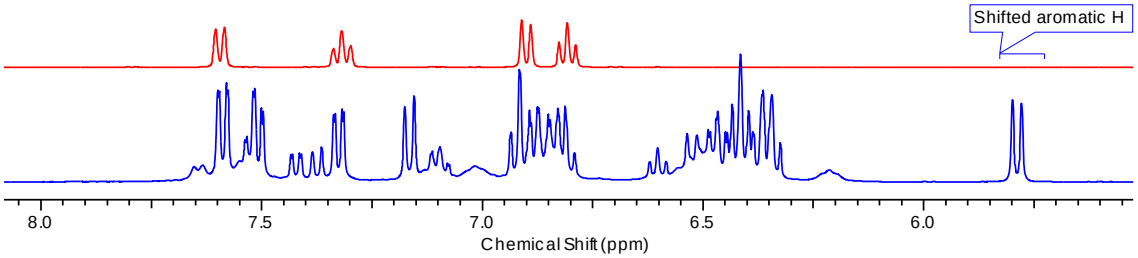

Figure 4.50: Expansion of the aromatic region of $Li_3[Y(Me_2\text{-}Ph)_6]$ (blue) vs H-Me_2-Ph (red) (*d*-THF, room temperature

This is unusual but it is supported by crystallographic data (Figure 4.51). Furthermore this has been experienced previously with other complexes of this type.[116]

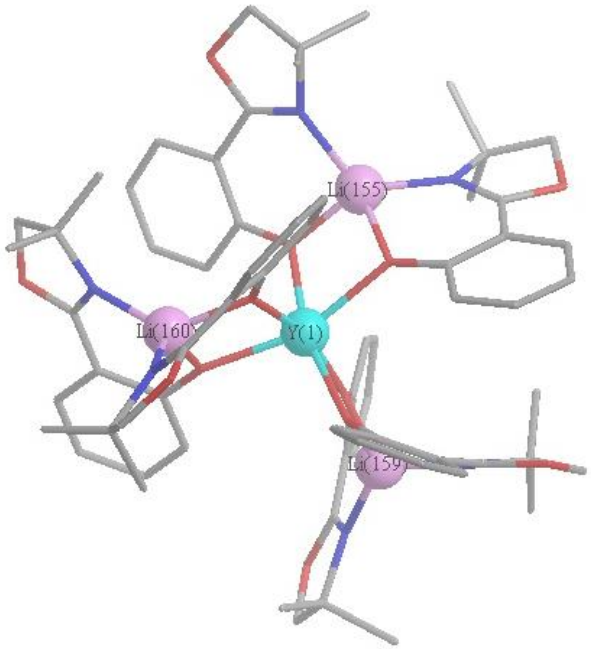

Figure 4.51: Crystal structure of $Li_3[Y(Me_2\text{-}Ph)_6]$ showing two ligands arranged perpendicular to each other

Anhydrous mass spectrometry of this complex yielded a mass fragment corresponding to loss of one ligand leading to $Li_3[Y(Me_2\text{-}Ph)_5]^+$ (Fig. 4.52), corresponding identically to the theoretical pattern produced for this complex.

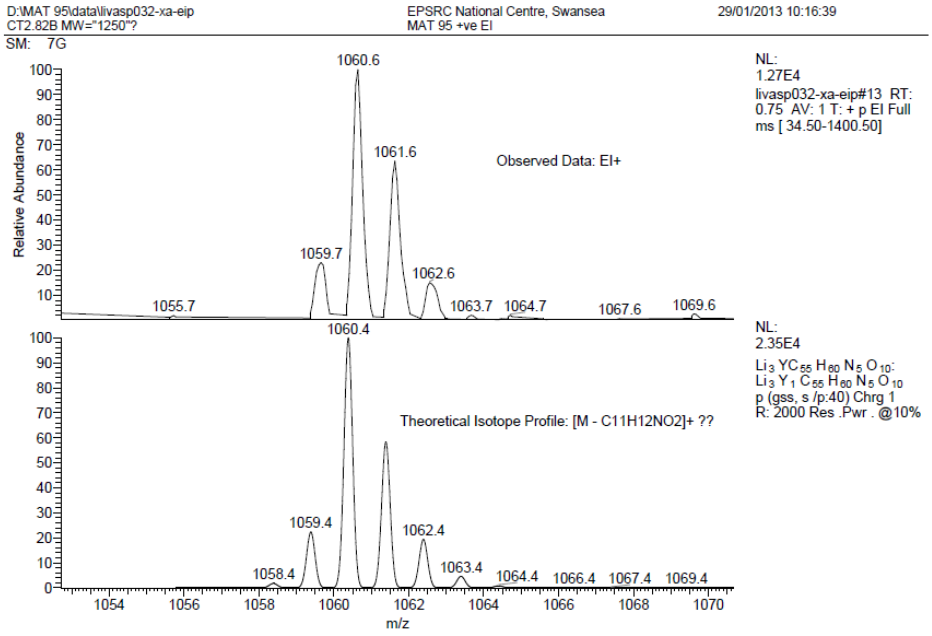

Figure 4.52: Mass spectrum of $Li_3[Y(Me_2\text{-}Ph)_6]$ showing the mass fragment at 1060.6m/z corresponding to $Li_3[Y(Me_2\text{-}Ph)_5]^{\pm}$

Table 4.4: Elemental Analysis results for $Li_3[Y(Me_2\text{-}Ph)_6]$

	$Li_3[Y(Me_2\text{-}Ph)_6]$ Calculated	$Li_3[Y(Me_2\text{-}Ph)_6]$ Found
Carbon (%)	63.35	63.40
Hydrogen (%)	5.76	5.68
Nitrogen (%)	6.72	6.63
C:N	9.43	9.56

Table 4.4 shows the elemental analysis results for the proposed complex $Li_3[Y(Me_2\text{-}Ph)_6]$ as can be seen the calculated and found values bare a close resemblance to each other deviating by 0.05% in carbon, 0.08% in hydrogen and 0.09% in nitrogen. This coupled with the mass

spectrometry, the crystal structure and the highly complex nature of the ^{1}H NMR strongly indicates the formation of the complex as $Li_3[Y(Me_2\text{-}Ph)_6]$.

4.4.2 Discussion of Data for Proposed Complex $Li_3[Y(^{i}Pr\text{-}Ph)_6]$

A crystal structure was also obtained for the chiral analogue of the complex discussed in section 4.4.1.

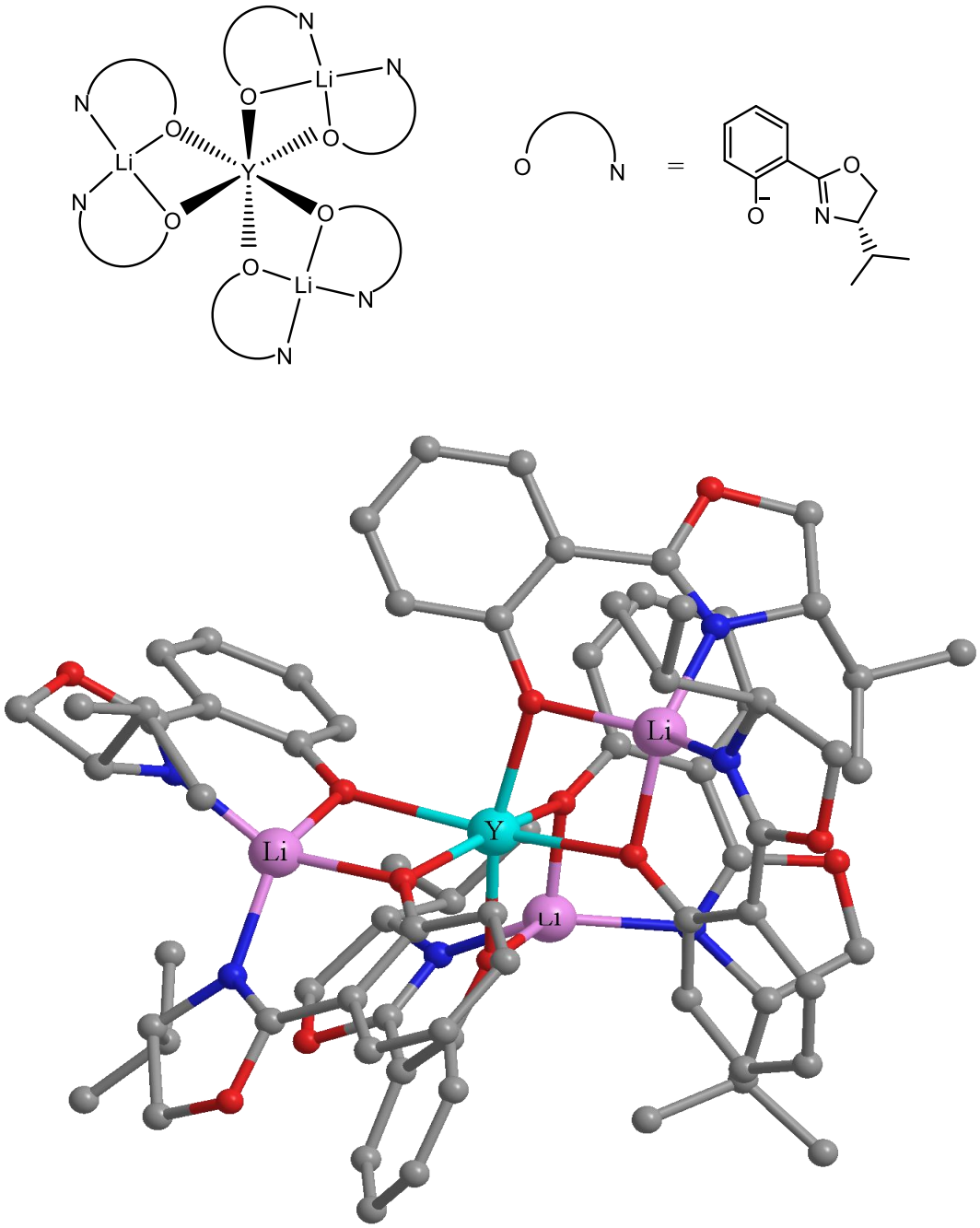

Figure 4.53: Crystal structure of $Li_3[Y(^{i}Pr\text{-}Ph)_6]$ synthesised during this study

As can be seen from figure 4.53 the binding motif in the above complex is the same as that seen in $Li_3[Y(Me_2\text{-}Ph)_6]$ (Fig. 4.40). The complex is made up of three repeat units (Fig. 4.53), much as for the achiral analogue, and also possesses the six membered chelate rings formed as lithium is held between a phenolate oxygen and an imine nitrogen.

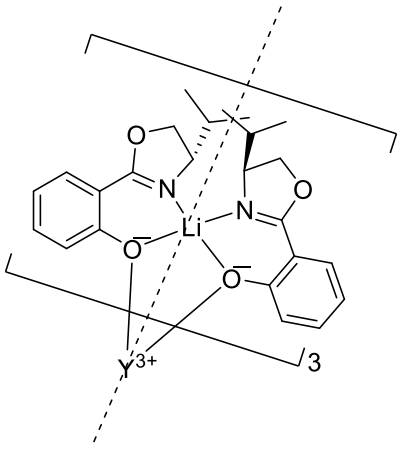

Figure 4.54: Repeat unit found in the $M_3[Ln(Ligand)_6]$ complex $Li_3[Y(^iPr\text{-}Ph)_6]$

Figure 4.54 also shows that the $Li[^iPr\text{-}Ph]_2$ have a C_2 symmetry axis running through the lithium centre and that the subunits are helically chiral due to the direction of rotation between the planar ^{i}Pr-Ph ligands. The complex possesses a crystallographic C_2 axis. The helical chirality of the complex is detailed below (table 4.5), with a full description of the complex being Λ-λδδ-$Li_3[Y(^iPr\text{-}Ph)_6]$ (Fig. 4.54). This is the preferred form in the solid state however in solution rapid thermal exchange processes will cause these two isomers (Δ or Λ) to average out with loss of splitting and resulting in peak broadening.

The average bond distance between the yttrium centre and the phenolate oxygens is 2.28Å. Compared against the structurally similar Shibasaki BINOL complexes, which have an average bond length of between 2.42Å (R.E=La) and 2.30Å (R.E.=Eu), this seems like a sensible bond distance given the smaller ionic radius (104pm) of yttrium (III) compared with europium (III) (108ppm) and lanthanum (115ppm).[2] As further comparison, the average Y-O(phenolate) bond distance in the four ligand complex, $Li[Y(Me_2\text{-}Me\text{-}Ph)_4]$ (Figure 4.11), is 2.23Å. It is important

to note that in the last comparison only the ligands also bound to the alkali metal have been included in the average. This is because they have the same binding mode as those in the six ligand $Li_3[Y(Me_2\text{-}Ph)_6]$ complex.

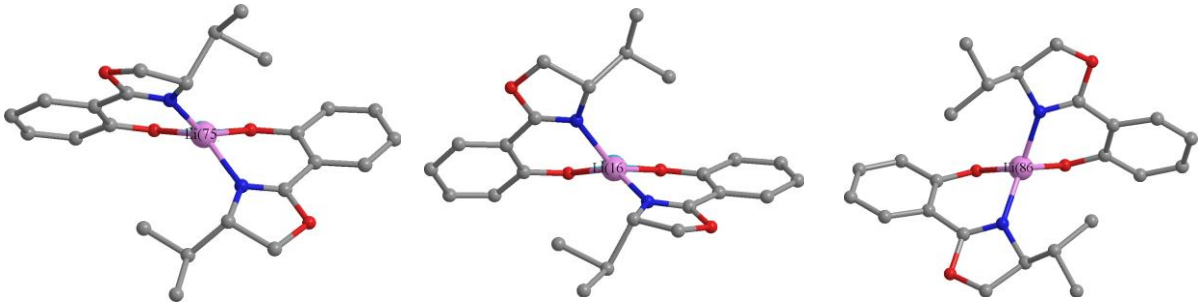

Figure 4.55: Chirality of the Li(^{i}Pr-Ph)$_2$ repeat units viewed along the lithium-yttrium axis, torsion angles given in the table below (lithium atom number given below each subunit)

Table 4.5: Account of the helical chirality about each lithium centre in $Li_3[Y(^i Pr\text{-}Ph)_6]$ (measured from N-C-C-C(O), determining the torsion between the oxazoline unit with respect to the phenol ring (see section 14.2 for tables of crystallographic data).

Lithium Number	Torsion Angle (°)	Chirality
Li75	-7.87(8), -14.46(8)	Δ
Li16	-7.87(5), -14.46(9)	Δ
Li86	27.44(15), 27.44(12)	Λ

As each subunit has two ligands the N-C-C-C(O) torsion angle has been measured for each ligand. Table 4.5 shows that the two δ subunits (Li (75) and Li (16)) have identical torsion angles, and that the two torsion angles measured for Li (86) are identical. These measurements

indicate a high degree of symmetry in the complex and that a C_2 axis runs along the Y-Li axis in the λ subunit, as indicated in figure 4.53.

From the crystal structure data we would expect ^{1}H NMR spectrum to consist of 2 sets of resonances in the ratio 2:1. However, due to the high similarity in crystal structure data between $Li_3[Y(Me_2\text{-}Ph)_6]$ (section 4.4.1) and $Li_3[Y(^i Pr\text{-}Ph)_6]$ we could expect a far more complicated ^{1}H NMR spectrum with a number of different isomers at room temperature.

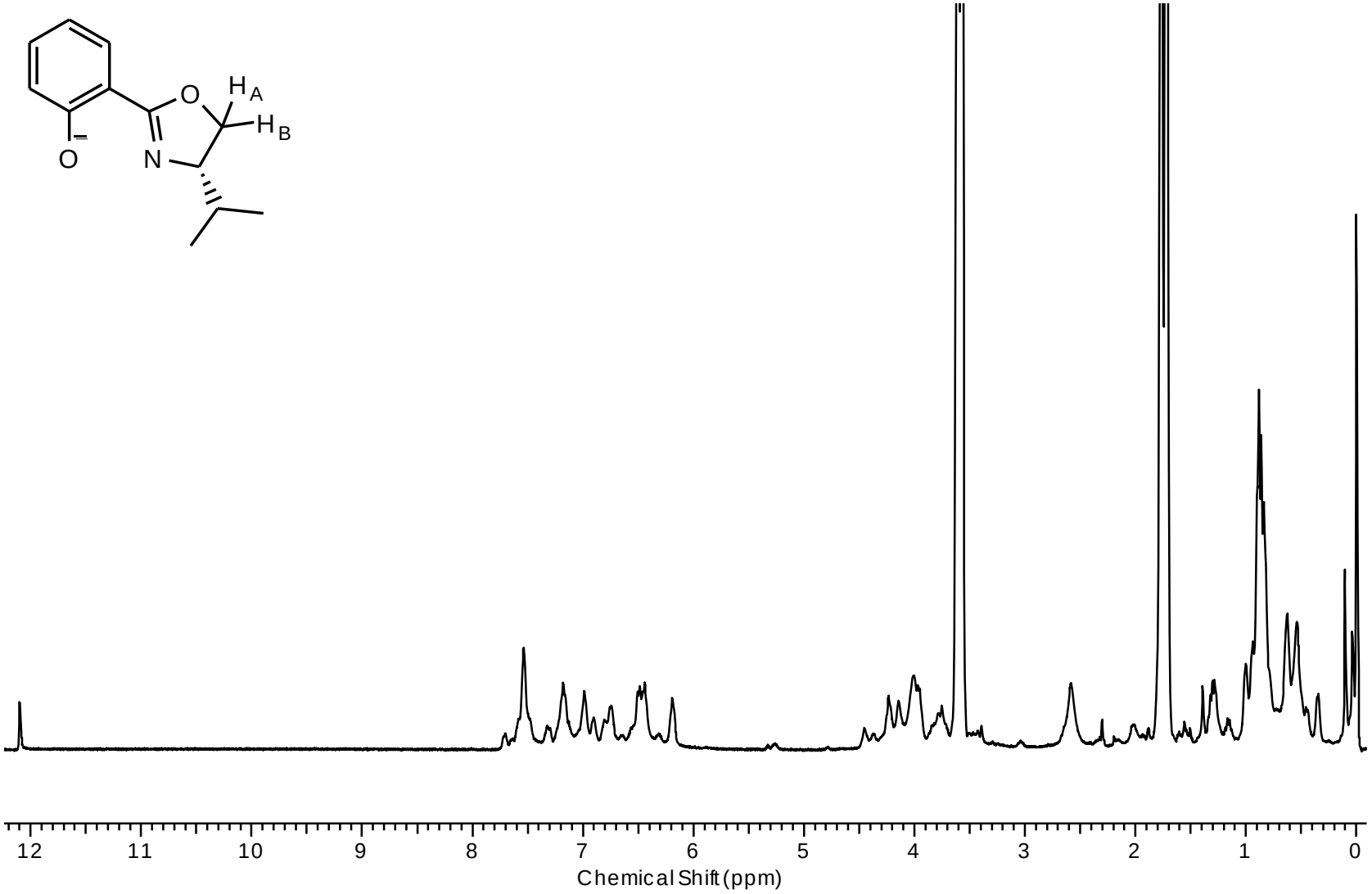

Figure 4.56: ^{1}H NMR spectrum of $Li_3[Y(^{i}Pr\text{-}Ph)_6$ at room temperature in *d*-THF

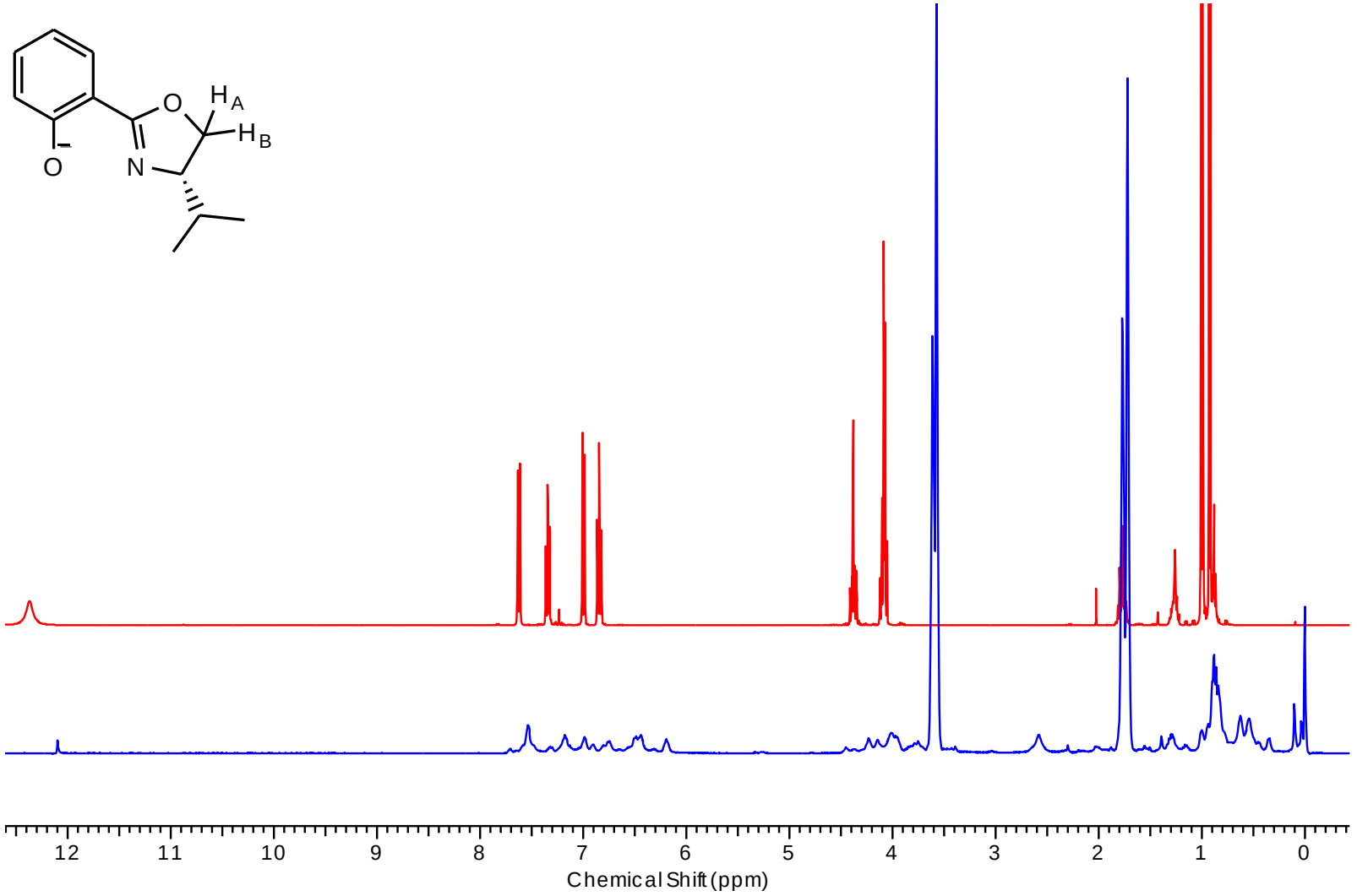

Figure 4.57: ^{1}H NMR comparison of free ligand H-^{i}Pr-Ph (red, top) vs $Li_3[Y(^{i}Pr\text{-}Ph)_6]$ (blue, bottom) at room temperature in d^8 THF

As can be seen from figure 4.56 the room temperature ^{1}H NMR is exceptionally broad. Comparison against the free ligand (Fig. 4.57) shows that although there are signs of a peak where we would expect free phenolic OH to appear in ^{1}H NMR there are no other peaks corresponding to free ligand.

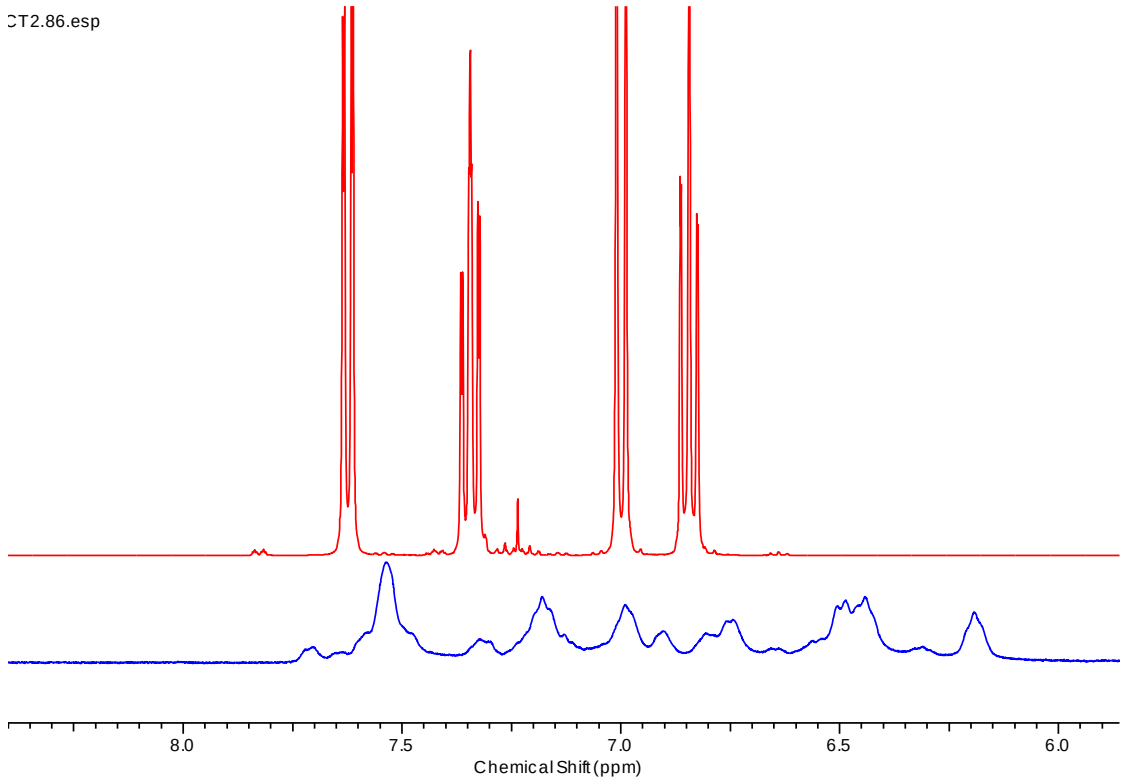

Figure 4.58: Expansion of the aromatic region of the ^{1}H NMR of free ligand H-^{i}Pr-Ph (red, top) vs $Li_3[Y(^{i}Pr\text{-}Ph)_6]$ (blue, bottom) at room temperature in d^8 THF

Figures 4.58, 4.59 and 4.60 show further comparison of the ^{1}H NMR spectra of the free ligand H-^{i}Pr-Ph against $Li_3[Y(^{i}Pr\text{-}Ph)_6]$. Figure 4.59 shows the oxazoline ring region (~5-3.75ppm), if the free ligand was present in a sizeable quantity we would expect to see highly defined peaks in this region, although there is likely to be some difficulty in seeing these peaks due to broadening of the peaks associated with the complex.

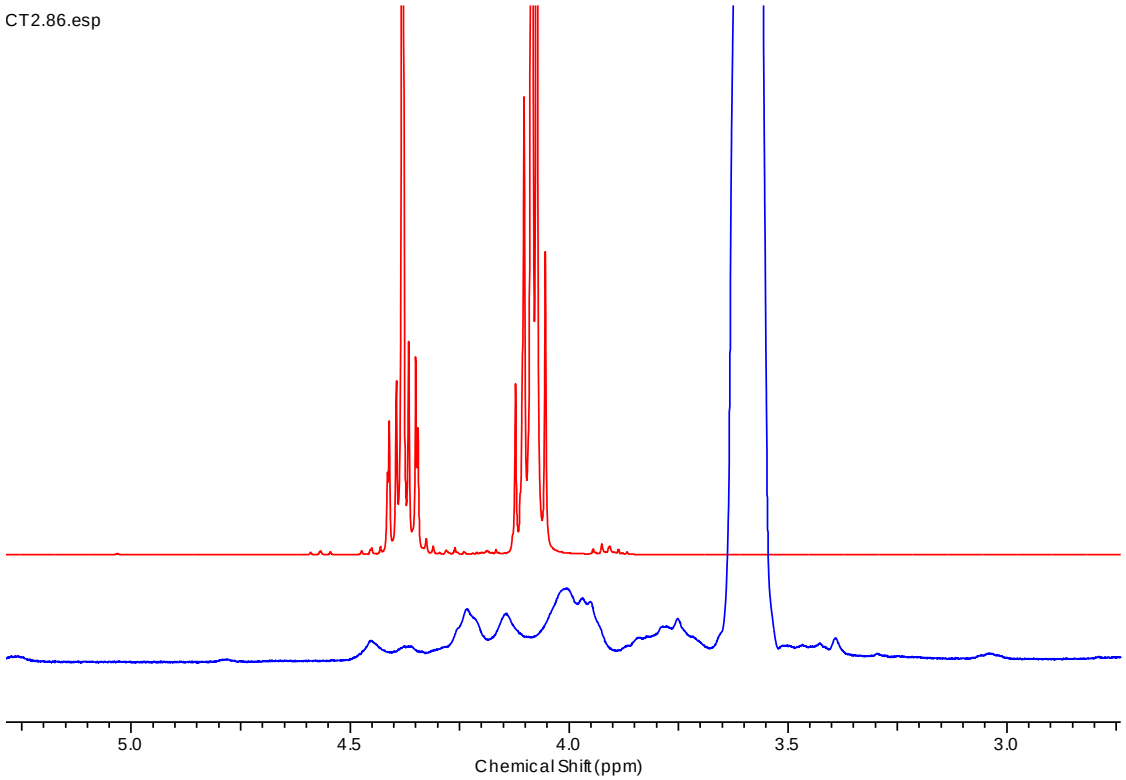

Figure 4.59: Expansion of the oxazoline ring region of the ^{1}H NMR spectrum of free ligand H-^{i}Pr-Ph (red, top) vs Li$_3$[Y(^{i}Pr-Ph)$_6$] (blue, bottom) at room temperature in *d*^{8} THF

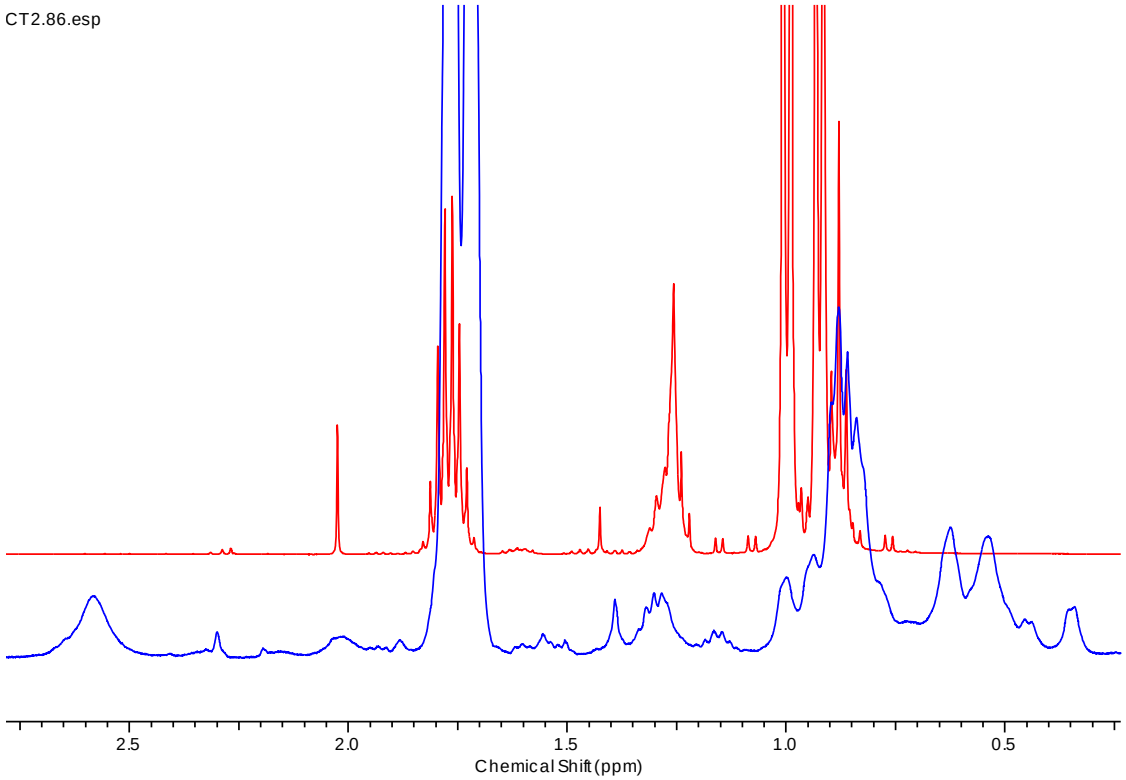

Figure 4.60: Expansion of the aliphatic region of the ^{1}H NMR spectrum of free ligand H-^{i}Pr-Ph (red, top) vs Li$_3$[Y(^{i}Pr-Ph)$_6$] (blue, bottom) at room temperature in *d*^{8} THF

Anhydrous mass spectrometry of $Li_3[Y(^iPr\text{-}Ph)_6]$ shows a mass peak at 1333.52 m/z (vs calculated 1334.57 m/z) using positive electrospray with a characteristic isotopic splitting pattern (Fig. 4.61).

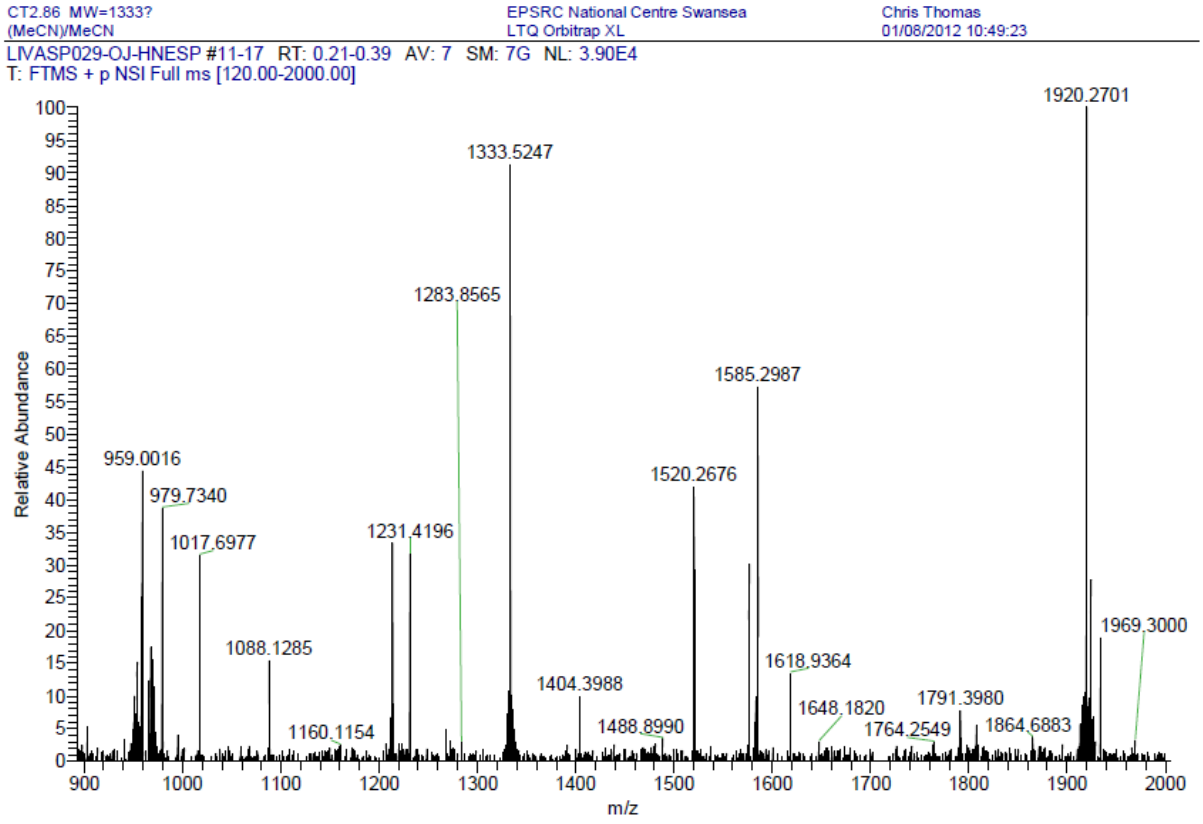

Figure 4.61: Mass spectrum of $Li_3[Y(^iPr\text{-}Ph)_6]$

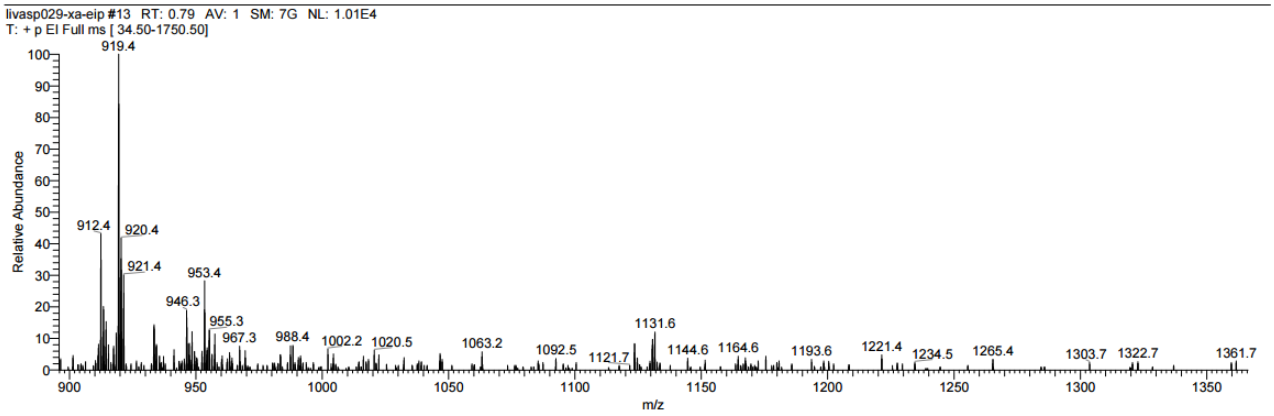

Figure 4.62: Mass Spectrum of $Li_3[Y(^iPr\text{-}Ph)_6]$ showing mass fragments at 1131.6 m/z and at 919.4 m/z

Figure 4.62 shows plausible mass fragments for $Li_3[Y(^iPr\text{-}Ph)_5]^{\pm}$ at 1131.6m/z and for $Li_2[Y(^iPr\text{-}Ph)_4]$ at 919.4 m/z again using positive electrospray.

Table 4.6: Elemental Analysis results for $Li_3[Y(^iPr\text{-}Ph)_6]$

	$Li_3[Y(^iPr\text{-}Ph)_6]$ Calculated	**$Li_3[Y(^iPr\text{-}Ph)_6]$ Found**
Carbon (%)	64.78	64.88
Hydrogen (%)	6.29	6.18
Nitrogen (%)	6.29	6.16
C:N	10.29	10.53

Table 4.6 shows the anhydrous elemental analysis results for the proposed complex $Li_3[Y(^iPr\text{-}Ph)_6]$. The calculated and found results are very similar deviating by 0.1% in carbon, 0.11% in hydrogen and 0.13% in nitrogen. The mass spectrometry and elemental analysis results coupled with the crystal structure and ^1H NMR data strongly support the formation of the complex as proposed as $Li_3[Y(^iPr\text{-}Ph)_6]$.

4.4.3 Discussion of Data for Proposed Complex $Li_3[Eu(Me_2\text{-}Ph)_6]$

Unfortunately a crystal structure was not obtained for this proposed complex nor was one isolated previously in the group. However we might expect the solid state structure to be similar to the yttrium analogue. It seems doubtful a dimer would form as the six ligands should co-ordinately saturate the metal centre. So we would expect the ^1H NMR spectrum to be very similar to that for the $Li_3[Y(Me_2\text{-}Ph)_6]$ complex, but with significant broadening due to europium's paramagnetism (Fig 4.63).

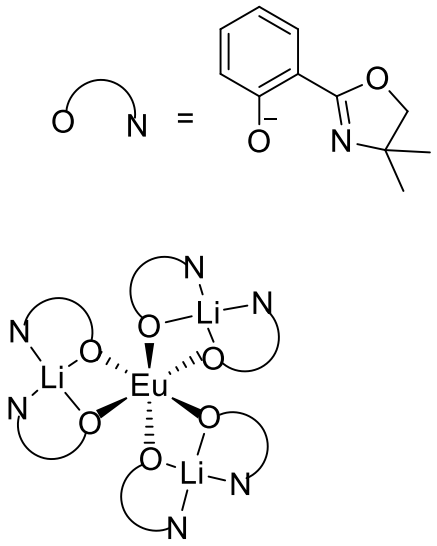

Figure 4.63: Proposed solid state structure of $Li_3[Eu(Me_2\text{-}Ph)_6]$

The ^1H NMR spectrum of $Li_3[Eu(Me_2\text{-}Ph)_6]$ was taken at room temperature in *d*-THF producing an extraordinarily simple spectrum (Fig. 4.64).

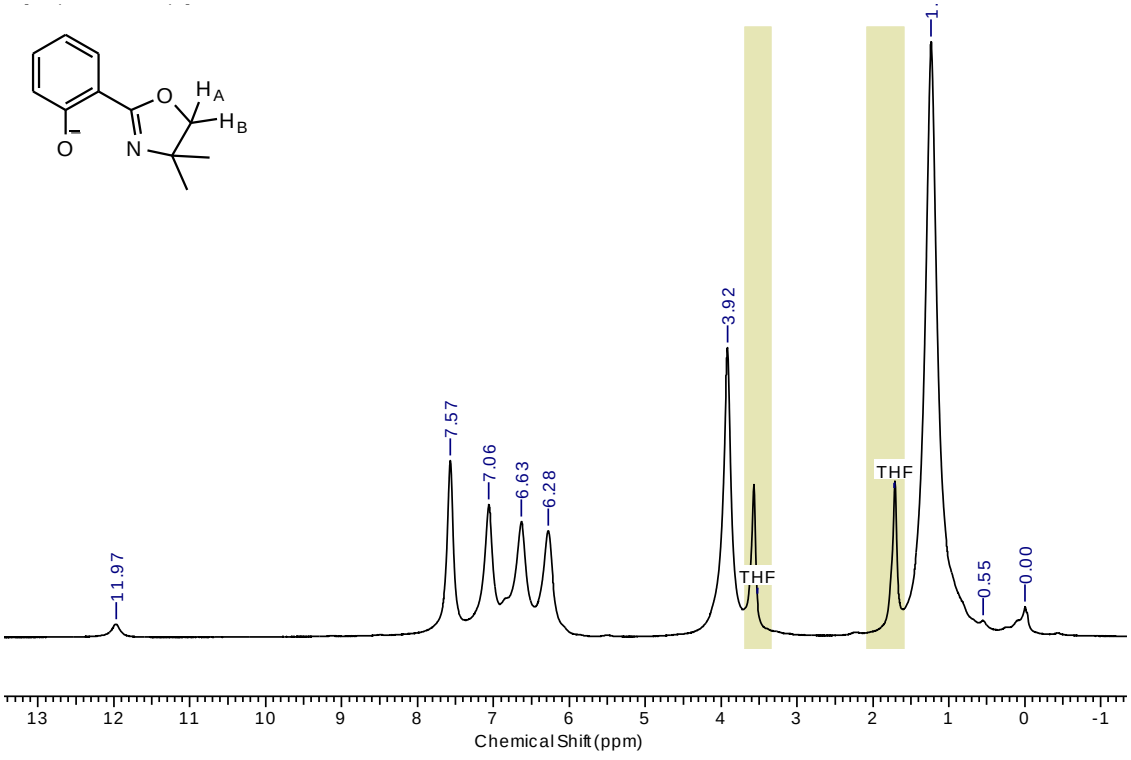

Figure 4.64: ^1H NMR spectrum of $Li_3[Eu(Me_2\text{-}Ph)_6]$ in *d*-THF at room temperature

Although there is a resonance at 11.97ppm there are no other signs of free ligand present in the NMR data, although due to the line broadening it is difficult to rule out the presence of free

ligand along the baseline. Integration of this resonance compared with the others in the ^{1}H NMR spectrum indicate that free phenol makes up less than 10% of the sample. Regardless of this there is significant peak shifting when the complex is compared against the free ligand (Fig. 4.65).

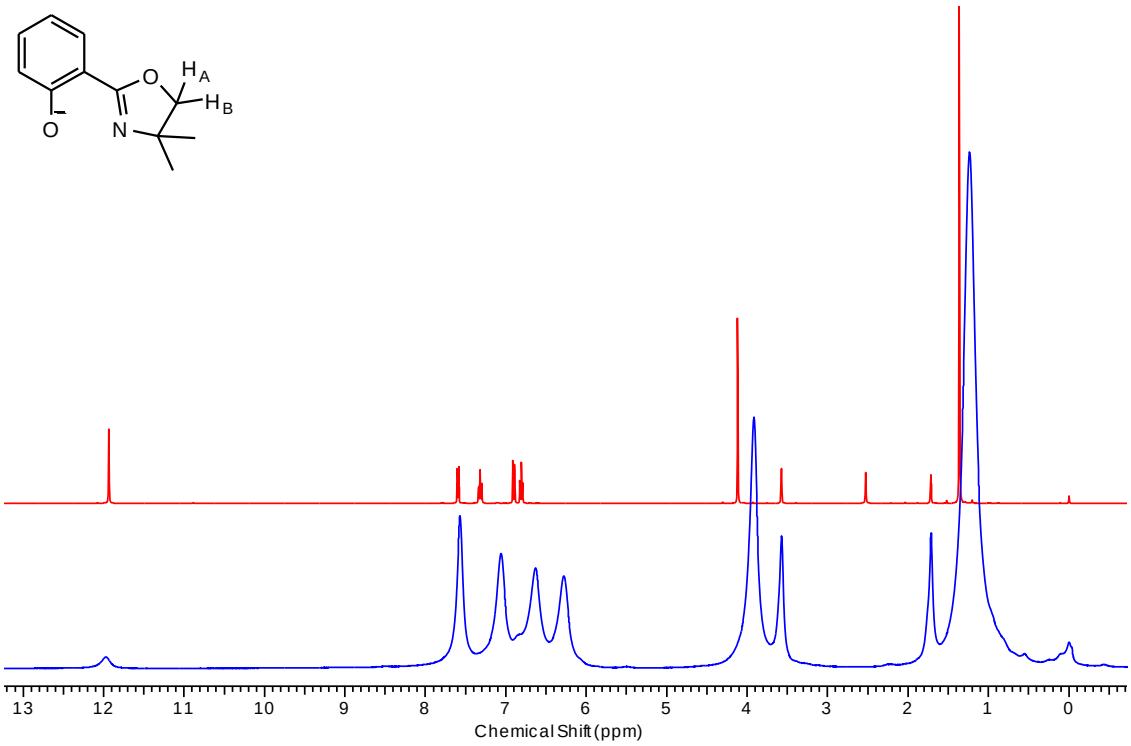

Figure 4.65: Comparison of H-Me$_2$-Ph (red) against Li$_3$[Eu(Me$_2$-Ph)$_6$] (blue) in *d*-THF at room temperature

Variable temperature ^{1}H NMR of the complex in figure 4.48 shows little overall structural change (Fig. 4.66). The temperature dependence of chemical shifts for the aromatic ^{1}H at 6.28 ppm is shown in figure 4.67.

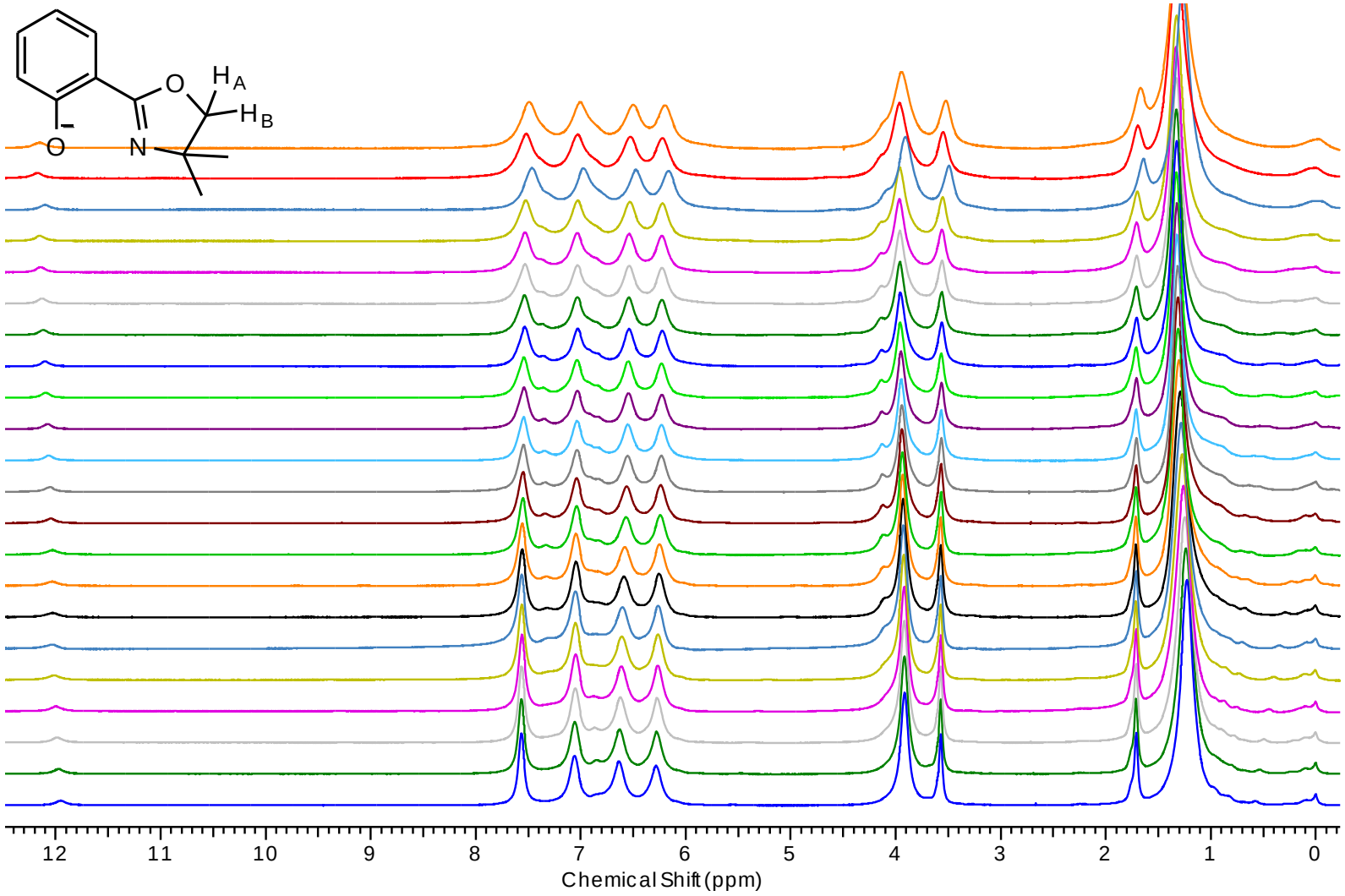

Figure 4.66: ^{1}H NMR data for the isopropyl region of $Li_3[Eu(Me_2\text{-}Ph)_6]$ showing the full range of temperatures explored from -80°C (red, top) to room temperature (blue, bottom) in 5°C increments in *d*-THF

A straight line would indicate no structural changes as the temperature drops and as can be seen from figure 4.67 the change in chemical shifts is linear. Figure 4.68 shows the temperature dependence of the methyl protons, it is worth noting the similarity of the two diagrams; both exhibit a roughly straight line until the 248K. The opposing slopes are due to geometric factors. Lower temperatures were considered however machine malfunction rendered this data unusable.

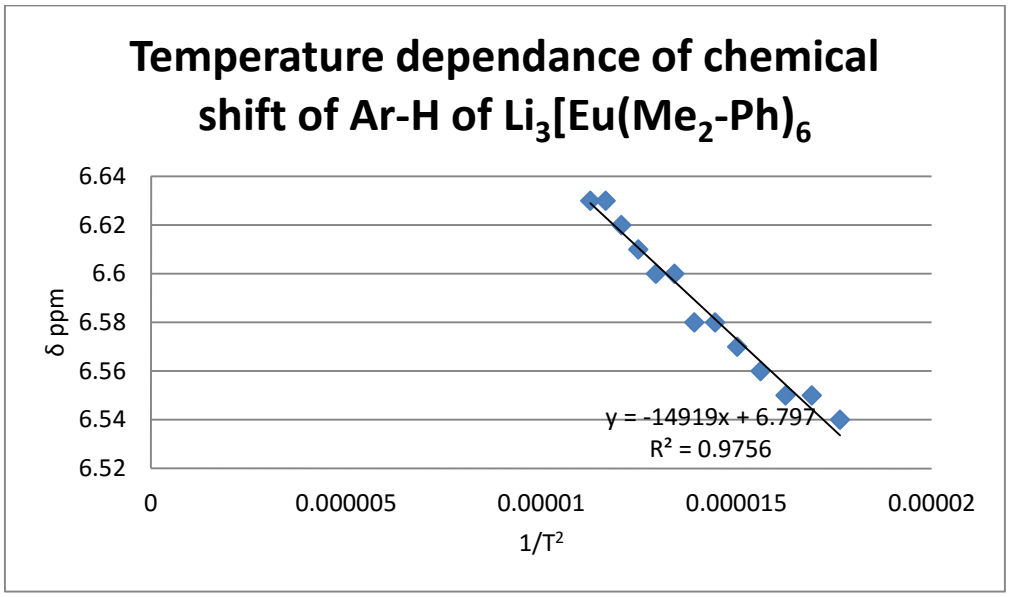

Figure 4.67: Temperature dependence of aromatic ^{1}H of $Li_3[Eu(Me_2\text{-}Ph)_6]$

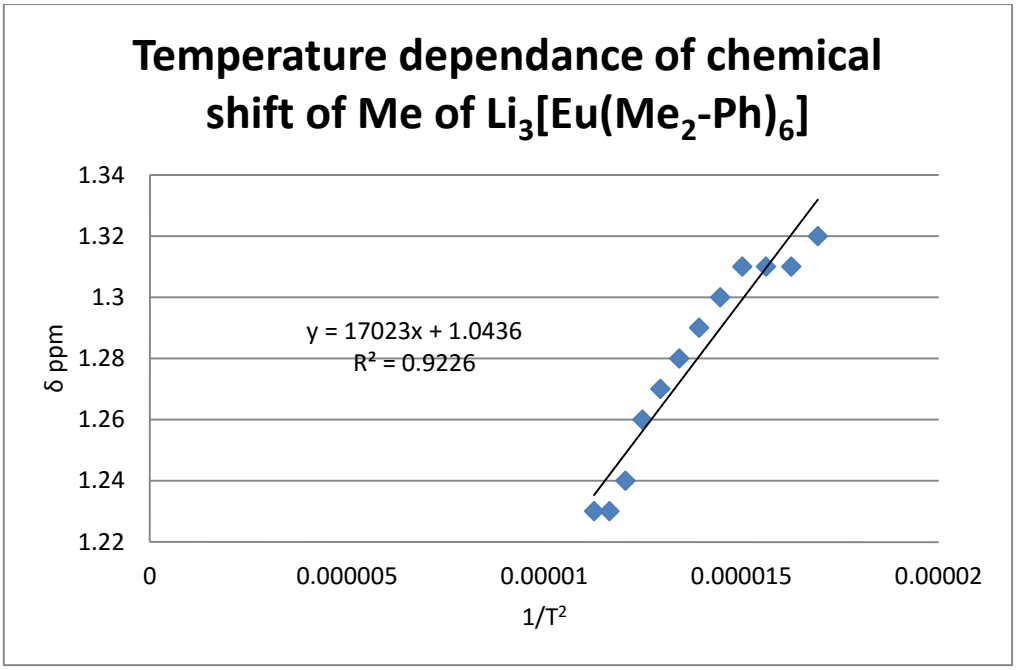

Figure 4.68: Temperature dependence of the methyl ^{1}H of $Li_3[Eu(Me_2\text{-}Ph)_6]$

The temperature dependence of the chemical shifts in the complex are examples of pseudocontact shifting, with the change in chemical shift increasing as the temperature is decreased. This effect is only observed when the complex has an uneven distribution of f-electrons as we would expect from a europium (III) complex. So the linear progressions demonstrated in figures 4.67 and 4.68 are good evidence of a europium complex forming.

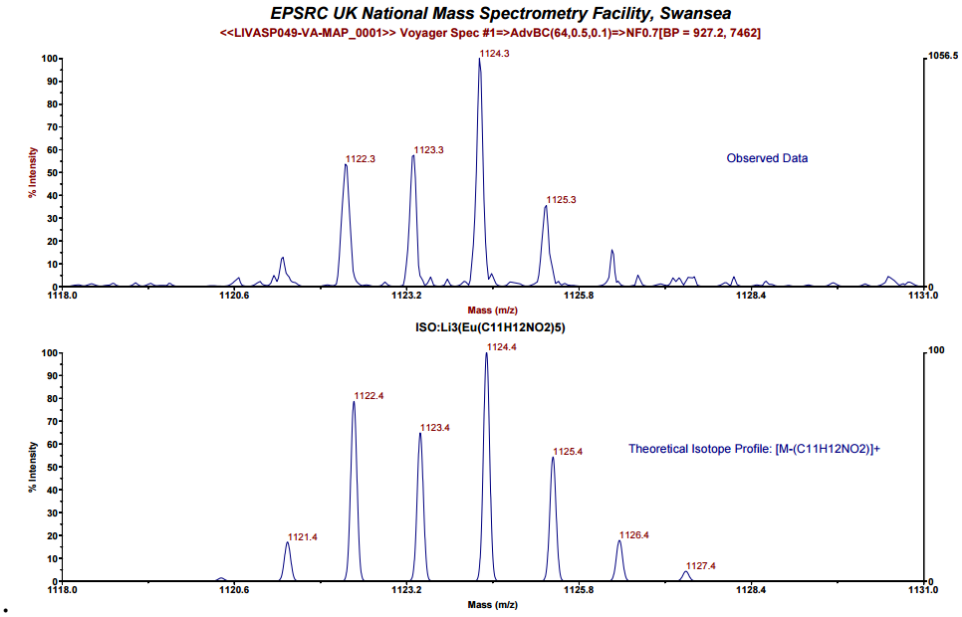

Figure 4.69: Mass spectrum of $Li_3[Eu(Me_2\text{-}Ph)_6$ showing the mass fragment at 1124.4m/z corresponding to $Li_3[Eu(Me_2\text{-}Ph)_5]\pm$

Figure 4.69 shows the anhydrous mass spectrum of $Li_3[Eu(Me_2\text{-}Ph)_6]$. As for the yttrium analogue the favoured mass fragment is $Li_3[Eu(Me_2\text{-}Ph)_5]^{\pm}$ at 1124.4m/z possessing the characteristic isotopic splitting pattern expected for this complex.

Table 4.7: Elemental Analysis results for $Li_3[Eu(Me_2\text{-}Ph)_6]$

	$Li_3[Eu(Me_2\text{-}Ph)_6]$ Calculated	$Li_3[Eu(Me_2\text{-}Ph)_6]$ Found
Carbon (%)	60.25	60.16
Hydrogen (%)	5.52	5.46
Nitrogen (%)	6.39	6.40
C:N	9.43	9.4

Table 4.7 shows the anhydrous elemental analysis results for $Li_3[Eu(Me_2\text{-}Ph)_6]$. There is a good correlation between the calculated and found values for this complex, deviating by 0.09% in carbon, 0.06% in hydrogen and 0.01% in nitrogen.

The ^1H NMR results coupled with the anhydrous mass spectrum and elemental analysis data strongly support the formation of the complex as proposed as $Li_3[Eu(Me_2\text{-}Ph)_6]$.

4.5 Conclusion

A range of rare earth heterobimetallic complexes with oxazoline ligands have been successfully synthesised and characterised. Both $M[Ln(Ligand)_4]$ and $M_3[Ln(Ligand)_6]$ complexes have been produced. The $M_3[Ln(Ligand)_6]$ complexes are of particular interest due to their similarity to Shibasaki's BINOL complexes.

During the course of this study a number of important trends have been identified. For example 4 ligand complexes of the general form $M[Ln(L)_4]$ were only stable for the substituted phenolic ligands Me_2-MePh or ^{i}Pr-MePh. However, 6 ligand complexes, of the general form $M_3[Ln(L)_6]$, were only stable for the unsubstituted phenolic ligands Me_2-Ph or ^{i}Pr-Ph. This was believed to be due to steric factors and was exemplified by the isolation of single crystals of 6 ligand complex from a bulk solution of 4 ligand complex. This proved to be the case for both modes of synthesis.

Only one complex showed a molecular mass ion in mass spectroscopy under anhydrous conditions, $Li_3[Y(^i Pr\text{-}Ph)_6]$, which showed a mass peak at 1333.52 m/z (vs calculated 1334.57 m/z) using positive electrospray with a characteristic isotopic splitting pattern (Fig. 4.47).

All other lithium-rare earth complexes showed mass fragments, with the achiral 6 ligand complexes showing a tendency to lose a ligand to form $Li_3[Ln(Ligand)_5]$ (Fig. 4.37 and Fig 4.55). These trends held for both yttrium (Fig. 4.37) and europium (Fig. 4.55), but whether this

shows something about the chemistry of these complexes or whether this was simply an artefact of the analysis technique is difficult to determine.

Catalytic Reactions

This chapter will detail examples of the catalytic utility of rare earths. This will then focus on the use of rare earth heterobimetallic complexes in the nitroaldol reaction and demonstrate the structural diversity of these complexes. This will then be followed by a discussion of the results of my research.

5. Introduction to Catalytic Reactions

5.1 Catalysis by rare earth complexes

The rare earths are a number of elements that possess a set of characteristics that make them uniquely suited for Lewis acid catalysis. These factors include: large ionic radii which allows for bulky substrate binding, the electrostatic nature of their bonds with ligands and a high oxidation state (+3). The electrostatic bonding makes metal to ligand bonds highly fluxional and labile. This in turn allows for a high rate of catalytic turnover, meaning high yields can often be achieved with relatively low catalyst loading.

The first examples of enantioselective rare earth catalysts were NMR shift reagents. This can largely be traced back to the fact that many of the characteristics required for an effective NMR shift reagent, such as large ionic radii a are the same as those necessary for an effective asymmetric catalyst. This was first demonstrated for $Eu(fod)_3$, one of the most popular NMR shift reagents, used in the production of dihydropyrans from aldehydes (Fig. 5.1). [117,74]

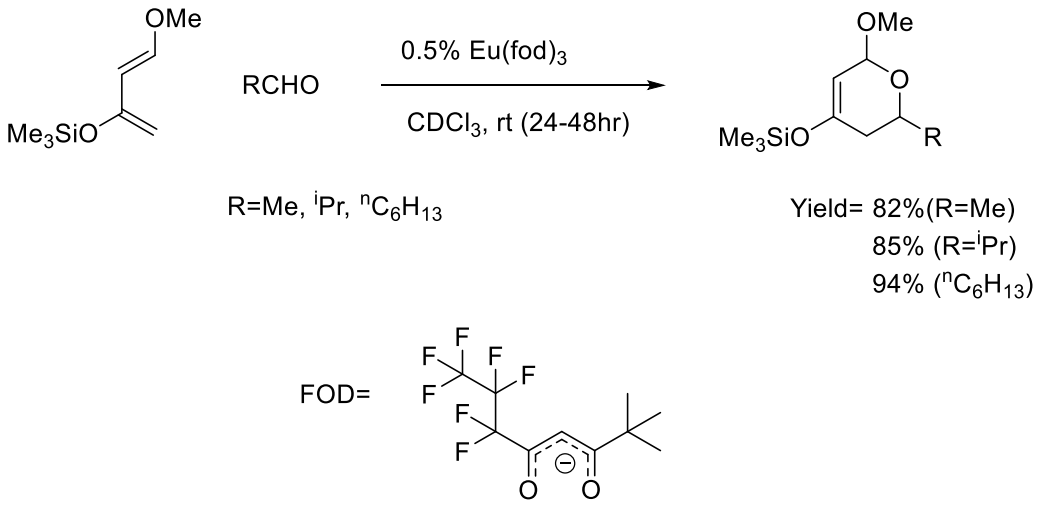

Figure 5.1: Diels-Alder reaction using $Eu(fod)_3$

5.2 The Nitroaldol (Henry) Reaction

The nitroaldol, or Henry reaction, is a base-catalysed C-C bond forming reaction between nitroalkanes and aldehydes or ketones (Fig. 5.2).[7] First discovered by L. Henry in 1895 the reaction, with mechanistic similarities to the aldol reaction discovered 23 years earlier, is a useful technique in organic chemistry due to the synthetic utility of the products (Fig. 5.4).[118] This is particularly evident in pharmaceuticals with the β-blocker (*S*)-propanolol, the HIV inhibitor Amprenavir and in the construction of anthracycline antibiotics all relying on nitroaldol adducts in their synthesis. [119,118]

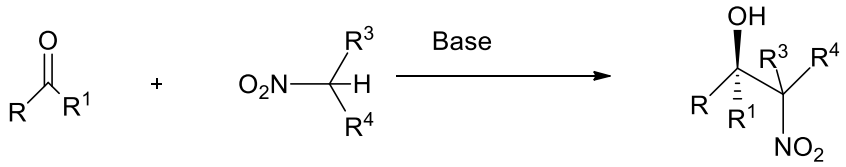

Figure 5.2: Generic Henry Reaction

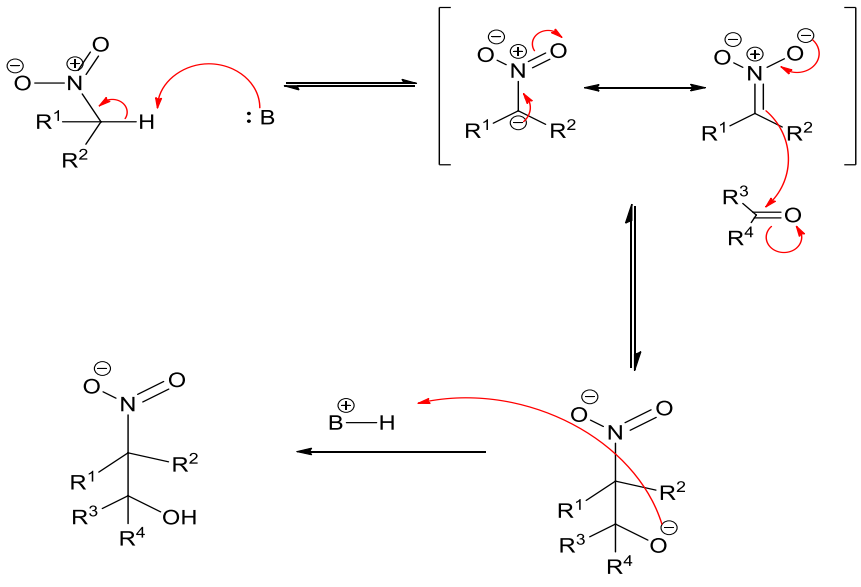

Figure 5.3: General Mechanism of the Henry Reaction

Traditionally, the reaction is carried out using a basic catalyst to deprotonate the nitroalkane to initiate the reaction (Fig. 5.3). Due to the reversibility of several steps in the reaction the reaction produces a mixture of enantiomers and diastereoisomers.[120]

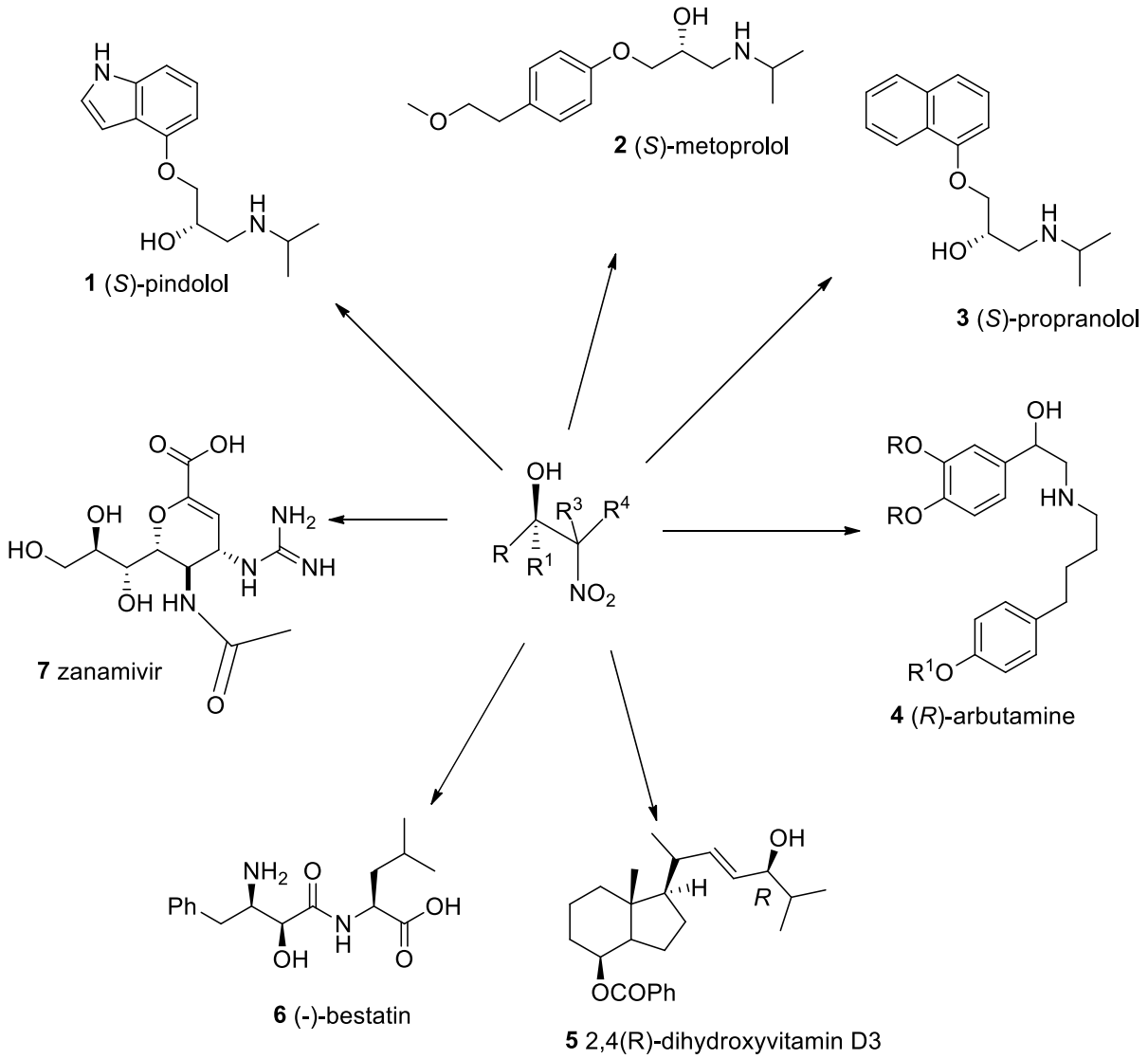

Figure 5.4: Pharmaceuticals synthesised via a nitroalcohol intermediate[118]

The reaction has undergone several modifications over the years to improve selectivity including high pressure and solvent free systems aimed at improving regio- and chemoselectivity, and the use of chiral metal catalysts to induce enantio- or diastereoselectivity.[7]

5.3 Development of the Henry Reaction Using Enantioselective Catalysts

The nitroaldol reaction has under gone a variety of different modifications: organic bases, inorganic bases, quaternary ammonium salts, protic solvents, aprotic solvents and solvent-less conditions.[118] Indeed the types of conditions that are employed often relate to the nature of the substrates, i.e. their functionality, solubility and the ease of deprotonation.

Considerable effort has been directed at developing asymmetric catalysts for the nitroaldol reaction as this coupled with a ready reduction of the corresponding nitroalcohol product, represents an efficient route to optically enriched amino alcohols. One of the earliest examples of this was provided by Shibasaki et al. in 1992 (Fig. 5.5). Here they describe the use of a mixture of $La_3(O^tBu)_9$ with (*S*)-binaphthol in THF, with LiCl (2 mol equiv. to La) and water (10 mol equiv. to La) which produced enantiomeric excesses between 71-90%.[81, 79]

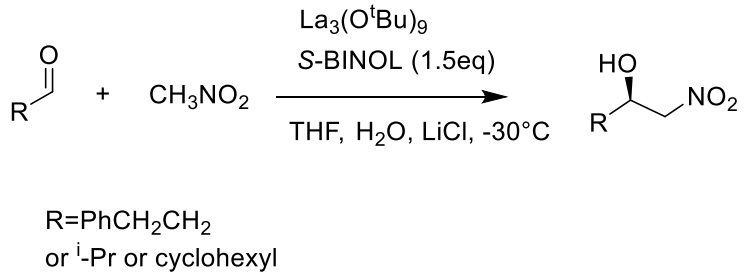

Figure 5.5: Nitroaldol reaction investigated by Shibasaki (1992)[79]

It was found that the addition of LiCl produced higher ee's and that water both increased the rate of reaction and the enantiomeric selectivity by as much as 20% when using isobutyraldehyde. [79]

In 1996 Shibasaki et al reported the efficient reaction of nitromethane with hydrocinnamaldehyde (Fig. 5.6).[121]

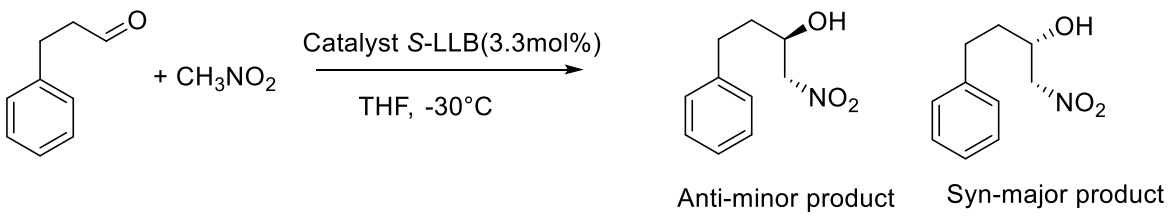

Figure 5.6: Nitroaldol reaction of hydrocinnamaldehyde investigated by Shibasaki (1996)[121]

The catalyst (*S*-LLB) represents a $Li_3[La(Binol)_3]$ complex (Fig. 5.7). The catalyst was formed *in-situ* by the addition much as for the earlier example. This initially achieved 39% ee, further investigation by the group led to improvement. It was eventually discovered that the use of sterically more bulky BINOL ligands provided both the best ee's and yields. The (tri-alkylsilyl)ethynyl derivatives were particularly effective giving an ee of 88% and yields of 85%, with a high degree of syn-selectivity (Fig. 5.7).

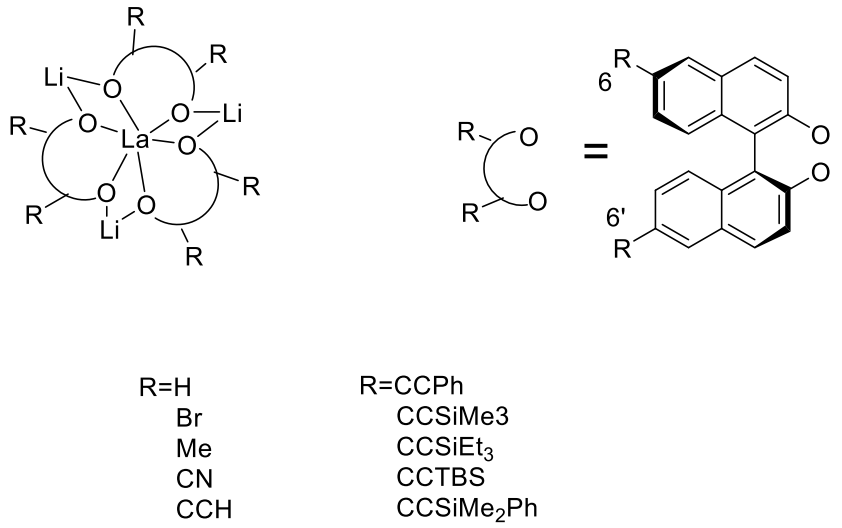

Figure 5.7: Catalyst used by Shibasaki et al. during their investigation of the nitroaldol reaction of hydrocinnamaldehyde[121]

Shibasaki used the lanthanide binaphtholate complexes in the synthesis of (*S*)-metoprolol with a chemical yield of 88%. This reaction proceeded through a nitroalcohol intermediate that was synthesised with a chemical yield of 76% and an ee of 92% (Fig. 5.8).

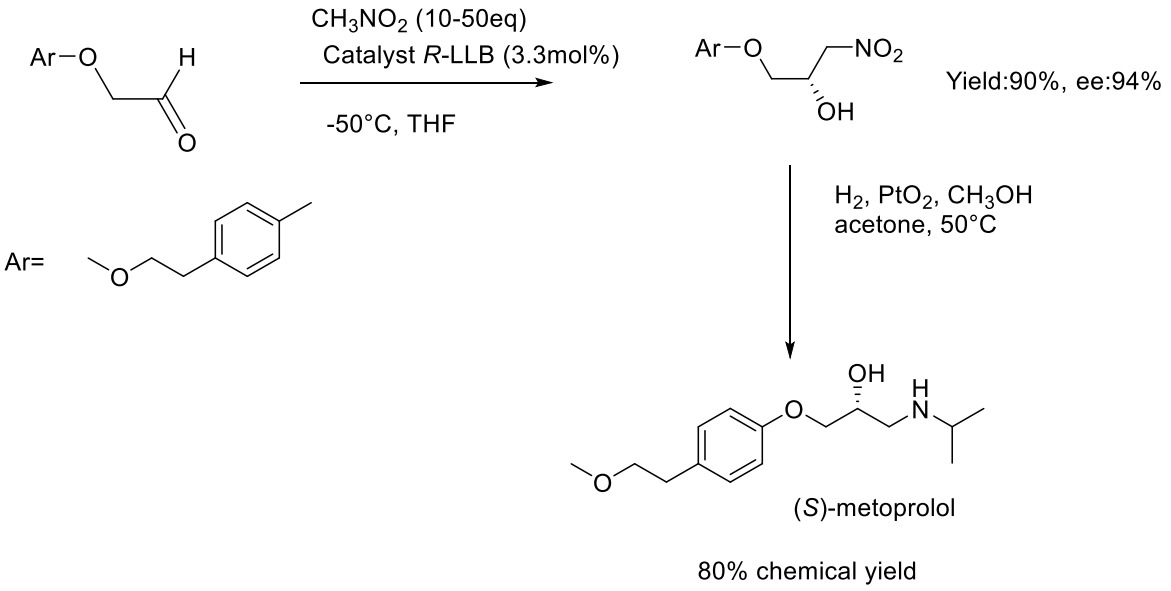

Figure 5.8: Synthesis of (*S*)-metoprolol[118]

The asymmetric synthesis of (*R*)-arbutamine reported by Shibasaki proceeds by reaction of an aldehyde with nitromethane in the presence of a samarium (*S*)-BINOL complex, water and n-butyllithium as the lithium source. This mixture was prepared in THF and immediately used in the reaction by addition of the aldehyde followed by an equivalent of nitromethane. This produced the aminoalcohol in 93% yield and 92% ee (Fig. 5.9).[118]

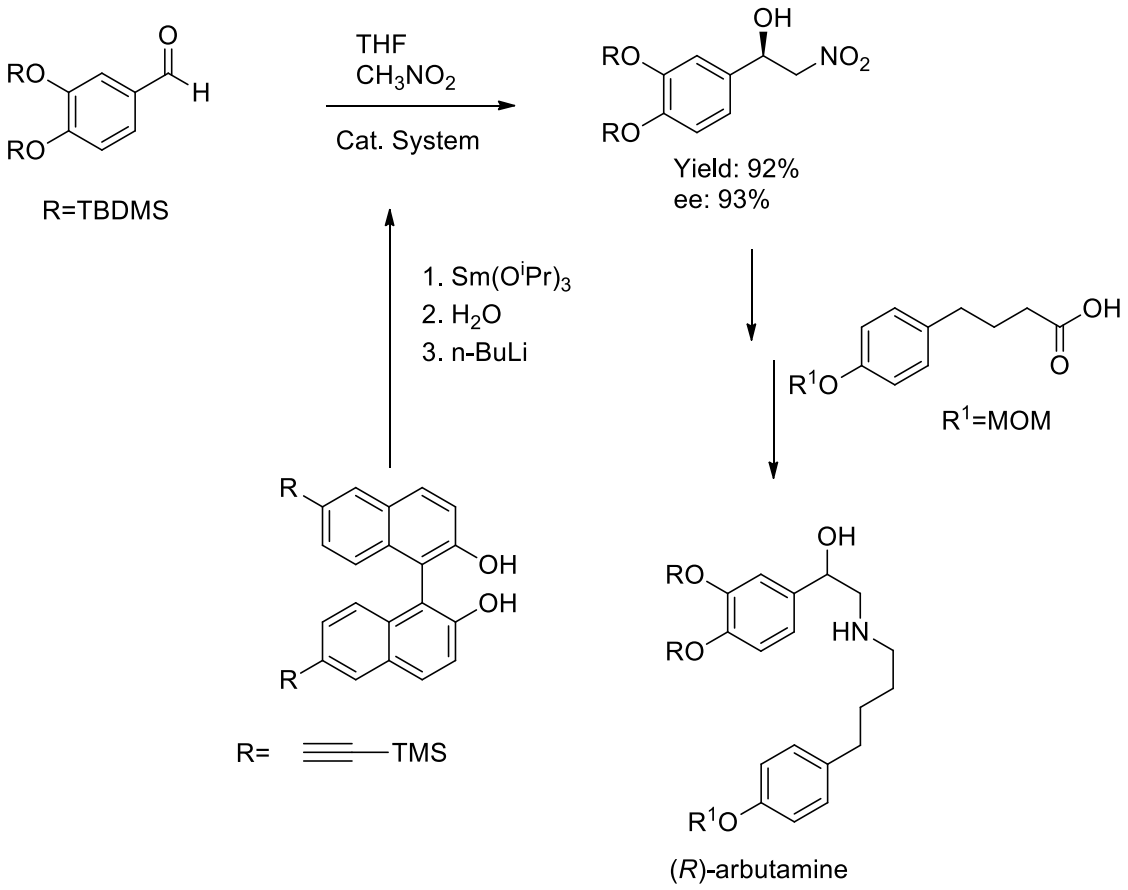

Figure 5.9: Synthesis of (*R*)-arbutamine[86]

(S)-Pindolol was synthesised by Shibasaki, starting from the commercially available 4-hydroxyindole. Treatment of the indole with 3-chloro-1,3-propanediol followed by periodate cleavage of the intermediate diol ether provided the aldehyde. This was condensed with nitromethane in the presence of a lanthanum-lithium (*R*)-BINOL catalyst (10mol%) to afford the nitroalcohol in 92% ee and 76% yield (Fig. 5.10).[86]

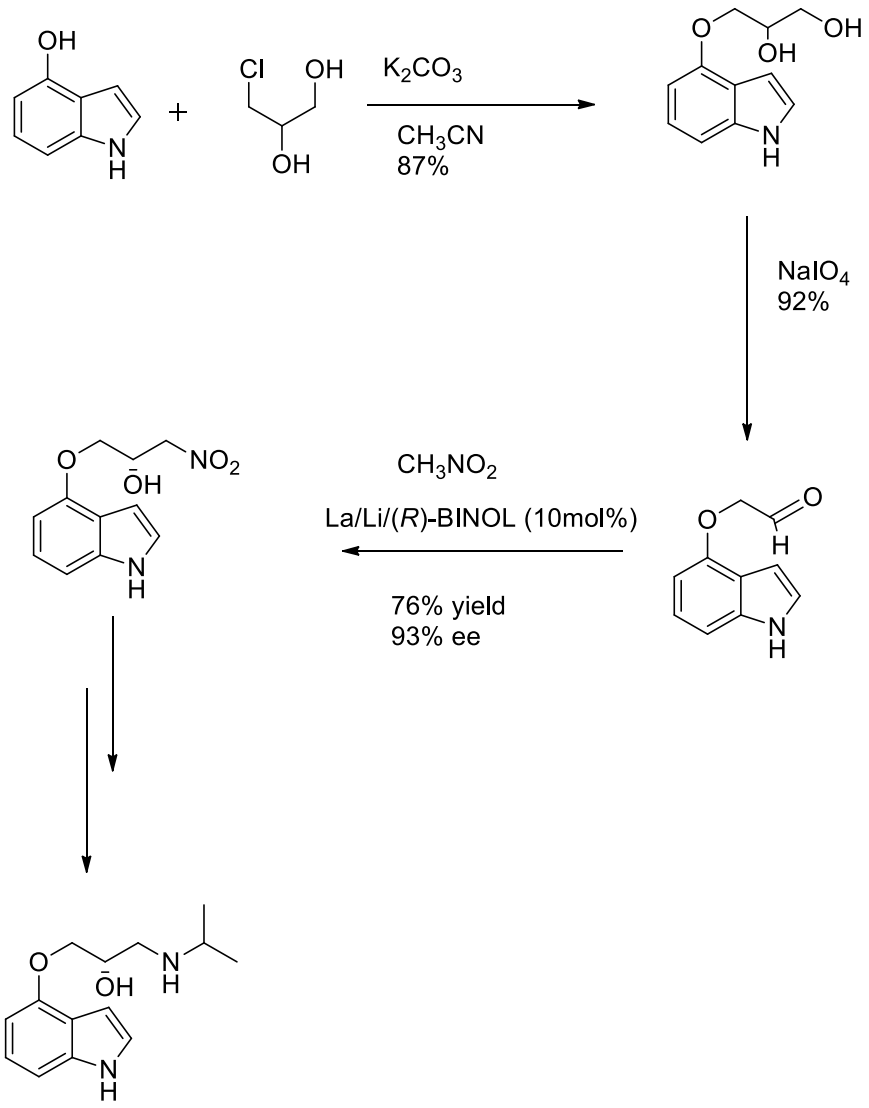

Figure 5.10: Synthesis of (*S*)-pindolol[119]

The lanthanum-(*R*)-binaphthol complex was used by Shibasaki et al. in the synthesis of (*S*)-propanolol. The overall process employed a mixture of an α-naphthol-derived aldehyde, nitromethane, $LaCl_3.H_2O$, dilithium (*R*)-(+)-binaphthoxide, sodium *tert*-butoxide and H_2O in THF. This produced the nitroaldol adduct in 80% yield, with 93% ee (Fig. 5.11).

Reduction/alkylation of the nitroalcohol function, through the aminoalcohol, was accomplished by hydrogenation over platinum oxide to give (*S*)-propanolol.

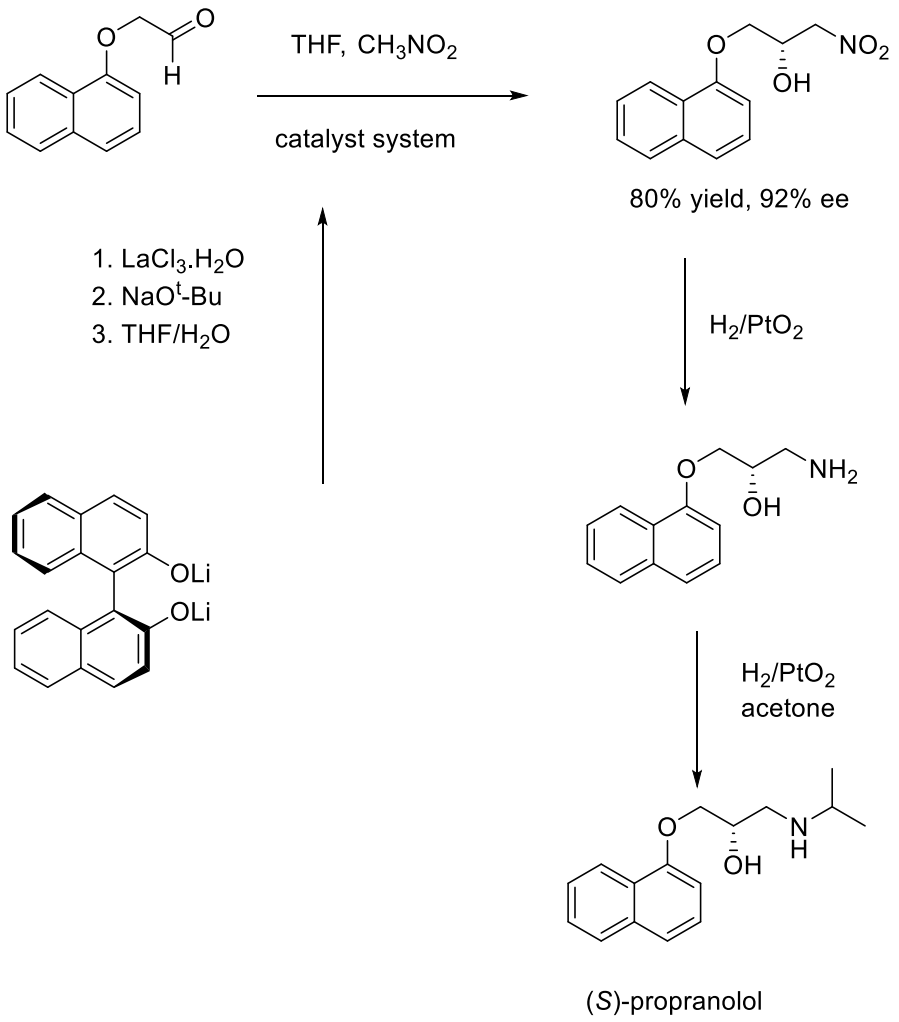

Figure 5.11: (*S*)-propranolol synthesis[119]

The use of a Na Nd heterobimetallic complex has been demonstrated by Shibasaki in the synthesis of Zanamivir, a neuraminidase inhibitor. The synthetic route employs a nitroaldol reaction as one of its key steps. The reaction (Fig. 5.12) was efficiently catalysed with a 71% yield and a 94% ee (anti) with an anti/syn=10:1.[122]

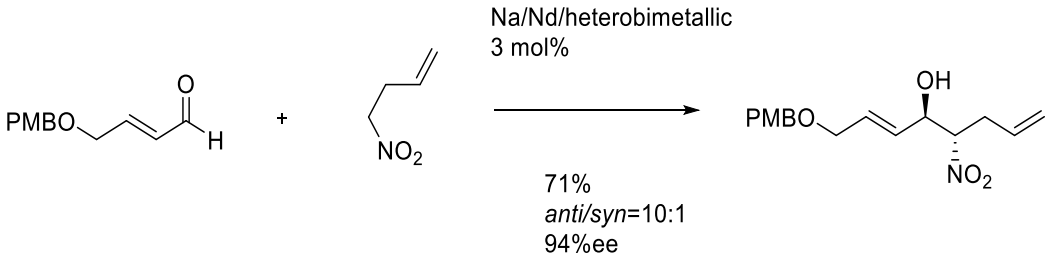

Figure 5.12: Key Henry reaction step during the synthesis of Zanamivir[122]

The catalyst was synthesised by mixing the (*R*) form of the ligand with $Nd_5O(O^iPr)_{13}$ and NaHMDS in a 2:1:2 ratio in the presence of nitroethane; this produced a white suspension which was centrifuged to isolate the active catalyst (Fig. 5.13).

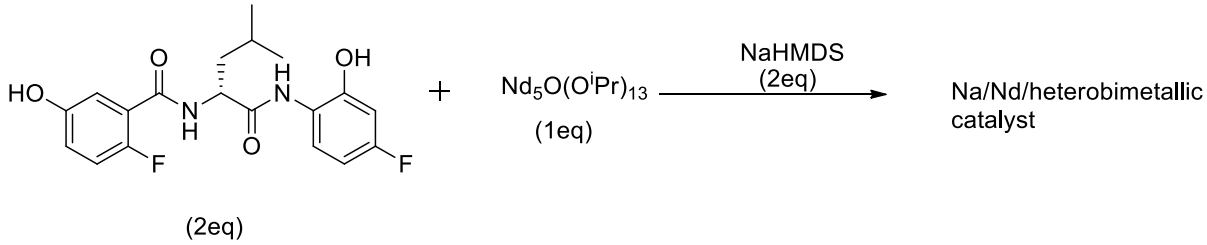

Figure 5.13: Synthesis of the catalyst used in the synthesis of Zanamivir[122]

A lanthanum/potassium (*S*)-BINOL complex was used to produce the 1a, 2,4R-dihydroxyvitamin D3 intermediate shown in figure 5.14. This was done stereoselectively. The reaction gave yields of 60-70% of the nitroalcohol with *R/S* ratios ranging from 92:8 to 94:6 (Fig. 5.14).[123]

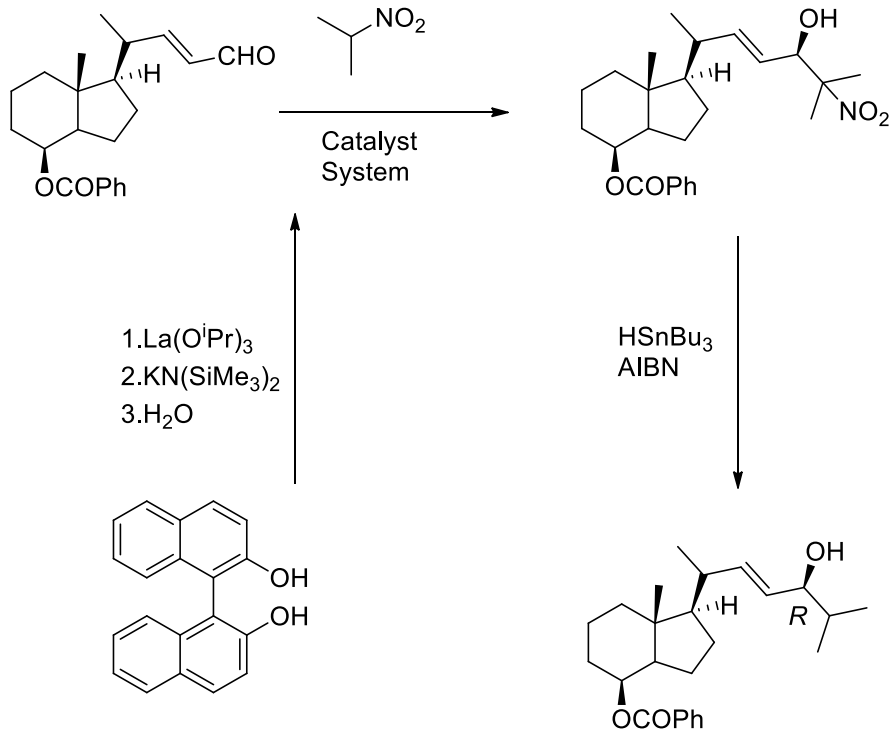

Figure 5.14: Synthesis of α,24(R)-dihydroxyvitamin D3[123]

Barua et al. employed the Shibasaki catalysts, i.e. La/Li/(*R*)-BINOL in their synthesis of (-)-bestatin, which produces the key nitroalcohol intermediate in 81% yield and 93% ee. The reaction was conducted at -50°C using a 10ml% catalytic loading of the La (*R*)-BINOL catalyst (Fig. 5.15).[124]

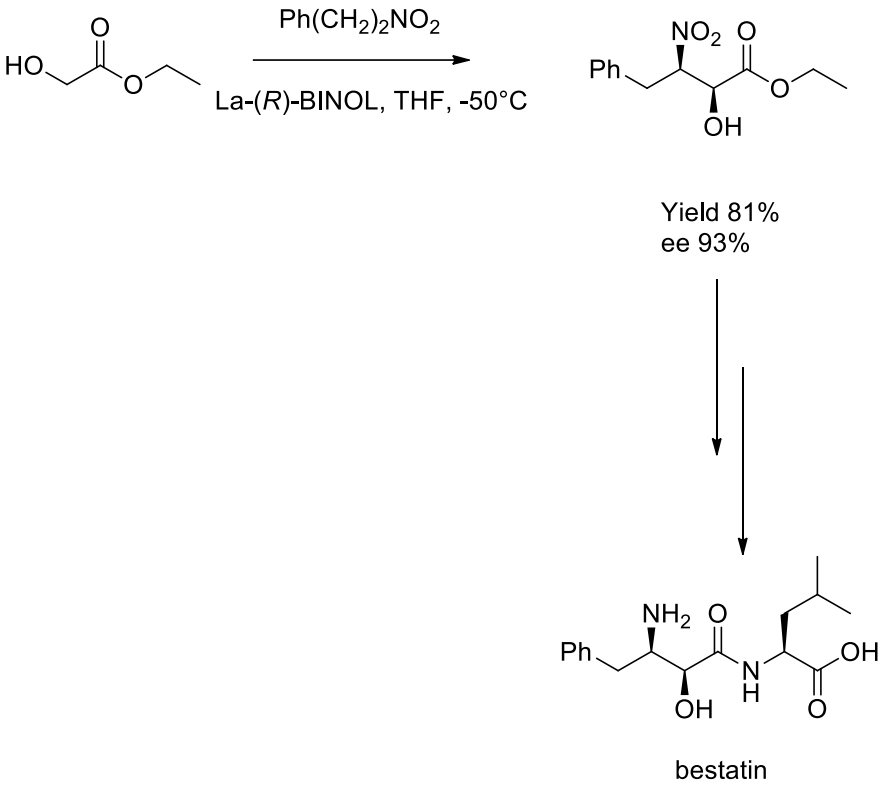

Figure 5.15: Synthesis of bestatin[124]

Formation of the nitroalcohol product was followed by protection of α-OH, followed by reduction over palladium on charcoal. This in turn was followed by BOC protection of the amine. The reaction then proceeded by addition of L-leucine as the benzyl ester followed by reduction to the carboxylic acid and finally cleavage of the protecting groups to yield (-)-bestatin (Fig. 5.15).

The most common example of the use of the lanthanide/alkali metal catalysis involves the use of a chiral BINOL ligand. Additionally the examples using lanthanum and lithium are far more numerous than those with different combinations of metal centres. It could be surmised that the combination of lanthanum and lithium is a particularly effective catalyst.

Water has proven crucial to many of the nitroaldol reactions catalysed by rare earth/alkali metal complexes. This was seen in one of the earliest examples of Shibasaki catalysts in the nitroaldol reaction and was further demonstrated during Shibasaki's testing of a sodium/neodymium complex.[125]

The addition of 9mol% of water to the reactions illustrated in figure 5.16 results in an increase in ee from 38% without water to 43% with water.[125]

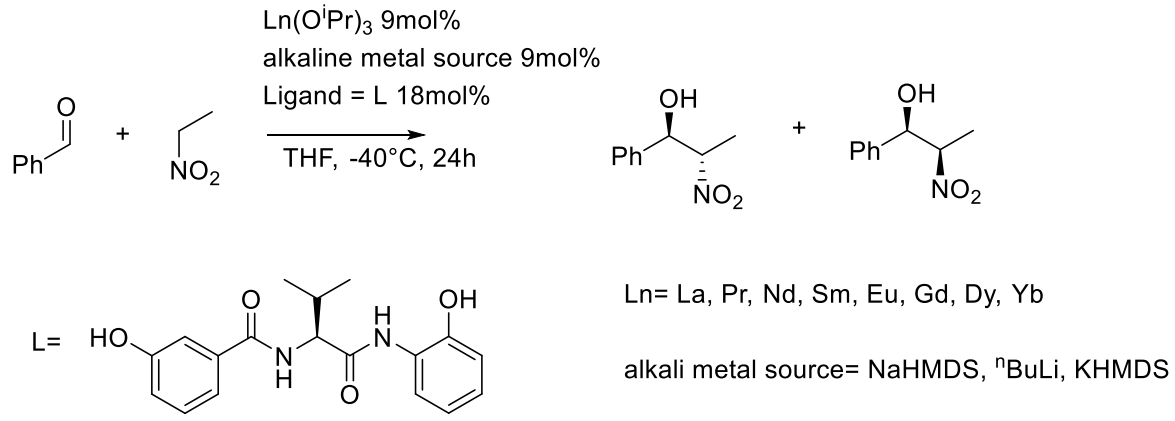

Figure 5.16:Nitroaldol reaction used by Shibasaki to demonstrate a new sodium/neodymium catalyst[125]

This result was in line with previous results by Shibasaki which noted an increase in both reaction rate and enantioselectivity (by ~20%) when 10mol% of water was used in the reaction.[79]

By varying the combination of rare earth/alkali metal/ligand and by taking into account the number of lanthanides available, a truly diverse range of catalysts can be produced based around this simple motif.[80] This effectively means a large number of potential substrates can

be efficiently catalysed, with tailoring of the catalyst possible by varying any number of the components. This fact coupled with the importance of the nitroaldol reaction in general makes the research of this class of catalysts interesting if not potentially crucial.

5.4 Research Aims

The aim of this section is to test the complexes I produced for catalytic potential, specifically in the synthetically important and relatively well understood Henry reaction. This is to explore any similarities between the work of Shibasaki et al. with whom our catalysts share a structural motif and thus illustrate the effects of catalyst structure on catalytic activity.

6. Discussion of Catalytic Reactions

6.1 Effect of varying the components of the catalyst

We chose to investigate the reaction between nitromethane and benzaldehyde. Figure 6.1 shows a general reaction scheme for the catalysis of the nitroaldol reaction. All reactions were carried out in THF and the optimum conditions for catalysis were room temperature, under atmospheric conditions, for approximately 16 hours. The reaction was sufficiently homogenous that stirring was not necessary.

Two work-up procedures were trialled during this study. The first procedure involved quenching the reaction with 2M HCl, followed by extraction of the product into diethyl ether. The organic phase was dried with magnesium sulfate, filtered and the solvent removed in vacuo to yield crude product. This was subsequently purified by column chromatography using a suitable eluent system.

The second procedure involved the addition of hexane to the crude reaction mixture; it was hoped this would result in the isolation and subsequent recovery of the catalyst. This formed a precipitate which was isolated by filtration and subsequently washed with further hexane before being allowed to dry in air. After this, the work-up proceeded as in the first procedure with the reaction mixture quenched with 2M HCl and the product removed into diethyl ether.

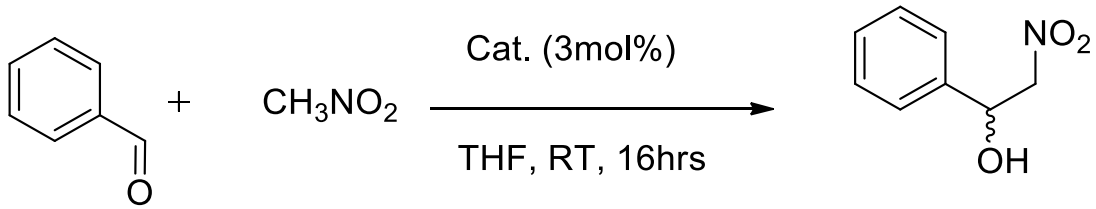

Figure 6.1: Nitroaldol reaction

As mentioned earlier, it was initially thought that the precipitate isolated was recovered catalyst. Analytical data proved inconclusive. Subsequent washing of the precipitate with

additional hexane did result in more of the precipitate dissolving. Furthermore the precipitate failed to catalyse a reaction in subsequent nitroaldol reactions.

As is shown in table 6.1 whenever hexane was added prior to the workup for the catalytic reactions there was a significant drop in product isolated from the reaction. Some of the precipitate eventually did dissolve in hexane after further washings. This improved the amount of product isolated and so it could be speculated that some of the precipitate is product.

Table 6.1: Catalysis of the nitroaldol reaction

Entry	Catalyst	L	Ln	M	Work up conditions	Time reaction seen by in TLC (Minutes)	Isolated Yield (%)
1	$M_3[Ln(L)_6]$	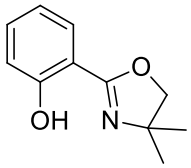	Y	Li	Hexane	30	31%
2	$M_3[Ln(L)_6]$	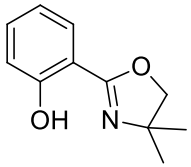	Y	Li	Acid	30	90%
3	$M_3[Ln(L)_6]$	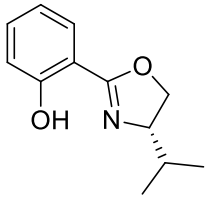	Y	Li	Hexane	30	33%
4	$M_3[Ln(L)_6]$	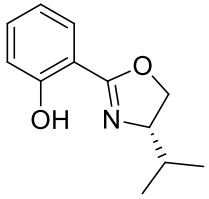	Y	Li	Acid	30	92%
5	$M[Ln(L)_4]$	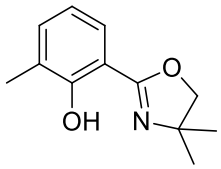	Y	Li	Hexane	30	30%

6	$M[Ln(L)_4]$	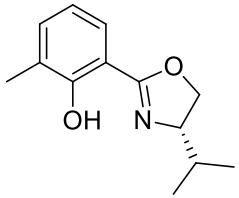	Y	Na	Acid	5	90
7	$M_3[Ln(L)_6]$	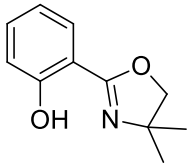	Eu	Li	Hexane	5	30
8	$M_3[Ln(L)_6]$	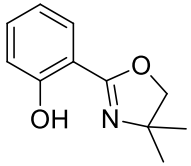	Eu	Li	Acid	5	89
9	$M[Ln(L)_4]$	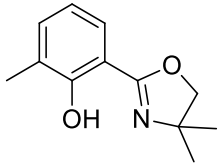	Eu	Li	Acid	5	90
10	$M_3[Ln(L)_6]$	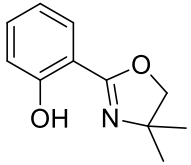	Y	Na	Acid	5	85

As can be seen from table 6.1 a number of different catalysts have been tested for the nitroaldol reaction (general reaction scheme given in Fig. 6.3). These catalysts all have the general formula $M_x[RE(L)_{x+3}]$; where M is an alkali metal, either sodium or lithium; RE is either yttrium or europium and L is an oxazolylphenolate ligand. There are two broad classes of catalyst, a four ligand complex $M_x[RE(L)_{x+3}]$ where x=1 and a six ligand complex $M_x[RE(L)_{x+3}]$ where x=3 (Fig. 6.2)

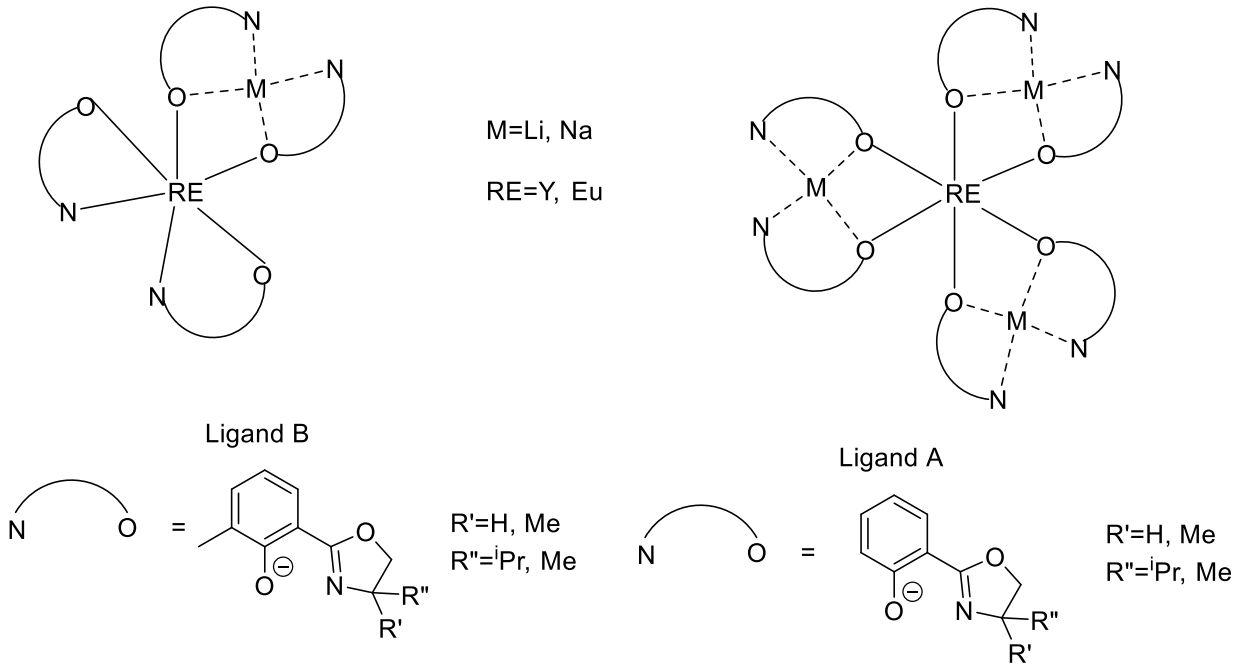

Figure 6.2: General structure of complexes used in this study

By varying the different components of the catalyst, we hoped to demonstrate the effect they each have on various aspects of the reaction and subsequently find the optimum combination of components for this particular reaction.

From table 6.1 there is a noticeable difference in activity (time taken for initial reaction to be seen by TLC). By comparing entries 2 and 7 it can be seen that the europium based catalysts are more active than yttrium based analogues. Similarly, substituting sodium for lithium seems to increase the activity; this can be seen when comparing entries 2 and 10. We believe this induction period to be a result of the formation of an active form of the catalyst. The rate at

which this is formed determines the speed with which an initial reaction is seen. This is evidenced by comparing entries 1 and 7, and 5 and 6. The reaction seems to be insensitive to the choice of ligand, as can be seen from entries 1 and 3 and again for entries 1 and 5. Changing the number of ligands around the metal centre also seemed to have no effect on the reaction as can be seen for entries 1 and 5. However as mentioned earlier due to steric reasons we were unable to synthesis M[Ln(Ligand)$_4$] complexes with ligand A and similarly we were unable to make M_3[Ln(Ligand)$_6$] complexes of ligand B (Fig. 6.2), so it is difficult to make a direct comparison between M_3[Ln(Ligand)$_6$] and M[Ln(Ligand)$_4$] complexes.

.

Table 6.2: Background testing of the nitroaldol reaction of benzaldehyde with nitromethane

Entry	Ligand (0.198 Molar eq)	LiCl/NaCl (0.099 Molar eq)	$Y(OH)_3$ (0.033 Molar eq)	$Y(OTf)_3/Eu(OTf)_3$ (0.033 Molar eq)	Catalyst[a] (0.033 Molar eq)	Benzaldehyde (1 Molar eq)	Nitromethane (1 Molar eq)		Benzoic acid (1 Molar eq)	THF	Reaction (Y/N)
							Non-dry	Dry			
1	✓					✓	✓			THF	N
2							✓		✓	THF	N
3	✓	✓		✓		✓	✓			THF	N
4		✓				✓	✓			THF	N
5				✓		✓	✓			THF	N
6		✓		✓		✓	✓			THF	N
7	✓	✓				✓	✓			THF	N
8	✓			✓		✓	✓			THF	N
9			✓			✓	✓			THF	N
10					✓		✓			THF	N
11					✓	✓				THF	N
12					✓	✓	✓			THF(Dry)	Y(~4%yield)
13					✓	✓	✓			THF	Y
14					✓	✓	✓			THF	Y
15					✓	✓	✓			THF	Y
16					✓	✓		✓		THF(Dry)	N
17[b]					✓	✓	✓			THF	Y
18[c]					✓	✓		✓		THF(Dry)	Y

a-The structure of the catalyst used is shown in figure 6.3, b-catalyst initially stirred in wet THF for 30 minutes, c-the catalyst in this case was purposely hydrated complex

From table 6.2, it can be seen that the individual components of the complexes do not catalyse the reaction either alone or in any combination, e.g. the addition of the ligand to a solution of benzaldehyde and nitromethane in THF produced no reaction.

6.2 Effect of Water

As can be seen from entries 12 and 16 in Table 6.3, one factor that did have a noticeable effect on the reaction was the presence of water. For entry 12 when anhydrous solvents were used along with wet nitromethane there was virtually no reaction. The small amount that did occur has been attributed to a small amount of water present in nitromethane (Fig. 6.3).

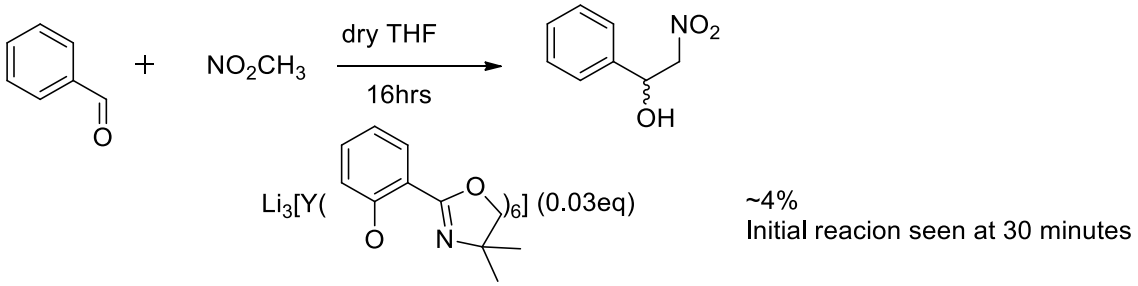

Figure 6.3: Reaction with non-dried nitromethane

Complete exclusion of water, using anhydrous nitromethane, significantly slowed down the rate of reaction with europium-lithium catalysts taking several hours to show initial reaction and the yttrium-lithium catalysts taking longer than a day to show any sign. Even after several days the isolated yields of these anhydrous reactions were small (≤ 4%) (Fig. 6.4).

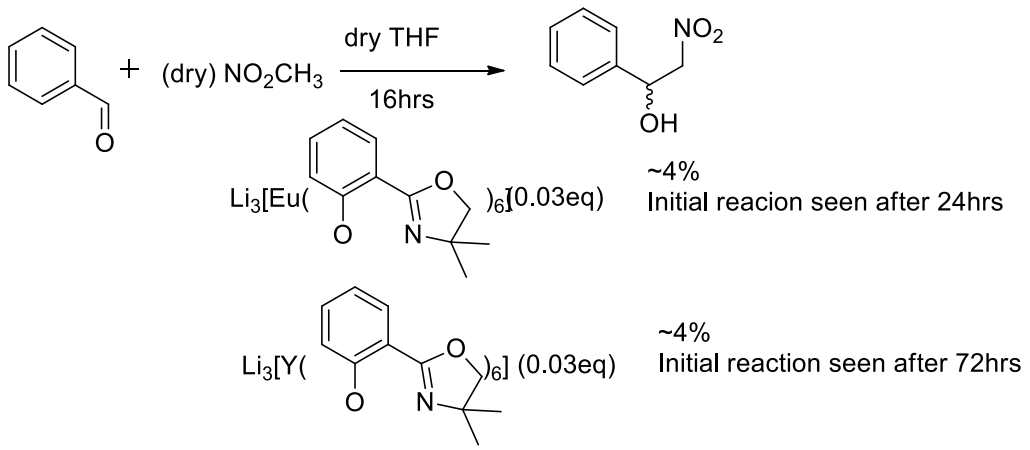

Figure 6.4: Reactions with dried nitromethane

Entry 17, in table 6.2, is of particular interest to the discussion of water's role in the reaction. The catalyst was initially stirred for 30 minutes at room temperature with non-dried THF; this was immediately followed by addition of the reactants. The mixture was then left at room temperature for 5 minutes and a TLC was taken which showed the presence of product (Fig. 6.5).

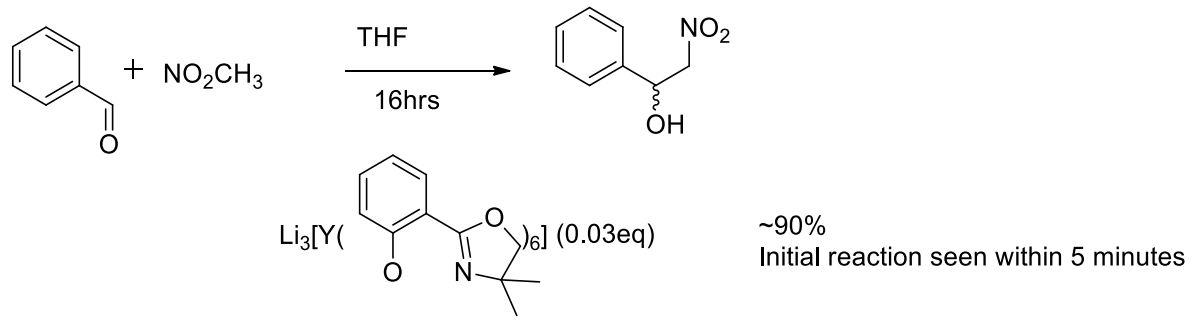

Figure 6.5: Catalyst initially stirred for 30 mins in wet THF

An yttrium centred catalyst was used here, which is usually characterised in this study by slower activity when compared with the europium catalysts. From entry 17, it appears that at least part of this slower activity is due to some reaction with water. We believe this reaction activates the catalyst and that the larger ionic radius of europium allows this active species to be formed faster resulting in the europium centred catalysts displaying greater activity.

These reactions demonstrate the importance of water in the catalytic reaction. However the precise role that water plays is unclear. Water associated with the complex in some way would provide a source of readily available labile protons near to the reaction centre, thereby acting as a proton exchange medium. The differences in activities noted between europium and yttrium catalysts could be explained by the rate at which the two react with water, with the larger europium centred catalyst being the more reactive due to its larger ionic radius. The increased activity of the sodium complexes compared with the lithium analogues could also be explained in a similar manner, i.e. the sodium ion is larger and in order to be incorporated into the complex pushes the ligands further apart. This latter point is evidenced by the difference in alkali metal-oxygen bond lengths (Na-O 2.409Å compared with Li-O 1.935Å) and the distance between nearest phenolic oxygens (O-O 3.124 Å in the sodium/yttrium complex against O-O 2.929 Å in the lithium/yttrium complex).

6.3 Moisture Stability of Rare Earth complexes, $Li_3[Y(Me_2\text{-}Ph)_6]$ and $Li_3[Eu(Me_2\text{-}Ph)_6]$.

During the course of catalytic testing of the complexes in this study, $Li_3[Y(Me_2\text{-}Ph)_6]$ and $Li_3[Eu(Me_2\text{-}Ph)_6]$, a number of test reactions were conducted. As mentioned earlier (Section 6.2) these reactions were run under ambient conditions and so the complexes were exposed to significant moisture. However there seemed to be very little evidence that this caused the complexes to decompose. In fact it was found eliminating water severely inhibited the reaction. We thought that the active species in the reaction might be a hydrated form of the complex and that the complexes must exhibit a degree of moisture stability.

Due to the work up conditions it was impossible to recover the catalyst from the reaction, so a quantity of previously anhydrous complex was recrystallized from wet THF. The complex dissolved readily in the solvent with no sign of decomposition. Petroleum ether (40:60) was

then added, forming a microcrystalline precipitate. This was white in the case of the yttrium complex and slightly yellow in the case of europium.

Mass spectrometry data of these samples proved exactly analogous to what was seen for anhydrous complex, showing a mass fragment peak corresponding to $Li_3[Ln(Ligand)_5]$. This was true for both the yttrium and europium complexes.

Attempts were made to isolate x-ray quality crystals for the hydrated versions of both $Li_3[Y(Me_2\text{-}Ph)_6]$ and $Li_3[Eu(Me_2\text{-}Ph)_6]$. However only crystals of $Li_3[Y(Me_2\text{-}Ph)_6]$ were able to form (Fig. 6.6).

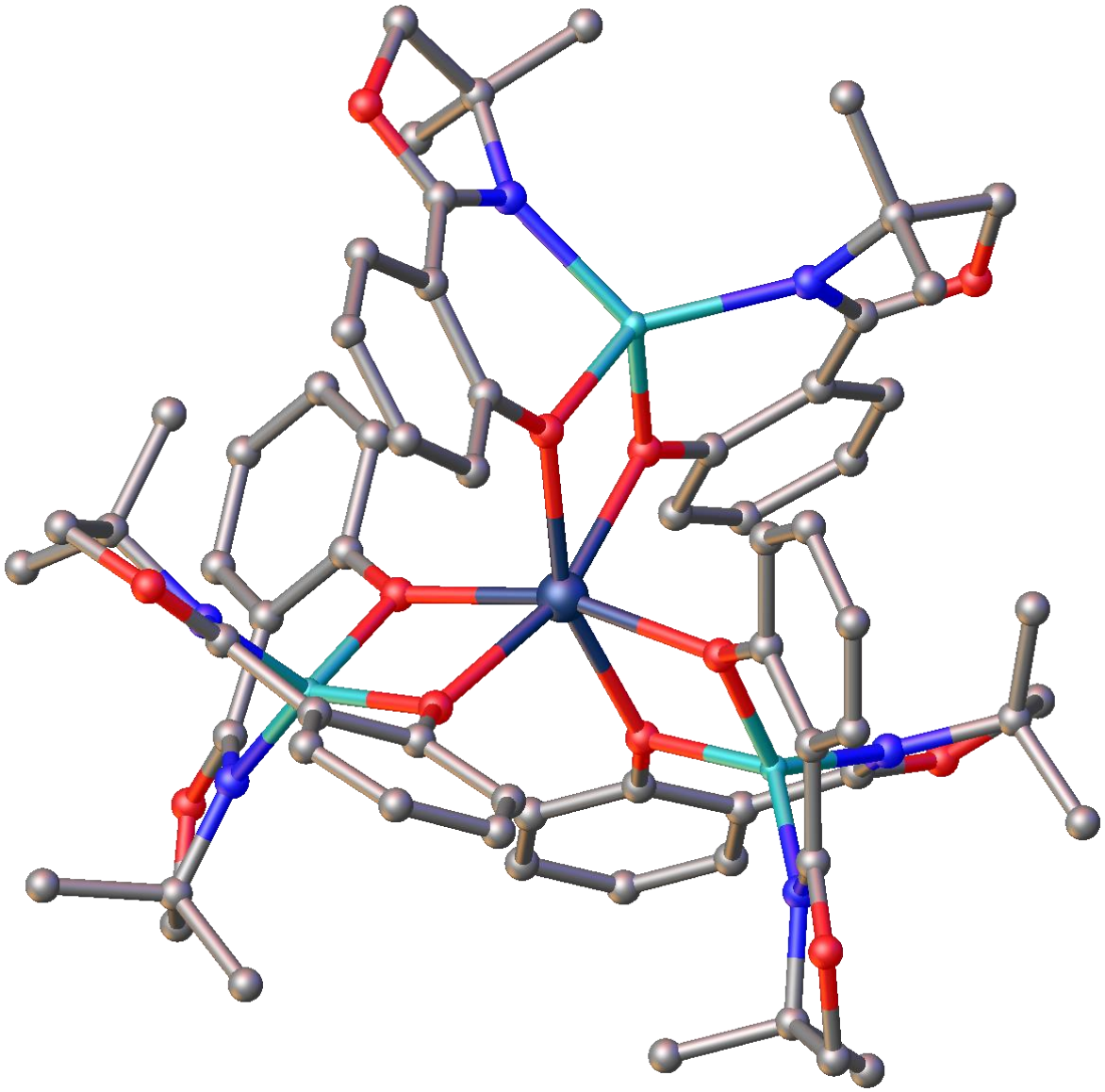

Figure 6.6: Crystal structure of $Li_3[Y(Me_2\text{-}Ph)_6]$ isolated from wet solvents.

The crystal structure of the hydrated $Li_3[Y(Me_2\text{-}Ph)_6]$ is identical to the anhydrous $Li_3[Y(Me_2\text{-}Ph)_6]$ (Fig. 6.7). There appears to be no water co-ordinated to the rare earth centre. Indicating that whatever water's role in the reaction is, it is not to do with formation of a water-complex adduct.

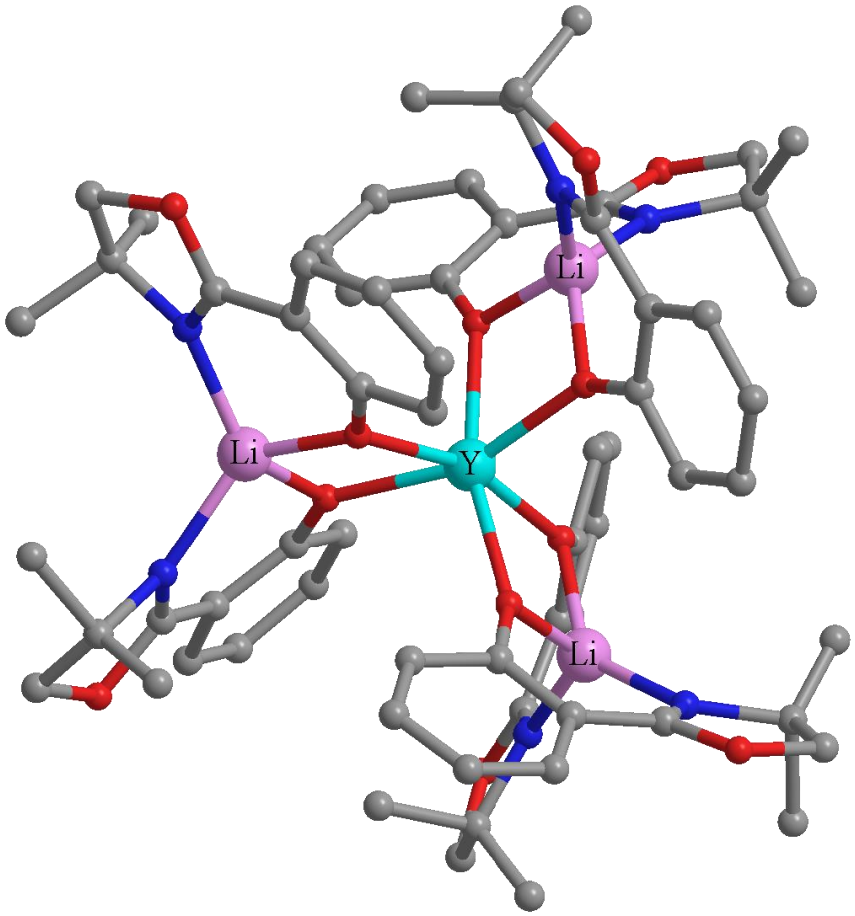

Figure 6.7: Crystal structure of $Li_3[Y(Me_2\text{-}Ph)_6]$ isolated from dry solvents.

^{1}H-NMR data for hydrated complexes also bears close resemblance to that of the anhydrous complex (Fig. 6.8 comparison of hydrated, anhydrous complexes with free ligand). However, the integration of the peak at ~12ppm, associated with phenolic OH, compared against an aromatic ^{1}H, thought to be associated with complex, increase from 6% in the anhydrous complex to 14% in the hydrated complex.

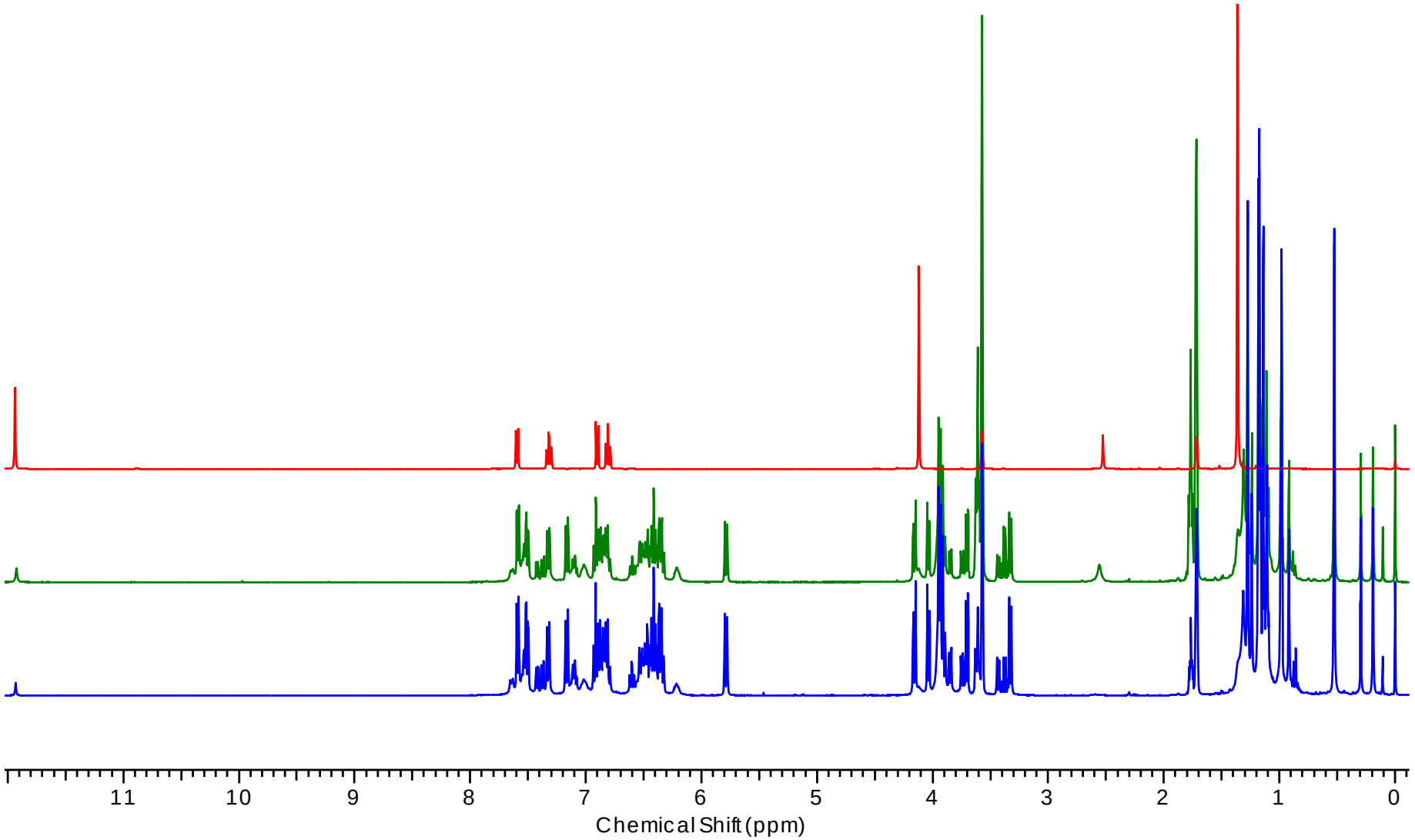

Figure 6.8: ^{1}H NMR spectra of "anhydrous" $Li_3[Y(Me_2\text{-}Ph)]$ (blue) vs "hydrated" complex $Li_3[Y(Me_2\text{-}Ph)_6].X\ H_2O$ (green) vs H-Me_2-Ph (red) (*d*-THF, room temperature).

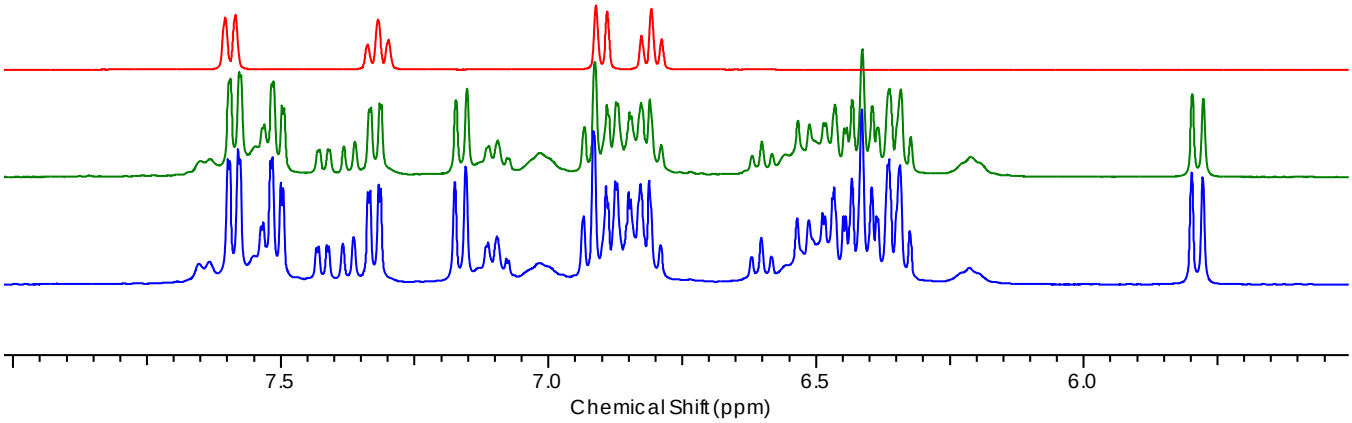

Figure 6.9: Expansion of the aromatic region of the ^{1}H NMR spectra of "anhydrous" $Li_3[Y(Me_2\text{-}Ph)]$ (blue) vs "hydrated" complex $Li_3[Y(Me_2\text{-}Ph)_6].X\ H_2O$ (green) vs H-Me_2-Ph (red) (*d*-THF, room temperature).

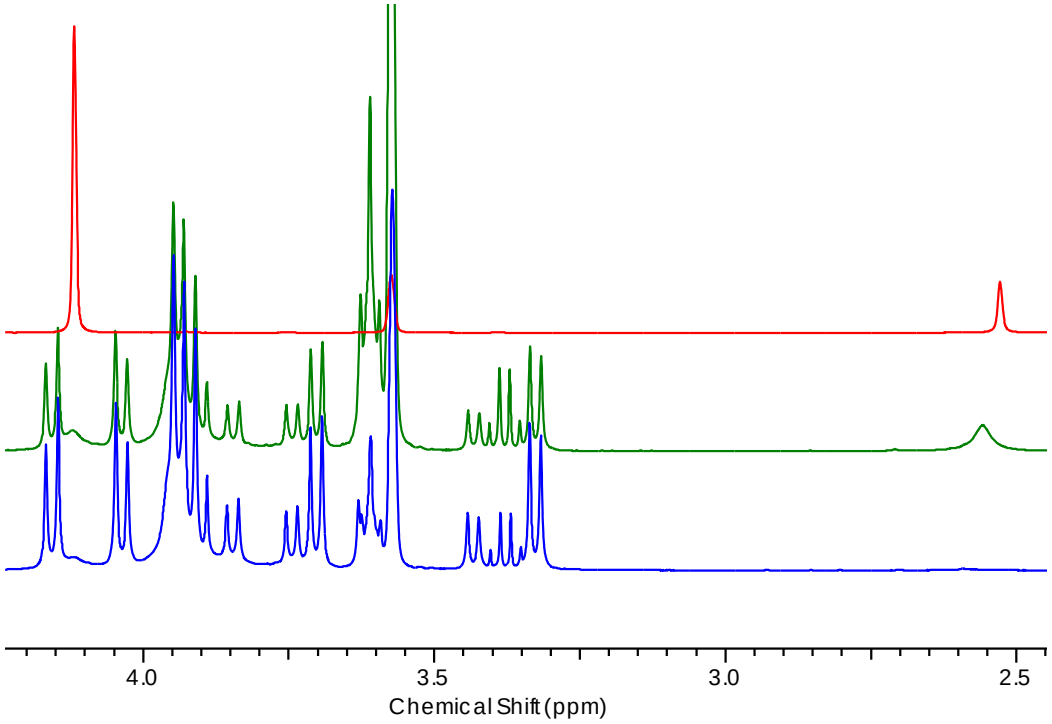

Figure 6.10: Expansion of the region from 4.5-2.5ppm of the ^{1}H NMR spectra of "anhydrous" $Li_3[Y(Me_2\text{-}Ph)]$ (blue) vs "hydrated" complex $Li_3[Y(Me_2\text{-}Ph)_6].X\ H_2O$ (green) vs H-Me_2-Ph (red) (*d*-THF, room temperature).

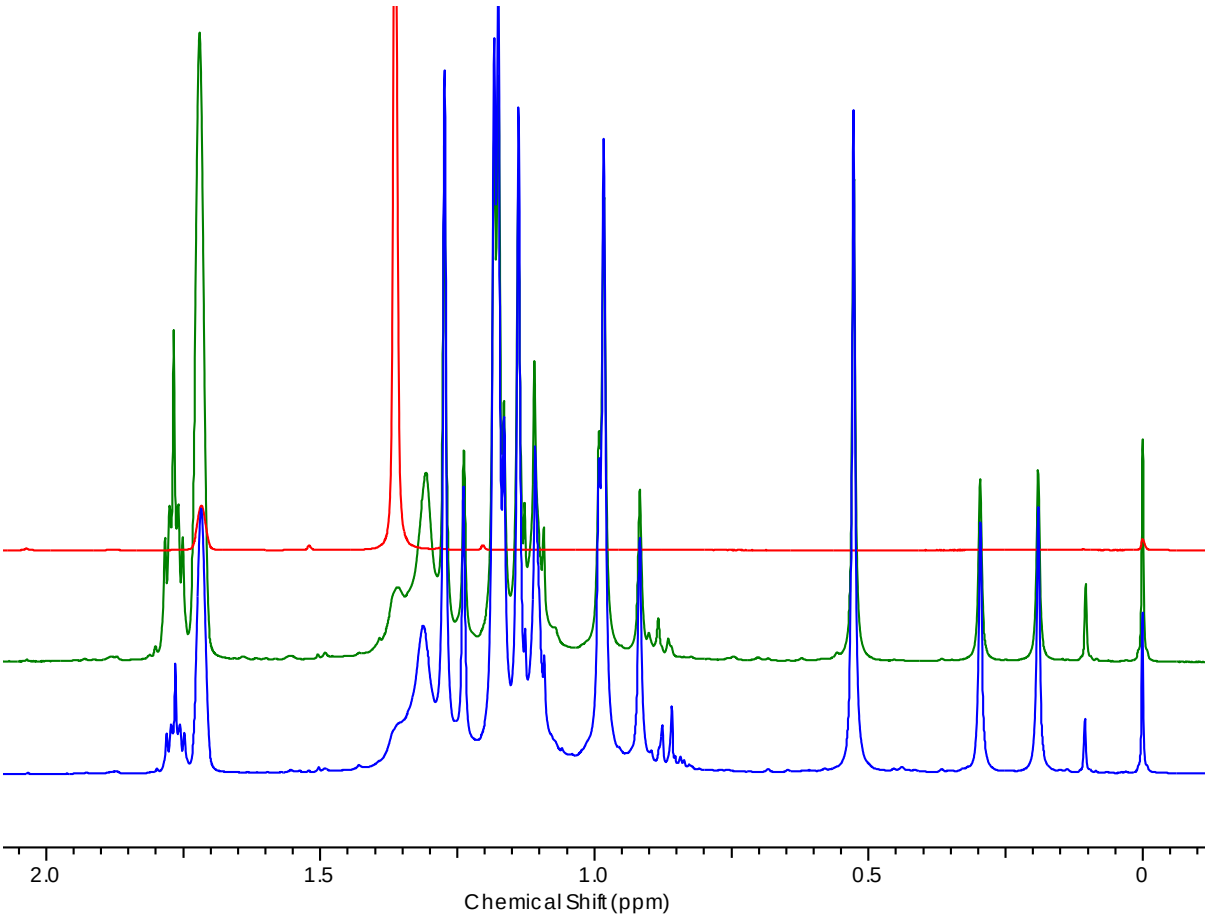

Figure 6.11: Expansion of the region from 2-0ppm of the ^{1}H NMR spectra of "anhydrous" $Li_3[Y(Me_2\text{-}Ph)]$ (blue) vs "hydrated" complex $Li_3[Y(Me_2\text{-}Ph)_6].X\ H_2O$ (green) vs H-Me_2-Ph (red) (*d*-THF, room temperature).

The ^{1}H NMR spectrum of the hydrated europium analogue seems to show a bigger deviation from that of the anhydrous complex (Fig. 6.12). There is clearly shifting in the peaks when compared against the ligand (Fig. 6.12). On closer inspection of the aromatic region (Fig. 6.13) and the region 4.5-2.5ppm (Fig. 6.14) the hydrated complex (green spectrum) shows peaks which correspond closely to those found in the free ligand. The integration of the peak at ~12ppm, associated with phenolic OH, compared against an aromatic ^{1}H increases from 10% in the anhydrous complex to 40% in the hydrated complex. This supports the theory that as the europium complex is the more active species it will be the more moisture sensitive of the complexes. Figure 6.13 shows ^{1}H NMR spectra of "anhydrous" $Li_3[Eu(Me_2\text{-}Ph)_6]$ (blue) vs "hydrated" $Li_3[Eu(Me_2\text{-}Ph)_6].XH_2O$ (green) vs H-Me_2-Ph (red).

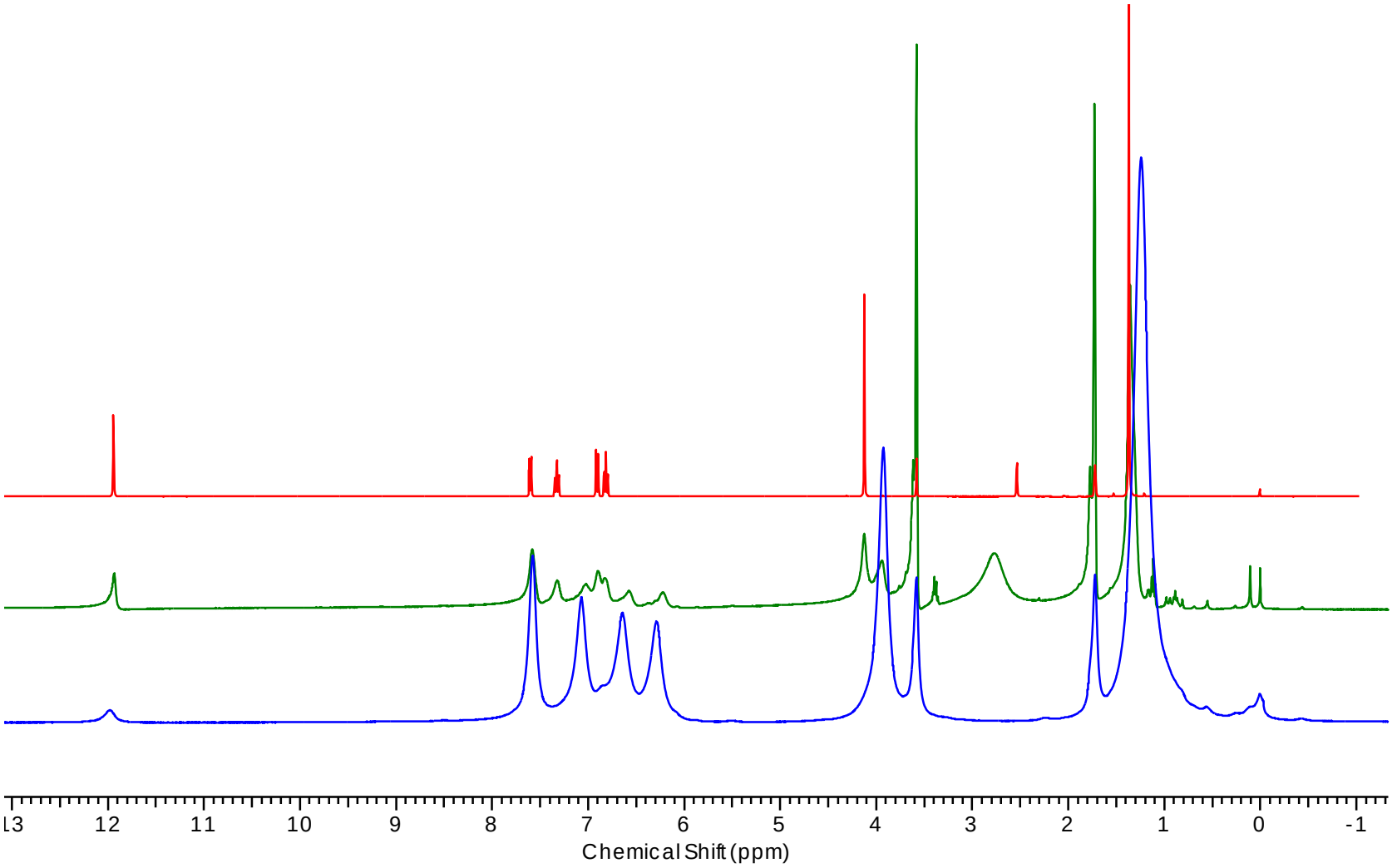

Figure 6.12: ^{1}H NMR spectra of "anhydrous" $Li_3[Eu(Me_2\text{-}Ph)_6]$ (blue) vs "hydrated" $Li_3[Eu(Me_2\text{-}Ph)_6].XH_2O$ (green) vs H-Me_2-Ph (red) (*d*-THF, room temperature)

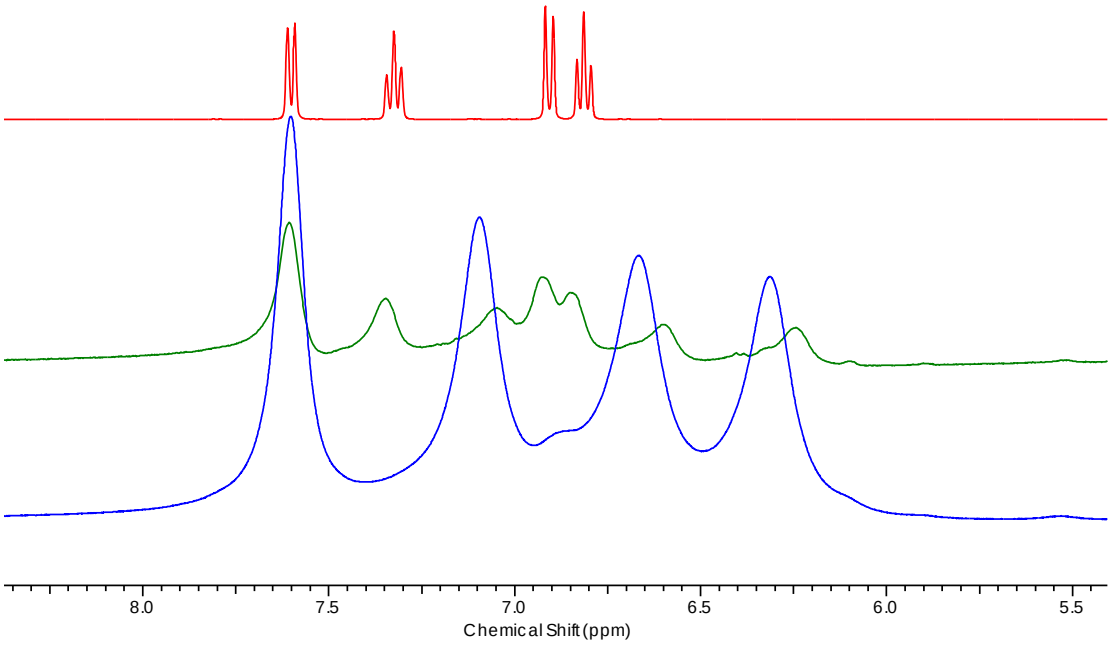

Figure 6.13: Expansion of the aromatic region of the ^{1}H NMR spectra of "anhydrous" $Li_3[Eu(Me_2\text{-}Ph)]$ (blue) vs "hydrated" complex $Li_3[Eu(Me_2\text{-}Ph)_6].X\ H_2O$ (green) vs H-Me_2-Ph (red) (*d*-THF, room temperature).

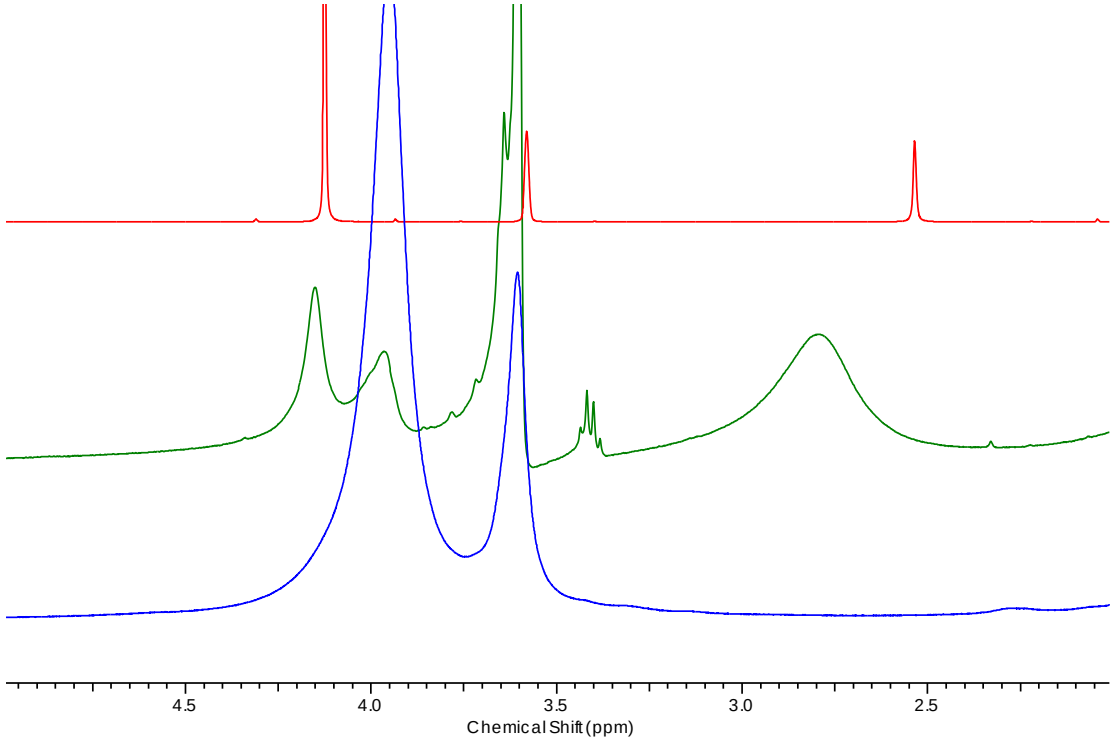

Figure 6.14: Expansion of the region from 4.5-2.5ppm of the ^{1}H NMR spectra of "anhydrous" $Li_3[Eu(Me_2\text{-}Ph)]$ (blue) vs "hydrated" complex $Li_3[Eu(Me_2\text{-}Ph)_6].X\ H_2O$ (green) vs H-Me_2-Ph (red) (*d*-THF, room temperature).

Direct comparison of the IR of the hydrated complexes (Fig. 6.16 and 6.17) against the free ligand (Fig. 6.15) showed a shift in the frequency of the imine stretch in the IR of the complexes and furthermore there was no sign of an imine stretch associated with free ligand. (yttrium complex imine stretch=1628.03cm^{-1}, europium complex imine stretch=1628.66cm^{-1}, free ligand imine stretch=1637.91cm^{-1}).

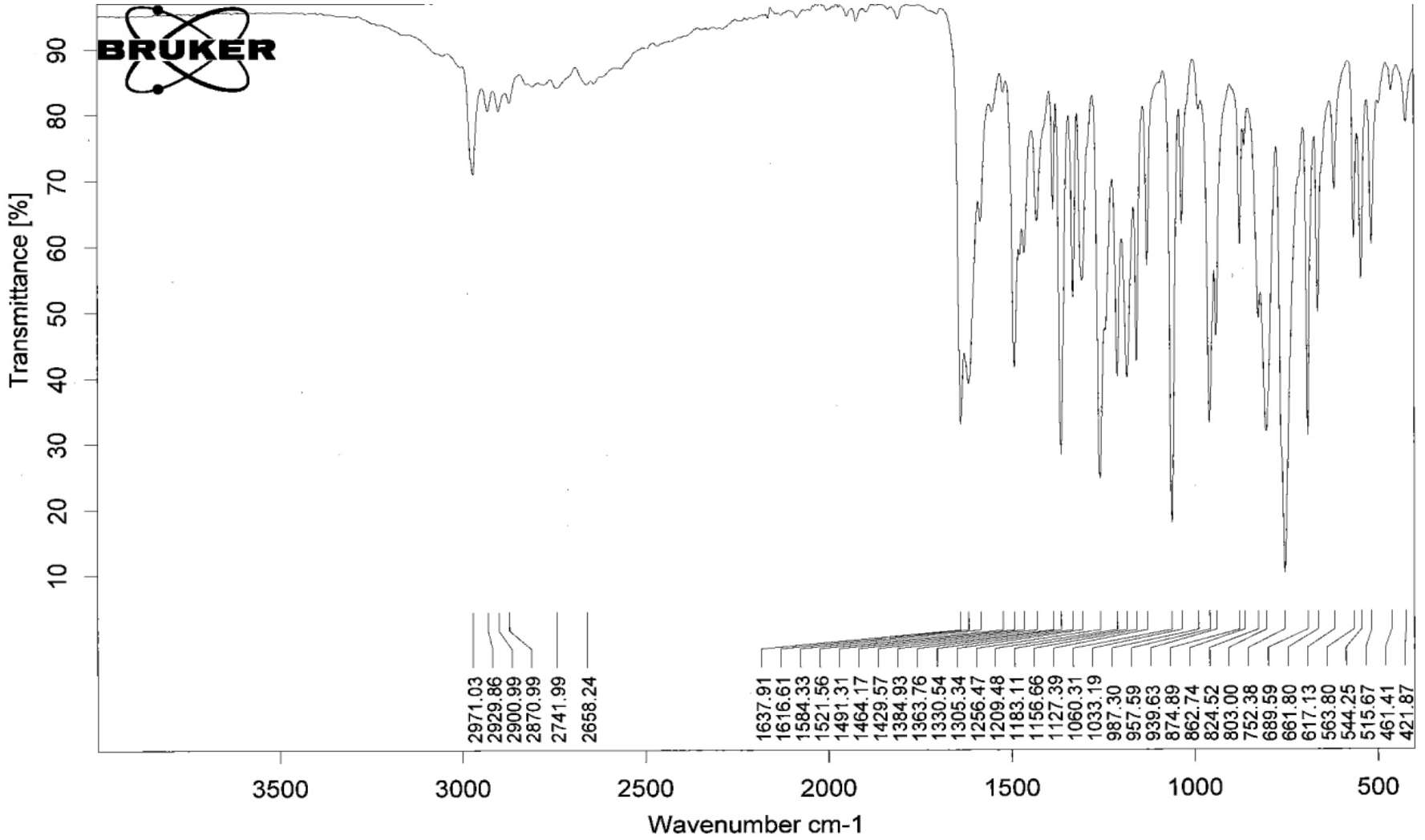

Figure 6.15: IR spectrum of uncoordinated ligand Me_2-Ph

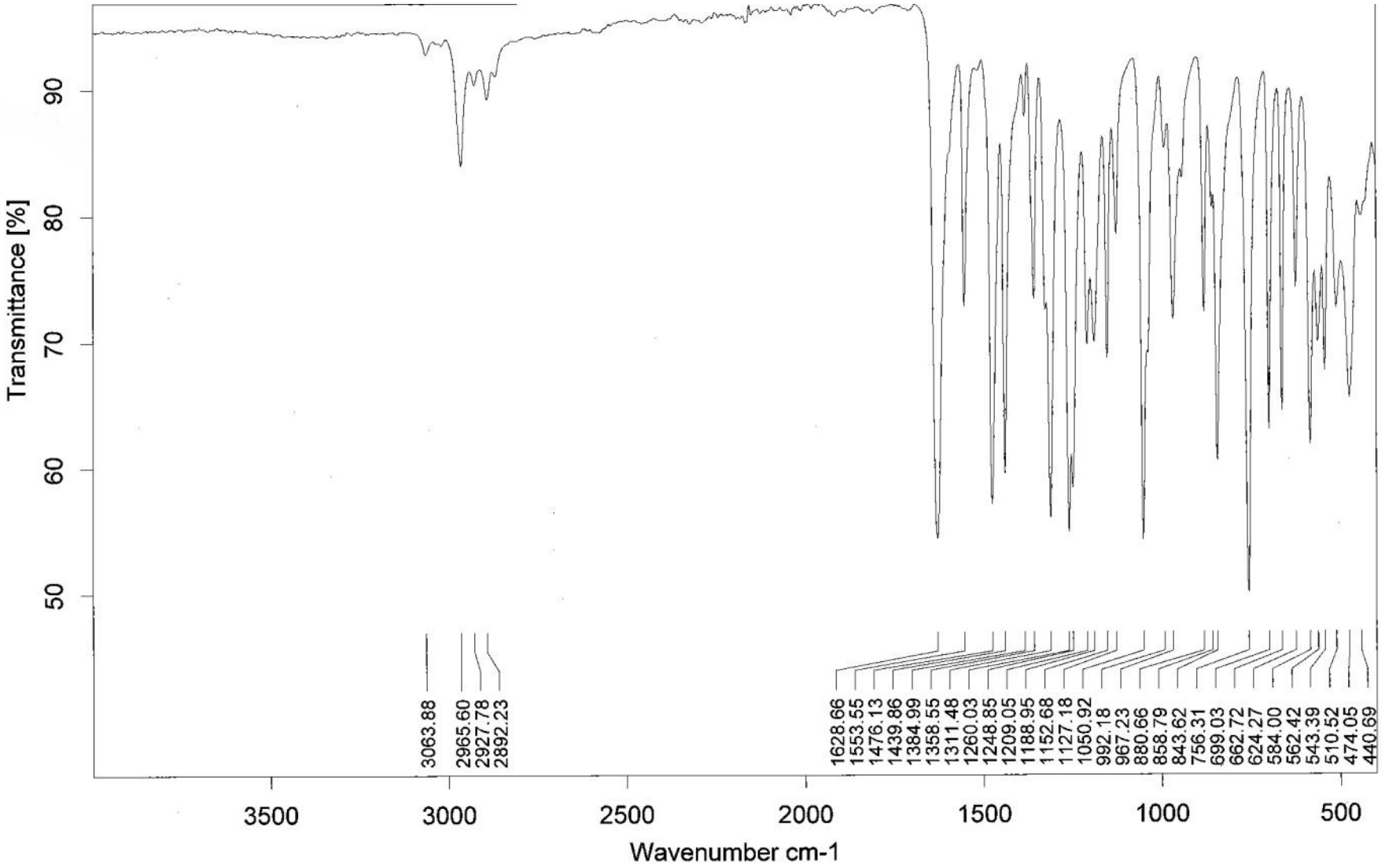

Figure 6.16: IR Spectrum of $Li_3[Eu(Me_2\text{-}Ph)_6]$ isolated from wet THF

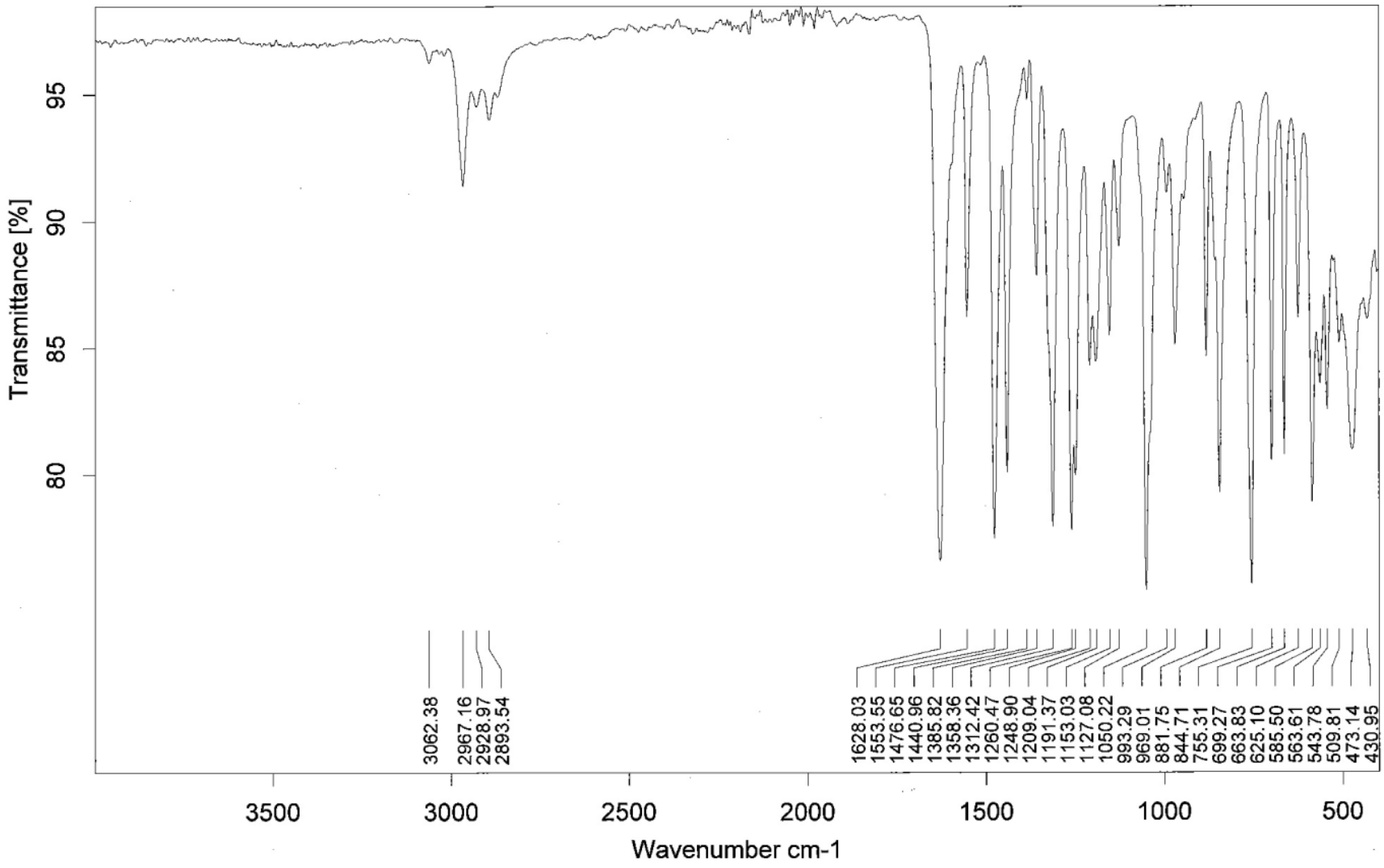

Figure 6.17: IR spectrum of $Li_3[Y(Me_2\text{-}Ph)_6]$ isolated from wet THF

As can be seen from figure 6.15 the free ligand has a distinctive imine stretch at 1637cm^{-1}. This stretch is absent in the IR spectra of either the europium complex (Fig. 6.16) or the yttrium complex (Fig. 6.17). Instead there is a stretch at ~1628cm^{-1} in both spectra, this downward shift of the peak is indicative of co-ordination to another atom, in this case lithium (Fig. 6.18).

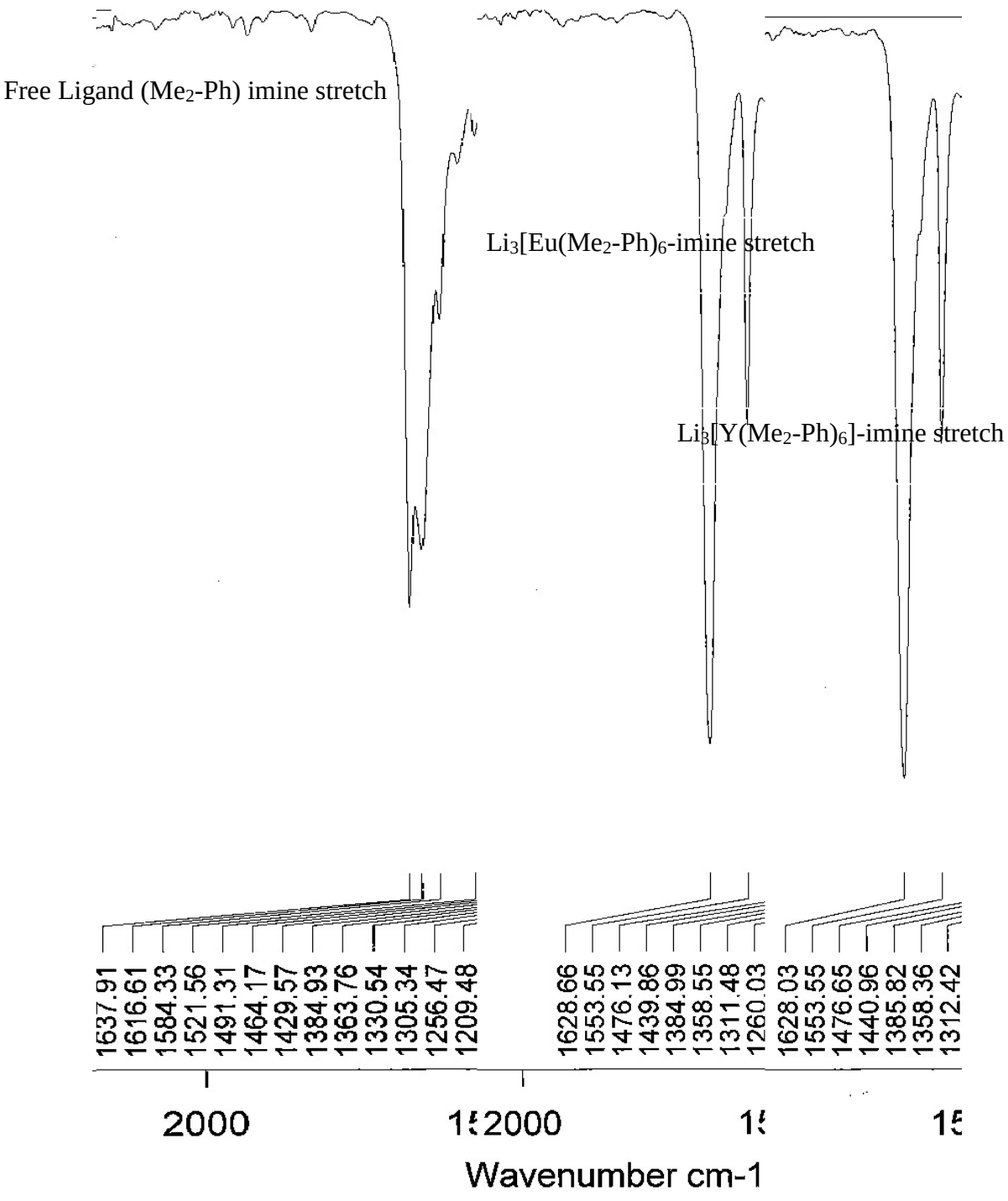

Figure 6.18: Comparison of imine stretch

From crystal structure data of the anhydrous complexes, it can be seen that the rare earth centre does not interact with the imine unit (Section 4.4). Consequently we would not anticipate much difference between the imine stretches of the yttrium and europium complexes.

The hydration level of the complexes was assessed by Karl-Fisher titration. This was conducted by first establishing a "baseline" by running Karl-Fisher on a pre-dried sample of THF; this solvent would be used throughout the rest of the experiment and was dried in bulk prior to the experiment. A known mass of anhydrous complex was then dissolved in the bulk THF and Karl-Fisher performed on the solution, there was no increase in the levels of water in the system. This procedure was then repeated for the hydrated complex. This time an increase in the amount of water in the system was detected, representing an increase of ~22ppm. This indicates the presence of water in the hydrated sample, meaning the water has remained associated with the complex without forming the hydroxide species and displacing ligands.

Elemental analysis of the hydrated complexes showed the greatest deviation from their anhydrous counterparts (Table 6.3).

Table 6.3: Comparison of elemental analysis for hydrated complexes a) $Li_3[Y(Me_2\text{-}Ph)_6].2H_2O$ and b) $Li_3[Eu(Me_2\text{-}Ph)_6].2H_2O$

	Calculated $Li_3[Y(Me_2\text{-}Ph)_6].2H_2O$	Found $Li_3[Y(Me_2\text{-}Ph)_6].2H_2O$	Calculated $Li_3[Eu(Me_2\text{-}Ph)_6].2H_2O$	Found $Li_3[Eu(Me_2\text{-}Ph)_6].2H_2O$
Carbon (%)	61.56	61.27	58.64	58.75
Hydrogen (%)	5.95	5.65	5.67	5.40
Nitrogen (%)	6.53	6.30	6.22	6.06
C:N	9.43	9.72	9.43	9.69

From the above results and more specifically due to the similarities in the C:N ratio it seems that there is very little change in the coordination sphere of the complex. This indicates that the ligand remains bound and that any discrepancy between the numbers is not due to formation of hydroxyl species and displacement of the ligand.

Furthermore with a lack of any evidence of free ligand in the NMR spectra for each of the complexes coupled with the Karl-Fisher results, then this difference in CHN values seems likely to be due to water incorporated into the crystal lattice .[126,127]

Reactions conducted with these hydrated complexes catalysed the reaction almost immediately with reaction seen within the first 5 minutes by TLC. Entry 18 in table 6.3 shows an attempt at using the hydrated complexes under anhydrous conditions. Previously when reactions were

conducted anhydrously it took several hours (europium centred catalyst) or days (yttrium centred catalyst) for any reaction to be seen. The yield from this reaction was 65%, which represents a drop in yield of ~25% compared to the "wet conditions", but still represents an improvement in yields for the anhydrous reactions. This reaction was then repeated, under both anhydrous and atmospheric conditions. The anhydrous reaction continued to demonstrate a low yield; however the reaction carried out under atmospheric conditions returned the yield to 90%. From this we can conclude that we require water for the reaction to proceed quickly and that the amount of water required is more than that trapped in the crystal lattice when the catalysts are isolated from "wet" solvents.

6.4 Proposed Catalytic Cycle

The catalytic cycle has already been proposed by Shibasaki et al. during their investigation into BINOL ligated alkali metal-rare earth complexes (LLBs) (Fig. 6.19)[128]. LLBs possess both Lewis acidity and Brønsted basicity, and the synergistic effects of the two functions provide unique catalytic activity. The unreactive substrates that bear moderately acidic hydrogens undergo deprotonation to generate reactive nucleophiles. Nitromethane forms the corresponding nitronate in the presence of catalytic amounts of LLB, and reacts with a variety of aliphatic and aromatic aldehydes.

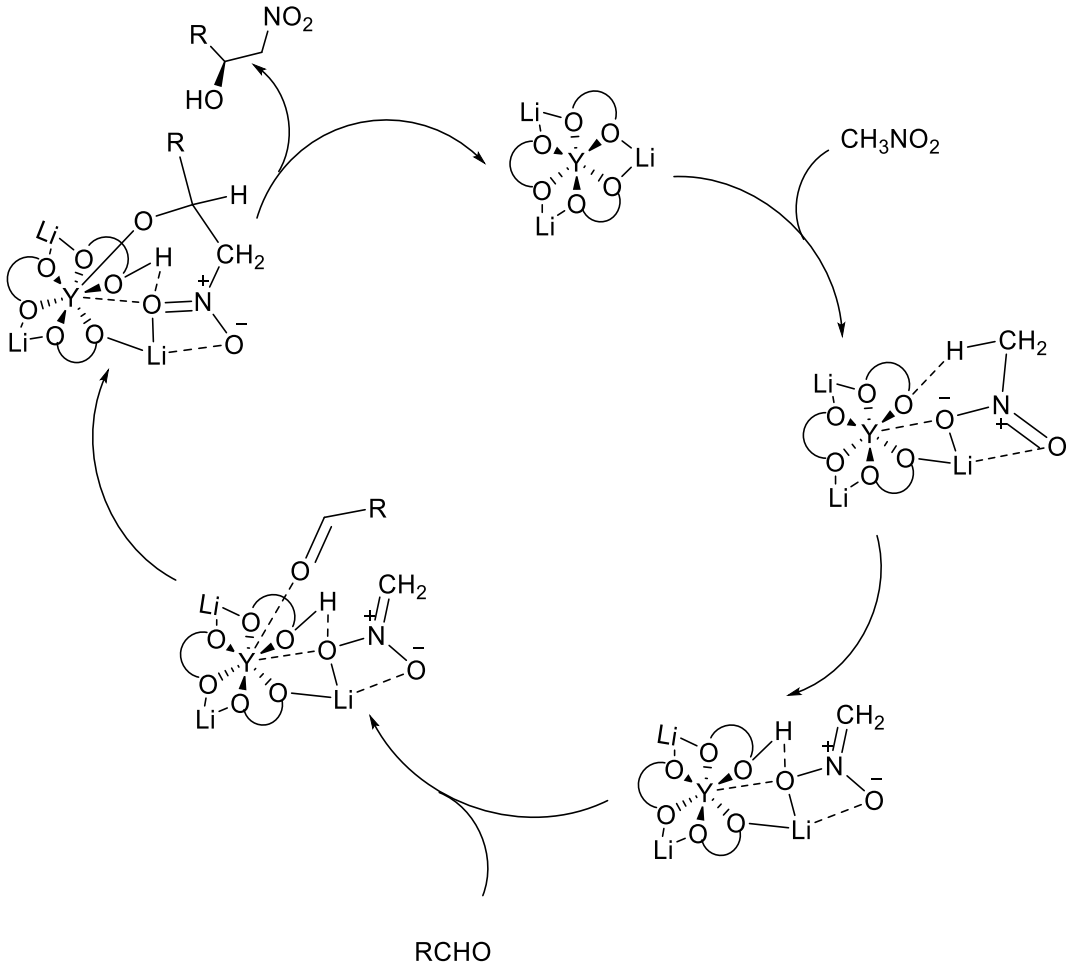

Figure 6.19: Catalytic cycle proposed by Shibasaki et al.[86]

The above catalytic cycle has water omitted for clarity, however it is noted that the presence of water is key to the efficient catalysing of the reaction and without it the rate of reaction was significantly reduced.[86]

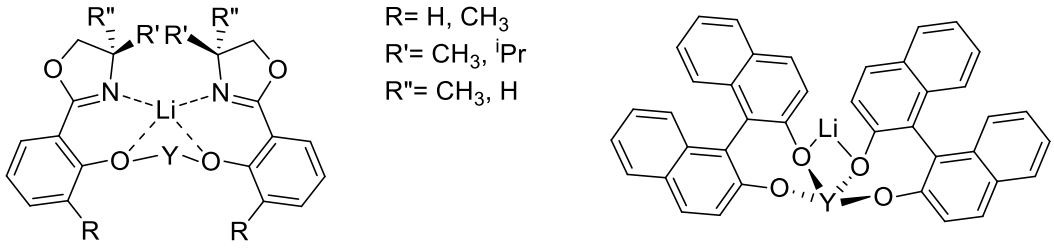

Figure 6.20: Simplified diagram illustrating the similarity in co-ordination sphere between the two different catalysts.

The underlying binding motif of the ligands used by Shibasaki bear a close resemblance to those used throughout this study, with the phenolic O binding to the lanthanide centre in place

of the BINOL. The lithium is held in a chelate ring between two oxazoline Ns with charge balancing and further co-ordination provided by the phenolic O (Fig. 6.20). The steric environment, which is controlled by the R groups, is held relatively close to the lanthanide centre.

Due to these similarities we believe analogies can be drawn between the systems of Shibasaki and our own.

In Shibasaki's cycle the nitromethane is activated by disrupting one of the O-Li bonds. This provides a BINOLate oxygen to deprotonate the nitromethane, and allows the nitro group to gain access to the rare earth centre and stabilise the negative charge. This is followed by co-ordination of the aldehyde to the rare earth centre, via the carbonyl oxygen, activating the carbonyl and leaving the carbonyl carbon more open to attack. Upon addition of the aldehyde to the system, co-ordination of the aldehyde to the lanthanide centre is indicated by a colour change. In our proposed system an oxygen-lithium bond is still disrupted, however, deprotonation of the nitromethane takes place at the phenolic oxygen. From here co-ordination of the aldehyde still takes place at the rare earth centre with additional stabilisation provided by the oxazoline nitrogen. The reaction then proceeds with final protonation of the carbonyl oxygen and product release, possibly aided by water.

We were unable to detect the presence of the nitronate intermediate in either case; this was ultimately attributed to its relatively short lifetime. It is thought that this is due to the presence of a relatively acidic OH group in close proximity to the reaction centre allowing for efficient protonation of the nitronate to give the nitroalkane and the catalyst.

6.4 Conclusion

We have successfully demonstrated the catalytic potential of a range of rare earth alkali metal heterobimetallic complexes with oxazolylyphenol ligands with regards to the nitroaldol

(Henry) reaction. In doing so we have effectively drawn comparisons between our work and the work of Shibasaki et al. and have expanded upon the understanding of the activity of these types of catalysts, specifically with regards to the importance of water within the reaction and the effects of varying components of the catalysts.

The moisture stability of the $M_3[Ln(Ligand)_6]$ complexes has been assessed and data supports their stability in wet solvents. The stability of these complexes seems to be strongly related to the steric environment experienced by the lanthanide centre, with relatively larger rare earths (eg. Eu) demonstrating relatively less stability than their smaller counterparts (eg. Y).

Conclusions

7. Conclusion

As discussed extensively in sections 1 and 3, rare earths and oxazoline ligands have both been shown to be very effective for asymmetric catalysis. However the use of both of these groups together has received little attention and therefore represents a potentially promising area of research. We believed that due to the lack of a simple synthetic route to oxazoline ligands, complexes containing them would be relatively unattractive to researchers and hence the potential of these two groups would remain untapped. In previous work conducted by the group we achieved what we felt would be significant steps towards this goal, and although that work did accomplish many of its objectives e.g. being versatile, easily scalable, relatively inexpensive and synthetically simplistic, we felt that more could be done. Significant advances were made reducing reaction times and employing vastly gentler conditions whilst maintaining yields by use of highly reactive hydroximonylchloride intermediates (Fig. 7.1).

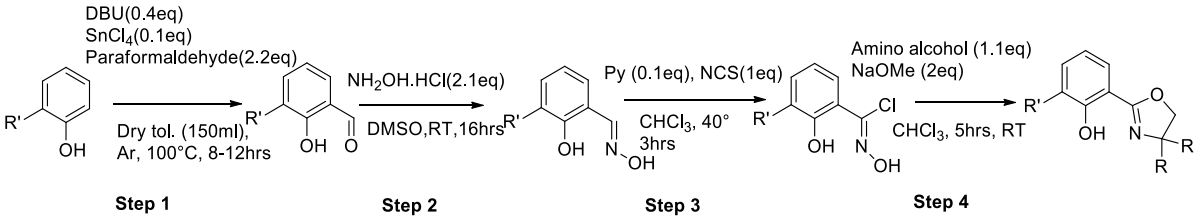

Figure 7.1: Overall synthesis developed in this study

Further work in this area should focus on a more reliable synthesis of the hydroximonyl chloride reactive intermediate (step 3 in Fig. 7.1). It was found that judicious choice of the base in this step was crucial, with pyridine producing the best results. Even when pyridine was used there were still significant amounts of "overchlorination", it rapidly became apparent that this was due at least in part to the structure of the starting material with relatively electron rich systems producing the most. Indeed the apparent success of the ligand synthesis is reliant on the relative ease with which steps 2 and 4 (Fig. 7.1) can be carried out and purified, their relative insensitivity to impurities and the ease of the synthesis as a whole.

Once a reasonably efficient synthesis of the ligands had been established the synthesis of a number of rare hetreobimetallic complexes were synthesised. Sterics seemed to play a key role in complex formation with less bulky ligands forming the $M_3[Ln(Ligand)_6]$ complex preferentially. Furthermore these $M_3[Ln(Ligand)_6]$ complexes demonstrate a degree of moisture stability which seem to be stable under atmospheric conditions for several weeks. This moisture stability seems to have its origins in the steric environment experienced at the rare earth centre with larger rare earth ions showing a greater degree of moisture sensitivity. Similarly the $M[Ln(Ligand)_4]$ complexes seemed to not exhibit as much moisture stability as their $M_3[Ln(Ligand)_6]$ counterparts; again this was believed to be due to a relative lack of steric "saturation" at the metal centre (Fig. 7.2).

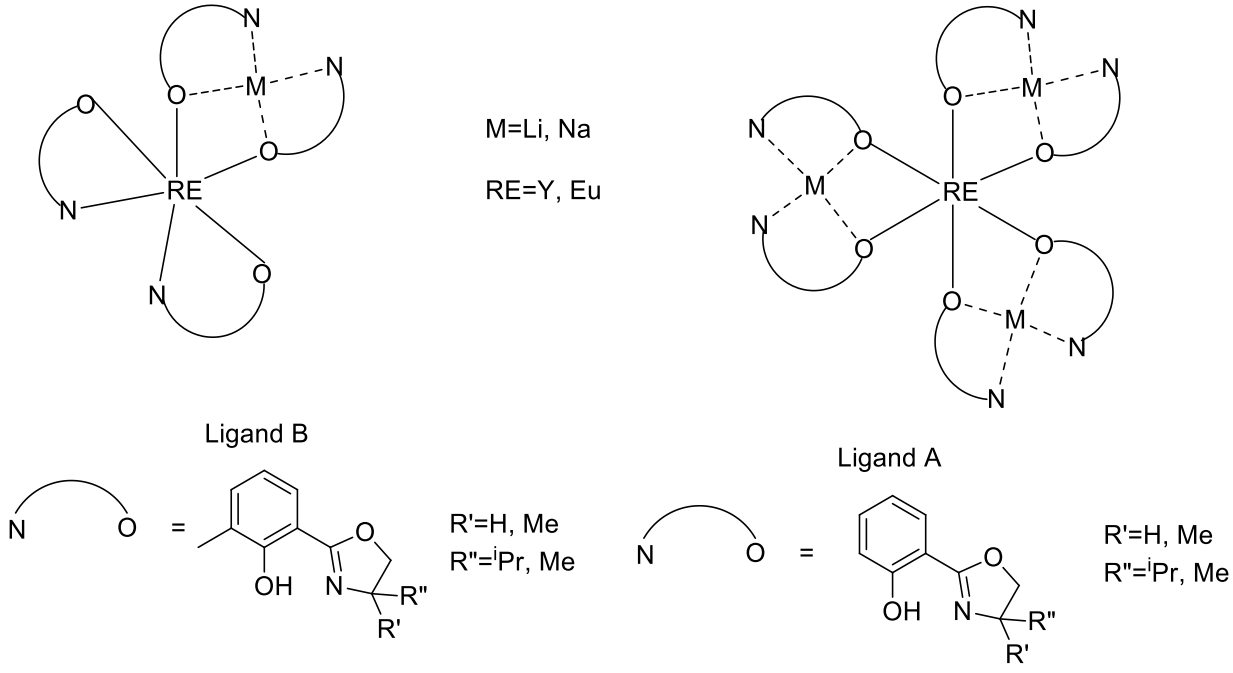

Figure 7.2: Overview of the structures produced in this study

Further work in this area should be focused on the production of a larger library of structures, particularly with sterically more demanding ligands, as these sterically more crowded complexes will have interesting applications in catalysis as well as potentially demonstrating further moisture stability.

The moisture stability of the complexes seems to produce a stable hydrated complex which is key to the catalytic activity of these complexes. This was shown to be applicable for a range of substrates including heterocyclic aldehydes, such as thiophene-2-carboxaldehyde. Attempts at anhydrous catalysis proved to be unsuccessful, demonstrating the key role that water plays in the catalytic cycle (Fig. 7.3).

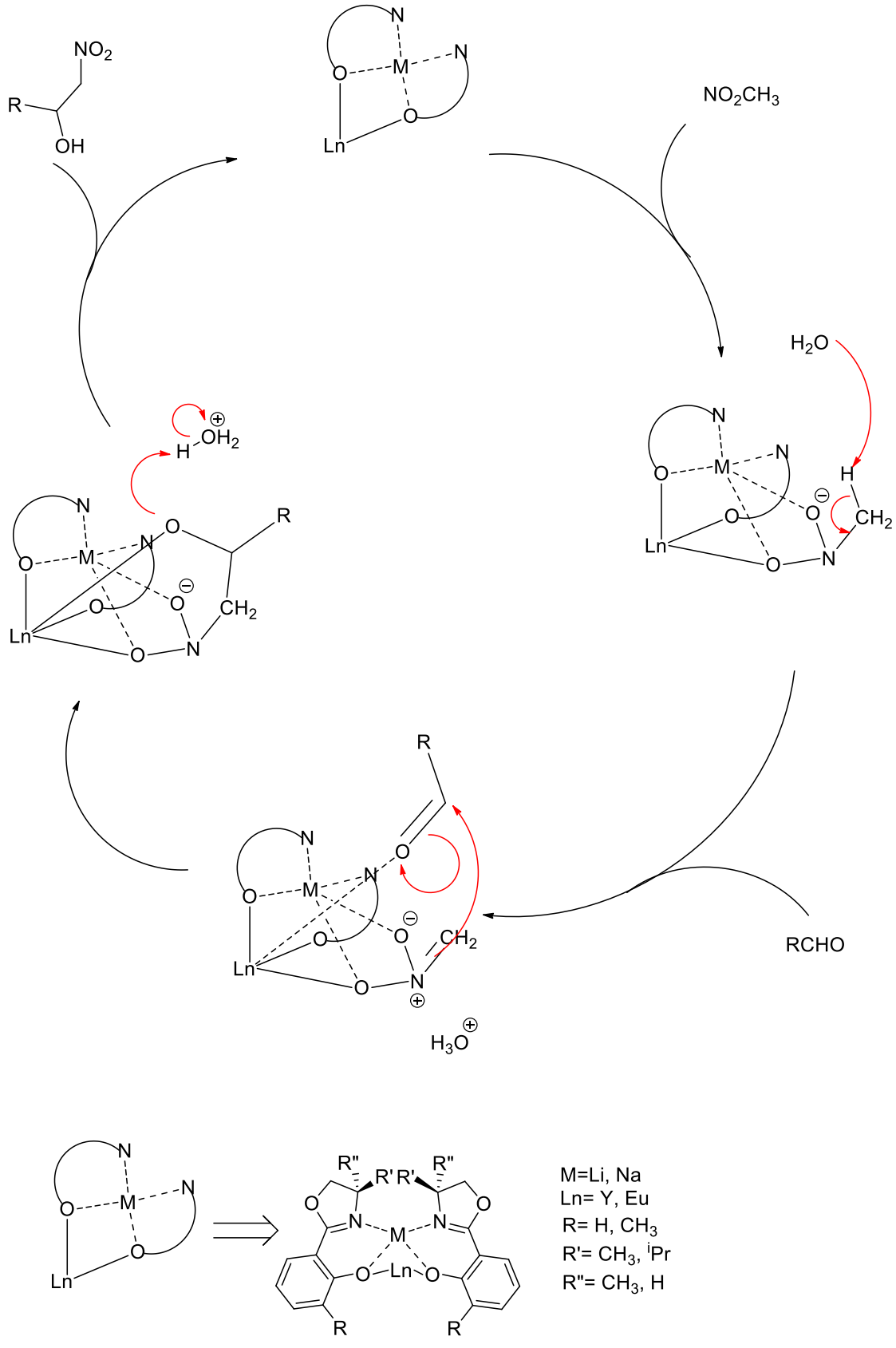

Figure 7.3: Catalytic cycle for the rare earth heterobimetallic complexes produced in this study.

The catalytic cycle has been proposed based on relatively limited data, an in situ NMR experiment might lend further evidence to the binding of the aldehyde to the metal centre although chemically it is the most likely to bind over the nitromethane. Further work should focus on the expansion of the substrate scope, possibly to incorporate further heterocycles and more sterically demanding substrates that aren't based on hydrocarbon chains to investigate the reason sterically more demanding aldehydes are significantly less active in the reaction. Additionally the potential to induce enantioselectivity has not been fully explored and there is some evidence from the literature that cooling the reaction could yield promising results in this area.[70,84,125]

In conclusion, a range of rare earth heterobimetallic complexes have been synthesised and characterised. Their moisture stability has been assessed by a number of methods and the level of hydration of these hydrated complexes assessed by Karl-Fisher. They have been tested for their catalytic potential in the nitroaldol reaction and proven to be promising candidates for further study. Through this an understanding of the catalytic cycle has been achieved, specifically the role of water in the reaction.

Experimental

This chapter contains a detailed account of the experimental procedures and analytical data for all compounds synthesised.

8. Ligand Experimental

Analysis

IR spectra were primarily collected as transmission spectra using a Perkin Elmer Spectrum RX1, however highly crystalline materials were analysed by attenuated total reflectance (ATR) using a Jasco FT/IR-4200. Mass spectrometry was carried using a Micromass LCT Mass Spectrometer or a Trio 1000 Spectrometer.

NMR spectra were recorded on a Bruker Avance 400 spectrometer. Analysis and post-processing was performed using ACDLABS v. 12.01. All carbon spectra have been referenced to their NMR solvents using the values stated in 'Structural determination of organic compounds" – Erno Pretch *et al*, 4th edition

General Synthesis

Formylation of the phenol compounds (3A) and (4A) was carried out using a modification of the Casiraghi reaction. Formylation of the napthol compound (5A) was carried out using the Reimer-Tiemann reaction.[51] Bis formylation (6A) was conducting using the Duff reaction.[52] Formation of the oxime (1-6B) was carried out by reaction of the aldehyde with hydroxylamine hydrogen chloride in DMSO. Chlorination of the oxime (1-6C) was conducted at 40°C using a catalytic amount of pyridine and NCS as the chlorinating agent. The cyclisation step (1-6D, 1-4E, 1-4F) was carried out at room temperature by drop wise

addition of a solution of (1-6C) in chloroform to a stirring solution of the amino alcohol in triethylamine.

(S)-valinol and (S)-phenyl alanol were prepared by the reduction of (S)-valine according to a published procedure.[129]

Purification

Formation of the Bis-formyl (4A) required flash column chromatography with neat DCM. Products of the Nitrile synthesis and subsequent cyclisations required purification via column chromatography with ethyl acetate: hexane systems. The cyclisation step (1-4D, 1-2E) required only trituration with neat hexane in order to yield products of analytical purity. All of the previously mentioned steps yielded product of sufficient purity that further purification was deemed unnecessary and they were “telescoped” through to the next stage.

8.1 Formylation Reactions

2-hydroxy-3-methylbenzaldehyde (**3A**): Ortho-cresol (10g, 1eq) and DBU (5.63ml, 0.4eq) were dissolved in dry toluene (100ml) under an argon atmosphere. This was cooled to 0°C and $SnCl_4$ (1.09ml, 0.1eq) added sub-surface. This was then stirred for 20 minutes and allowed to come to room temperature. Paraformaldehyde (6.1g, 2.2eq) was then added and the reaction heated to 100°C for 8hrs. The reaction was cooled to room temperature and the reaction was quenched with 2M HCl (100ml) and the product extracted with diethyl ether (3x100ml) and the combined organic phase washed with brine (100ml0, dried (Mg_2SO_4), filtered and concentrated to yield a dark orange oil (10.18g, 81%).

IR (NaCl, thin film): ArOH 3142.2, Ar-H 3050.6, CHO 2846.5, C=O 1644.0; MS (Cl^+, NH_3): *m*/*z*=135 (M-H, 100%); ^{1}H NMR (400 MHz, $CDCl_3$) δ ppm 11.28 (1 H, s, OH), 9.87 (1 H, s, CHO),7.38 (2 H, d, *J* = 7.6 Hz, H's 4+6), 6.91 (1 H, t, *J* = 7.5 Hz, H5) 2.26 (3 H, s, CH_3); ^{13}C NMR (100 MHz, $CDCl_3$) δ ppm 197.1 (CHO), 160.4 (COH), 138.2 (C4), 131.8 (C6), 127.2 (C1), 120.4 (C3), 119.8 (C5), 15.5 (CH_3); Elemental analysis found: C 70.41%, H 6.06%; ($C_8H_8O_2$) requires: C 70.57%, H 5.92%

3-(tert-butyl)-2-hydroxy-5-methylbenzaldehyde (4A): Reaction was conducted as for (3A) except using 2-(tert-butyl)-4-methylphenol (8.225g, 1eq) and the

reaction was heated for 12hrs; this yielded product as a yellow crystalline solid (8.16 g, 85 %).

IR (NaCl, thin film): Ar-H 2964.0, CHO 2869.0, C=O 1651.6; MS (Cl^+, NH_3): *m*/*z*=193 ($M+H^+$, 100%); ^1H NMR (400 MHz, $CDCl_3$) δ ppm 11.61 (1 H, s, OH), 9.83 (1 H, s, CHO), 7.33 (1 H, d, *J* = 2.18 Hz, H4), 7.18 (1 H, d, *J* = 1.47 Hz, H5) 2.33 (3 H, s, CH_3), 1.41(6 H, s ^tBu); ^{13}C NMR (100 MHz, $CDCl_3$) δ ppm 197.5 (CHO), 159.6 (COH), 138.4 (C3), 135.8 (C4), 131.8 (C6), 128.6 (C5), 120.8 (C1), 35.2 ($C(CH_3)_3$), 29.6 ($C(CH_3)_3$), 21.0 (CH_3); Elemental analysis found: C 74.78%, H 8.38%; ($C_{12}H_{16}O_2$) requires: C 74.97%, H 8.39%.

2-hydroxy-1-napthaldehyde (**5A**): 2-Napthol (10g, 1eq) and TBAB (0.09g, 0.004eq) were dissolved in 40% w/v NaOH (40ml) and 1,4-dioxane (60ml). This produced a turbid brown solution which was heated to 70°C and $CHCl_3$ (7.2ml, 1.3eq) added over 5 minutes. The colour of the reaction gradually changed from brown to green to blue. The reaction was heated at 70°C for 2 hours during which a precipitate formed. The reaction was cooled to 0°C and filtered to yield a green sold. This was washed with 1M NaOH (40ml) and 1,4-dioxane (40ml) to leave a yellow solid. This was dissolved in 2M HCl (200ml) and the product extracted wit diethyl ether (3x100ml). The combined organic was dried (Mg_2SO_4), filtered and reduced to yield product as an orange solid (3.63g, 31%).

IR (ATR): Ar-H 3058.6, C=O 1635.3; MS (Cl^+, NH_3): *m*/*z*=173.0 ($M+H^+$, 100%); ^1H NMR (400 MHz, $CDCl_3$) δ ppm 13.16 (1 H, s, OH), 10.81 (1 H, s, CHO), 8.34-8.36 (1 H, d, *J* = 8.54 Hz, H8), 7.97-7.99 (1 H, d, *J* = 9.01 Hz, H4), 7.79-7.81 (1 H, d, *J* = 8.11 Hz, H5) 7.60-7.64 (1 H, pt, *J* = 8.24 Hz, H7), 7.44-7.46 (1 H, pt, *J* = 7.82 Hz, H6), 7.13-7.15 (1 H, d, *J* = 9.01 Hz, H3); ^{13}C NMR (100 MHz, $CDCl_3$) δ ppm 193.7 (CHO), 165.4 (C2), 139.6 (C4), 133.3 (C10), 129.9 (C6), 129.6 (C8) 128.2 (C5), 124.9 (C7), 119.6 (C3), 119.0 (C9), 111.7 (C1); Elemental analysis found: C 76.38%, H 4.67%; ($C_{11}H_8O_2$) requires: C 76.73%, H 4.68%.

2-hydroxy-5-methylisophthalaldehyde (**6A**): TFA (100ml) was placed under an argon atmosphere and cooled to 0°C, hexamine (34.2g, 2.1eq) was added portion wise and then para-creosol (12.8ml, 1eq) added. This was stirred and allowed to come to room temperature. This resulted in a bright yellow solution which was heated at 85°C for 20hrs. This formed a viscous orange mix which was quenched with water (300ml) and the product extracted with DCM (4x100ml). The combined organic phase was washed with water (2x100ml), dried (Mg_2SO_4), filtered and concentrated to yield crude product as orange oil (22.58g)

IR (NaCl, Nujol mull): Ar-H 2930.8, C=O 1681.1; MS (Cl^+, NH_3): *m*/*z*=182.2 ($M+NH_4^+$, 100%); ^1H NMR (400 MHz, $CDCl_3$) δ ppm 11.46 (1 H, s, OH), 10.21 (2 H, s, CHO), 7.77 (2 H, s, H's 4+6), 2.39 (3 H, s, CH_3); ^{13}C NMR (100 MHz, $CDCl_3$) δ ppm 192.6 (COH), 162.1 (2xCHO), 138.4 (C's 4+6), 130.0 (C's 1+3), 123.3 (C5),

20.5 (CH_3); Elemental analysis found: C 65.62%, H 4.95%; ($C_9H_8O_2$) requires: C 65.85%, H 4.91%.

8.2 Synthesis of oximes

2-hydroxybenzaldehyde oxime (**1B**): Salicylaldehyde (1A) (10g, 1eq) and hydroxylamine hydrogen chloride (11.88g, 2.1eq) were dissolved in DMSO (100ml) and stirred at room temperature for 6 hours. The reaction was quenched with water (200ml) and the product extracted with diethyl ether (3x100ml). The combined organic was washed with brine (100ml), dried (Mg_2SO_4), filtered and concentrated to yield product as a clear oil which crystallised on standing to produce a white crystalline solid (10.29g, 91%).

IR (NaCl): N-OH 3409.5, Ar-H 3058.6, C=N 1616.1; MS (Cl^+, NH_3): *m/z*=138.0 ($M+H^+$, 100%); ^{1}H NMR (400 MHz, $CDCl_3$) δ ppm 9.95 (1 H, s, OH), 8.23 (1 H, s, CHN), 7.32-7.26 (1 H, m, H3), 7.22-7.15 (1 H, dd, J=7.7,1.7Hz, H4), 7.02-6.98 (1 H, dt, J=8.3,0.5, H1), 6.90-6.95 (1 H, tp, J=7.5, H2); ^{13}C NMR (400MHz, $CDCl_3$) δ ppm 158.8 (C-OH), 152.5 (C=N), 132.0 (C5), 130.7 (C2), 121.8 (C3), 118.4(C4), 117.8(C1); Elemental analysis found: C 60.39%, H 5.18%, N 10.2%; ($C_7H_7NO_2$) requires: C 61.29%, H 5.11%, N 10.20%.

2-hydroxy-3-methoxy benzaldehyde oxime (**2B**): Reaction was conducted as for 1B except using ortho-vanillin (2A) (9.17g, 1eq). This yielded product as a light yellow crystalline powder (7.35g, 74%).

IR (NaCl): N-OH 3332.3, Ar-H 3066.2, C=N 1581.3; MS (Cl^+, NH_3): *m/z*=168.1 ($M+H^+$, 100%); H^1 NMR (400MHz, $CDCl_3$) δ ppm 9.92(1 H, s, OH), 8.24 (1 H, s,

CHN), 6.94-6.82 (3 H, m, H1,H2,H3), 3.91 (3 H, s, OCH_3); ^{13}C NMR (400MHz, $CDCl_3$) δ ppm 152.59 (C=N), 148.38 (C-OMe), 147.17 (C-OH), 122.65 (C3), 119.92 (C4), 117.22 (C-C=N), 113.48 (C5), 56.55 (CH_3-O); Elemental analysis found: C 55.36%, H 5.50%, N 7.78%; ($C_8H_9NO_3$) requires: C 57.43%, H 5.38%, N 8.37%

2-hydroxy-3-methylbenzaldehyde oxime (**3B**): Reaction was conducted as for 1B except using 2-hydroxy-3-methylbenzaldehyde (3A) (10g, 1eq). This yielded product as a brown solid (8.65g, 78%).

IR (NaCl): N-OH 3332.2. Ar-H 3068.2, C=N 1585.3; MS (Cl^+, NH_3): *m/z*=152.6 ($M+H^+$, 100%); ^1H NMR (400 MHz, $CDCl_3$) δ ppm 8.23 (1H, s, CHN), 7.18-7.16 (1H, dd, *J*=7.4, 0.7 Hz, Ar-H1), 7.06-7.04 (1H, dd, *J*=7.6, 1.3 Hz, Ar-H3), 6.87-6.83 (1H, pseudo tp, Ar-H2), 2.30 (3H, s, Ar-CH_3); C^{13} NMR (400MHz, $CDCl_3$) δ ppm 153.83 (C-OH), 153.51 (C=N), 132.89 (C4), 128.94 (C3), 126.13 (C2), 119.74 (C2), 116.15 (C1), 16.16 (Ar-CH_3); Elemental analysis found C:62.94%, H: 5.94%, N:9.20%; ($C_8H_9NO_2$) requires: C 63.55%, H 6.00%, N 9.27%.

3-(tert-butyl)-2-hydroxy-5-methylbenzaldehyde oxime (**4B**): Reaction was conducted as for 1B except using 3-(tert-butyl)-2-hydroxy-5-methylbenzaldehyde (4A) (8.16g, 1eq). This yielded product as a yellow solid (7.05g, 80%).

IR (NaCl): N-OH 3332.3, Ar-H 3069.2, C=N 1595.3; MS (Cl^+, NH_3): *m/z*=208.3 ($M+H^+$,100%); ^1H NMR (400MHz, $CDCl_3$) δ ppm 8.21 (1H, s, CHN), 7.13 (1H, d, *J*=2Hz, Ar-H4), 6.86 (1H, d, *J*=1.9Hz, Ar-H2), 2.30 (3H, s, Ar-CH_3), 1.44 (9H, s, Ar-$CH(CH_3)_3$); C^{13} NMR (400MHz, $CDCl_3$) δ ppm 154.71 (C-OH), 154.19 (C=N), 137.34 (C5), 130.08 (C4), 129.54 (C2), 128.22 (C1), 116.66 (C1), 29.85 (Ar-$C(CH_3)_3$), 21.02 (Ar-CH_3); Elemental analysis found: C 68.77%, H 8.17%, N 6.68%; ($C_{12}H_{17}NO_2$) requires: C 69.52%, H 8.27%, N 6.76%.

2-hydroxy-1-napthaldehyde oxime (**5B**): Reaction was conducted as for 1B except using 2-hydroxy-1-napthaldehyde (5A) (3.63g, 1eq). This yielded product as a fluffy off-white solid (3.73g, 95%).

IR (NaCl): N-OH 3332.3, C=N 1631.4; MS (Cl^+, NH_3): *m/z*=188.2 ($M+H^+$, 55%), 172.2 (M^+-OH, 100%); ^1H NMR (400 MHz, $CDCl_3$) δ ppm 9.13 (1 H, s, CHN), 7.99-7.94 (1 H, d, J=8.5Hz, H4), 7.82-7.76 (2 H, m, H5 H6), 7.56-7.50 (1H, ddd, J=8.5, 7, 1.4 Hz, H7), 7.40-7.35 (1 H, ddd, J=8.1, 7, 1Hz, H8), 7.28-7.23 (1 H, m, H9); ^{13}C NMR (100MHz, $CDCl_3$) δ ppm 158.11 (C-OH), 150.07 (C-C=N), 133.37 (C3), 132.35 (C8), 129.46 (C4), 128.74 (C5), 128.04 (C6), 124.05(C7), 120.56(C9), 119.16(C10), 66.31 (C=N); Elemental analysis found: C 70.53%, H 4.79%, N 7.38%; ($C_{11}H_9NO_2$) requires: C 70.52%, H 4.81%, N 7.48%

(1N,1'N)-2-hydroxy-3-((N)-(hydroxyimino)methyl)-5-methylbenzaldehyde oxime (**6B**)**:** Reaction was conducted as for 1B except using 2-hydroxy-5-methylisophthalaldehyde (6A) (5g, 1eq). This yielded product as an off-white solid (3.6g 65%).

IR (NaCl, Nujol mull): Ar-H 2930.8, C=N 1621.1; MS (Cl^+, NH_3): *m/z*=195.7 ($M+H^+$, 100%); ^1H NMR (400MHz, $CDCl_3$) 8.19 (2H, s, CHN), 7.12-7.09 (2H, dd, J=8.4, 6.1 Hz, Ar-H), 2.29 (3H, s, Ar-CH_3); Elemental analysis found: C 55.64%, H 5.11%, N 14.38%; ($C_9H_{10}N_2O_3$) requires: C 55.67%, H 5.19%, N 14.43%.

8.3 Chlorination of oximes

N,2-dihydroxybenzimidoyl chloride (**1C**): 2-hydroxybenzaldehyde oxime (1B) (10g, 1eq) and pyridine (1.15g, 0.2eq) were dissolved in $CHCl_3$ (80ml) and heated to 40°C. NCS (9.73g, 1eq) was then added and the reaction heated at 40°C for 3hrs. The reaction was cooled to room temperature and diluted with DCM (100ml). The organic phase was washed with water (2x100ml) and brine (100ml), dried (Mg_2SO_4), filtered and concentrated to yield product as pale yellow powder (10.49g, 84%).

IR (NaCl): N-OH 3305.3, C=N 1612.2; MS (Cl^+, NH_3): *m/z*=172.0 ($M+H^+$, 10%), 138.2 (M-Cl, 100%); ^{1}H NMR (400 MHz, $CDCl_3$) δ ppm 9.90 (1H, s, OH), 7.84-7.79 (1H, dd, J=8, 1.5Hz, H3), 7.38-7.32 (1H, m, H4), 7.02-6.97 (2H, t, J=7.9, H5, H6); Elemental analysis found: C 48.89%, H 3.34%, N 8.01%; ($C_7H_5NO_2Cl$) requires: C 49.12%, H 3.51%, N 8.19%.

N,2-dihydroxy-3-methoxybenzimidoyl chloride (**2C**): Reaction conducted as for (1C) except using 2-hydroxy-3-methoxy benzaldehyde oxime (2B) (10g, 1eq). To yield product as an orange solid (11.75g, 99%).

IR (NaCl): N-OH 3293.5, Ar-H 2977.5, C=N 1465.6; MS (Cl^+, NH_3): *m/z*=201.7 (M, 10%), 183.1 (M-OH, 100%), 168.1 (M-Cl, 80%); ^{1}H NMR (400 MHz, $CDCl_3$) δ ppm 10.34 (1H, s, OH), 8.59 (1H, s, N-OH), 7.45-7.41 (1H, dd, J=8.1, 1.6Hz, H6), 7.01-6.97 (1H, m, H5), 6.95-6.90 (1H, m, H4), 3.93 (3H, s, O-CH_3); ^{13}C NMR (100 MHz,

$CDCl_3$) 148.19 (C-OH), 146.4 (C-C=N), 120.88 (C3), 119.19 (C4), 116.05 (C5), 113.81 (C6), 56.26 (O-CH_3); Elemental analysis found: C 49.31%, H 4.05%, N 6.92%; ($C_8H_8NO_3Cl$) requires: C 47.64%, H 3.97%, N 6.95%.

N,2-dihydroxy-3-methylbenzimidoyl chloride (**3C**): Reaction conducted as for (1C) except using 2-hydroxy-3-methylbenzaldehyde oxime (3B) (5g, 1eq). To yield product as a brown oil (5.2g, 85%).

IR (NaCl): N-OH 3293.5, Ar-H 2983.2, C=N 1598.9; MS (Cl^+, NH_3): *m/z*= 185.02 (M, 10%), 150.06 (M-Cl, 100%); ^{1}H NMR (400MHz, $CDCl_3$) δ ppm 7.68-7.65 (1H, dd, *J*=8.1, 0.8 Hz, Ar-H4), 7.22-7.20 (1H, m, Ar-H2), 6.78-6.74 (1H, J=7.8 Hz x2, pseudo t, Ar-H3), 2.21 (3H, s, Ar-CH_3); ^{13}C NMR (400MHz, $CDCl_3$) δ ppm 155.86 (Cl-C=N), 153.65 (C-OH), 133.74 (C5), 132.96 (C4), 128.98 (C3), 127.48 (C2), 119.73 (C1), 16.16 (Ar-CH_3); Elemental analysis found: C 52.54%, H 5.12%, N 7.54%; $C_8H_8NO_2Cl$ requires: C 51.89%, H 4.36%, N 7.57%.

3-(tert-butyl)-N,2-dihydroxy-5-methylbenzimidoyl chloride (**4C**): Reaction conducted as for (1C) except using 3-(tert-butyl)-2-hydroxy-5-methylbenzaldehyde oxime (4B) (5g, 1eq). To yield product as a brown oil (5.02g, 86%)

IR (NaCl): N-OH 3293.5, Ar-H 2985.3, C=N 1612.2; MS (Cl^+, NH_3): *m/z*= 241.07 (M, 10%), 206.12 (M-Cl, 100%); ^{1}H NMR (400MHz, $CDCl_3$) δ ppm 7.50 (1H, m, Ar-H4),

7.16 (1H, d, *J*=1.9 Hz, Ar-H2), 2.31 (1H, s, Ar-CH_3), 1.41 (1H, s, Ar-C(CH_3)$_3$); ^{13}C NMR (400MHz, $CDCl_3$) δ ppm 154.71 (Cl-C=N), 153.99 (C-OH), 147.77 (C5), 143.60 (C1), 137.54 (C4), 137.26 (C2), 29.82 (Ar-C(CH_3)$_3$), 21.09 (Ar-CH_3); Elemental analysis found: C 61.02%, H 6.72%, N 5.70%; ($C_{12}H_{16}NO_2Cl$) requires: C 59.73%, H 6.69%, N 5.81%.

8.4 Achiral cyclizations

2-(4,4-dimethyl-4,5-dihydrooxazol-2-yl)phenol (**1D**): N,2-dihydroxybenzimidoyl chloride (1C) (2.33g, 1eq) was dissolved in $CHCl_3$ (100ml). This was added drop-wise to a solution of NaOMe (1.38g, 1eq) and 2-amino-2-methylpropan-1-ol (2.55g, 2.1eq) over 5hrs at room temperatures. The reaction was quenched with 1M NaOH (100ml) and the aqueous phase extracted with diethyl ether (2x100ml), the combined organic phase was washed with NH_4Cl (100ml). The organic phase was then dried (Mg_2SO_4), filtered and concentrated to yield crude product as a brown oil (1.8g). This was then triturated with hexane (30ml) to yield product as white crystals (1.35g, 52%).

MS (Cl^+, NH_3): *m/z*=192.25 ($M+H^+$, 100%); ^{1}H NMR (400 MHz, $CDCl_3$) δ ppm 7.57-7.54 (1H, dd, J=7.8, 1.7Hz, H3), 7.31-7.26 (1H, m, H4), 6.94-6.91 (1H, dd, J=8.4, 0.9Hz, H5), 6.81-6.77 (1H, td, J=7.5Hz, H6), 4.02 (2H, s, CH_2), 1.32 (6H, s, $(CH_3)_2$); ^{13}C NMR (100 MHz, $CDCl_3$) 163.88 (C-OH), 160.21 (C-Ox), 133.57 (C3), 128.26 (C4), 118.97 (C5), 117.06 (C6), 111.30 (N-C-O), 78.76 (O-C-C), 67.52 (C-C-N), 28.94 ($(CH_3)_2$); Elemental analysis found: C 68.14%, H 6.82%, N 7.32%; ($C_{11}H_{13}NO_2$) requires: C 69.09%, H 6.85%, N 7.32%.

2-(4,4-dimethyl-4,5-dihydrooxazol-2-yl)-6-methoxyphenol (**2D**): Reaction conducted as for (1D) except using *N,2-dihydroxy-3-methoxybenzimidoyl chloride* (2C) (1.73g, 1eq). To yield crude product as a brown oil (1.33g). This was

then triturated with hexane (30ml) to yield product as pale yellow crystals (0.89g, 45%).

MS (Cl^+, NH_3): *m/z*= 222.33 ($M+H^+$, 100%); ^1H NMR (400 MHz, $CDCl_3$) δ ppm 7.19-7.16 (1H, dd, J=8, 1.5, H4), 6.92-6.88 (1H, dd, J=8.1, 1.5, H5), 6.77-6.72 (1H, m, H6), 4.03 (1H, s, CH_2), 3.84 (1H, s, O-CH_3), 1.33 (1H, s, $(CH_3)_2$); ^{13}C NMR (100 MHz, $CDCl_3$) 164.08 (C-OCH_3), 150.56 (C-OH), 148.65 (C-Ox), 119.78 (C4), 118.47 (C5), 115.11 (C6), 111.45 (N-C-O), 78.79 (O-C-C), 67.51 (C-C-N), 56.56 (O-CH_3), 28.91 ($(CH_3)_2$); Elemental analysis found: C 64.11%, H 6.90%, N 6.10%; ($C_{12}H_{15}NO_3$) requires: C 65.14%, H 6.83%, N 6.33%.

2-(4,4-dimethyl-4,5-dihydrooxazol-2-yl)-6-methylphenol (**3D**): Reaction conducted as for (1D) except using *N*,2-dihydroxy-3-methylbenzimidoyl chloride (3C) (1.6g, 1eq). To yield crude product as a brown oil (0.51g, 30%). This was triturated with hexane (100ml) and refluxed overnight (66°C, 16 hrs). This yielded product as a brown oil (0.33g, 19%)

IR (ATR): Ar-H 2970.1, C=N 1634.1; MS (CI+, NH3): m/z=206.3 (M+H+, 100%);

1H NMR (400 MHz, CDCl3) δ ppm 12.46 (1 H, br. s., OH), 7.48 (1 H, ddd, J=7.9,

1.7, 0.5 Hz, H3), 7.22 (1 H, ddd, J=7.4, 1.7, 0.9 Hz, H5), 6.77 (1 H, pt, J=7.6 Hz,

H4), 4.08 (2 H, s, H5'), 2.28 (3 H, s, CH3), 1.38 (6 H, s, (CH3)2); 13C NMR (100

MHz, CDCl3) δ ppm 163.9 (C2'), 158.1 (COH), 134.0 (C5), 125.6 (C6), 125.4 (C3), 118.0 (C4), 110.1 (C2), 78.3 (C5'), 67.0 (C4'), 28.5 ((CH3)2), 15.8 (CH3); Elemental analysis found: C 70.04, H 7.77, N 7.03; ($C_{12}H_{15}NO_2$) requires: C 70.22, H 7.37, N 6.82;

2-(tert-butyl)-6-(4,4-dimethyl-4,5-dihydrooxazol-2-yl)-4-methylphenol (**4D**): Reaction conducted as for (1D) except using 3-(tert-butyl)-N,2-dihydroxy-5-methylbenzimidoyl chloride (4C) (1.6g, 1eq).

IR (ATR): Ar-H 2920.0, C=N 1634.2; MS (CI+, NH3): m/z=262.4 (M+H+, 100%);

1H NMR (400 MHz, CDCl3) δ ppm 12.53 (1 H, s, OH), 7.34 (1 H, d, J=2.1 Hz, H3), 7.18 (1 H, d, J=2.1 Hz, H5), 4.07 (2 H, s, H5'), 2.28 (3 H, s, Ar-CH3), 1.43 (9 H, s, tBu), 1.40 (6 H, s, (CH3)2); 13C NMR (100 MHz, CDCl3) δ ppm 164.2 (C2'), 156.83 (COH), 136.8 (C2), 131.3 (C3), 126.5 (C4), 125.6 (C5), 110.5 (C6), 78.1 (C5'), 67.1(C4'), 34.8 (CH(CH3)3) 29.4 (CH(CH3)3), 28.5 ((CH3)2) 20.7 (ArCH3);

Elemental analysis found: C 73.64%, H 8.91%, N 5.36%; ($C_{16}H_{23}NO_2$) requires: C 73.53%, H 8.87%, N 5.36%.

8.5 Chiral cyclisations: (S)-Valinol

(S)-2-(4-isopropyl-4,5-dihydrooxazol-2-yl)phenol (**1E**): Conducted as for (**1D**) except using N,2-dihydroxybenzimidoyl chloride (1C) (3.06g, 1eq) and (S)-Valinol (3.87g, 2.1eq). This was then triturated with hexane to yield product as orange/brown oil (1.01g, 28%).

IR (NaCl): OH 2961.3, Ar-H 2873.8, N=C 1642.7; MS(Cl^+,NH_3): *m/z*=206.3 ($M+H^+$,100%); ^{1}H NMR (400 MHz, $CDCl_3$) δ ppm 7.65-7.60 (1H, dd, J=7.8, 1.7 Hz, H3), 7.38-7.31 (1H, m, H4), 7.02-6.98 (1H, m, H5), 6.89-6.82 (1H, td, J=7.5 Hz, H6), 4.45-4.35 (1H, m, CH(C_3H_7)), 4.16-4.05 (2H, m, O-CH_2-CH), 1.85-1.73 (1H, m, CH($CH_{3)2}$), 1.05-0.97 (3H, d, J=6.8, CH_3), 0.96-0.91 (3H, d, J=6.7, CH_3); Elemental analysis found: C 70.24%, H 7.45%, N 6.91%; ($C_{12}H_{15}NO_2$) requires: C 70.22%, H 7.37%, N 6.82%.

(S)-2-(4-isopropyl-4,5-dihydrooxazol-2-yl)-6-methoxyphenol (**2E**): Reaction was conducted as for (1E) except using N,2-dihydroxy-3-methoxybenzimidoyl chloride (2C) (1.1g, 1eq). This yielded crude product as light brown oil (1.27g, 98%). This was triturated with hot hexane (100ml) to yield product as light yellow solid. (0.34g, 27%)

IR (ATR): Ar-H 2966.0, C=N 1639.2; MS (CI+, NH3): m/z=236.3 (M+H+, 100%);

1H NMR (400 MHz, CDCl3) δ ppm 12.79 (1 H, br. s, OH), 7.25 (1 H, dd, J=8.0, 1.5

Hz, H5), 6.97 (1 H, dd, J=8.0, 1.5 Hz, H3), 6.81 (1 H, pt, J=8.2 Hz, H4), 4.38 - 4.49 (1 H, m H4'), 4.08 - 4.19 (2 H, m, H5'), 3.91 (3 H, s, OCH3), 1.80 (1 H, psxt, J=6.7 Hz CH(CH3)2), 1.01 (3 H, d, J=6.7 Hz, (CH(CH3A), 0.95 (3 H, d, J=6.7 Hz, (CH(CH3B); 13C NMR (100 MHz, CDCl3) δ ppm 165.3 (C2'), 150.3 (COH), 148.3 (C6), 119.4 (C5), 118.0 (C4), 114.7 (C3), 110.8 (C2), 71.3 (C5'), 70.0 (C4'), 56.1 (OCH3), 33.0 (CH(CH3)2), 18.6 (CH(CH3A), 18.5 (CH(CH3B); Elemental analysis found: C 66.21%, H 7.37%, N 5.91%; ($C_{13}H_{17}NO_3$) requires: C 66.36%, H 7.28%, N 5.95%.

(S)-2-(4-isopropyl-4,5-dihydrooxazol-2-yl)-6-methylphenol (**3E**): Reaction was conducted as for (1E) except using N,2-dihydroxy-3-methylbenzimidoyl chloride (3C) (1.6g, 1eq). This yielded crude product as light brown oil (0.43g, 23%). This was triturated with hot hexane (100ml) this yielded product as a light brown oil which crystallised on standing (0.37g, 20%).

IR (ATR): Ar-H 2958.3, C=N 1635.3; MS (Cl^+, NH_3): *m/z*=220 ($M+H_+$, 100%); $_1$H NMR (400 MHz, $CDCl_3$) δ ppm 12.59 (1 H, br. s. OH), 7.49 (1 H, dd, *J*=7.8, 1.6 Hz, H5), 7.23 (1 H, dd, *J*=7.4, 0.8 Hz, H3), 6.77 (5 H, *p*t, *J*=7.6 Hz, H4), 4.37 - 4.46 (1 H, m, H4'), 4.06 - 4.17 (2 H, m, H5'), 2.29 (3 H, s, CH_3), 1.79 (1 H, *p*sxt, *J*=6.7 Hz, C**H**(CH_3)$_2$), 1.02 (3 H, d, *J*=6.7 Hz, CH(C**H**$_{3A}$), 0.95 (3 H, d, *J*=6.7 Hz, CH(C**H**$_{3B}$); $_{13}$C

NMR (100 MHz, $CDCl_3$) δ ppm 165.4 (C2'), 158.2 (COH), 134.1 (C5), 125.7 (C6), 125.5 (C3), 118.0 (C4), 109.9 (C2), 71.5 (C5'), 69.9 (C4'), 33.0 (**C**H$(CH_3)_2$), 18.7 (CH(**C**$H_3)_2$), 15.9 (CH_3); Elemental analysis found: C 71.21%, H 7.81%, N 6.42%; ($C_{13}H_{17}NO_2$) requires: C 71.21%, H 7.81%, N 6.39%.

(S)-2-(tert-butyl)-6-(4-isopropyl-4,5-dihydrooxazol-2-yl)-4-methylphenol (4E): Reaction was conducted as for (1E) except using 3-(tert-butyl)-N,2-dihydroxy-5-methylbenzimidoyl chloride (4C) (1.6g, 1eq).

IR (ATR): Ar-H 2958.3, C=N 1631.5; MS (Cl^+, NH3): m/z=276.1 (M+H+, 100%);

1H NMR (400 MHz, CDCl3) δ ppm 12.65 (1 H, s, OH), 7.34 (1 H, d, J=2.18 Hz, H4), 7.18 (1 H, d, J=2.2 Hz, H3), 4.40 (1 H, td, J=7.5, 1.19 Hz, H4'), 4.06 - 4.13 (2 H, m, H5'), 2.27 (3 H, s, Ar-CH3), 1.75 (1 H, psxt, J=6.83 Hz, CH(CH3)2), 1.43 (9 H, s, tBu), 1.04 (3 H, d, J=6.69 Hz, CH(CH3A)), 0.95 (3 H, d, J=6.74 Hz, CH(CH3B)); 13C NMR (100 MHz, CDCl3) δ ppm 165.7 (C2'), 156.0 (COH), 136.8 (C2), 131.4 (C3), 126.5 (C4), 125.7 (C5), 110.3 (C6), 71.7 (C5'), 69.6 (C4'), 34.8 (C(CH3)3) 33.1 (CH(CH3)2), 29.4 (C(CH3)3), 20.7 (Ar-CH3), 18.9 (CH(CH3A), 18.7 (CH(CH3B); Elemental analysis found: C 74.17%, H 9.04%, N 4.99%; ($C_{17}H_{25}NO_2$) requires: C 74.14%, H 9.15%, N 4.98%.

8.6 Chiral cyclisations: (S)-Phenyl alanol

(S)-2-(4-benzyl-4,5-dihydrooxazol-2-yl)-6-methoxyphenol (**2F**): Reaction was conducted as for (1F) except using N,2-dihydroxy-3-methoxybenzimidoyl chloride (2C) (1.1g, 1eq). This yielded crude product as light brown oil (0.85g, 55%). This was titurated with hot hexane (100ml) to yield product as light yellow solid (0.52g, 33%).

IR (ATR): Ar-H 2989.3, C=N 1633.2; MS (Cl^+, NH_3): *m/z*=284.32(M+H, 100%); ^1H NMR (400MHz, $CDCl_3$) 7.26-7.21 (3H, m, Ar"-H2, Ar"-H3, Ar"-H4), 7.17-7.12 (3H, m, Ar"-H1, Ar"-H5, Ar-H3), 6.92-6.90 (1H, dd, *J*=8, 1.5Hz, Ar-H1), 6.79-6.72 (1H, pseudo t, Ar-H2), 4.58-4.54 (1H, m, Ar'-H4), 4.37-4.32 (1H, pseudo t, Ar'-$H5_A$), 4.09-4.05 (1H, pseudo t, Ar'-$H5_B$), 3.85 (3H, s, Ar-CH_3), 3.46-3.41 (1H, m, -CH_{2A}-), 3.04-2.99 (1H, m, -CH_{2B}-); Elemental analysis found: C 72.01%, H 6.10%, N 5.03%; ($C_{17}H_{17}NO_3$) requires: C 72.07%, H 6.05%, N 4.94%.

8.7 Nitrile synthesis

2-Hydroxybenzonitrile: Salicylaldehyde (7.00g, 1.0eq) and $NH_2OH.HCl$ (6.18g, 2.2eq) were dissolved in DMSO and initially stirred for 20 minutes at room temperature before being heated at 100°C for 6hr. Crude product was isolated as an orange solid (7.41g) which was purified by flash chromatography (product adhered to silica, eluting with 1:9 EtOAc in hexane, R_f = 0.67) to yield the title compound as a yellow-white solid (6.78g, 98%).

IR (NaCl, nujol mull): ArOH 3301.5, C≡N 2233.8; MS (Cl^+, NH_3): *m*/*z*=137.1 ($M+NH_4^+$, 100%); ^1H NMR (400 MHz, $CDCl_3$) δ ppm 7.35 (1 H, m, H4), 7.33 (1 H, m, H6), 6.90 (1 H, *p*t, *J*=7.7 Hz, H5), 5.93 (1 H, s, OH); ^{13}C NMR (100 MHz, $CDCl_3$) δ ppm 157.4 (COH), 136.4 (C4), 130.5 (C6), 126.6 (C3), 121.4 (C5), 117.2 (CN), 99.2 (C1); CHN ($C_8H_7O_2$) found: C 70.35%, H 4.28%, N 11.39%; required: C 70.56%, H 4.23%, N 11.76%.

2-Hydroxy-3-methylbenzonitrile: Repeated as for the synthesis of **5B'** except using **3A** and refluxing for 6hrs. This produced a foul smelling orange oil. Product of sufficient purity could be obtained by refluxing in hexane, before cooling and trituration. For analysis product was purified by flash chromatography (product adhered to silica, eluting with 1:9 EtOAc in hexane, Rf=0.32) to yield title compound as orange red solid (10.05g, 70%).

IR (NaCl, nujol mull): ArOH 3301.5, C≡N 2233.8; MS (Cl^+, NH_3): *m*/*z*=151.1 ($M+NH_4^+$, 100%); ^1H NMR (400 MHz, $CDCl_3$) δ ppm 7.35 (1 H, m, H4), 7.33 (1 H, m, H6), 6.90 (1 H, *p*t, *J*=7.7 Hz, H5), 5.93 (1 H, s, OH), 2.29 (3 H, s, CH_3) ^{13}C NMR (100 MHz, $CDCl_3$) δ ppm 157.4 (COH), 136.4 (C4), 130.5 (C6), 126.6 (C3), 121.4 (C5), 117.2 (CN), 99.2 (C1), 16.3 (CH_3); CHN ($C_8H_7O_2$) found: C 72.35%, H 5.28%, N 10.39%; required: C 72.16%, H 5.30%, N 10.52%.

8.8 $ZnCl_2$ catalysed cyclisations

2-(4,4-dimethyl-4,5-dihydrooxazol-2-yl)phenol (**1D**): $ZnCl_2$ (1.14g, 0.1 equiv.) was charged to a 250ml schlenk flask and heated under vacuum until molten (heatgun) before being allowed to cool under an argon atmosphere. 2-amino-2-methylpropan-1-ol (11.21g, 1.5 equiv.) and **2-hydroxybenzonitrile** (10g, 1.0eq) were dissolved in chlorobenzene (150ml) and charged in one go. The resulting bright yellow solution was heated to 131°C for 72 hours, before being cooled and stripped. The resulting yellow solid was quenched into 2M HCl (100ml) and extracted with DCM (5 x 100ml). The combined organic phases were washed with water (100ml) which was re-extracted with DCM (2 x 50ml). The combined organic phases were dried (Mg_2SO_4) and stripped to give a yellow solid (7.71g), which was purified by flash chromatography (product adhered to silica, eluting with 1:9 EtOAc in hexane, R_f = 0.72) to yield the title compound as a dark oil (5.4g, 52%).).

MS (Cl^+, NH_3): *m/z*=192.25 ($M+H^+$, 100%); ^{1}H NMR (400 MHz, $CDCl_3$) δ ppm 7.57-7.54 (1H, dd, J=7.8, 1.7Hz, H3), 7.31-7.26 (1H, m, H4), 6.94-6.91 (1H, dd, J=8.4, 0.9Hz, H5), 6.81-6.77 (1H, td, J=7.5Hz, H6), 4.02 (2H, s, CH_2), 1.32 (6H, s, $(CH_3)_2$); ^{13}C NMR (100 MHz, $CDCl_3$) 163.88 (C-OH), 160.21 (C-Ox), 133.57 (C3), 128.26 (C4), 118.97 (C5), 117.06 (C6), 111.30 (N-C-O), 78.76 (O-C-C), 67.52 (C-C-N),

28.94 ($(CH_3)_2$); CHN ($C_{11}H_{13}NO_2$) found: C 68.14%, H 6.82%, N 7.32%; required: C 69.09%, H 6.85%, N 7.32%.

2-(4,4-dimethyl-4,5-dihydrooxazol-2-yl)-6-methylphenol (**3D**): Reaction conducted as for (**1D**) except using 2-hydroxy-3-methylbenzonitrile. To yield crude product as a brown oil, this was refluxed in hexane over charcoal. This yielded product as a yellow oil (1.23g, 60%)

IR (ATR): Ar-H 2970.1, C=N 1634.1; MS (Cl_+, NH_3): *m/z*=206.3 ($M+H_+$, 100%); $_1$H NMR (400 MHz, $CDCl_3$) δ ppm 12.46 (1 H, br. s., OH), 7.48 (1 H, ddd, *J*=7.9, 1.7, 0.5 Hz, H3), 7.22 (1 H, ddd, *J*=7.4, 1.7, 0.9 Hz, H5), 6.77 (1 H, *p*t, *J*=7.6 Hz, H4), 4.08 (2 H, s, H5'), 2.28 (3 H, s, CH_3), 1.38 (6 H, s, $(CH_3)_2$); ^{13}C NMR (100 MHz, $CDCl_3$) δ ppm 163.9 (C2'), 158.1 (COH), 134.0 (C5), 125.6 (C6), 125.4 (C3), 118.0 (C4), 110.1 (C2), 78.3 (C5'), 67.0 (C4'), 28.5 ($(CH_3)_2$), 15.8 (CH_3); CHN ($C_{12}H_{15}NO_2$) found: C 70.04, H 7.77, N 7.03; required: C 70.22, H 7.37, N 6.82;

(S)-2-(4-isopropyl-4,5-dihydrooxazol-2-yl)phenol (**1E**): Conducted as for (**5E'**) except using **2-hydroxybenzonitrile** and (S)-Valinol. This was then triturated with hexane to yield product as orange/brown oil (3.01g, 45%).

IR (NaCl): OH 2961.3, Ar-H 2873.8, N=C 1642.7; MS(Cl^+,NH_3): *m/z*=206.3 ($M+H^+$,100%); ^{1}H NMR (400 MHz, $CDCl_3$) δ ppm 7.65-7.60 (1H, dd, J=7.8, 1.7 Hz, H3), 7.38-7.31 (1H, m, H4), 7.02-6.98 (1H, m, H5), 6.89-6.82 (1H, td, J=7.5 Hz,

H6), 4.45-4.35 (1H, m, CH(C_3H_7)), 4.16-4.05 (2H, m, O-CH_2-CH), 1.85-1.73 (1H, m, CH(CH_3)$_2$), 1.05-0.97 (3H, d, J=6.8, CH_3), 0.96-0.91 (3H, d, J=6.7, CH_3); CHN ($C_{12}H_{15}NO_2$) found: C 70.24%, H 7.45%, N 6.91%; required: C 70.22%, H 7.37%, N 6.82%.

(S)-2-(4-isopropyl-4,5-dihydrooxazol-2-yl)-6-methylphenol (**3E**): Reaction was conducted as for (1E) except using 2-hydroxy-3-methylbenzonitrile (1.6g, 1eq). This yielded crude product as light brown oil (0.43g, 23%). This was triturated with hot hexane (100ml) this yielded product as a light orange oil which crystallised on standing (5.6g, 52%).

IR (ATR): Ar-H 2958.3, C=N 1635.3; MS (Cl_+, NH_3): *m*/*z*=220 (M+H_+, 100%); $_1$H NMR (400 MHz, $CDCl_3$) δ ppm 12.59 (1 H, br. s. OH), 7.49 (1 H, dd, *J*=7.8, 1.6 Hz, H5), 7.23 (1 H, dd, *J*=7.4, 0.8 Hz, H3), 6.77 (5 H, *p*t, *J*=7.6 Hz, H4), 4.37 - 4.46 (1 H, m, H4'), 4.06 - 4.17 (2 H, m, H5'), 2.29 (3 H, s, CH_3), 1.79 (1 H, *p*sxt, *J*=6.7 Hz, C**H**(CH_3)$_2$), 1.02 (3 H, d, *J*=6.7 Hz, CH(C**H**$_{3A}$), 0.95 (3 H, d, *J*=6.7 Hz, CH(C**H**$_{3B}$); $_{13}$C NMR (100 MHz, $CDCl_3$) δ ppm 165.4 (C2'), 158.2 (COH), 134.1 (C5), 125.7 (C6), 125.5 (C3), 118.0 (C4), 109.9 (C2), 71.5 (C5'), 69.9 (C4'), 33.0 (**C**H(CH_3)$_2$), 18.7 (CH(**C**H_3)$_2$), 15.9 (CH_3); CHN ($C_{13}H_{17}NO_2$) found: C 71.21%, H 7.81%, N 6.42%; required: C 71.21%, H 7.81%, N 6.39%.

8.9 Amino Alcohol reduction

(S)-2-amino-3-methylbutan-1-ol (**(S)-valinol**): (S)-valine (11.80g, 1.0 eq) and $NaBH_4$ (8.32g, 2.2 eq) were suspended in THF (75ml) to give a white slurry. This was cooled to 0°C before the drop-wise addition of I_2 (25.38g, 1.0 eq) in THF (50ml) over 15min. Once the slurry had returned to white it was heated to reflux for 16 h. The white slurry was then cooled to 0°C before careful quenching with methanol (50ml, or until an opaque solution formed, significant H_2 off-gassing). This was concentrated to give a white semi-solid, which was dissolved in 20% w/v NaOH (150ml) and extracted in diethyl ether (3x100ml). Combined organic was washed with brine (100ml) dried (Mg_2SO4) and stripped to give a slightly opaque oil (8.71g). This was purified by Kugelrohr distillation (150°C, 8 mbar) to yield the title compound as clear colourless oil (6.89g, 67%).

IR (ATR): OH + NH_2 3344.0; MS (Cl+, NH_3): *m/z*=104.2 ($M+H^+$, 100%); ^1H NMR (400 MHz, $CDCl_3$) δ ppm 5.03 (1 H, br. s., OH), 3.64 (1 H, dd, J=10.75, 3.72 Hz, H1A), 3.34 (1 H, dd, J=10.75, 8.52 Hz, H1B), 3.05 (2 H, s, NH_2), 2.59 (1 H, ddd, J=8.48, 6.37, 3.75 Hz, H2), 1.61 (1 H, psxt, J=6.60 Hz, H3), 0.92 (1 H, d, J=6.83 Hz, CH_3A), 0.92 (1 H, d, J=6.78 Hz CH_3B); ^{13}C NMR (100 MHz, $CDCl_3$) δ ppm 64.31 (C1), 58.30 (C2), 30.92 (C3), 19.18 (CH_3A), 18.30 (CH_3B); Elemental analysis found: C 58.33%, H 13.29%, N 11.30%; ($C_5H_{13}NO$) requires: C 58.21%, H 12.70%, N 13.58%.

(S)-2-amino-3-phenylpropan-1-ol (**(S)-Phenyl alanol**): Reaction conducted as for (S)-valinol except using (S)-phenyl alanol (10g, 1eq). This yielded crude product (12.97g) as clear oil which crystallised on standing. This was dissolved in toluene to yield product as white powdery solid (4.55g, 50%)

IR (ATR): NH 2927.4, CO 1049.0; MS (Cl^+, NH_3): *m/z*= 152.1($M+H^+$, 100%); ^1H NMR (400 MHz, $CDCl_3$) δ ppm 7.06 - 7.26 (m, 5H), 3.55 (dd, *J*=10.9, 3.7 Hz, 1H), 3.32 (dd, *J*=10.8, 7.4 Hz, 1H), 2.90 - 3.11 (m, 3H), 2.69 (dd, *J*=13.6, 5.4 Hz, 1H), 2.47 (dd, *J*=13.3, 8.7 Hz, 1H); ^{13}C NMR (101 MHz, $CDCl_3$) δ ppm 138.66, 129.65, 129.05, 126.96, 65.97, 54.68, 40.54; Elemental analysis found: C 71.44%, H 8.85%, N 9.18%; ($C_9H_{13}NO$) requires: C 71.49%, H 8.67%, N 9.26%.

9. Complex Formation

9.1 Synthesis of rare earth starting materials

Anhydrous rare earth chlorides:

RE_2O_3 (1.0 equiv) and an excess of NH_4Cl (4.0 equiv) were dissolved in conc. HCl (200 ml, 36% w/v) to give a pale yellow solution. This was evaporated to dryness, giving a white solid which was oven baked overnight (~160°C). The off-white solid was ground into a fine powder and transferred to the ampoule of the sublimation glassware. This was placed under high vacuum (mercury diffusion pump) and the ampoule and heated to 200°C for 2 hr (tube furnace) before increasing the temperature to 360°C at approximately 10°C per 30 min were it was held for 12 hrs. During this process NH_4Cl sublimed out of the ampoule to coat the inside of the rest of the glassware. The sample was allowed to cool and the (now anhydrous) $LnCl_3$ was isolated by flame sealing the ampoule under N_2. Removal of the NH_4Cl was confirmed by Elemental analysis.[107]

Anhydrous rare earth chlorides via dehydration with thionyl chloride:

Ln_2O_3 (1.0 equiv) was dissolved in conc. HCl (200 ml, 36% w/v) to give a clear solution. This was slowly evaporated to dryness over several hours, giving a white solid.

Thionyl chloride, $SOCl_2$ (150ml) was refluxed (~90°C) for ~30 minutes over linseed oil (6.25ml). $SOCl_2$ (~100ml) distilled off over 4 hours at (~95°C).

Hydrated $LnCl_3$ ground to a fine powder and $SOCl_2$ added, this produced a small amount of effervescence and a fine white suspension this was heated at reflux (~95°C) for ~48 hours.

The resultant suspension was heated under vacuum for 5days to drive off residual $SOCl_2$. This produced anhydrous $LnCl_3$ as on off white solid.

Yields:

YCl_3-98%

$EuCl_3$-95%

Lanthanide silylamide, $[Ln(N\{SiMe_3\}_2)_3]$:

nBuLi (2.95eq) placed in a flask and cooled to 0°C and HMDS (2.95eq) added carefully via syringe injection under argon. A white crystalline precipitate formed which dissolved upon the addition of dry THF. $LnCl_3$ added with cooling under argon and the resultant pale yellow solution stirred at room temperature overnight. This resulted in an orange solution with a small amount of white precipitate that was heated to reflux (~100°C) for ~3 hours to ensure complete reaction. The resultant cloudy orange suspension was allowed to cool to room

temperature and settle out, producing white precipitate. This was reduced to dryness and heated for ~2 hours at ~90°C, before cooling and addition of dry toluene (~250ml). The solution was vigorously stirred at room temperature before a white solid was allowed to settle out and the solvent transferred to a clean flask.

The orange solution was reduced by half under vacuum and cooled for ~72 hours to allow crystals to form. These crystals were then removed by Schlenck filtration and stored under argon in a Schlenck flask as a yellow white fluffy solid. Product confirmed by NMR.

Yields:

$Y(Si(N(CH_3)_3)_2)_3$-75%

$Eu(Si(N(CH_3)_3)_2)_3$-58%

9.2 Rare earth complexes prepared *via* the silylamide route

Synthesis of $Li_3[Y(Me_2\text{-}Ph)_6]$: Me_2-Ph (1g, 6eq) was dissolved in dry THF and cooled before careful addition of 2.5M n-BuLi (1.009ml, 0.167g, 3eq). The resultant bright yellow solution was stirred for 20 minutes with cooling before being allowed to warm to room temperature.

A flask containing $Y(N(SiMe_3)_2)_3$ (1.49g, 1eq) was cooled and dry THF (~100ml) added. To this the partially deprotonated ligand solution was added via cannula

to produce a clear solution that was stirred at room temperature overnight. Solvent and HMDS were removed in vacuum to produce the title compound as an off-white amorphous solid (0.98g, 90%).

MS (EI^+, NH_3): *m/z*=1060.6 ($Li_3[Y(Me_2\text{-}Ph)_5]$, 20%); ^1H NMR (400MHz, $CDCl_3$) δ ppm 7.46-7.44 (1H, d, *J*=7.9Hz, H1), 7.41-7.38 (2H, d, *J*=7.8, 1.6Hz, H1), 7.34-7.32 (2H, m, H2), 7.25-7.22 (1H, dd, *J*=7.8, 1.7Hz, H4), 7.19-7.17 (1H, d, *J*=8 Hz, H4), 7.15-7.12 (1H, dd, *J*=7.8, 1.7Hz, H1), 6.98-6.69 (1H, d, *J*=8.1Hz, H4), 6.93-6.88 (1H, m, H2), 6.74-6.70 (2H, m, H2), 6.68-6.60 (4H, m, H2, H3), 6.43-6.39 (1H, t, *J*=7.4Hz x2, H3), 6.34-6.32 (1H, m, H2), 6.30-6.13 (8H, m, H2, H3), 5.61-5.59 (1H, d, *J*=8.2 Hz, H1), 3.98-3.96 (1H, d, *J*=8.1 Hz, H5'), 3.86-3.84 (1H, d, *J*=8.1 Hz, $H5_A$'), 3.76-3.74 (1H, d, *J*=7.2 Hz, H5'), 3.72-3.70 (1H, m, H5'), 3.67-3.65 (1H, d, *J*=7.8 Hz, H5'), 3.56-3.54 (1H, d, *J*=7.8 Hz, $H5_A$') 3.52-3.50 (1H, d, *J*=7.7, H5'), 3.25-3.23 (1H, d, *J*=7.8 Hz, $H5_A$') 3.20-3.18 (1H, d, *J*=7Hz, H5'), 3.15-3.13 (1H, d, *J*=7.8 Hz, $H5_A$'), 1.08 (3H, s, CH_3), 1.05 (3H, s, CH_3), 0.99 (3H, s, CH_3), 0.98 (3H, s, CH_3), 0.97 (3H, br. s, CH_3), 0.95 (3H, s, CH_3), 0.92 (3H, s, CH_3), 0.80 (3H, s, CH_3), 0.79 (3H, s, CH_3), 0.73 (3H, s, CH_3), 0.34 (3H, s, CH_3), 0.30 (2H, s CH_3), 0.19 (3H, s, CH_3); ^{13}C NMR (400MHz, $CDCl_3$) δ ppm 165.6 (C-OH) 165.6 (C-OH), 165.4 (C-OH), 165.4 (C-OH), 164.9 (C-OH), 164.2 (C-Ox), 164.1 (C-Ox), 163.2 (C-Ox), 163.0 (C-Ox), 162.80 (C-Ox), 132.4 (C1), 132.3 (C1), 131.8 (C1), 131.8 (C1), 131.6 (C1), 129.2 (C4), 128.9 (C4), 128.7 (C4), 128.5 (C4), 128.4 (C4), 124.0 (C2), 123.8 (C2), 123.6 (C2),

123.5 (C2), 123.1 (C2), 115.6 (C3), 115.3 (C3), 115.2 (C3), 114.6 (C3), 114.5 (C3), 114.4 (O-C=N), 114.3 (O-C=N), 114.1 (O-C=N), 114.0 (O-C=N), 113.7 (O-C=N), 77.7 (O-C-C), 77.5 (O-C-C), 77.3 (O-C-C), 77.0 (O-C-C), 76.9 (O-C-C), 67.3 (N-C-C), 67.2 (N-C-C), 67.1 (N-C-C), 66.9 (N-C-C), 66.7 (N-C-C), 28.8 (CH_3), 28.5 (CH_3), 28.5 (CH_3), 28.3 (CH_3), 28.2 (CH_3), 28.2 (CH_3), 28.1 (CH_3), 27.9 (CH_3), 27.1 (CH_3), 27.1 (CH_3), 26.7 (CH_3), 25.9 (CH_3), 25.4 (CH_3), 24.8 (CH_3), 24.6 (CH_3), 24.4 (CH_3); Elemental analysis found C 63.40%, H 5.68%, N 6.63%; ($Li_3C_{66}H_{72}N_6O_{12}Y$) requires C 63.34%, H 5.80%, N 6.72%.

Synthesis of $Li_3[Y(^iPr\text{-}Ph)_6]$: Synthesised in the same was as **$Li_3[Y(Me_2\text{-}Ph)_6]$**but using ^{i}Pr-Ph (2g, 4eq) as the ligand. $Li_3[Y(^iPr\text{-}Ph)_6]$ isolated as a crystalline white solid (1.49g, 70%).

MS (NSI^+): *m/z*=1333.52 ($M+H^+$, 20%); ^{1}H NMR (400MHz, $CDCl_3$) δ ppm 7.63-7.60 (1H, m, Ar-H1), 7.56-7.53 (1H, m, Ar-H4), 7.48-7.46 (2H, d, *J*=7.3Hz, Ar-H1, Ar-H4), 7.42ppm (2H, br. s, Ar-H2), 7.09 (5H, br. s), 6.64 (2H, m, Ar-H3), 6.54 (1H, m, Ar-H4), 6.46 (1H, m, Ar-H4), 6.36 (1H, br. s, Ar-H1), 4.37 (3H, br. s, H5'), 3.98 (5H, br. s, H5'), 3.88 (2H, br. s, H5'), 0.86 (3H, br. s, CH(C**H$_{3A}$**)), 0.8 (3H, br. s, CH(C**H$_{3B}$**)), 0.51 (3H, d, *J*=6.1 Hz, CH(C**H$_{3A}$**)), 0.47 (3H, d, *J*=6.1 Hz, CH(C**H$_{3B}$**)), 0.35-0.33 (3H, d, *J*=6.7 Hz, CH(C**H$_{3A}$**)), 0.25-0.24 (3H, d, *J*=6.7 Hz, CH(C**H$_{3B}$**)); ^{13}C NMR (400MHz, $CDCl_3$) δ ppm 164.0 (C-OH), 158.8 (C-Ox), 132.1 (C1), 126.9 (C2), 117.3 (C2), 115.6 (C3), 109.6 (O-C=N), 70.4 (O-C-C), 68.8 (N-C-C), 32.0 (**C**H$(CH_3)_2$), 17.6

(CH_{3A}), 17.5 (CH_{3B}); Elemental analysis found C 64.88%, H 6.18%, N 6.16%; ($Li_3C_{72}H_{84}N_6O_{12}Y$) requires C 64.78%, H 6.298%, N 6.298%.

Synthesis of $Li_3[Eu(Me_2\text{-}Ph)_6]$: Synthesised as for **$Li_3[Y(Me_2\text{-}Ph)_6]$** but using $Eu(N(SiMe_3)_2)_3$ (g,1eq) and Me_2-Ph(6eq). $Li_3[Eu(Me_2\text{-}Ph)_6]$ isolated as a pale yellow solid (1.2g, 90%).

MS (NSI^+): *m/z*=1124.4 ($Li_3[Eu(Me_2\text{-}Ph)_5]$, 20%); ^{1}H NMR (400MHz, $CDCl_3$) δ ppm 7.57 (1H, br. s, Ar-H1), 7.06 (1H, br. s, Ar-H4), 6.63 (1H, br. s, Ar-H2), 6.28 (1H, br. s, Ar-H3), 3.92 (2H, br. s, H5'), 1.23 (6H, br. s, $(CH_3)_2$); ^{13}C NMR (400MHz, $CDCl_3$) δ ppm 164.3 (C-OH), 132.3 (C-Ox), 130.0 (C1), 122.4 (C2), 113.2 (C3), 76.7 (O-C-C), 27.8 (CH_3); Elemental analysis found C 60.16%, H 6.40%, N 5.46%; ($Li_3C_{66}H_{72}N_6O_{12}Eu$) requires C 60.25%, H 6.39%, N 5.52%.

9.3 Rare earth complexes prepared *via* salt metathesis

Synthesis of $Na[Y(Me_2\text{-}Ph)_4]$: Anhydrous YCl_3 (0.085g, 1eq) was transferred to a Schlenk flask in a glove box and placed under an inert atmosphere. In a separate flask NaH (0.127g, 60% suspension in mineral oil, 8.8eq) was weighed out, placed under an inert atmosphere and suspended in dry petroleum ether. This was stirred at room temperature for 1hr, the resulting suspension was allowed to settle before removal of the pet. ether/mineral oil solution via cannula. The now activated NaH was resuspended in dry THF and cooled to 0°C before addition of Me_2-Ph (0.49g, 4eq) as a solution in dry THF. This was done with care

as hydrogen gas is produced during the addition. This was stirred at room temperature for 2hrs before being allowed to settle giving a pale yellow solution (Na-Me_2-Ph) and white precipitate. The YCl_3 was now suspended in dry THF and sonicated, the pale yellow solution was carefully transferred to the YCl_3 suspension with cooling and the mixture stirred overnight at room temperature before being allowed to settle (slowly). The resultant yellow solution was transferred by cannula to a clean Schlenk flask, leaving behind a white precipitate (NaCl). The solution was reduced to dryness and redissolved in dry toluene to ensure complete removal of all NaCl. The supernatant was then removed via cannula again in to a clean Schlenk flask and concentrated to give product as a white solid (0.58g, 50%)

MS ($^+$MALDI): *m/z*=895.22 (Na_2[Y(Me_2-Ph)$_4$], 85%); ^{1}H NMR (400MHz, $CDCl_3$, 25°C) δ ppm 7.56 (1H, d, *J*= 7.8 Hz, Ar-H1), 7.07 (1H, t, *J*= 6.6 Hz, Ar-H2), 6.54 (1H, d, *J*=7.8 Hz, Ar-H4), 6.43 (1H, t, *J*=6.9 Hz x2, Ar-H3), 3.87 (2H, br. s, H5'), 1.13-1.10 (6H, m, $(CH_3)_2$); ^{1}H NMR (400MHz, $CDCl_3$, -80°C) δ ppm 7.66-7.64 (1H, dd, *J*=7.9, 1.5 Hz), 7.63-7.61 (1H, m), 7.47-7.45 (2H, m), 7.27-7.24 (2H, m), 7.07-7.03 (1H, m), 6.97-6.94 (1H, d, *J*=8.2 Hz), 6.89 (1H, s), 6.62-6.60 (1H, d, *J*=8.2 Hz), 6.49-6.45 (1H, t, *J*=7.4 Hzx2), 6.41-6.39 (1H, d, *J*=8 Hz), 4.20 (1H, s), 4.10-4.08 (1H, d, *J*=7.6 Hz), 4.02-3.98 (2H, t, *J*=7.4 Hz x2), 3.49-3.47 (1H, d, *J*=7.8 Hz), 1.39 (6H, s), 1.32 (3H, br. s), 1.25 (3H, br. s), 0.82 (3H, br. s), 0.68 (3H, br. s); ^{13}C NMR

(400MHz, $CDCl_3$) δ ppm 164.7 (C-OH), 130.2 (C-Ox), 127.8 (C2), 120.1 (C3), 113.5 (C4), 111.6 (C5), 75.6 (O-C=N), 66.0 (O-C-C), 25.1 (N-C-C), 23.5 ($(CH_3)_2$); Elemental analysis found C 60.78%, H 5.55%, N 6.43%; ($Na_3C_{66}H_{72}N_6O_{12}Y$) requires C 60.99%, H 5.59%, N 6.47%.

Synthesis of Na[Y(^{i}Pr-MePh)$_4$]: Synthesised as for **Na[Y(Me$_2$-Ph)$_4$]**, except using ^{i}Pr-MePh(4eq). This produced Na[Y(^{i}Pr-MePh)$_4$] as an amorphous white solid (0.56g, 48%).

MS ($^+$MALDI): *m/z*=747.19 (Na_2[Y(^{i}Pr-Ph)$_3$], 30%); ^{1}H NMR (400MHz, $CDCl_3$, 25°C) δ ppm 7.41-7.39 (3H, dd, *J*=7.9, 1.2 Hz, Ar-H), 7.29-7.27 (1H, d, *J*=7.5 Hz, Ar-H), 7.11-7.10 (1H, d, *J*=6.5 Hz, Ar-H), 6.97 (3H, br. s, Ar-H), 6.32-6.28 (2H, t, *J*=7.4 Hz x2), 4.22-4.21 (2H, d, *J*=3.6 Hz, H5') 4.04-4.03 (5H, d, *J*=4.6 Hz, H5'), 3.98 (3H, br. s, H5'), 3.77-3.75 (1H, m, H5'), 2.87 (1H, t, *J*=8.3 Hz x2, H4'), 2.79 (1H, br. s, H4'), 2.49 (3H, s, H4'), 2.1 (10H, br. s, $CH(CH_3)_2$)), 0.91 (8H, d, *J*=6.1 Hz, $(CH_3)_2$), 0.83 (8H, m, $(CH_3)_2$), 0.76-0.74 (4H, d, *J*=6.9, $(CH_3)_2$), 0.44-0.42 (4H, d, *J*=6.4, $(CH_3)_2$); ^{1}H NMR (400MHz, $CDCl_3$, -80°C) δ ppm 7.48-7.46 (1H, d, *J*=6.8 Hz), 7.38-7.37 (2H, d, *J*=7 Hz), 7.30-7.28 (1H, d, *J*=7.2 Hz), 7.17-7.15 (1H, dd, *J*=7.8, 1.8 Hz), 6.97-6.96 (1H, d, *J*=5.5 Hz), 6.91-6.89 (1H, d *J*=5.7 Hz), 6.81-6.77 (1H, t, *J*=7.6 Hz x2), 6.05-6.01 (1H, t, *J*=7.3 Hz x2), 5.95 (1H, br. s), 4.67-4.65 (1H, d, *J*=8.4 Hz), 4.55-4.51 (1H, m), 4.26-4.22 (1H, m), 4.19-4.15 (1H, dd, *J*=9.3, 7.1 Hz), 4.08 (1H, br. s), 3.99 (3H, br. s), 2.47 (3H, s), 2.23 (3H, s), 2.07 (6H, br. s), 1.03-1.01 (3H, d, *J*=6.7 Hz),

0.96-0.94 (3H, d, *J*=6.7 Hz), 0.91-0.87 (6H, m), 0.78-0.72 (6H, m), 0.70-0.68 (3H, d, *J*=6.1 Hz), 0.29-0.28 (3H, d, *J*=6.1 Hz); Elemental analysis found C 62.91%, H 6.43%, N 5.53%; ($Na_3C_{72}H_{84}N_6O_{12}Y$) requires C 63.13%, H 6.93%, N 5.73%.

9.4 Rare earth complexes from rare earth chlorides produced *via* trimethyl orthoformate dehydration

Synthesis of $Na[Y(Me_2\text{-}Ph)_6](OH)(THF)_2$: Y_2O_3 (1.0 equiv, 0.074g) was dissolved in conc. HCl (40 ml, 36% w/v) to give a clear solution. This was heated to dryness, giving a white solid. This was then dissolved in water, transferred to a Schlenk flask and the water removed *in vacuo.* Trimethyl orthoformate (260 equiv, 29.83g, 30ml) was then added and the reaction refluxed (~115°C) for 2hrs. This was then reduced to dryness to produce an off-white solid before being suspended in dry THF (~30ml).

NaH(0.138g, 60% suspension in mineral oil, 17.62eq) was weighed out, placed under an inert atmosphere and suspended in dry petroleum ether This was stirred at room temperature for 1hr, the resulting suspension was allowed to settle before removal of the pet. ether/mineral oil solution via cannula. The now activated NaH was resuspended in dry THF and cooled to 0°C before addition of Me_2-Ph (0.5g, 8eq) as a solution in dry THF. This was done with care as hydrogen gas is produced during the addition. This was stirred at room temperature for 2hrs before being allowed to settle giving a pale yellow solution (Na-Me_2-Ph) and white precipitate. The YCl_3 was now suspended in dry THF and sonicated, the pale yellow solution was carefully transferred to the YCl_3 suspension with cooling and the mixture stirred overnight at room temperature before being

allowed to settle (slowly). The resultant yellow solution was transferred by cannula to a clean Schlenk flask, leaving behind a white precipitate (NaCl). The solution was reduced to dryness and redissolved in dry toluene to ensure complete removal of all NaCl. The supernatant was then removed via cannula again in to a clean Schlenk flask and concentrated to give product as a white solid (0.58g, 50%)

9.5 Rare earth complexes prepared *via* rare earth nitrate tetraglyme ($RE(NO_3)_3$(Tetraglyme))

Synthesis of [Na(Tetraglyme)$(THF)_2$][La(Me_2-Ph)$_4$]: La_2O_3 (1.0 equiv, 0.551g) was dissolved in conc. HNO_3 (40 ml, 36% w/v) to give a clear solution. This was heated to dryness, giving a white solid. To this tetraglyme (0.869g, 2eq) was added as a solution in ethyl acetate (50ml). This was followed by a distillation at 80°C to remove water.[110]

NaH(0.138g, 60% suspension in mineral oil, 17.6eq) was weighed out, placed under an inert atmosphere and suspended in dry petroleum ether This was stirred at room temperature for 1hr, the resulting suspension was allowed to settle before removal of the pet. ether/mineral oil solution via cannula. The now activated NaH was resuspended in dry THF and cooled to 0°C before addition of Me_2-Ph (0.5g, 8eq) as a solution in dry THF. This was done with care as hydrogen gas is produced during the addition. This was stirred at room temperature for

2hrs before being allowed to settle giving a pale yellow solution (Na-Me_2-Ph) and white precipitate. The YCl_3 was now suspended in dry THF and sonicated, the pale yellow solution was carefully transferred to the YCl_3 suspension with cooling and the mixture stirred overnight at room temperature before being allowed to settle (slowly). The resultant yellow solution was transferred by cannula to a clean Schlenk flask, leaving behind a white precipitate ($NaNO_3$). The supernatant was then removed via cannula in to a clean Schlenk flask and concentrated to give product as a white solid (0.58g, 50%).

10. Catalytic reactions

10.1General procedure:

0.033 molar equivalents of catalyst was dissolved in THF (~5ml). To this nitromethane (1eq) and aldehyde (1eq) was added and the reaction stirred at room temperature overnight.

Reaction solution was quenched 2M HCl and product extracted with EtOAc (2x~25ml). The combined organic layers were washed with brine (~50ml). This was dried ($MgSO_4$), filtered and stripped to yield a yellow/orange oil. This was purified by column chromatography (1:5, EtOAc:Hex).

Structure	Nomenclature
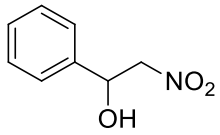	2-nitro-1-phenylethanol

2-nitro-1-phenylethanol: Prepared as for the general procedure described above except using benzaldehyde (1eg, 0.072g) and nitromethane (0.041g, 1eq). This produced product as a clear, slightly yellow oil (0.095, 90%).

MS (CI^+, NH_3): *m/z*= 120.1 (M-NO_2, 10%), 107.1 (M-CH_2NO_2, 100%); ^1H NMR (400MHz, $CDCl_3$) δ ppm 7.30 (5H, s, Ar-H1, Ar-H2, Ar-H3, Ar-H4, Ar-H5), 5.36-5.31 (1H, dd, *J*=9.2, 3.1 Hz, CH), 4.55-4.36 (2H, m, CH_A, CH_B), 3.02 (1H, br, s, C-OH); Elemental analysis found: C 58.14%, H 5.31%, N 8.86%; ($C_8H_9NO_2$) requires C 57.48%, H 5.43%, N 8.38%.[130]

Bibliography

1 M. Shibasaki, M. Kanai and K. Funabashi, *Chem. Commun. (Camb).*, 2002, 1989–1999.

2 M. Shibasaki, H. Sasai and T. Arai, *Angew. Chem. Int. Ed. Engl.*, 1997, **36**, 1236–1256.

3 J. V Allen, J. F. Bower and J. M. J. Williams, *Tetrahedron: Asymmetry*, 1994, **5**, 1895–1898.

4 R. Andreasch, *Monatshefte für Chemie - Chem. Mon.*, 1884, **5**.

5 S. Gabriel, *Berichte der Dtsch. Chem. Gesellschaft*, 1889, **22**, 1139–1154.

6 C. Henvichs and H. Brunner, *Tetrahedron Lett.*, 1995, **6**, 653–656.

7 a. Ebru Aydin and S. Yuksekdanaci, *Tetrahedron: Asymmetry*, 2013, **24**, 14–22.

8 G. C. Hargaden and P. J. Guiry, *Chem. Rev.*, 2009, **109**, 2505–50.

9 K. Schwekendiek and F. Glorius, *Synthesis (Stuttg).*, 2006, **2006**, 2996–3002.

10 L. E. N. Allan, G. J. Clarkson, D. J. Fox, A. L. Gott and P. Scott, *J. Am. Chem. Soc.*, 2010, **132**, 15308–15320.

11 M. Gómez, G. Muller and M. Rocamora, *Coord. Chem. Rev.*, 1990, **105**, 769–835.

12 A. K. Ghosh, P. Mathivanan and J. Cappiello, *Tetrahedron*, 1998, **9**, 1–45.

13 T. R. Ward, *Organometallics*, 1996, **7333**, 2836–2838.

14 B. D. Ward and L. H. Gade, *Chem. Commun. (Camb).*, 2012, **48**, 10587–99.

15 C. Bolm, T. Kim, K. Luongq and K. Harmsa, *Chem. Ber.*, 1997, 887–890.

16 K. Kempe, M. Lobert, R. Hoogenboom and U. S. Schubert, *J. Comb. Chem.*, 2009, **11**, 274–80.

17 H. Brunner, *J. Organomet. Chem.*, 1986, **316**, 6–8.

18 H. Nishiyama, H. Sakaguchi, T. Nakamura, M. Horlhata, M. Kondo and K. Itoh, *Organometallics*, 1989, **5**, 846–848.

19 H. Nishiyama, H. Sakaguchi, T. Nakamura, M. Horlhata, M. Kondo and K. Itoh, *Organometallics*, 1989, **5**, 846–848.

20 R. E. Lowenthal, A. Abiko and S. Masamune, *Tetrahedron Lett.*, 1990, 6005–6008.

21 J. Comelles, A. Pericas, M. Moreno-Mañas, A. Vallribera, G. Drudis-Solé, A. Lledos, T. Parella, A. Roglans, S. García-Granda and L. Roces-Fernández, *J. Org. Chem.*, 2007, **72**, 2077–2087.

22 J. Ito and H. Nishiyama, *Synlett*, 2012, **23**, 509–523.

23 T. G. Gant, A. I. Meyers, F. Collins, A. Oxazolines, C. Metalation, A. Oxazolines and A. Metalations, *Tetrahedron*, 1994, **50**.

24 H. C. Aspinall, J. F. Bickley, N. Greeves, R. V Kelly and P. M. Smith, *Organometallics*, 2005, **24**, 3458–3467.

25 P. Segl and M. Jamniclj, *Inorganica Chim. Acta*, 1993, **205**, 221–229.

26 H. W. Görlitzer, M. Spiegler and R. Anwander, *Dalton Trans.*, 1999, **222**, 4287–4288.

27 G. Helmchen and a Pfaltz, *Acc. Chem. Res.*, 2000, **33**, 336–45.

28 G. J. Dawson and S. J. Coote, 1993, **34**, 3149–3150.

29 A. Togni and L. M. Venanzi, *Angew. Chemie Int. Ed. English*, 1994, **33**, 497–526.

30 R. A. Gossage, *Dalton Trans.*, 2011, **40**, 8733–44.

31 G. A. Snow, *J. Chem. Soc.*, 1954, 4080–4093.

32 T. Peterson, K. Falk, S. A. Leong, M. P. Klein and J. B. Neilands, *J. Am. Chem. Soc.*, 1980, **102**, 7715–7718.

33 G. Desimoni, G. Faita, F. Piccinini and M. Toscanini, *European J. Org. Chem.*, 2006, 5228–5230.

34 G. Mugesh, H. B. Singh and R. J. Butcher, *Eur. J. Inorg. Chem.*, 2001, 669–678.

35 K. Kandasamy, H. B. Singh, R. J. Butcher, J. P. Jasinski, H. U. V, K. S. College and N. Hampshire, 2004, **43**, 5704–5713.

36 P. G. Cozzit, C. Floriani, D. Chimica and U. Parma, *Inorg. Chem.*, 1995, 2921–2930.

37 P. G. Cozzi and C. Floriani, *Perkin Tranactions*, 1995, **604**.

38 S. Jansat, G. Muller, D. Panyella, M. Font-bardía and X. Solans, *Dalton Trans.*, 1997, 3755–3764.

39 M. D. Godbole, M. P. Puig, S. Tanase, H. Kooijman, A. L. Spek and E. Bouwman, *Inorganica Chim. Acta*, 2007, **360**, 1954–1960.

40 R. Appel, *Angew. Chemie Int. Ed. English*, 1975, **14**, 801–811.

41 O. D. Beckingham, 2012.

42 H. Vorbruggen, *Tetrahedron*, 1993, **49**, 9353–9372.

43 H. Witte, *Liebigs Ann Chem*, 1974, **408**, 996–1009.

44 S. T. Chill and R. C. Mebane, *Synth. Commun.*, 2009, **39**, 3601–3606.

45 H. C. Aspinall, O. Beckingham, M. D. Farrar, N. Greeves and C. D. Thomas, *Tetrahedron Lett.*, 2011, **52**, 5120–5123.

46 J. V Allen and J. M. J. Williams, *Tetrahedron: Asymmetry*, 1994, **5**, 2–7.

47 J. W. Bode, Y. Hachisu, T. Matsuura and K. Suzuki, *Org. Lett.*, 2003, **5**, 391–394.

48 J. W. Bode, Y. Hachisu, T. Matsuura and K. Suzuki, *Tetrahedron Lett.*, 2003, **44**, 3555–

3558.

49 B. G. Casiraghi, G. Casnati, G. Puglia, G. Sartori, G. Terenghi, C. Organica and V. M. D. Azeglio, *Perkin Elmer*, 1978.

50 A. Kochnev, I. Oleynik, S. Ivanchev and G. Tolstikov, *Russ. Chem. Bull.*, 2007, **56**, 1125–1129.

51 G. V Kalechits and A. G. Osinovskii, *Russ. J. Appl. Chem.*, 2002, **75**, 962–964.

52 L. F. Lindoy and G. V Meehan, *Synthesis (Stuttg).*, 2006, 1029–1032.

53 A. V Dubrovskiy and R. C. Larock, *Org. Lett.*, 2010, **12**, 1180–1183.

54 I. Thomsen and K. B. G. Torssell, *Acta Chem. Scand.*, 1988, **B42**, 303–308.

55 H. U. I. Chiang, *J. Org. Chem.*, 1971, **36**, 2146–2155.

56 A. Dondoni, *J. Org. Chemsitry*, 1972, **37**, 3564–3566.

57 G. Lee, *Synthesis (Stuttg).*, 1982, 508–509.

58 B. Kou-Chang Liu, *J. Org. Chemsitry*, 1980, **45**, 3916–3918.

59 P. Y. S. Lam, J. J. Adams, C. G. Clark, W. J. Calhoun, J. M. Luettgen, R. M. Knabb and R. R. Wexler, *Bioorg. Med. Chem. Lett.*, 2003, **13**, 1795–1799.

60 M. Bigdeli, *J. Chem. Res.*, 2007.

61 D. Halstead, 1970, pp. 2016–2018.

62 I. U. of P. and A. Chemistry, *Nomenclature of Inorganic Chemistry: IUPAC Recomendations 2005*, 2005.

63 S. Cotton, *Lanthanide and Actinide Chemistry*, John Wiley & Sons, 2006.

64 T. Moeller, *J. Chem. Educ.*, 1970, **47**.

65 K. Dehnicke and A. Greiner, *Angew. Chem. Int. Ed. Engl.*, 2003, **42**, 1340–1354.

66 H. C. Aspinall, *Chemistry of the f-Block elements*, Gordon and Breach Science Publishers, 2001.

67 A. L. Gemal and J. L. Luche, *J. Am. Chem. Soc.*, 1981, **103**, 5454–5459.

68 K. Dehnicke and A. Greiner, *Angew. Chemie - Int. Ed.*, 2003, **42**, 1340–1354.

69 H. C. Aspinall, N. Greeves and P. M. Smith, *Tetrahedron Lett.*, 1999, **40**, 1763–1766.

70 K. Hara, S. Tosaki, V. Gnanadesikan, H. Morimoto, S. Harada, M. Sugita, N. Yamagiwa, S. Matsunaga and M. Shibasaki, *Tetrahedron*, 2009, **65**, 5030–5036.

71 Michael D. McCreary; Daniel W. Lewis; David L., *J. Am. Chem. Soc.*, 1974, **96**, 1038–1054.

72 C. C. Hinckley, *J. Am. Chem. Soc.*, 1969, **91**, 5160–5162.

73 a. D. Sherry, J. Ren, J. Huskens, E. Brücher, É. Tóth, C. F. C. G. Geraldes, M. M. C. a. Castro and W. P. Cacheris, *Inorg. Chem.*, 1996, **35**, 4604–4612.

74 M. Bednarski and S. Danishefsky, *J. Am. Chem. Soc.*, 1983, 3716–3717.

75 M. Bednarski, C. Maring, S. Danishefsky and N. Haven, *Tetrahedron Lett.*, 1983, 3451–3454.

76 M. Q. and K. Jankowski, *J. Chem. Soc. Chem. Commun.*, 1987, 676–677.

77 K. Nakai, T. Masahiro and T. Makami, *Tetrahedron: Asymmetry*, 1991, **2**, 993–996.

78 K. Nakai, T. Masahiro and T. Makami, *J. Org. Chem.*, 1991, **56**, 5456–5459.

79 H. Sasai, *J. Am. Chem. Soc.*, 1992, **114**, 4418–4420.

80 H. Sasai, T. Suzuki, N. Itoh, S. Arai and M. Shibasaki, *Tetrahedron Lett.*, 1993, **34**, 2657–2660.

81 H. Sasai, W. Kim, T. Suzuki and M. Shibasaki, *Tetrahedron Lett.*, 1994, **35**, 6123–6126.

82 H. Sasai, M. Bougauchi, T. Arai and M. Shibasaki, *Tetrahedron Lett.*, 1997, **38**, 2717–2720.

83 K. Funabashi, Y. Saida, M. Kanai and M. Shibasaki, *Tetrahedron Lett.*, 1998, **39**, 7557–7558.

84 T. Morita, T. Arai, H. Sasai and M. Shibasaki, *Tetrahedron: Asymmetry*, 1998, **9**, 1445–1450.

85 H. Sasai, E. Emori, T. Arai and M. Shibasaki, *Tetrahedron Lett.*, 1996, **37**, 5561–5564.

86 M. Shibasaki and N. Yoshikawa, *Chem. Rev.*, 2002.

87 Helen C. Aspinall, *Chem. Rev.*, 2002, **102**, 1807–1850.

88 A. I. Sanchez-blanco, K. V Gothelf and K. A. Jergensen, *Tetrahedron Lett.*, 1997, **38**, 7923–7926.

89 C. Qian and L. Wang, *Tetrahedron Lett.*, 2000, **41**, 2203–2206.

90 R. C. Evans, P. Douglas and C. J. Winscom, *Coord. Chem. Rev.*, 2006, **250**, 2093–2126.

91 B. Karimi and A. Maleki, *Chem. Commun. (Camb).*, 2009, 5180–5182.

92 R. Anwander, O. Runte, J. Eppinger, G. Gerstberger and M. Spiegler, *Dalton Trans.*, 1998, 847–858.

93 S. Hong, S. Tian, M. V. Metz and T. J. Marks, *J. Am. Chem. Soc.*, 2003, **125**, 14768–14783.

94 A. Alaaeddine, A. Amgoune, C. M. Thomas, S. Dagorne, S. Bellemin-Laponnaz and J. F. Carpentier, *Eur. J. Inorg. Chem.*, 2006, 3652–3658.

95 J. Zhou and Y. Tang, *Chem. Soc. Rev.*, 2005, **34**, 664–76.

96 B. D. Ward, *Angew. Chem. Int. Ed. Engl.*, 2002, **41**, 3473.

97 B. D. Ward, S. Bellemin-Laponnaz and L. H. Gade, *Angew. Chemie - Int. Ed.*, 2005, **44**,

1668–1671.

98 L. Lukesová, B. D. Ward, S. Bellemin-Laponnaz, H. Wadepohl and L. H. Gade, *Dalton Trans.*, 2007, 920–922.

99 B. D. Ward, L. Lukešová, H. Wadepohl, S. Bellemin-Laponnaz and L. H. Gade, *Eur. J. Inorg. Chem.*, 2009, **3**, 866–871.

100 B. D. Ward, *Organometallics*, 2007, 4652.

101 A. V. Pawlikowski, A. Ellern and A. D. Sadow, *Inorg. Chem.*, 2009, **48**, 8020–8029.

102 H. Guillon, S. Daniele, L. G. Hubert-Pfalzgraf and J. . Letoffe, *Polyhedron*, 2004, **23**, 1467–1472.

103 D. J. Berg, C. Zhou, T. Barclay, X. Fei, S. Feng, K. a Ogilvie, R. a Gossage, B. Twamley and M. Wood, *Can. J. Chem.*, 2005, **83**, 449–459.

104 H. Morimoto, G. Lu, N. Aoyama, S. Matsunaga and M. Shibasaki, *J. Am. Chem. Soc.*, 2007, **129**, 9588–9589.

105 A. Rodger, *Inorg. Chem.*, 1988, **27**, 3061–3062.

106 D. C. Bradley, J. S. Ghotra and A. Hart, *Dalton Trans.*, 1973, 1021–1023.

107 C. P. Carter and M. D. Taylor, *J. Inorg. Nucl. Chem.*, 1962, **24**, 387–391.

108 A. Merbach, M.-N. Pitteloud and P. Jaccard, *Helv. Chim. Acta*, 1972, **55**, 44–52.

109 A. Lebrun, J.-L. Namy and H. B. Kagan, *Tetrahedron Lett.*, 1991, **32**, 2355–2358.

110 H. C. Aspinall and M. Williams, *Inorg. Chem.*, 1996, **35**, 255–257.

111 Y. Hirashima, *Chem. Lett.*, 1979, 463–464.

112 Y. Hirashima, *J. Chem. Soc. Japan*, 1983, **56**, 738–743.

113 S. Akerboom, E. T. Hazenberg, I. Schrader, S. F. Verbeek, I. Mutikainen, W. T. Fu and E. Bouwman, *Eur. J. Inorg. Chem.*, 2014, n/a–n/a.

114 M. D. Hobbs, 2007.

115 D. L. Davies, K. Singh, S. Singh and B. Villa-Marcos, *Chem. Commun. (Camb).*, 2013, **49**, 6546–8.

116 H. C. Aspinall, J. Bacsa, O. D. Beckingham, E. G. B. Eden, N. Greeves, M. D. Hobbs, F. Potjewyd, M. Schmidtmann and C. D. Thomas, *Dalton Trans.*, 2014, **43**, 1434–42.

117 G. Gerstberger, C. Palm and R. Anwander, *Chem. a Eur. J.*, 1999, 997–1005.

118 F. A. Luzzio, *Tetrahedron*, 2001, **57**, 915–945.

119 H. Sasai, N. Itoh, T. Suzuki and M. Shibasaki, *Tetrahedron Lett.*, 1993, **34**, 855–858.

120 N. Ono, *The Nitro Group in Organic Synthesis*, John Wiley & Sons, Inc., 2002.

121 H. Sasai, T. Tokunaga, S. Watanabe, T. Suzuki, N. Itoh and M. Shibasaki, *J. Org. Chemsitry*, 1996, 7388–7389.

122 T. Nitabaru, N. Kumagai and M. Shibasaki, *Angew. Chem. Int. Ed. Engl.*, 2012, **51**, 1644–7.

123 H. Sasai, S. Arai, Y. Tahara and M. Shibasaki, *J. Org. Chem.*, 1996, 6656–6657.

124 N. Gogoi, J. Boruwa and N. C. Barua, *Tetrahedron Lett.*, 2005, **46**, 7581–7582.

125 T. Nitabaru, N. Kumagai and M. Shibasaki, *Tetrahedron Lett.*, 2008, **49**, 272–276.

126 M.-L. Chen, S. Gao and Z.-H. Zhou, *Dalton Trans.*, 2012, **41**, 1202–9.

127 J. R. Robinson, X. Fan, J. Yadav, P. J. Carroll, A. J. Wooten, M. a Pericàs, E. J. Schelter and P. J. Walsh, *J. Am. Chem. Soc.*, 2014.

128 S. Matsunaga and M. Shibasaki, *Chem. Commun. (Camb).*, 2014, **50**, 1044–57.

129 A. I. Meyers, *J. Org. Chemsitry*, 1993, **58**, 3568–3571.

130 C. Wolf and H. Xu, *Chem. Commun. (Camb).*, 2011, **47**, 3339–3350.

Appendix

11. ^{1}H and ^{13}C NMR Spectra of Intermediates and Final Ligands.

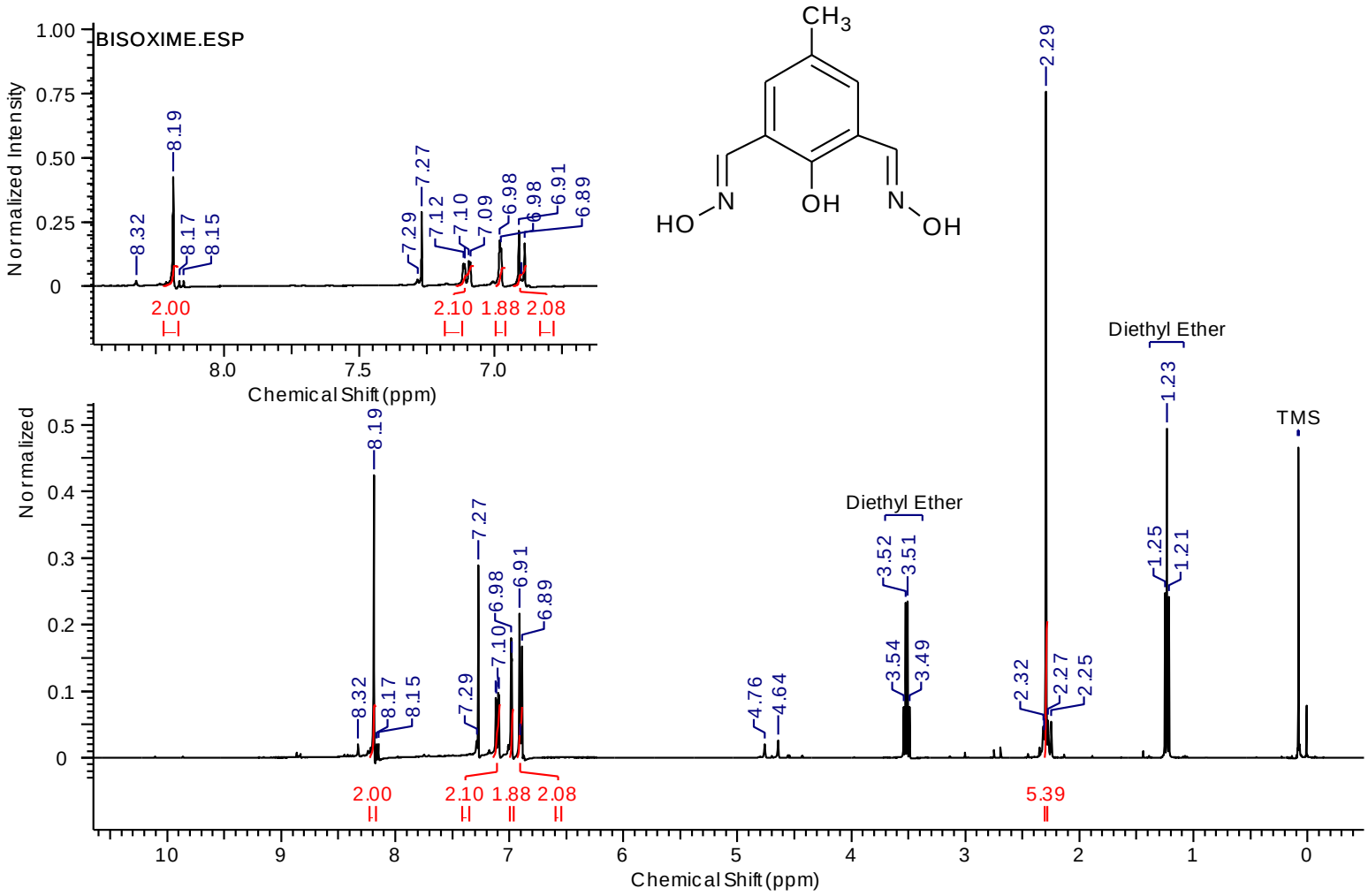

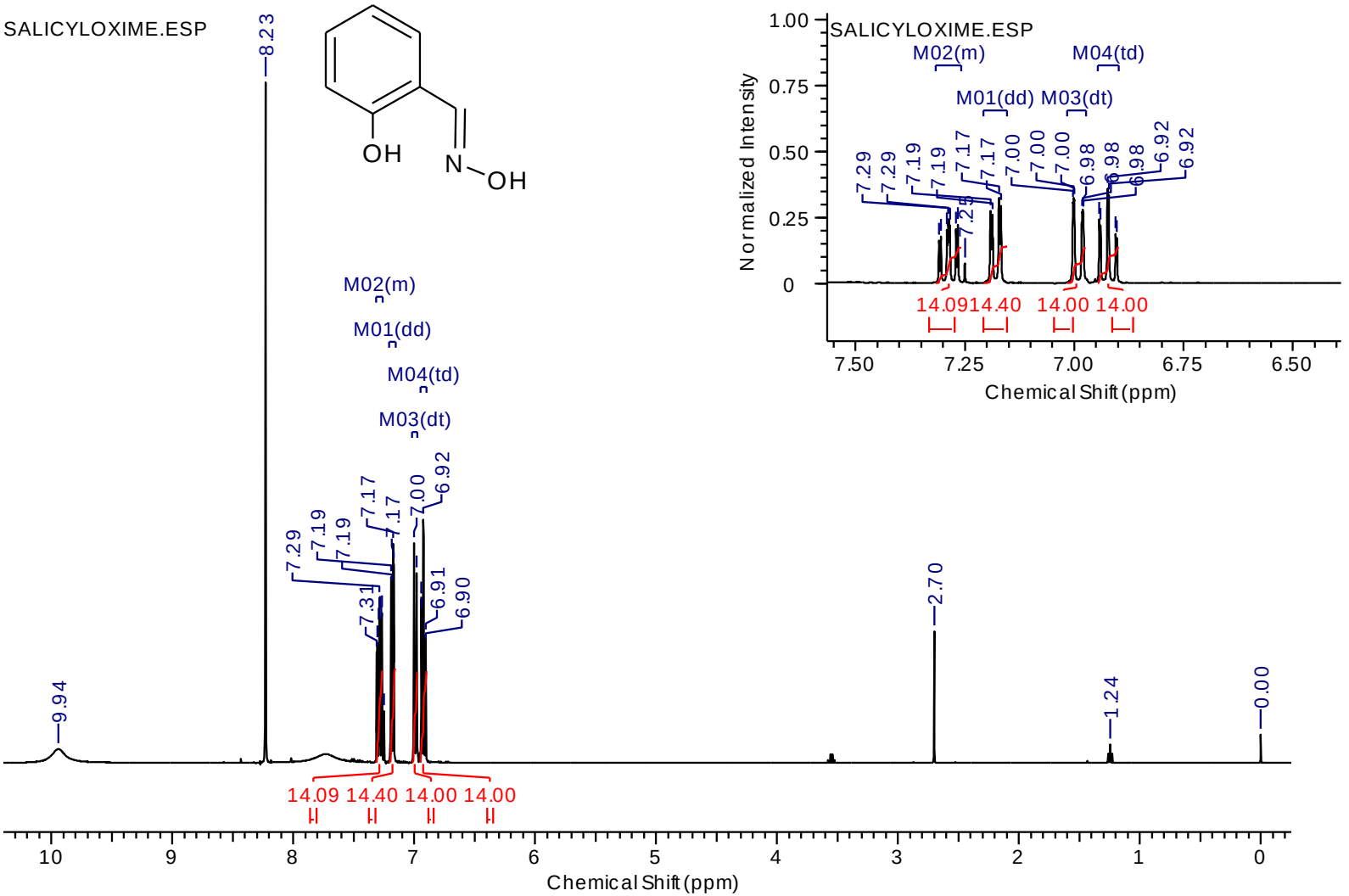
SALICYLOXIME.ESP
8.23
OH
N
OH
M02(m)
M01(dd)
M04(td)
M03(dt)
7.29
7.19
7.19
7.17
7.17
7.00
6.92
7.31
6.91
6.90
9.94
2.70
1.24
0.00
14.09 14.40 14.00 14.00
Chemical Shift (ppm)
SALICYLOXIME.ESP
M02(m)
M04(td)
M01(dd) M03(dt)
Normalized Intensity
14.09 14.40 14.00 14.00
Chemical Shift (ppm)

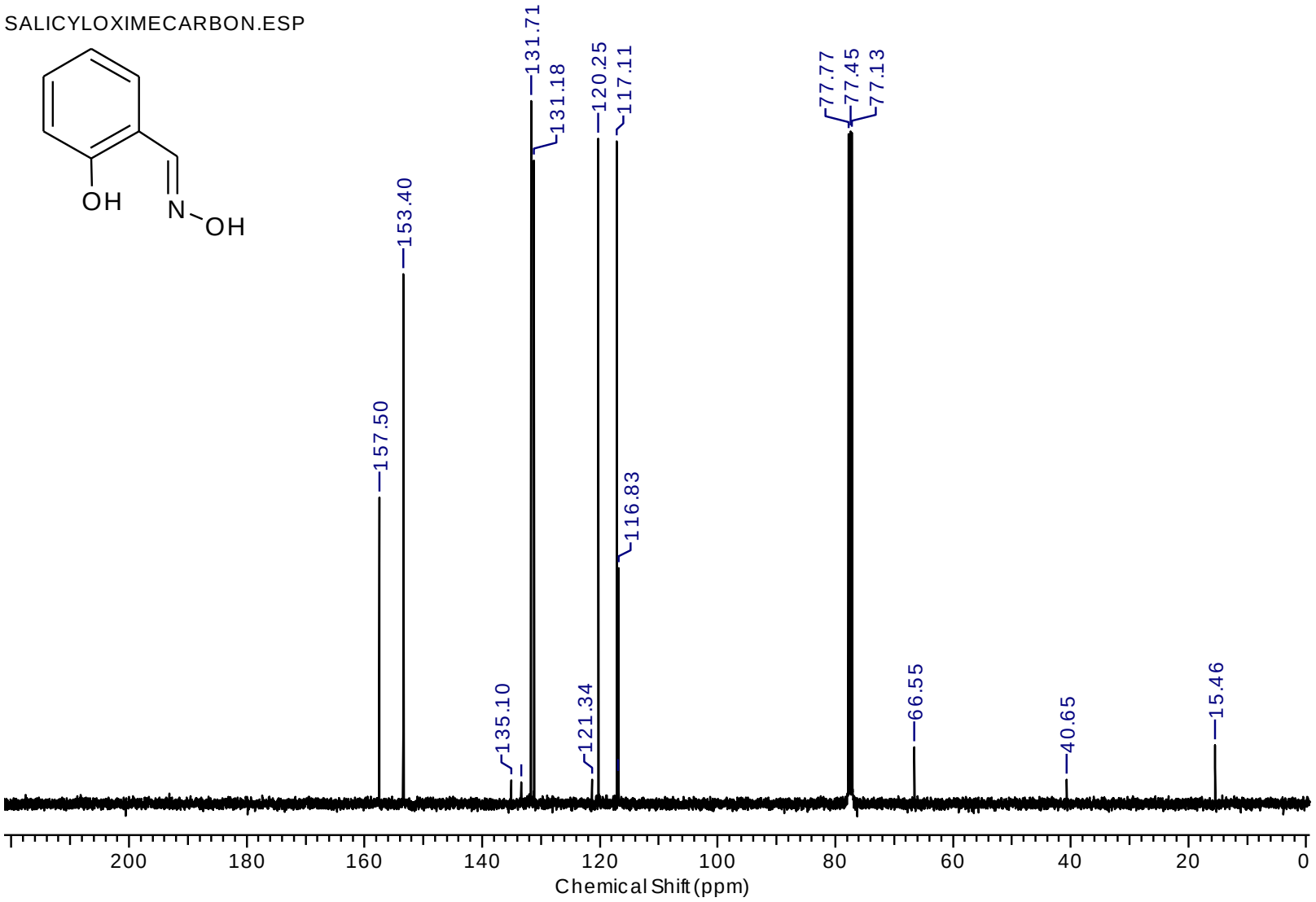
SALICYLOXIMECARBON.ESP
OH
N
OH
157.50
153.40
135.10
131.71
131.18
121.34
120.25
117.11
116.83
77.77
77.45
77.13
66.55
40.65
15.46
200
180
160
140
120
100
80
60
40
20
0
Chemical Shift (ppm)

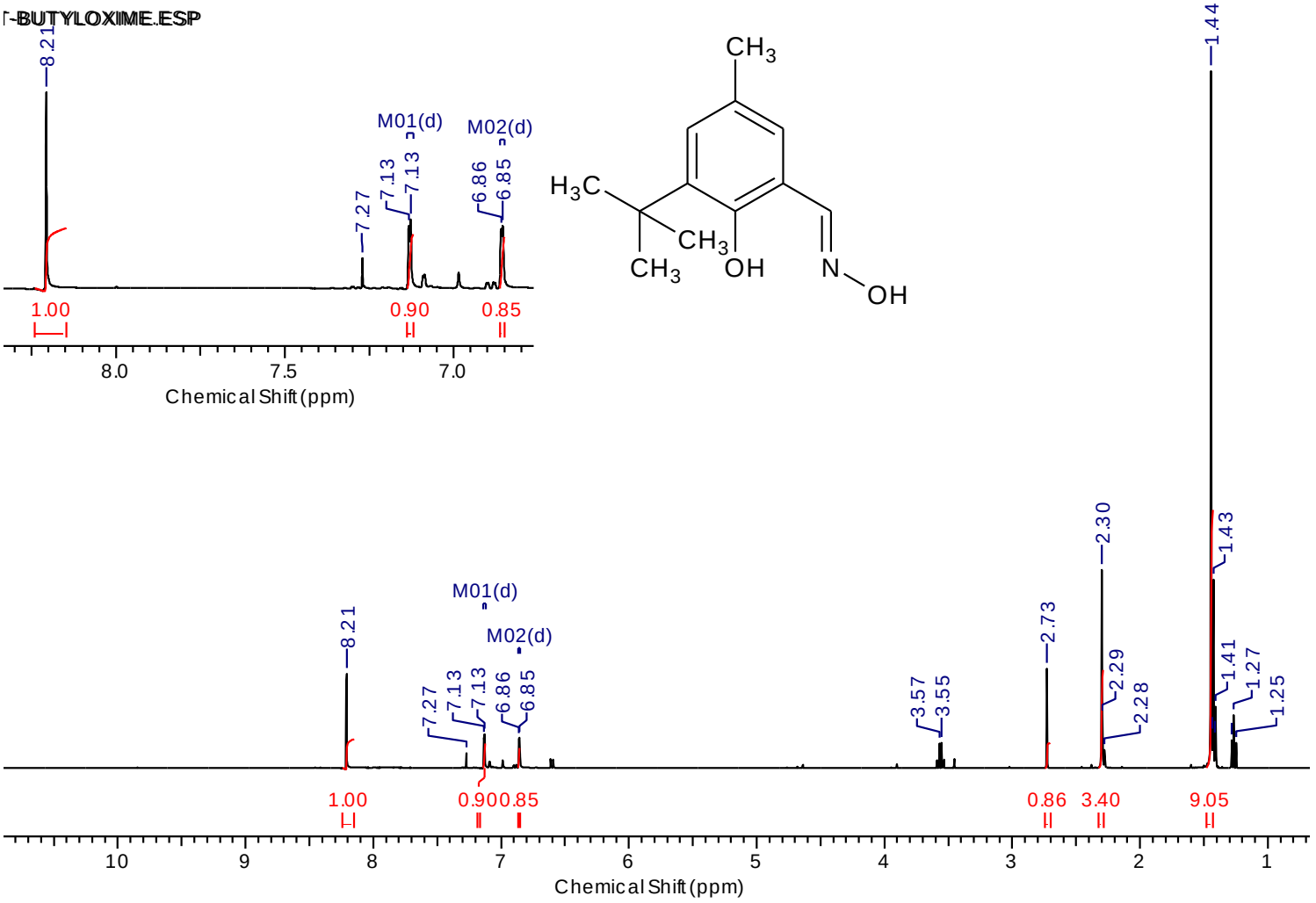
T-BUTYLOXIME.ESP
8.21
M01(d)
M02(d)
7.27
7.13
7.13
6.86
6.85
1.00
0.90
0.85
8.0
7.5
7.0
Chemical Shift (ppm)
CH3
H3C
CH3
CH3
OH
N
OH
1.44
2.30
1.43
2.73
2.29
2.28
1.41
1.27
1.25
3.57
3.55
1.00
0.90
0.85
0.86
3.40
9.05
10
9
8
7
6
5
4
3
2
1
Chemical Shift (ppm)

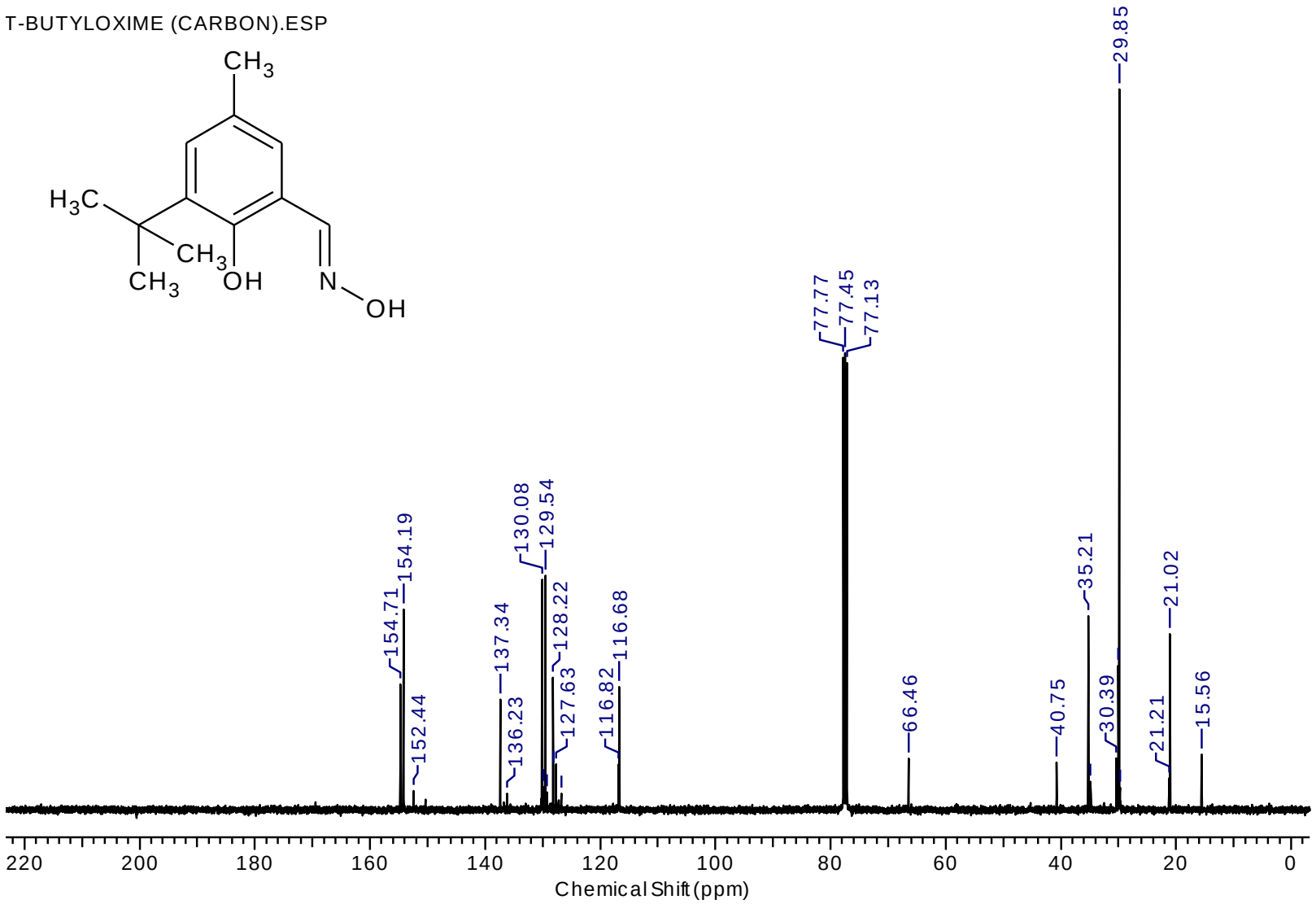
T-BUTYLOXIME (CARBON).ESP
CH3
H3C
CH3
CH3
OH
N
OH
29.85
77.77
77.45
77.13
154.71
154.19
152.44
137.34
136.23
130.08
129.54
128.22
127.63
116.82
116.68
66.46
40.75
35.21
30.39
21.21
21.02
15.56
220
200
180
160
140
120
100
80
60
40
20
0
Chemical Shift (ppm)

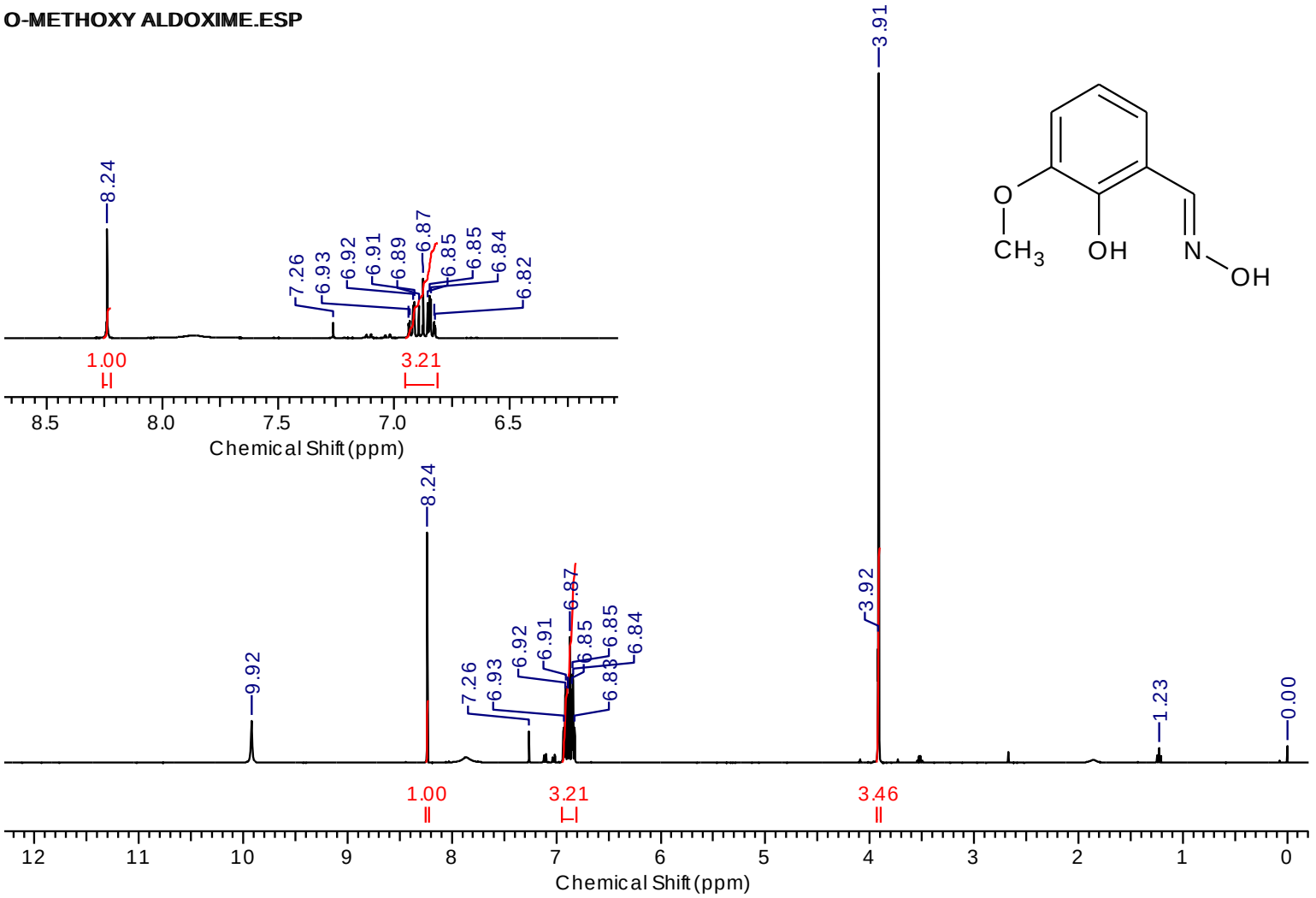
O-METHOXY ALDOXIME.ESP
8.24
7.26
6.93
6.92
6.91
6.89
6.87
6.85
6.84
6.82
1.00
3.21
8.5
8.0
7.5
7.0
6.5
Chemical Shift (ppm)
3.91
O
CH3
OH
N
OH
8.24
9.92
7.26
6.93
6.92
6.91
6.87
6.85
6.84
6.83
3.92
1.23
0.00
1.00
3.21
3.46
12
11
10
9
8
7
6
5
4
3
2
1
0
Chemical Shift (ppm)

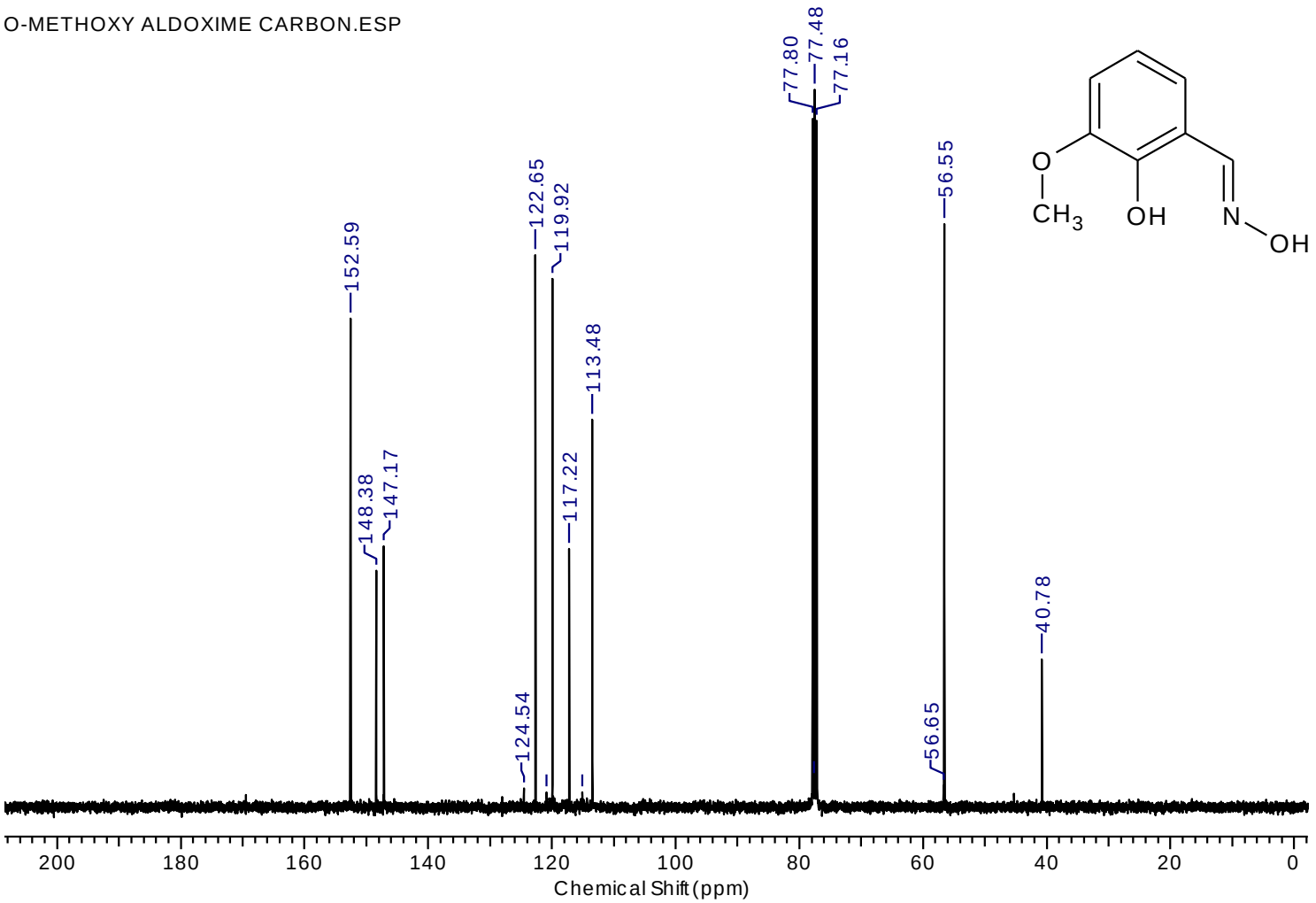
O-METHOXY ALDOXIME CARBON.ESP
152.59
148.38
147.17
124.54
122.65
119.92
117.22
113.48
77.80
77.48
77.16
56.65
56.55
40.78
O
CH3
OH
N
OH
200
180
160
140
120
100
80
60
40
20
0
Chemical Shift (ppm)

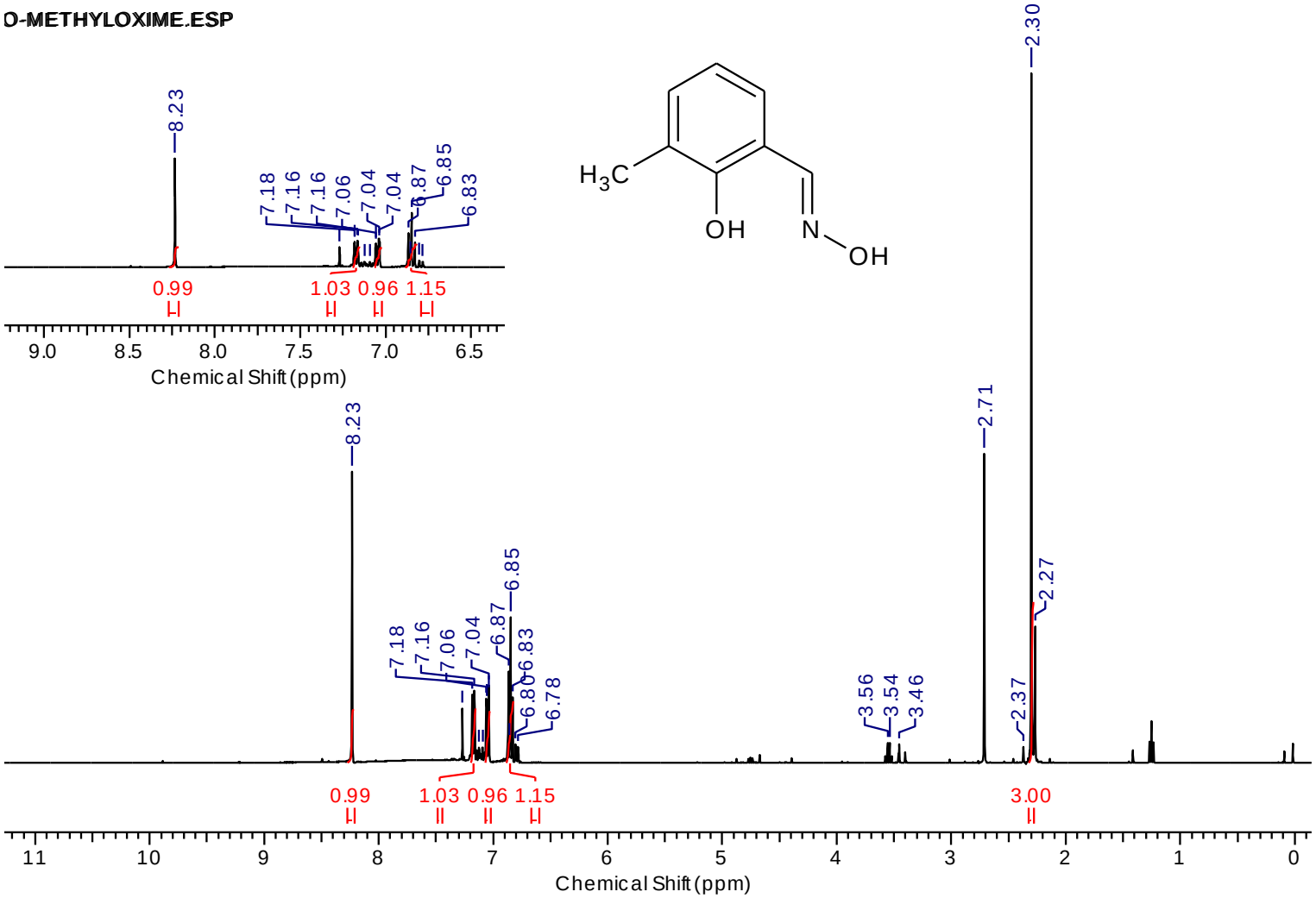
O-METHYLOXIME.ESP
8.23
7.18
7.16
7.16
7.06
7.04
7.04
6.87
6.85
6.83
0.99
1.03
0.96
1.15
9.0
8.5
8.0
7.5
7.0
6.5
Chemical Shift (ppm)
H3C
OH
N
OH
2.30
2.71
2.27
2.37
3.56
3.54
3.46
6.78
3.00
11
10
9
8
7
6
5
4
3
2
1
0
Chemical Shift (ppm)

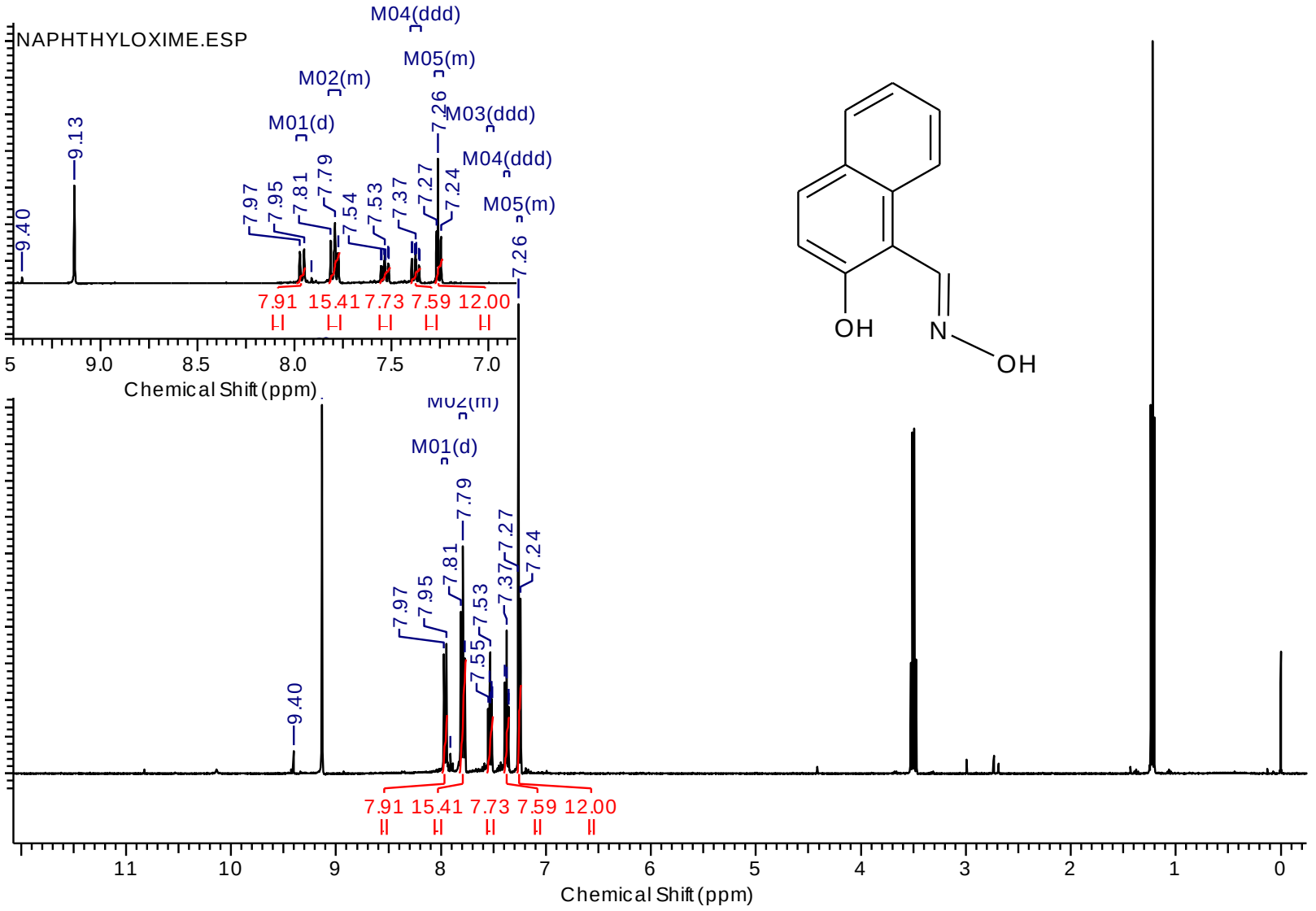
NAPHTHYLOXIME.ESP
M04(ddd)
M05(m)
M02(m)
M01(d)
M03(ddd)
M04(ddd)
M05(m)
9.40
9.13
7.97
7.95
7.81
7.79
7.54
7.53
7.37
7.27
7.26
7.24
7.91 15.41 7.73 7.59 12.00
Chemical Shift (ppm)
OH
N
OH

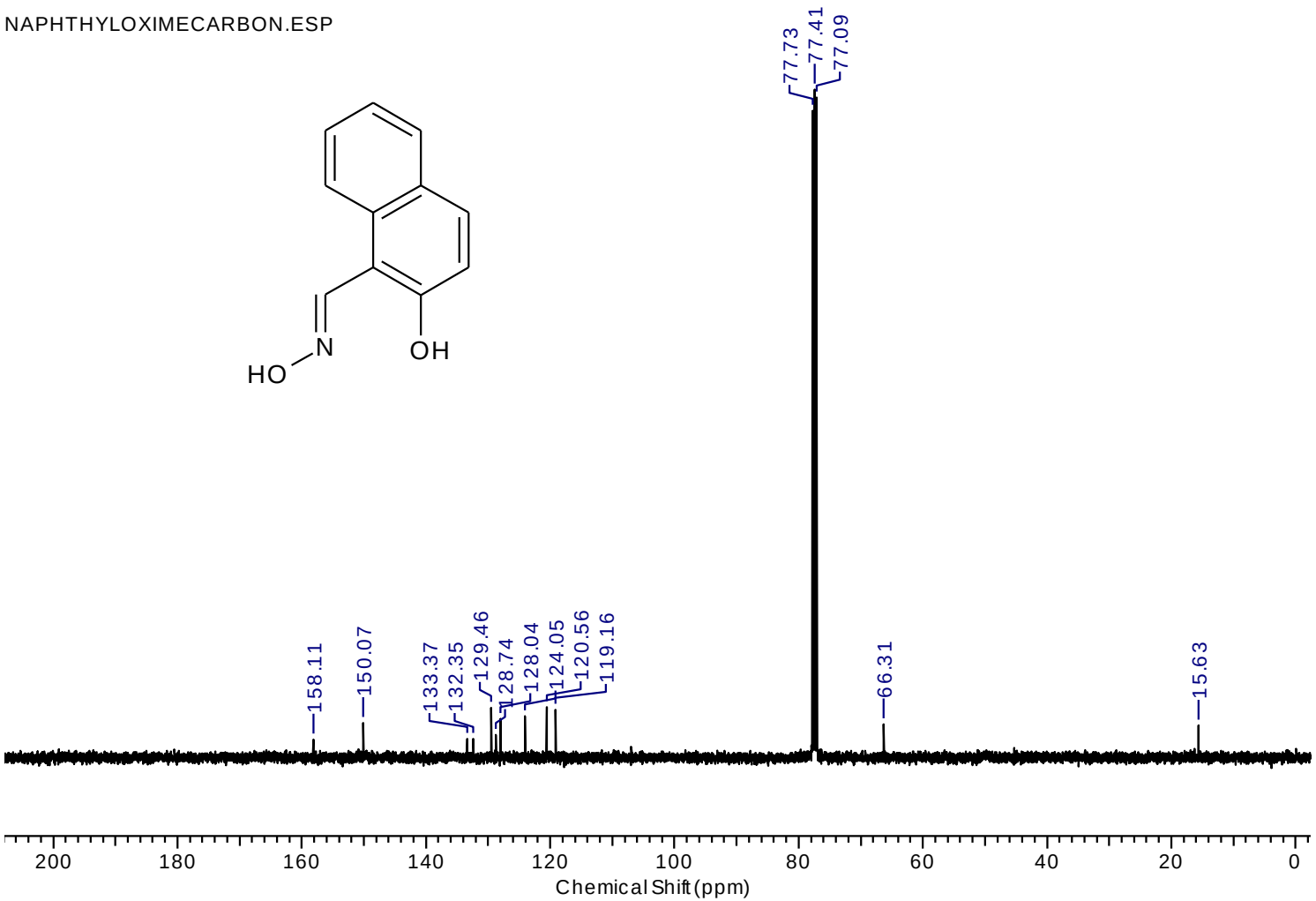
NAPHTHYLOXIMECARBON.ESP
HO
N
OH
77.73
77.41
77.09
158.11
150.07
133.37
132.35
129.46
128.74
128.04
124.05
120.56
119.16
66.31
15.63
200
180
160
140
120
100
80
60
40
20
0
Chemical Shift (ppm)

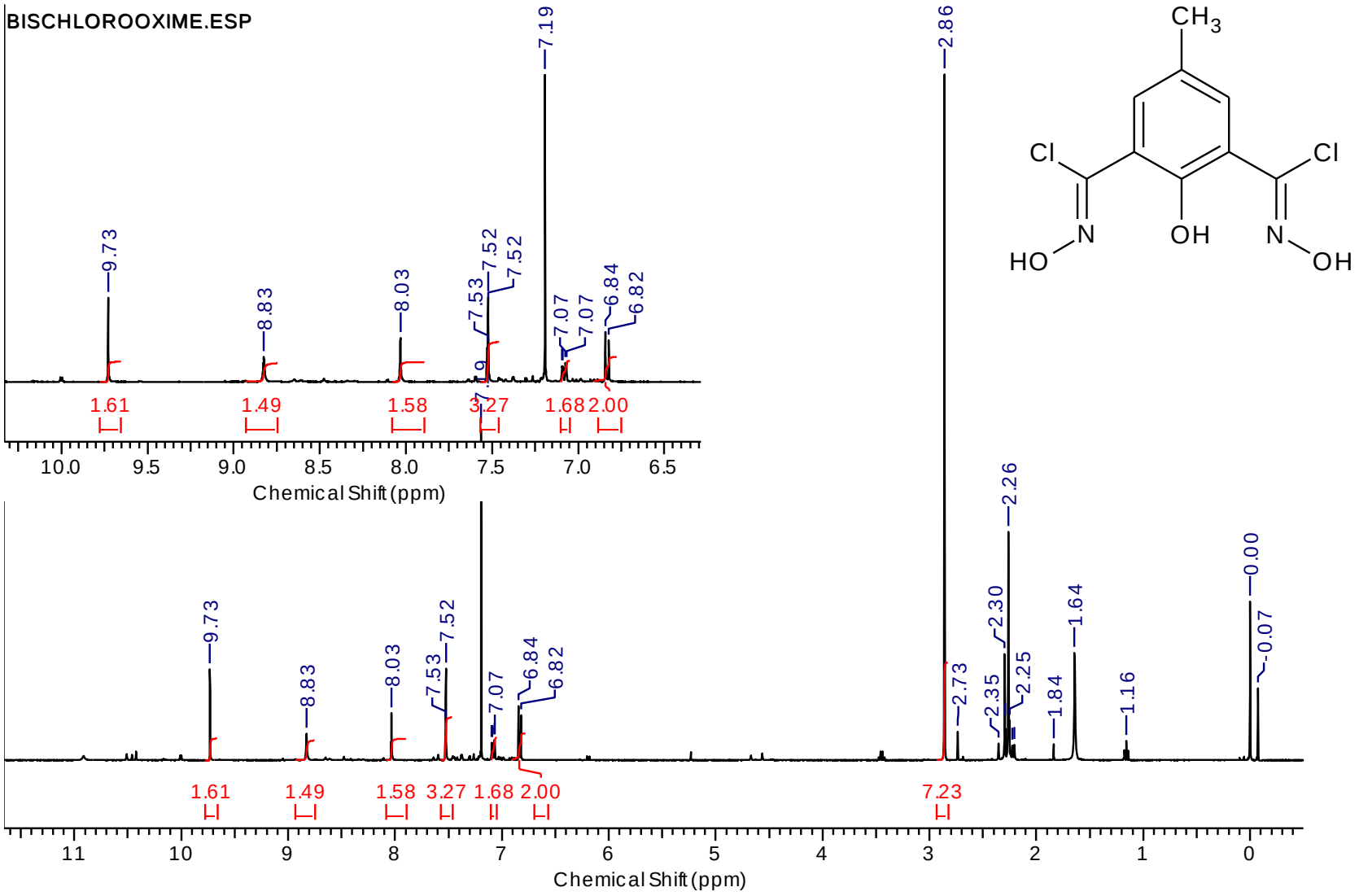
BISCHLOROOXIME.ESP
9.73
8.83
8.03
7.53
7.52
7.52
7.19
7.07
7.07
6.84
6.82
1.61
1.49
1.58
3.27
1.68
2.00
10.0
9.5
9.0
8.5
8.0
7.5
7.0
6.5
Chemical Shift (ppm)
2.86
CH3
Cl
Cl
N
OH
N
HO
OH
2.26
2.30
2.25
2.35
1.84
1.64
1.16
0.00
-0.07
2.73
7.23
11
10
9
8
7
6
5
4
3
2
1
0
Chemical Shift (ppm)

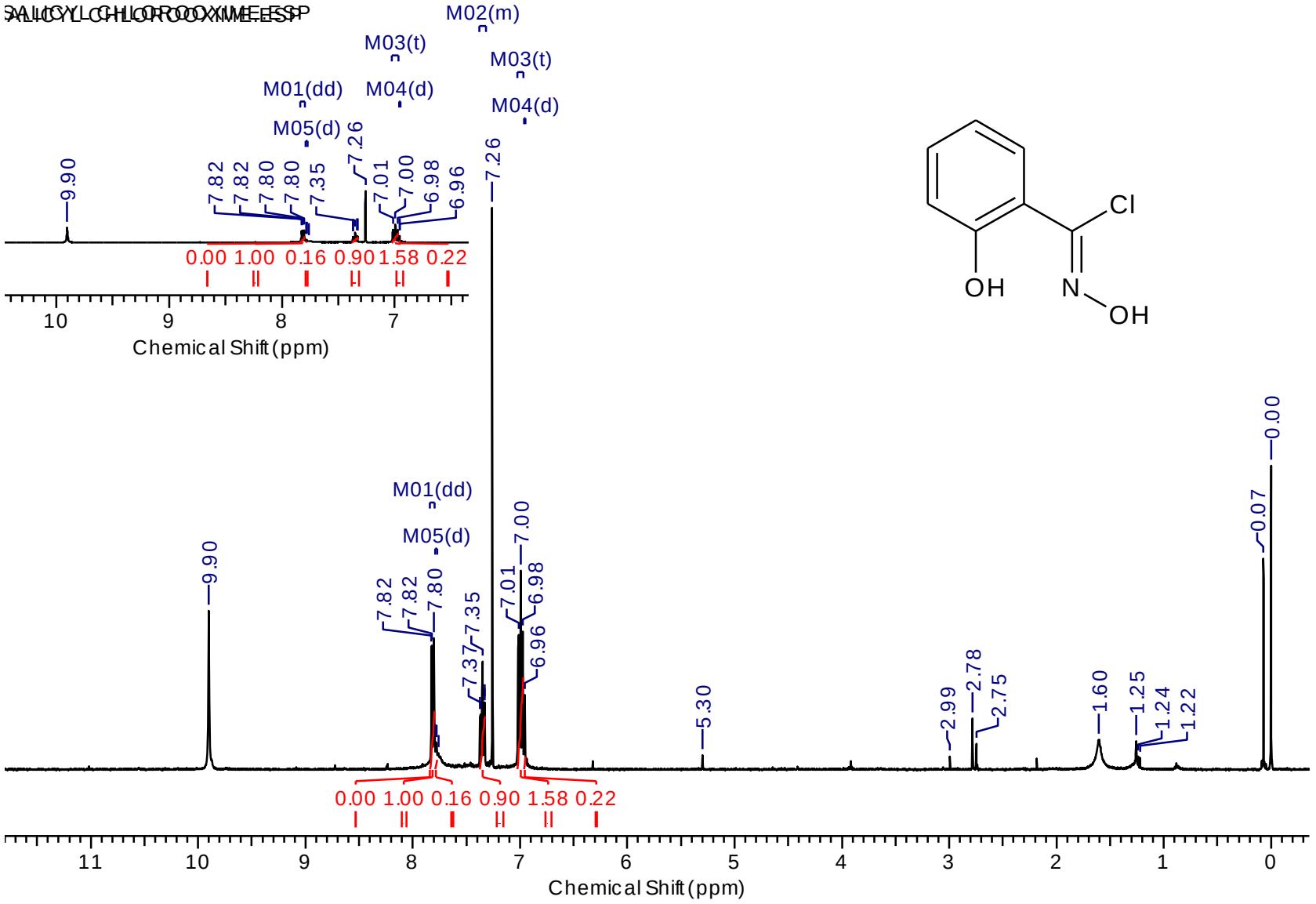
M02(m)
M03(t)
M03(t)
M01(dd)
M04(d)
M04(d)
M05(d)
9.90
7.82
7.82
7.80
7.80
7.35
7.26
7.01
7.00
6.98
6.96
0.00 1.00 0.16 0.90 1.58 0.22
10
9
8
7
Chemical Shift (ppm)
Cl
OH
N
OH
M01(dd)
M05(d)
9.90
7.82
7.82
7.80
7.37
7.35
7.26
7.01
7.00
6.98
6.96
5.30
2.99
2.78
2.75
1.60
1.25
1.24
1.22
0.07
0.00
0.00 1.00 0.16 0.90 1.58 0.22
11
10
9
8
7
6
5
4
3
2
1
0
Chemical Shift (ppm)

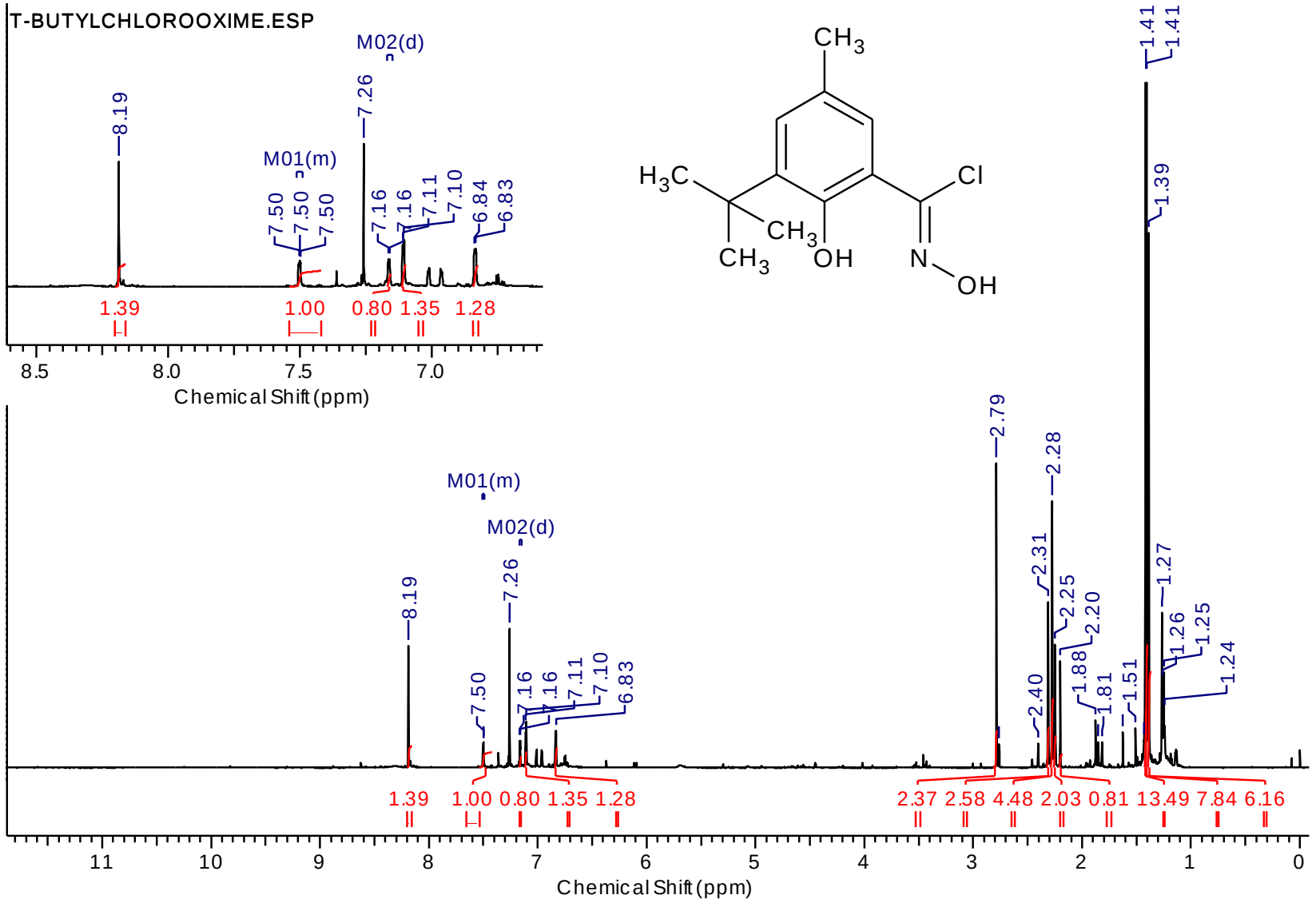
T-BUTYLCHLOROOXIME.ESP
M02(d)
M01(m)
8.19
7.26
7.50
7.50
7.50
7.16
7.16
7.11
7.10
6.84
6.83
1.39
1.00
0.80
1.35
1.28
8.5
8.0
7.5
7.0
Chemical Shift (ppm)
CH3
H3C
CH3
CH3
OH
Cl
N
OH
1.41
1.41
1.39
2.79
2.28
2.31
2.25
2.20
1.88
1.81
1.51
2.40
1.27
1.26
1.25
1.24
M01(m)
M02(d)
8.19
7.26
7.50
7.16
7.16
7.11
7.10
6.83
1.39
1.00
0.80
1.35
1.28
2.37
2.58
4.48
2.03
0.81
13.49
7.84
6.16
11
10
9
8
7
6
5
4
3
2
1
0
Chemical Shift (ppm)

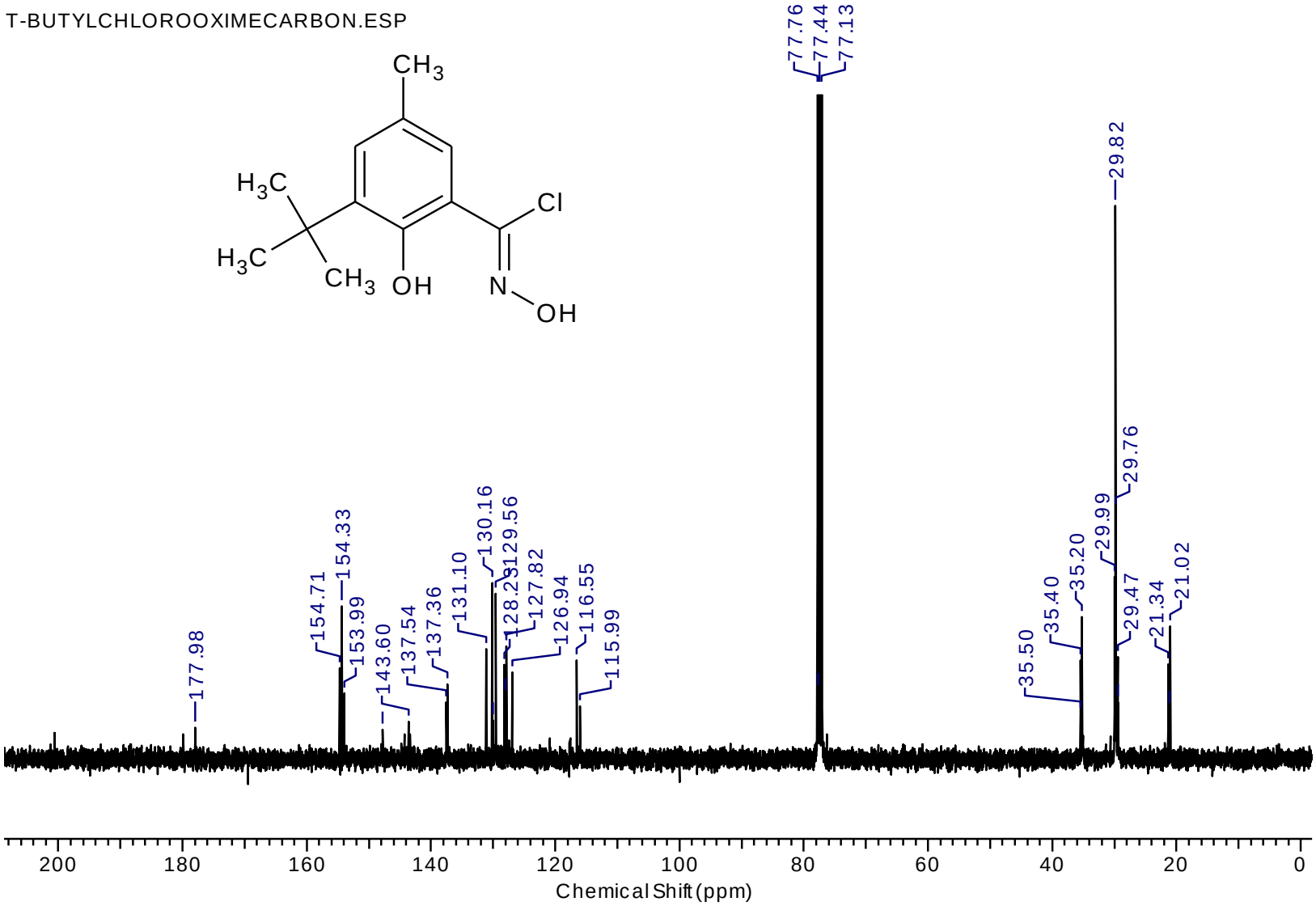
T-BUTYLCHLOROOXIMECARBON.ESP
CH3
H3C
H3C
CH3
OH
Cl
N
OH
77.76
77.44
77.13
29.82
29.76
29.99
35.20
35.40
35.50
29.47
21.34
21.02
177.98
154.71
154.33
153.99
143.60
137.54
137.36
131.10
130.16
129.56
128.23
127.82
126.94
116.55
115.99
200
180
160
140
120
100
80
60
40
20
0
Chemical Shift (ppm)

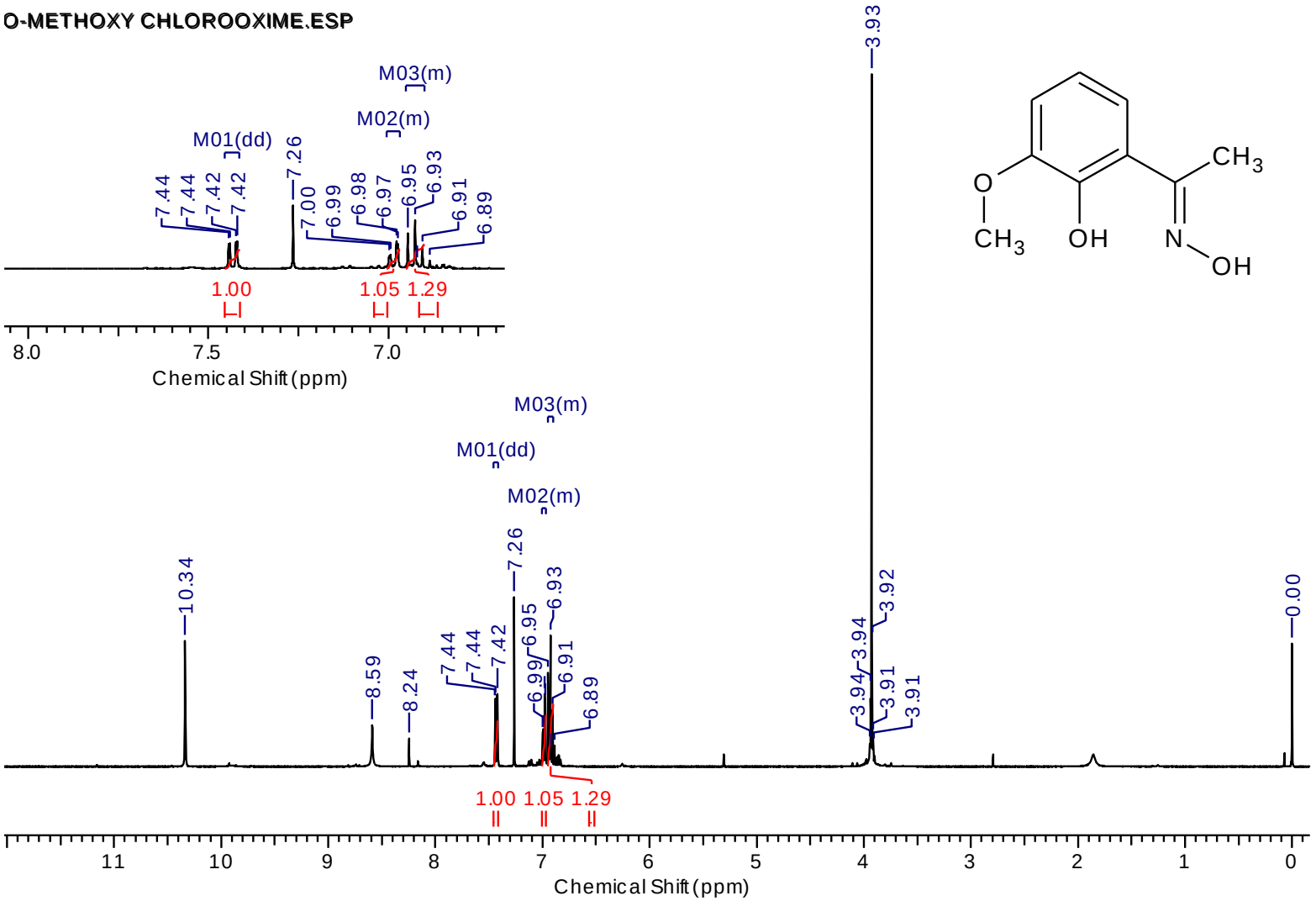
O-METHOXY CHLOROOXIME.ESP
M03(m)
M02(m)
M01(dd)
7.44
7.44
7.42
7.42
7.26
7.00
6.99
6.98
6.97
6.95
6.93
6.91
6.89
1.00
1.05
1.29
8.0
7.5
7.0
Chemical Shift (ppm)
3.93
CH3
O
CH3
OH
N
OH
M03(m)
M01(dd)
M02(m)
10.34
8.59
8.24
7.44
7.44
7.42
7.26
6.95
6.93
6.99
6.91
6.89
3.92
3.94
3.94
3.91
3.91
0.00
1.00
1.05
1.29
11
10
9
8
7
6
5
4
3
2
1
0
Chemical Shift (ppm)

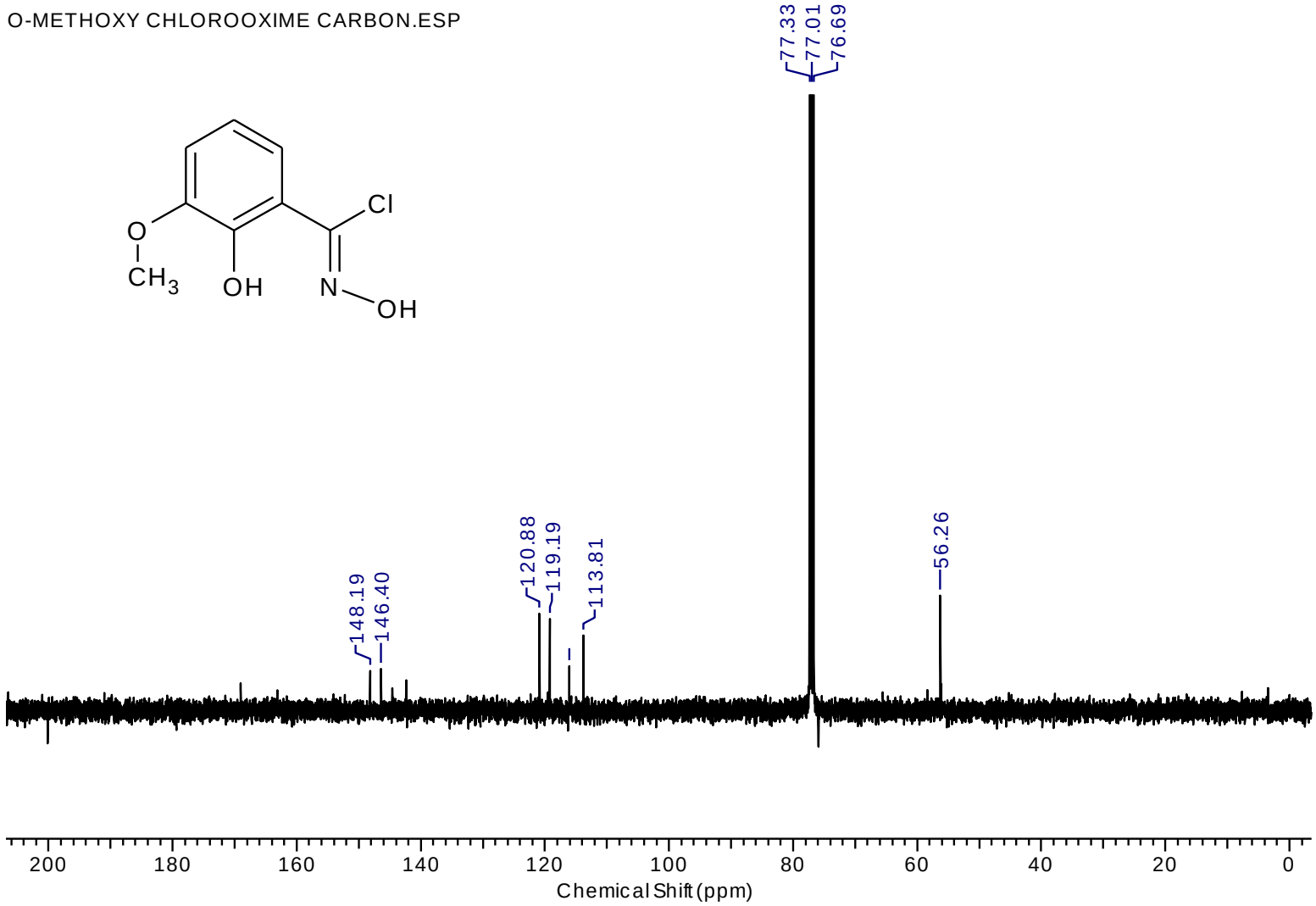
O-METHOXY CHLOROOXIME CARBON.ESP
77.33
77.01
76.69
148.19
146.40
120.88
119.19
113.81
56.26
Cl
O
CH3
OH
N
OH
200
180
160
140
120
100
80
60
40
20
0
Chemical Shift (ppm)

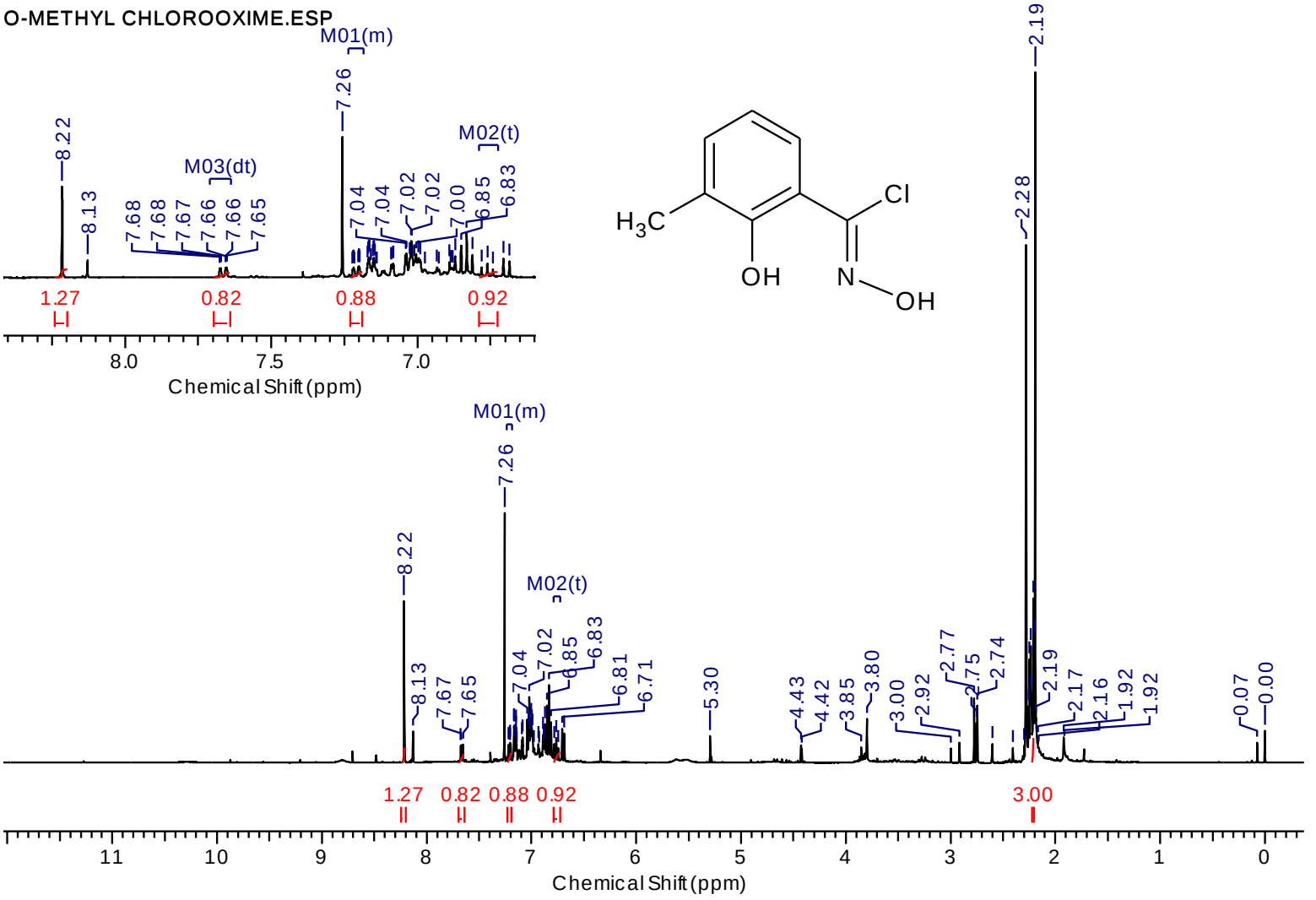
O-METHYL CHLOROOXIME.ESP
M01(m)
M02(t)
M03(dt)
8.22
8.13
7.68
7.68
7.67
7.66
7.66
7.65
7.26
7.04
7.04
7.02
7.02
7.00
6.85
6.83
1.27
0.82
0.88
0.92
8.0
7.5
7.0
Chemical Shift (ppm)
H3C
OH
N
Cl
OH
2.19
2.28
M01(m)
7.26
8.22
M02(t)
8.13
7.67
7.65
7.04
7.02
6.85
6.83
6.81
6.71
5.30
4.43
4.42
3.85
3.80
3.00
2.92
2.77
2.75
2.74
2.19
2.17
2.16
1.92
1.92
0.07
0.00
1.27
0.82
0.88
0.92
3.00
11
10
9
8
7
6
5
4
3
2
1
0
Chemical Shift (ppm)

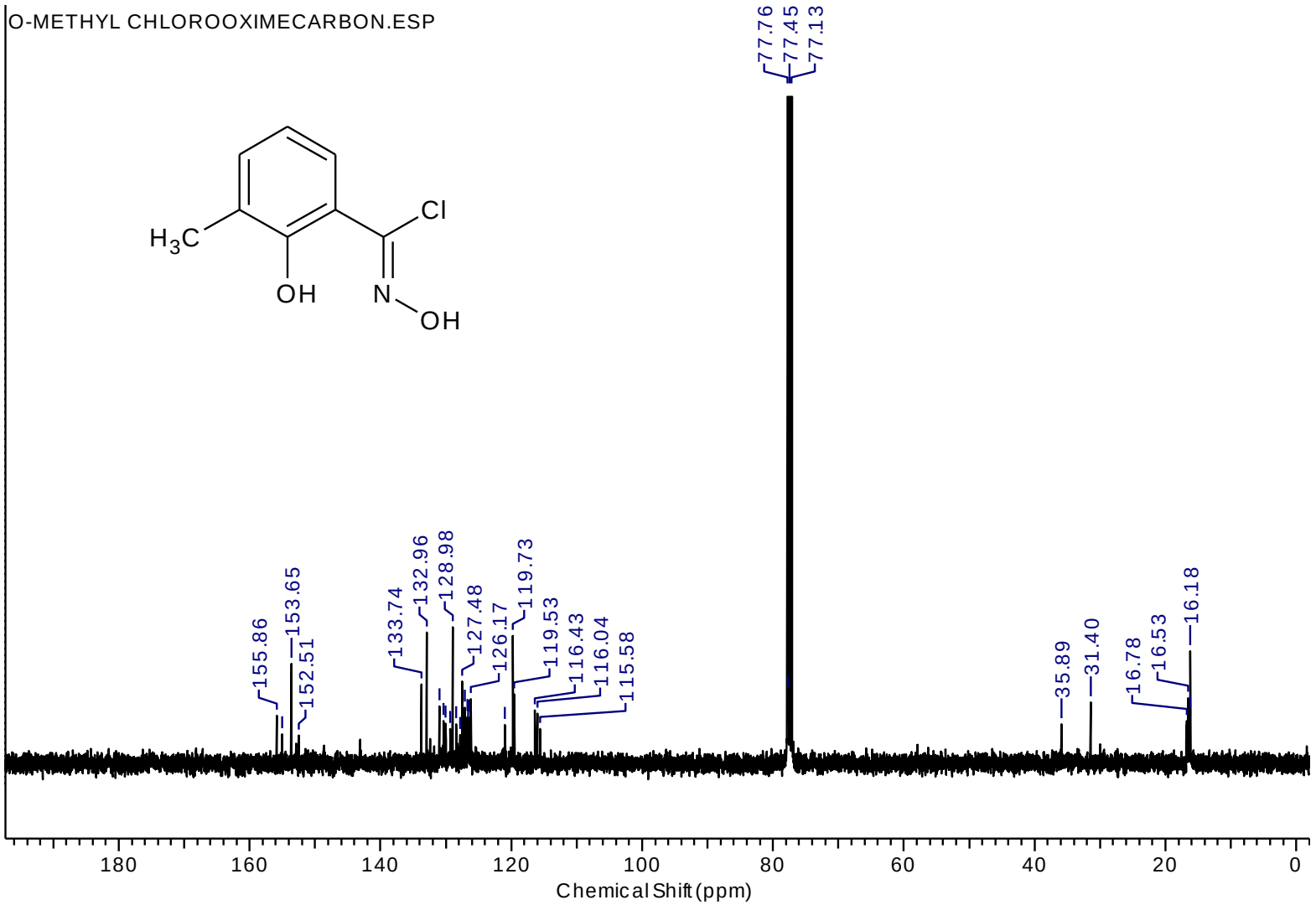
O-METHYL CHLOROOXIMECARBON.ESP
H3C
OH
Cl
N
OH
77.76
77.45
77.13
155.86
153.65
152.51
133.74
132.96
128.98
127.48
126.17
119.73
119.53
116.43
116.04
115.58
35.89
31.40
16.78
16.53
16.18
180
160
140
120
100
80
60
40
20
0
Chemical Shift (ppm)

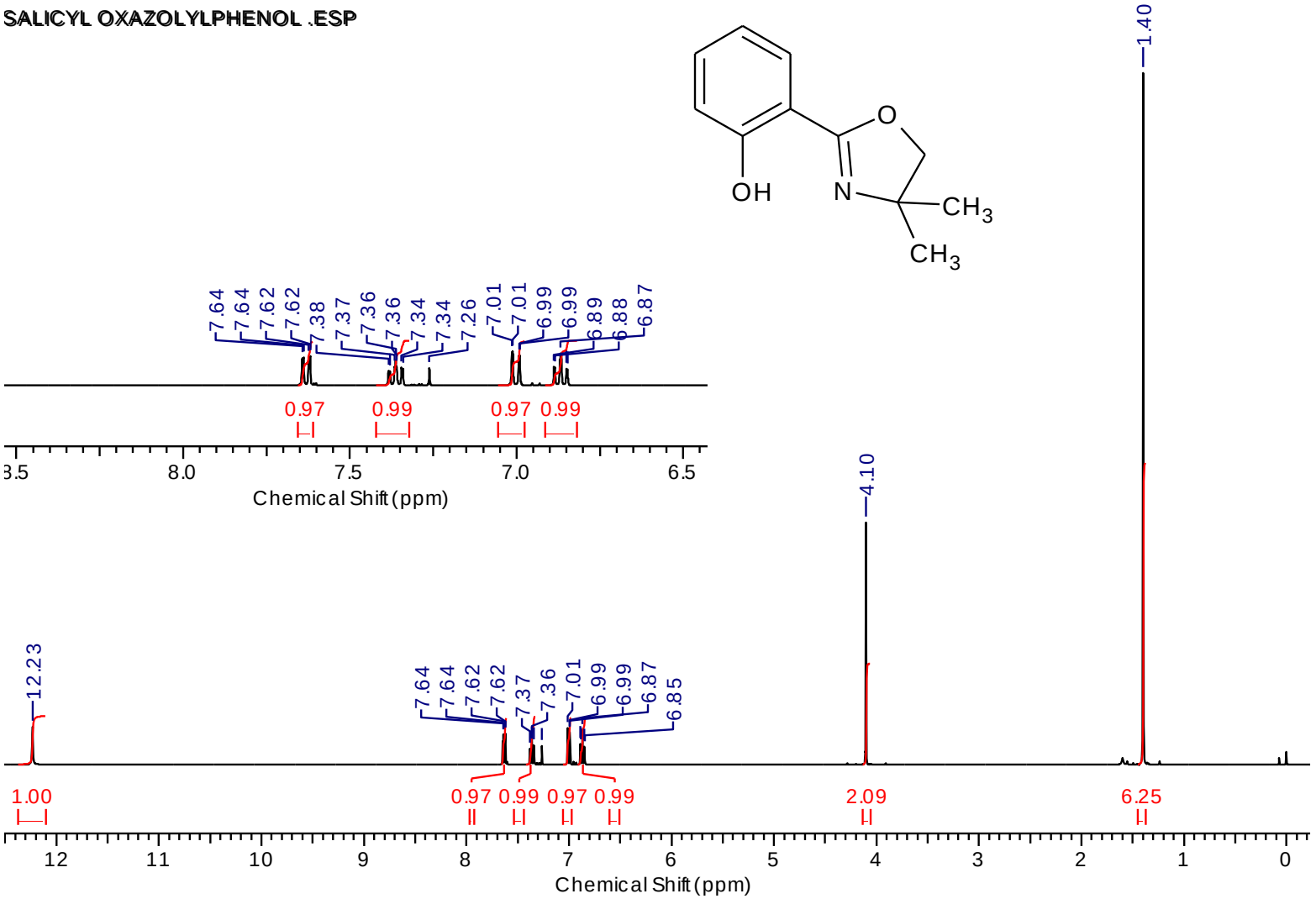
SALICYL OXAZOLYLPHENOL .ESP
OH
N
O
CH3
CH3
1.40
4.10
12.23
7.64
7.64
7.62
7.62
7.38
7.37
7.36
7.36
7.34
7.34
7.26
7.01
7.01
6.99
6.99
6.89
6.88
6.87
6.85
0.97
0.99
0.97
0.99
1.00
0.97
0.99
0.97
0.99
2.09
6.25
Chemical Shift (ppm)
Chemical Shift (ppm)

SALICYL OXAZOLYLPHENOL CARBON.ESP

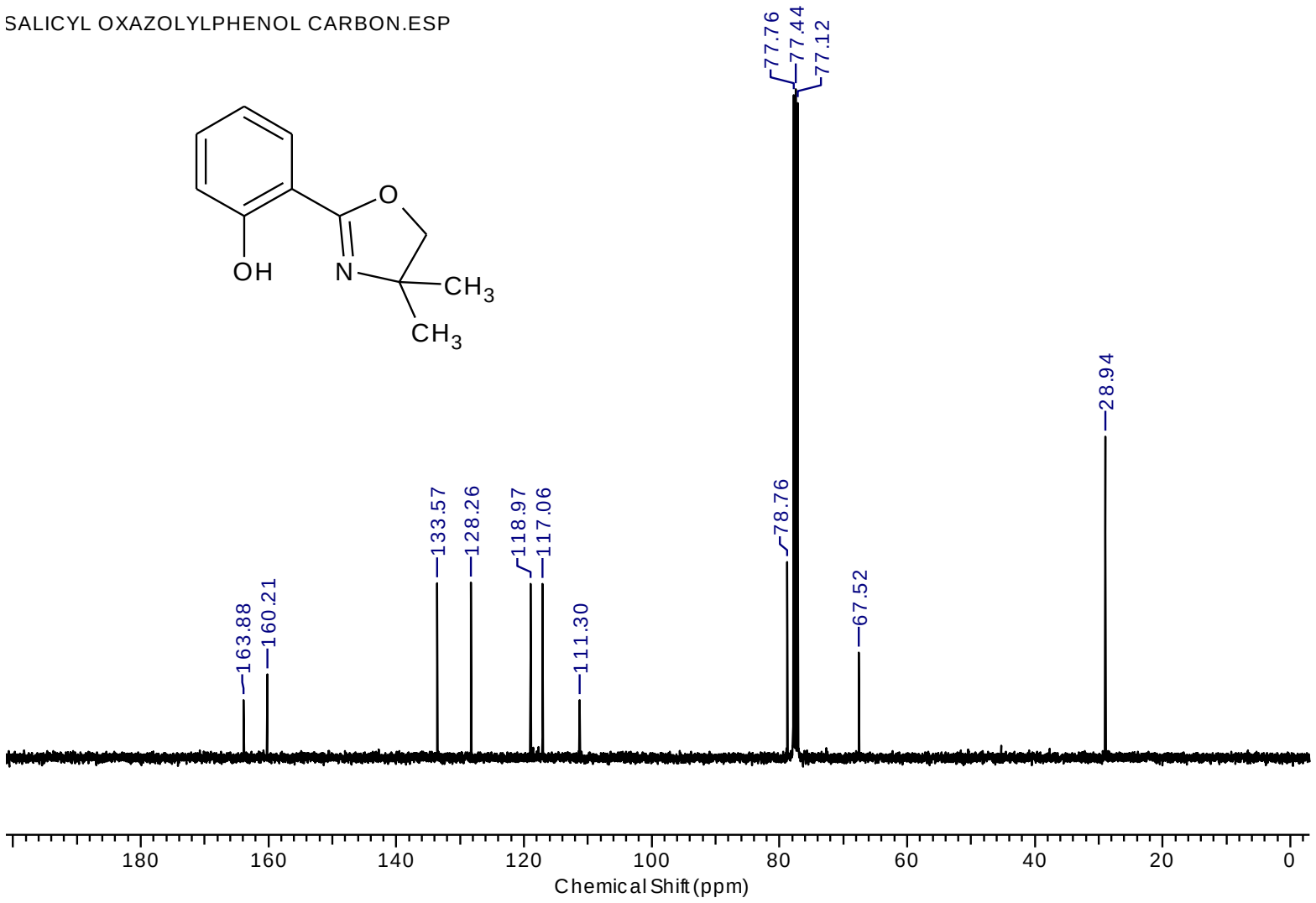

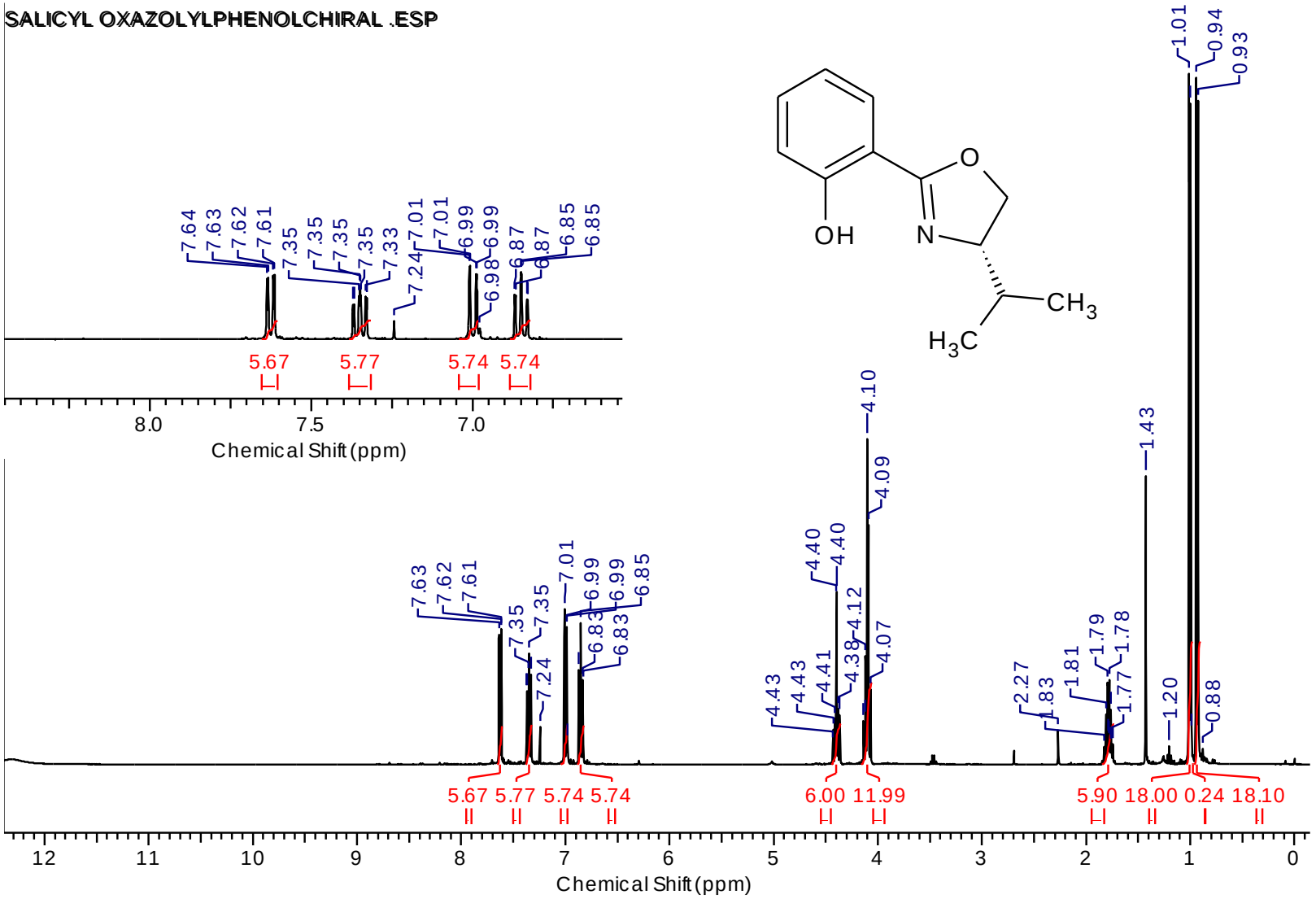
SALICYL OXAZOLYLPHENOLCHIRAL .ESP
OH
N
O
CH3
H3C
Chemical Shift (ppm)
Chemical Shift (ppm)

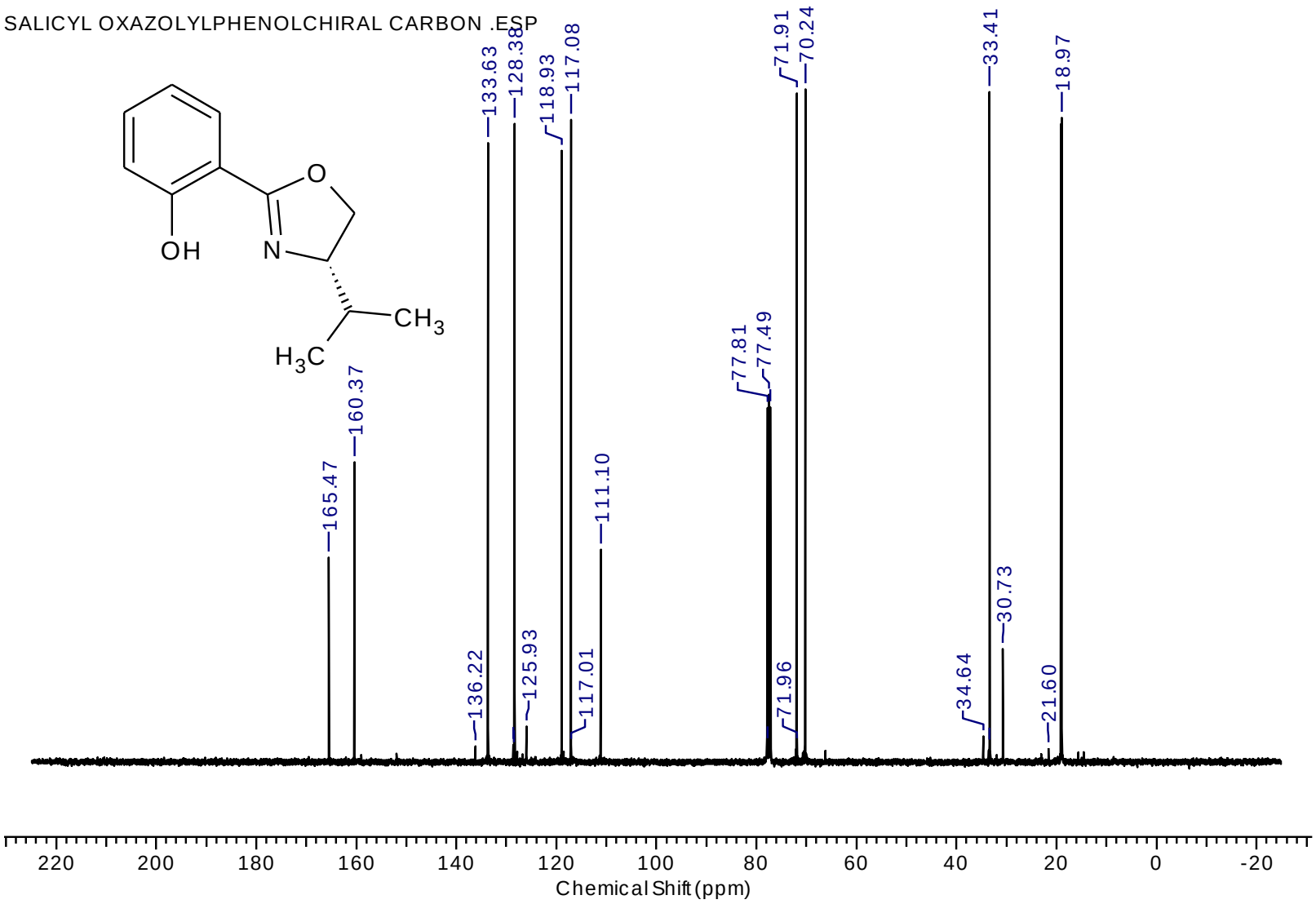
SALICYL OXAZOLYLPHENOLCHIRAL CARBON .ESP
OH
N
O
CH3
H3C
165.47
160.37
136.22
133.63
128.38
125.93
118.93
117.08
117.01
111.10
77.81
77.49
71.96
71.91
70.24
34.64
33.41
30.73
21.60
18.97
220
200
180
160
140
120
100
80
60
40
20
0
-20
Chemical Shift (ppm)

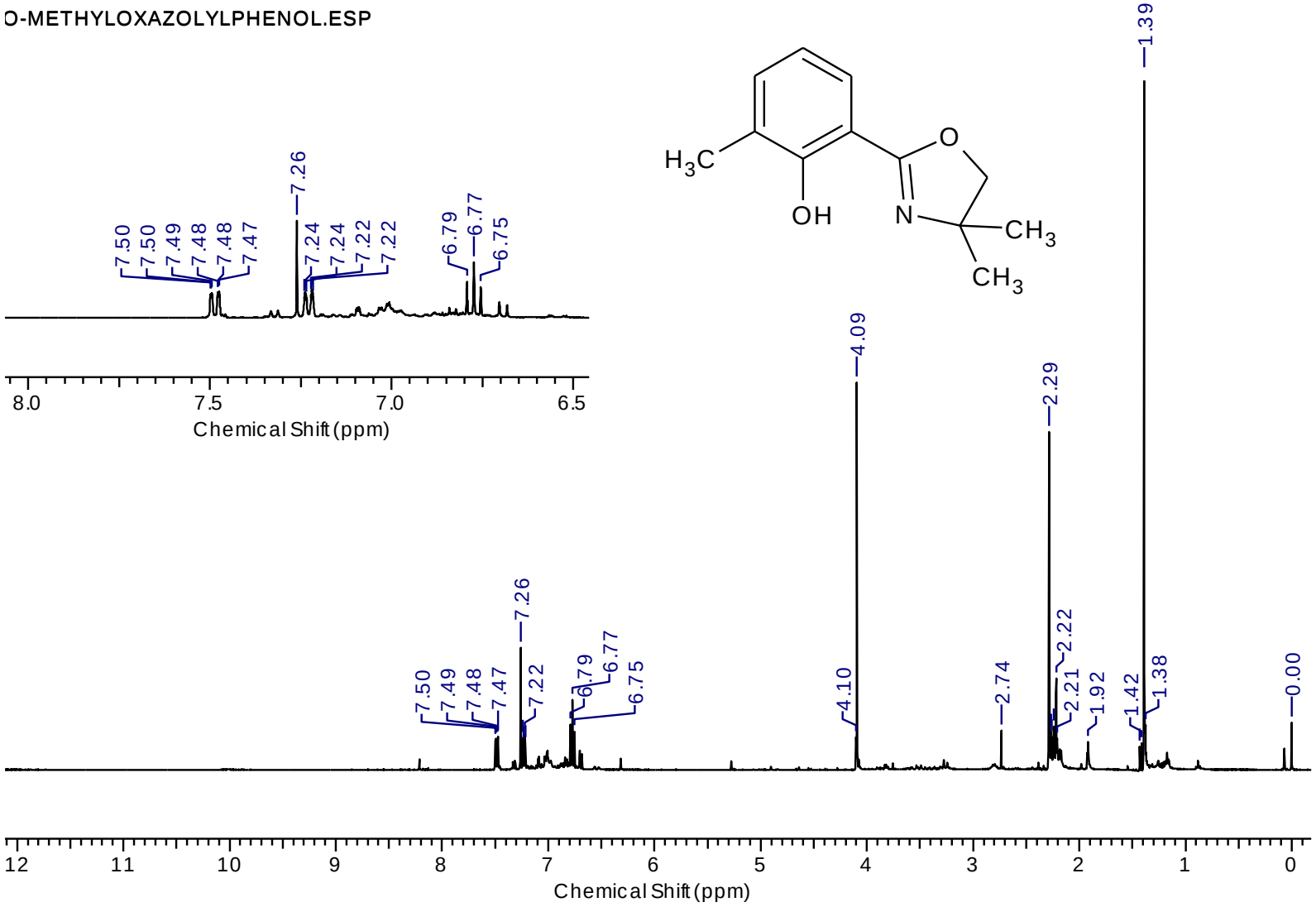
O-METHYLOXAZOLYLPHENOL.ESP
7.50
7.50
7.49
7.48
7.48
7.47
7.26
7.24
7.24
7.22
7.22
6.79
6.77
6.75
8.0
7.5
7.0
6.5
Chemical Shift (ppm)
H3C
OH
O
N
CH3
CH3
1.39
4.09
2.29
7.26
7.50
7.49
7.48
7.47
7.22
6.79
6.77
6.75
4.10
2.74
2.22
2.21
1.92
1.42
1.38
0.00
12
11
10
9
8
7
6
5
4
3
2
1
0
Chemical Shift (ppm)

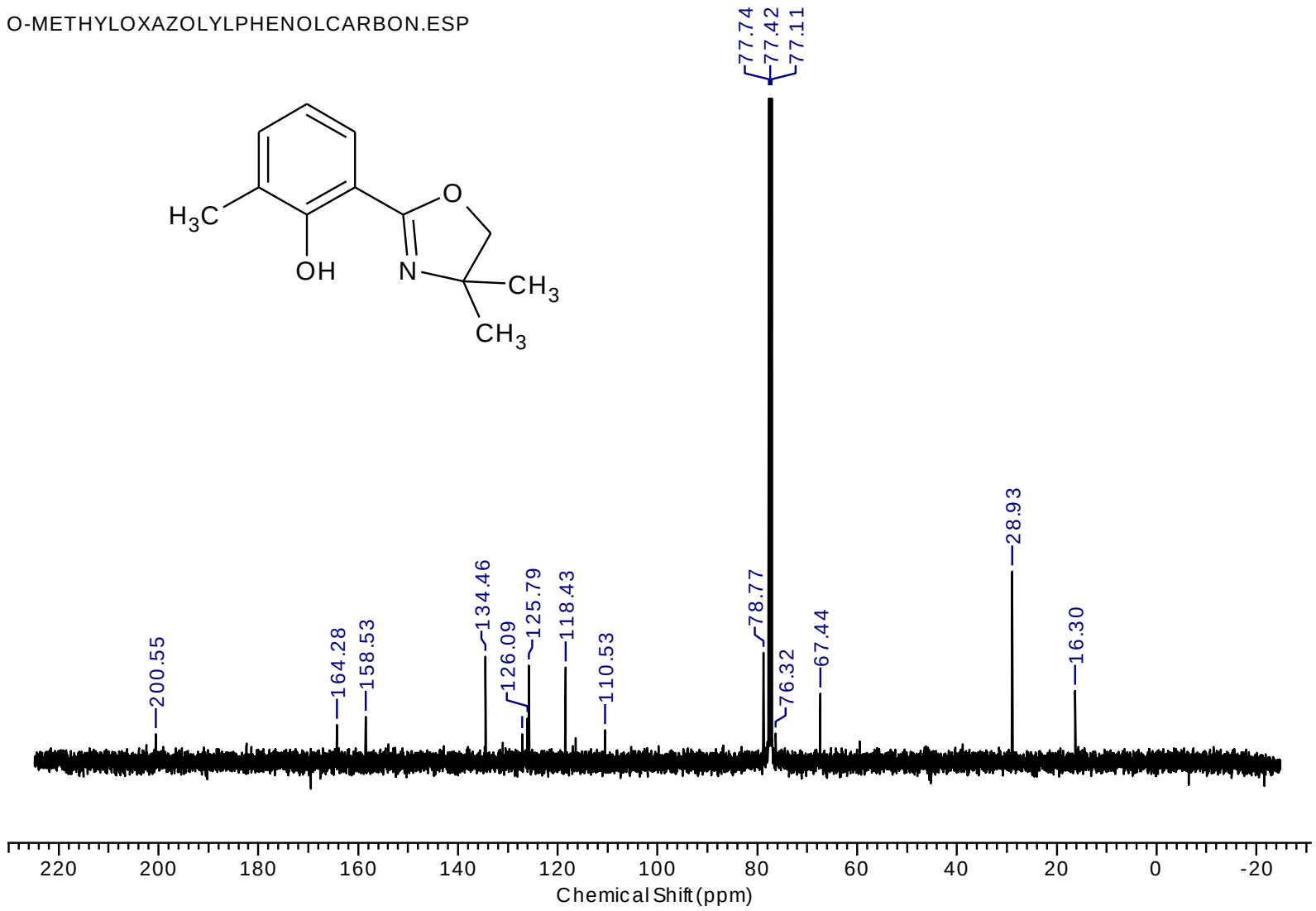
O-METHYLOXAZOLYLPHENOLCARBON.ESP
H3C
OH
N
O
CH3
CH3
77.74
77.42
77.11
200.55
164.28
158.53
134.46
126.09
125.79
118.43
110.53
78.77
76.32
67.44
28.93
16.30
220
200
180
160
140
120
100
80
60
40
20
0
-20
Chemical Shift (ppm)

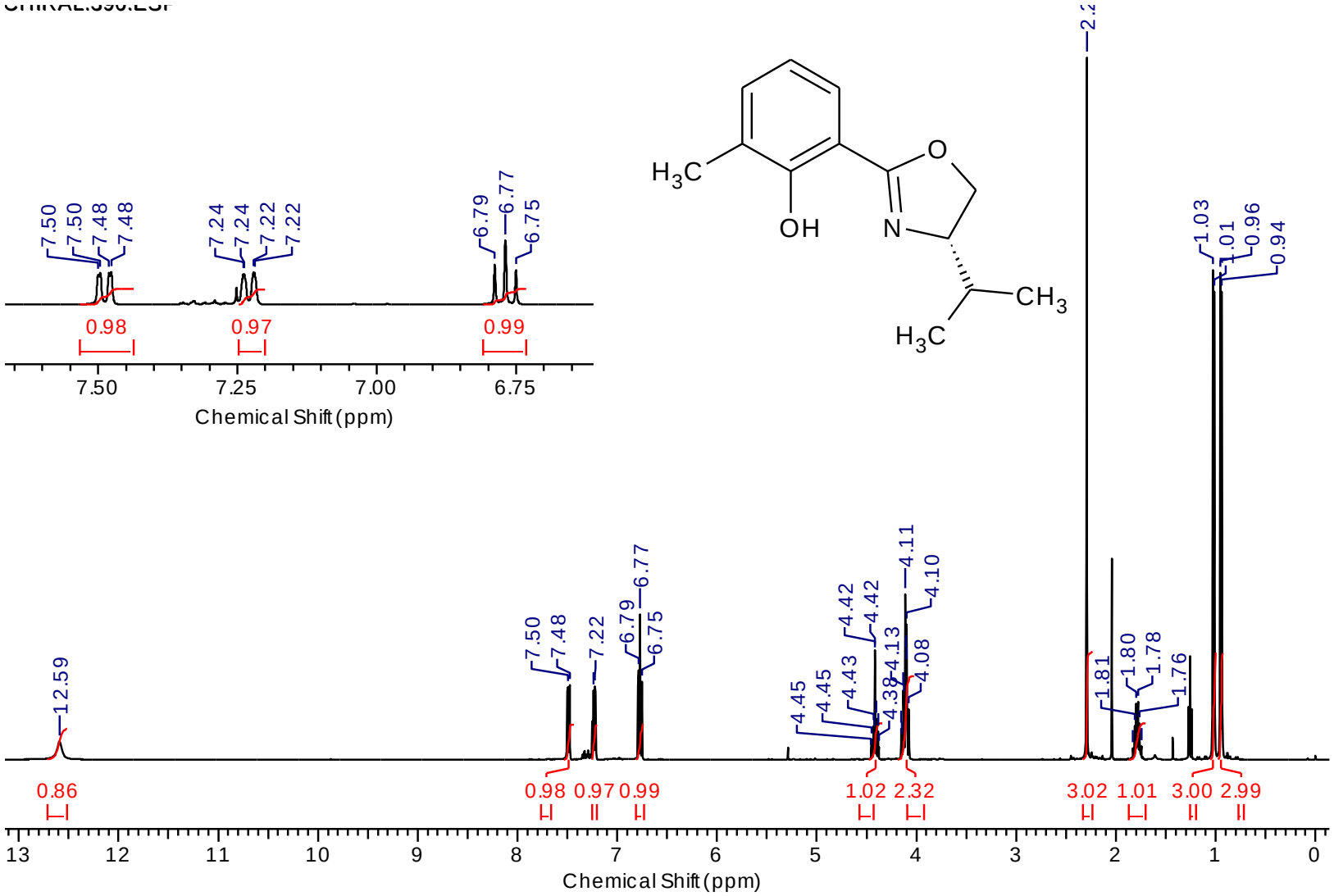
7.50
7.50
7.48
7.48
7.24
7.24
7.22
7.22
6.79
6.77
6.75
0.98
0.97
0.99
7.50
7.25
7.00
6.75
Chemical Shift (ppm)
H3C
OH
O
N
CH3
H3C
12.59
7.50
7.48
7.22
6.79
6.77
6.75
4.45
4.45
4.43
4.42
4.42
4.39
4.13
4.11
4.10
4.08
1.81
1.80
1.78
1.76
1.03
1.01
0.96
0.94
0.86
0.98
0.97
0.99
1.02
2.32
3.02
1.01
3.00
2.99
13
12
11
10
9
8
7
6
5
4
3
2
1
0
Chemical Shift (ppm)

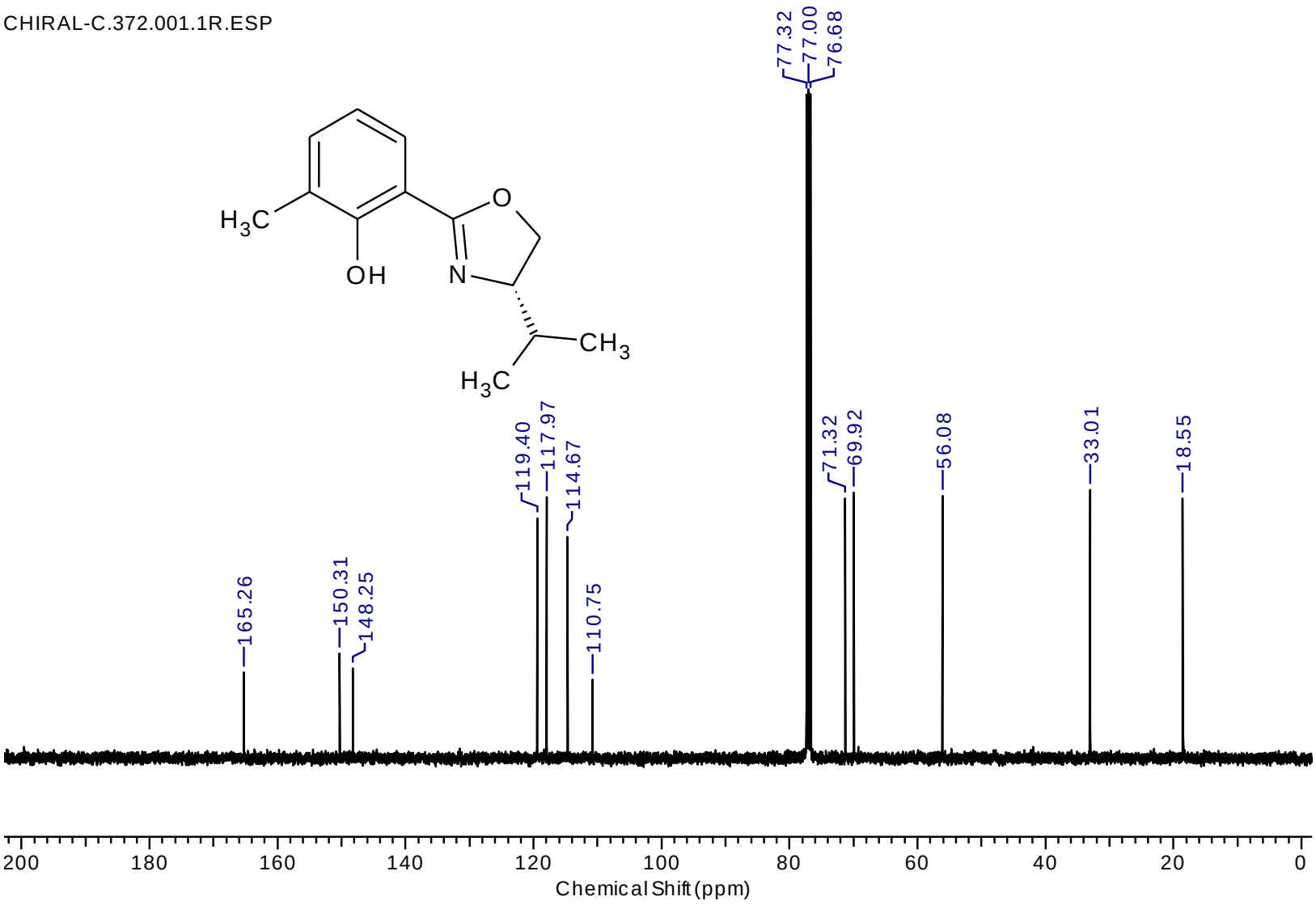
CHIRAL-C.372.001.1R.ESP
77.32
77.00
76.68
71.32
69.92
56.08
33.01
18.55
119.40
117.97
114.67
110.75
165.26
150.31
148.25
H3C
OH
N
O
CH3
H3C
200
180
160
140
120
100
80
60
40
20
0
Chemical Shift (ppm)

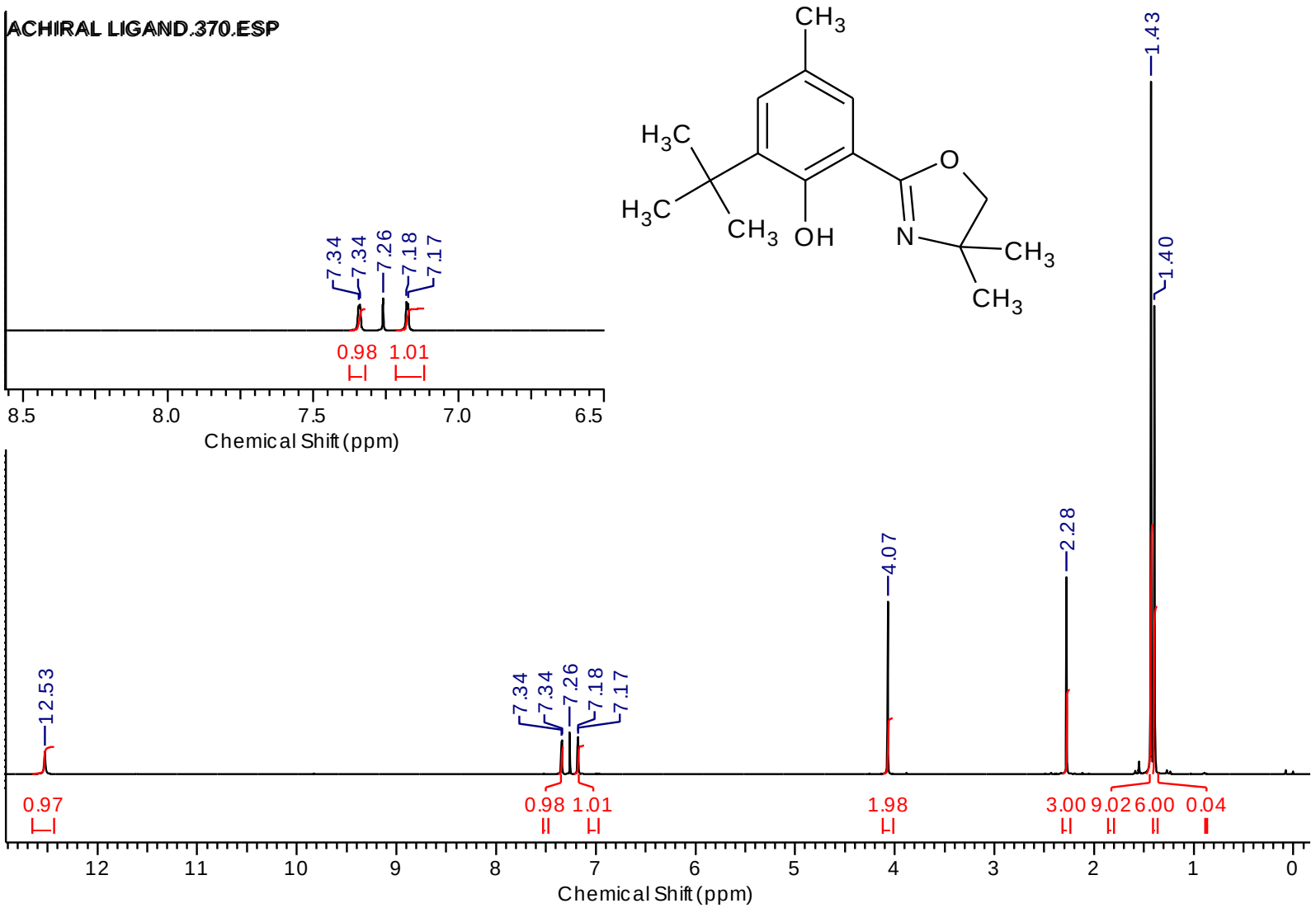
ACHIRAL LIGAND.370.ESP
7.34
7.34
7.26
7.18
7.17
0.98
1.01
8.5
8.0
7.5
7.0
6.5
Chemical Shift (ppm)
CH3
H3C
H3C
CH3
OH
O
N
CH3
CH3
1.43
1.40
12.53
7.34
7.34
7.26
7.18
7.17
4.07
2.28
0.97
0.98
1.01
1.98
3.00
9.02
6.00
0.04
12
11
10
9
8
7
6
5
4
3
2
1
0
Chemical Shift (ppm)

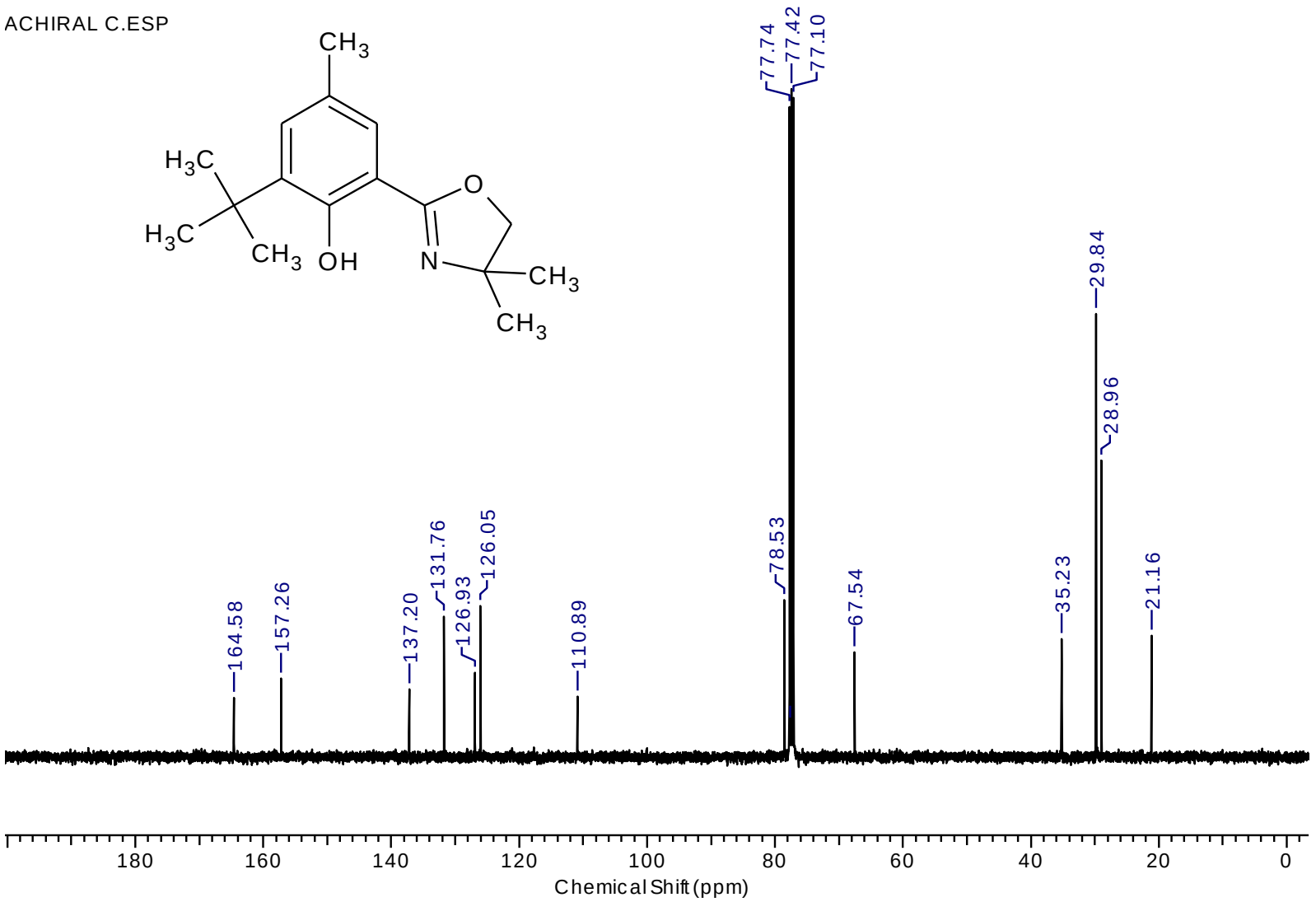
ACHIRAL C.ESP
CH3
H3C
H3C
CH3
OH
O
N
CH3
CH3
77.74
77.42
77.10
29.84
28.96
164.58
157.26
137.20
131.76
126.93
126.05
110.89
78.53
67.54
35.23
21.16
180
160
140
120
100
80
60
40
20
0
Chemical Shift (ppm)

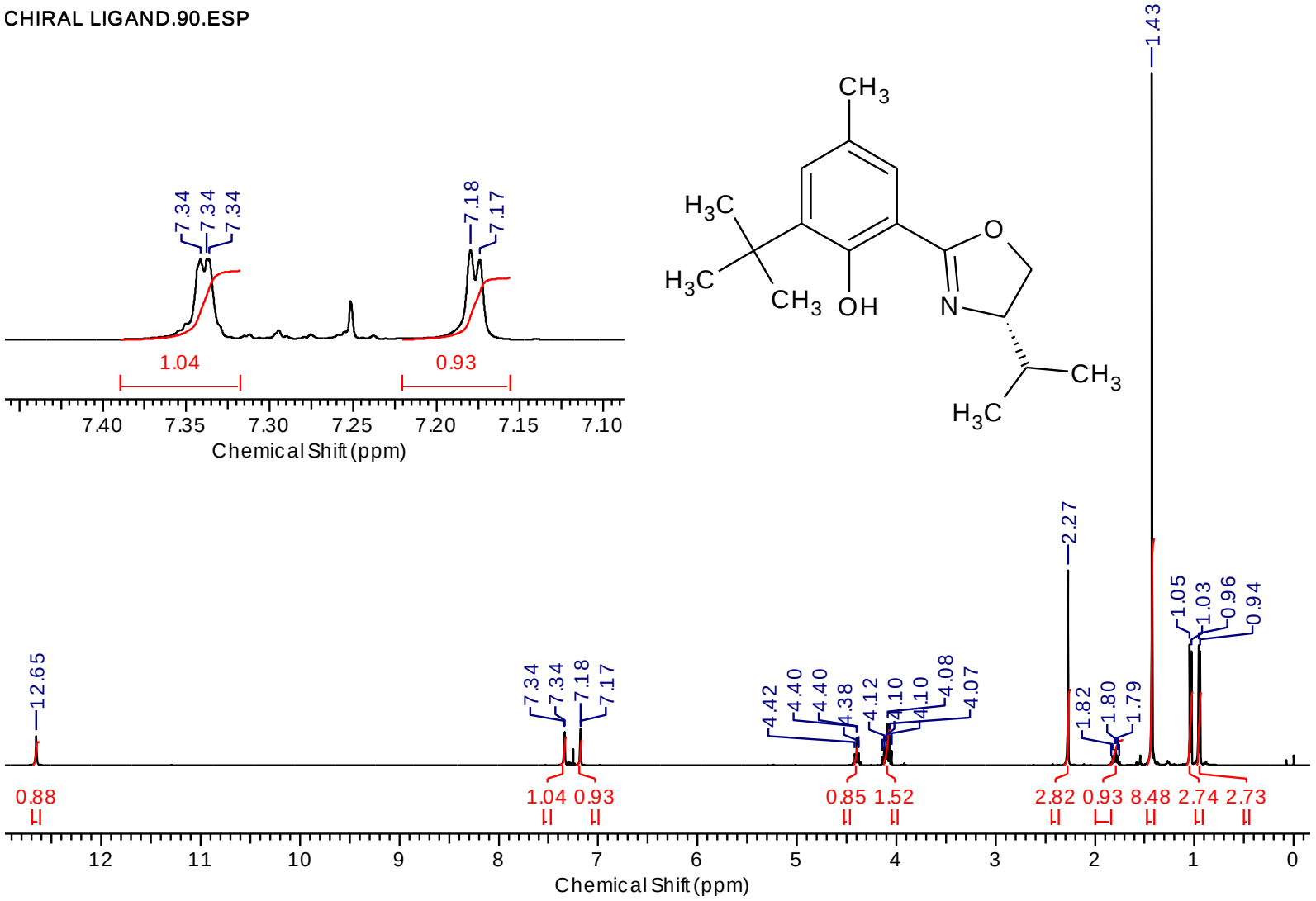
CHIRAL LIGAND.90.ESP
7.34
7.34
7.34
7.18
7.17
1.04
0.93
7.40
7.35
7.30
7.25
7.20
7.15
7.10
Chemical Shift (ppm)
CH3
H3C
H3C
CH3
OH
O
N
CH3
H3C
1.43
12.65
7.34
7.34
7.18
7.17
4.42
4.40
4.40
4.38
4.12
4.10
4.10
4.08
4.07
2.27
1.82
1.80
1.79
1.05
1.03
0.96
0.94
0.88
1.04
0.93
0.85
1.52
2.82
0.93
8.48
2.74
2.73
12
11
10
9
8
7
6
5
4
3
2
1
0
Chemical Shift (ppm)

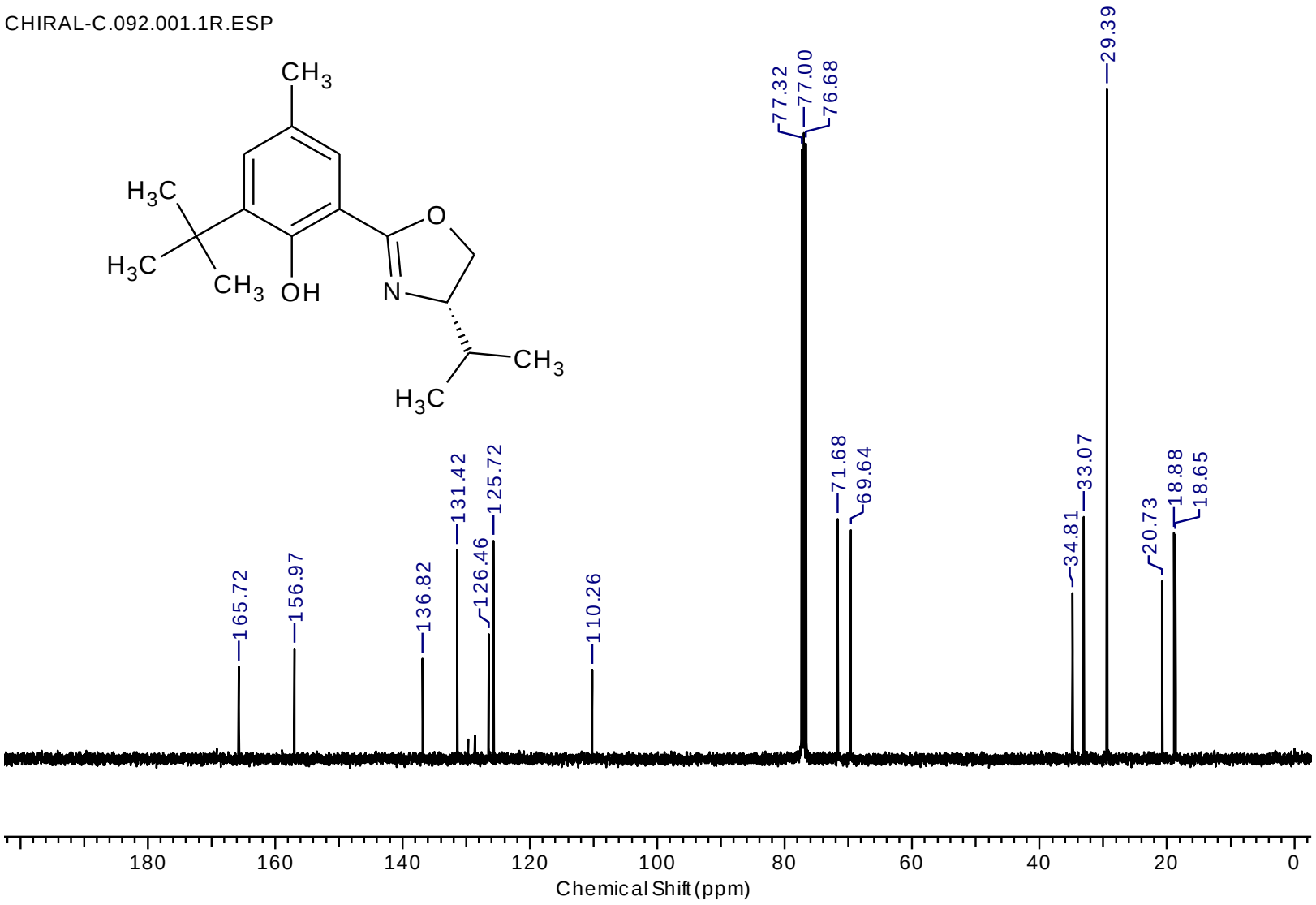
CHIRAL-C.092.001.1R.ESP
CH3
H3C
H3C
CH3
OH
O
N
CH3
H3C
165.72
156.97
136.82
131.42
126.46
125.72
110.26
77.32
77.00
76.68
71.68
69.64
34.81
33.07
29.39
20.73
18.88
18.65
180
160
140
120
100
80
60
40
20
0
Chemical Shift (ppm)

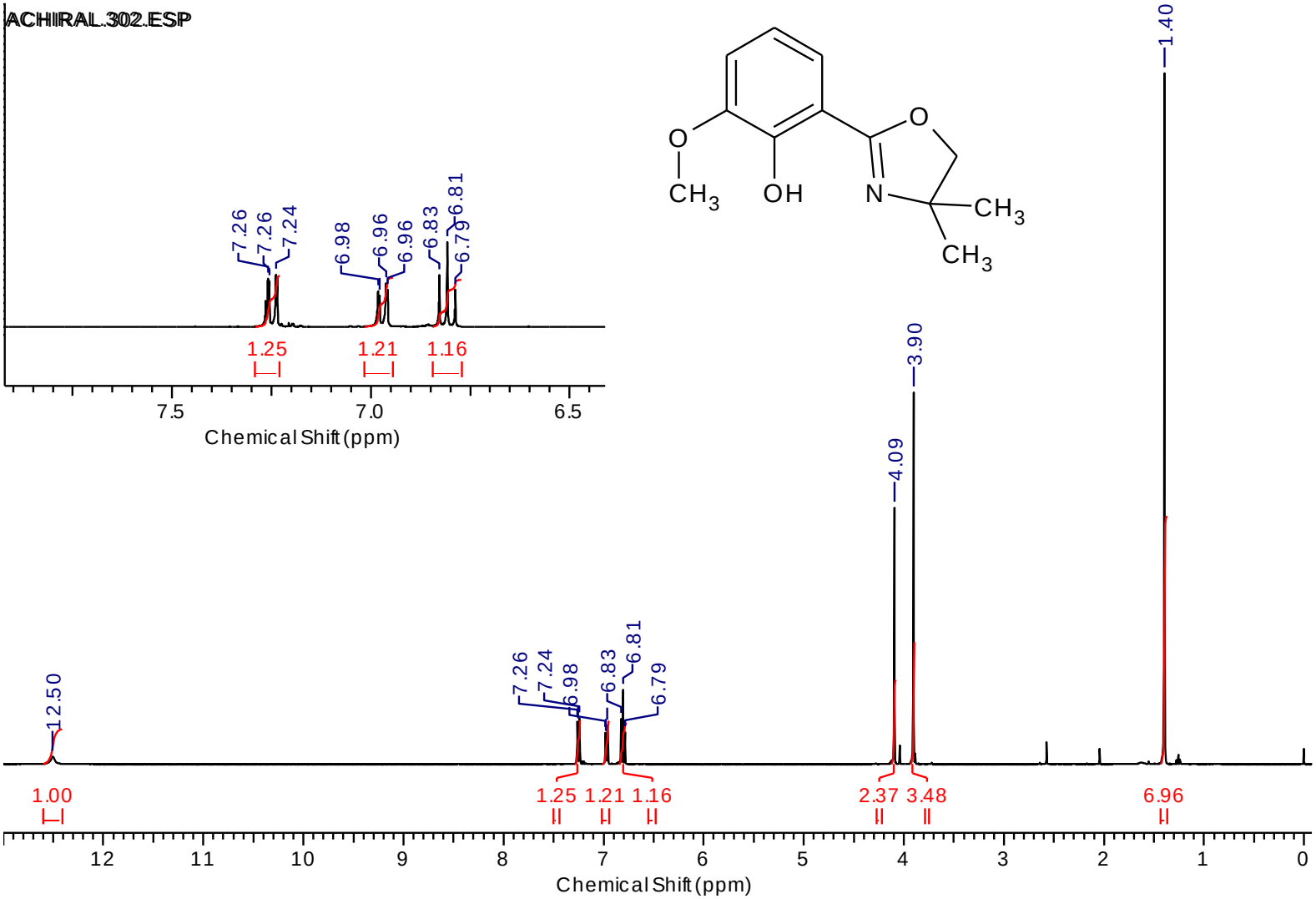
ACHIRAL.302.ESP
7.26
7.26
7.24
6.98
6.96
6.96
6.83
6.81
6.79
1.25
1.21
1.16
7.5
7.0
6.5
Chemical Shift (ppm)
O
CH3
OH
N
O
CH3
CH3
1.40
3.90
4.09
12.50
7.26
7.24
6.98
6.83
6.81
6.79
1.00
1.25
1.21
1.16
2.37
3.48
6.96
12
11
10
9
8
7
6
5
4
3
2
1
0
Chemical Shift (ppm)

CHIRAL.370.ESP

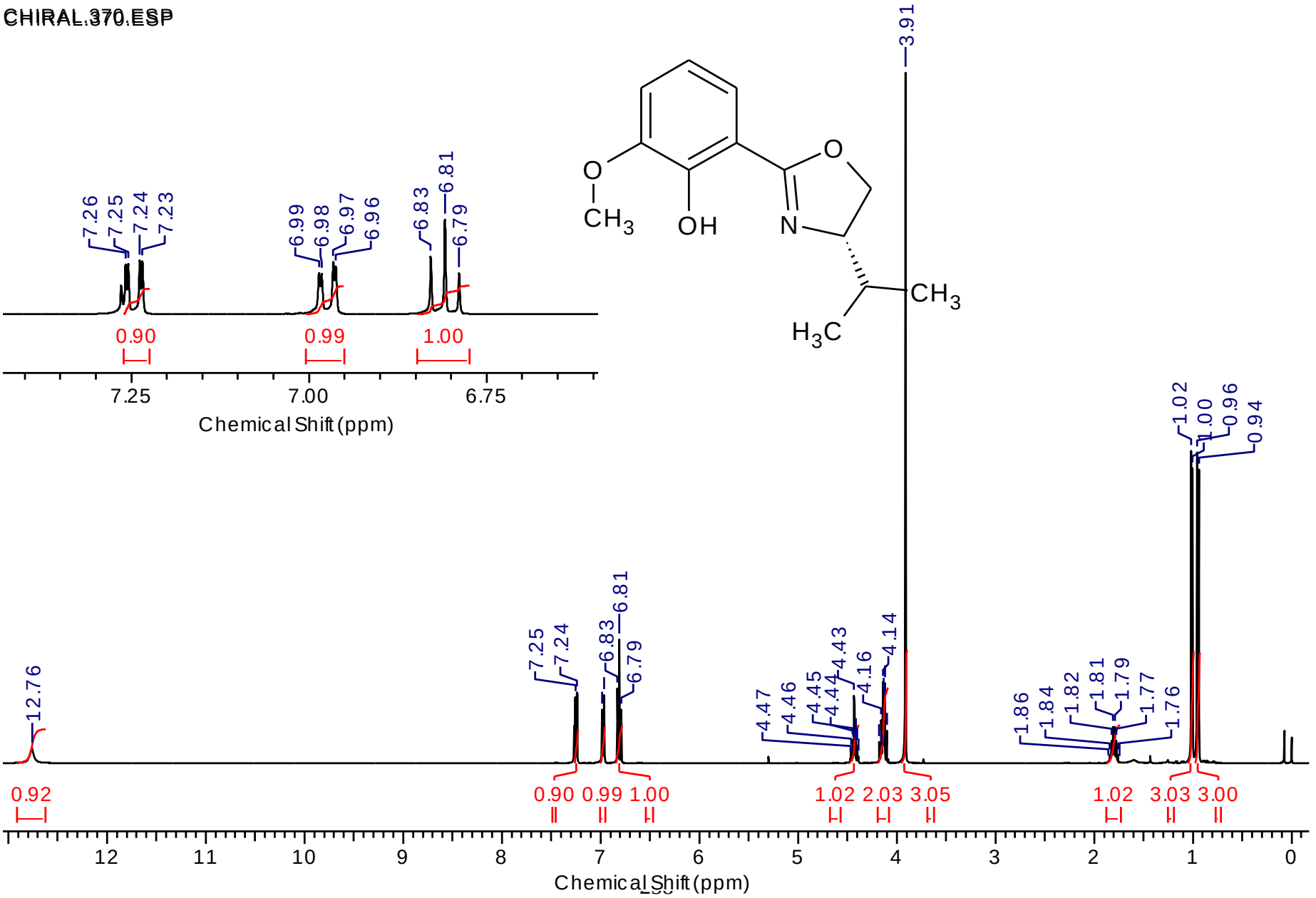

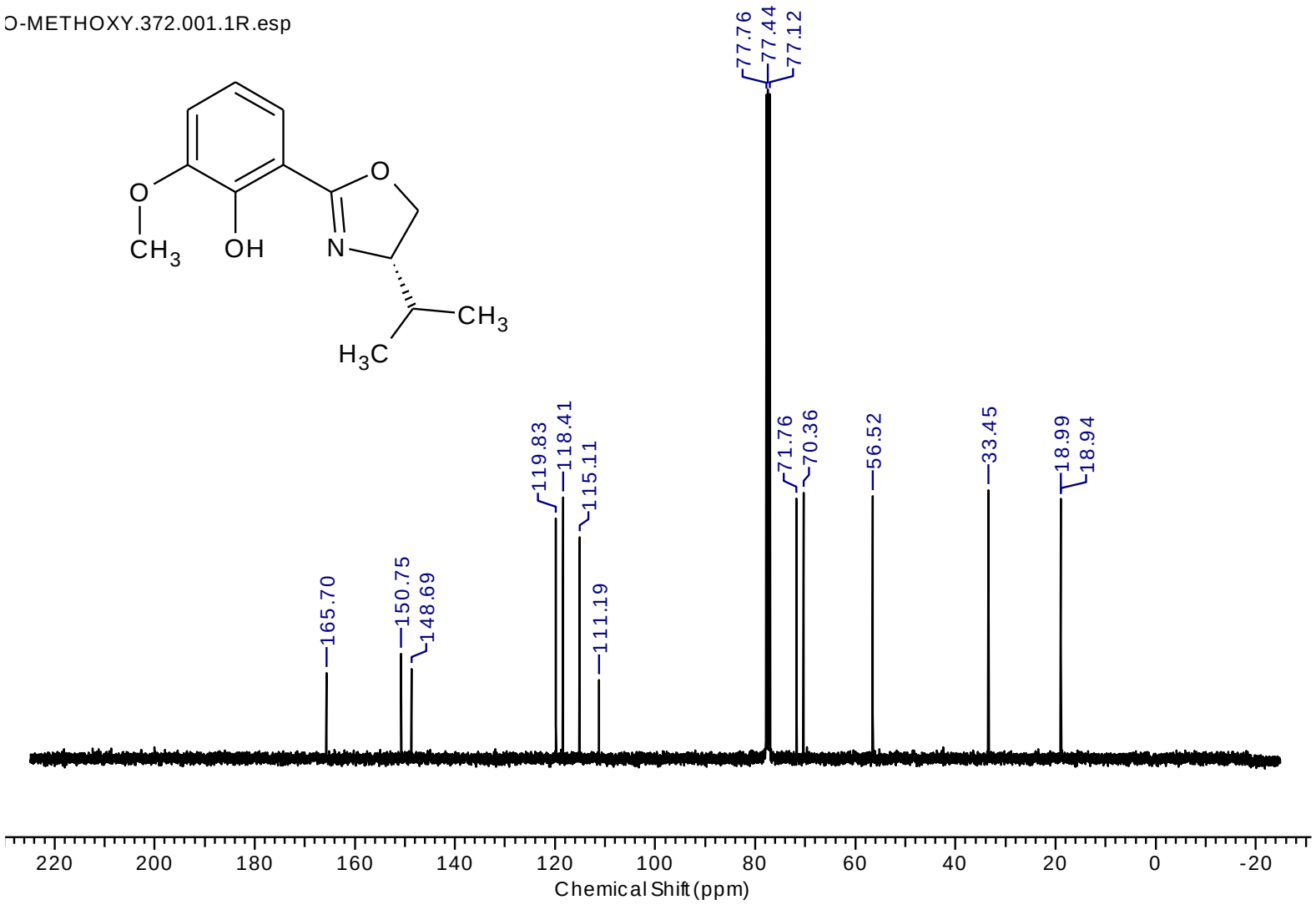
O-METHOXY.372.001.1R.esp
O
CH3
OH
N
O
CH3
H3C
77.76
77.44
77.12
119.83
118.41
115.11
71.76
70.36
56.52
33.45
18.99
18.94
165.70
150.75
148.69
111.19
220
200
180
160
140
120
100
80
60
40
20
0
-20
Chemical Shift (ppm)

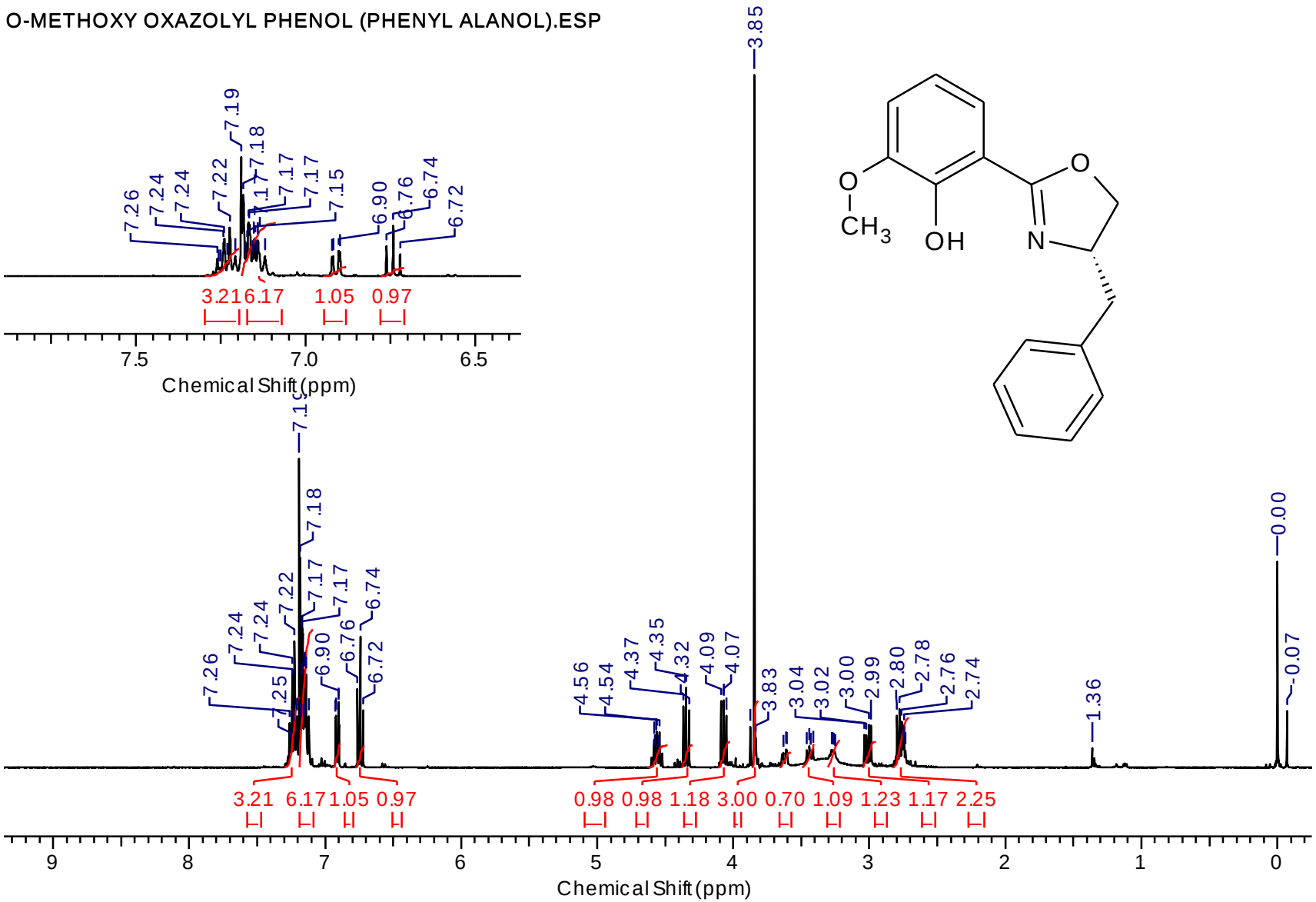
O-METHOXY OXAZOLYL PHENOL (PHENYL ALANOL).ESP
7.26
7.24
7.24
7.22
7.19
7.18
7.17
7.17
7.15
6.90
6.76
6.74
6.72
3.21
6.17
1.05
0.97
7.5
7.0
6.5
Chemical Shift (ppm)
3.85
O
CH3
OH
N
O
7.26
7.24
7.24
7.22
7.18
7.17
7.17
6.74
6.90
6.76
6.72
7.25
4.56
4.54
4.37
4.35
4.32
4.09
4.07
3.83
3.04
3.02
3.00
2.99
2.80
2.78
2.76
2.74
1.36
0.00
-0.07
3.21
6.17
1.05
0.97
0.98
0.98
1.18
3.00
0.70
1.09
1.23
1.17
2.25
9
8
7
6
5
4
3
2
1
0
Chemical Shift (ppm)

12. ^{1}H of Catalyst Products

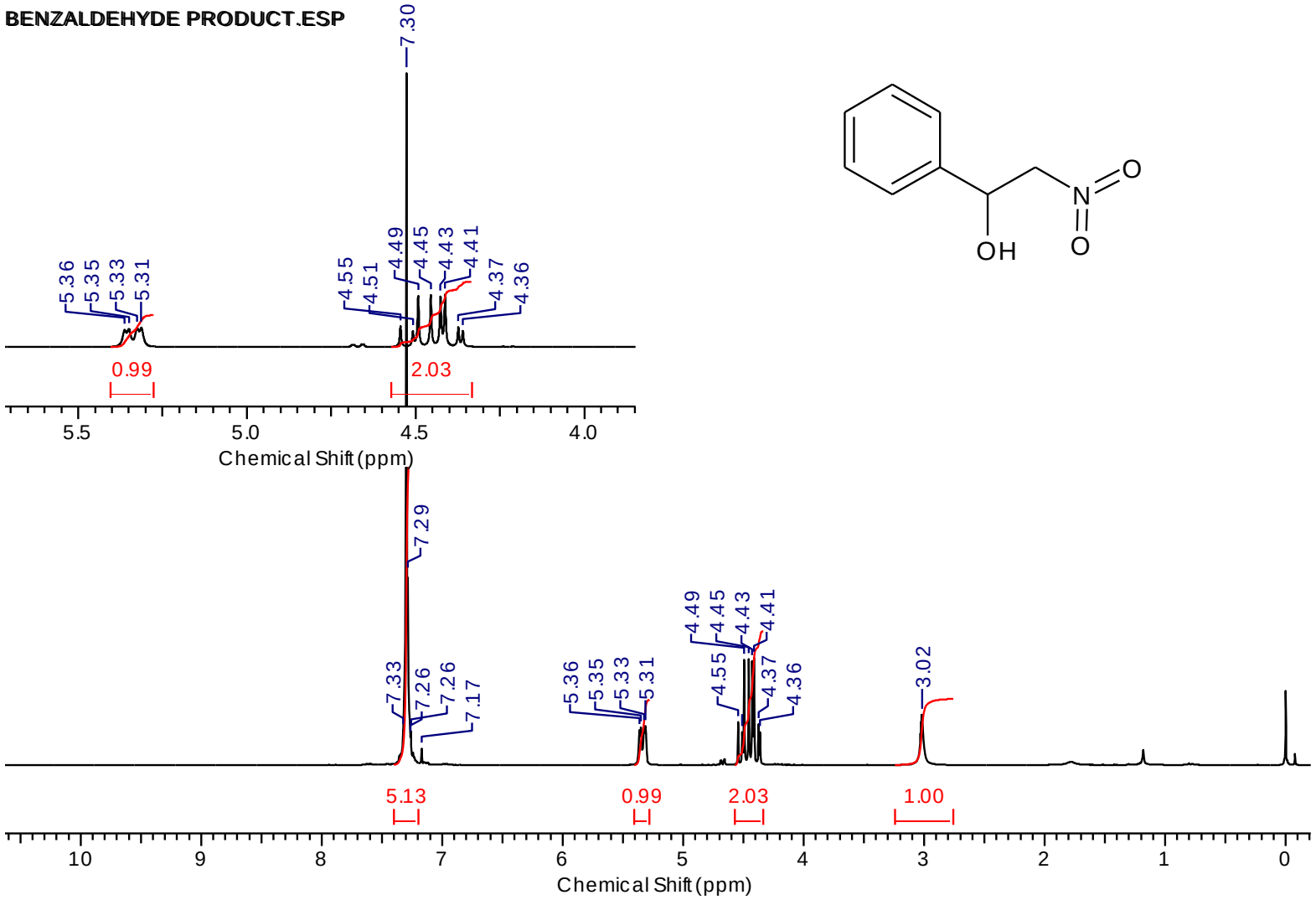

13. ^{1}H and ^{13}C NMR Spectrum of Rare Earth Complexes

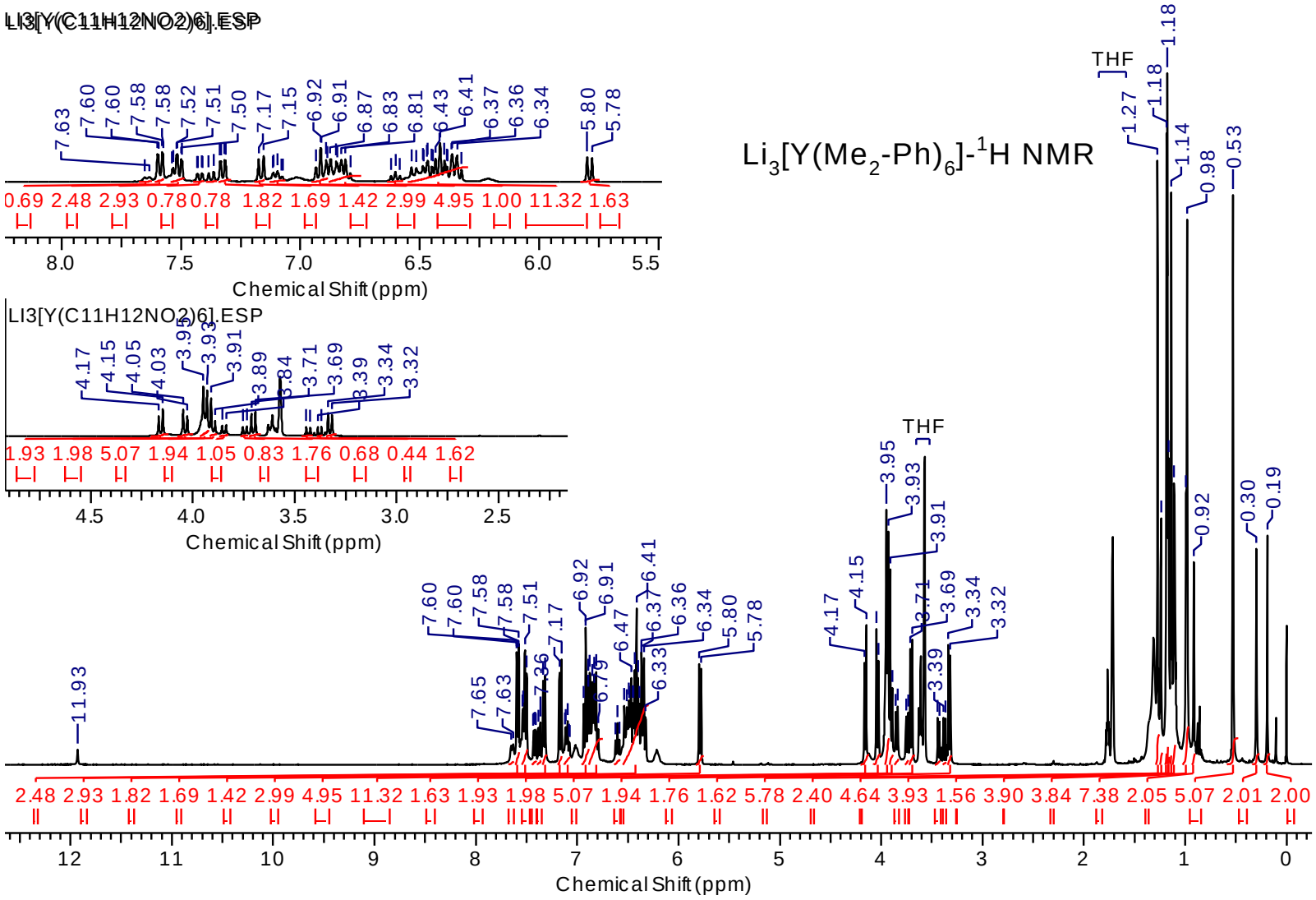

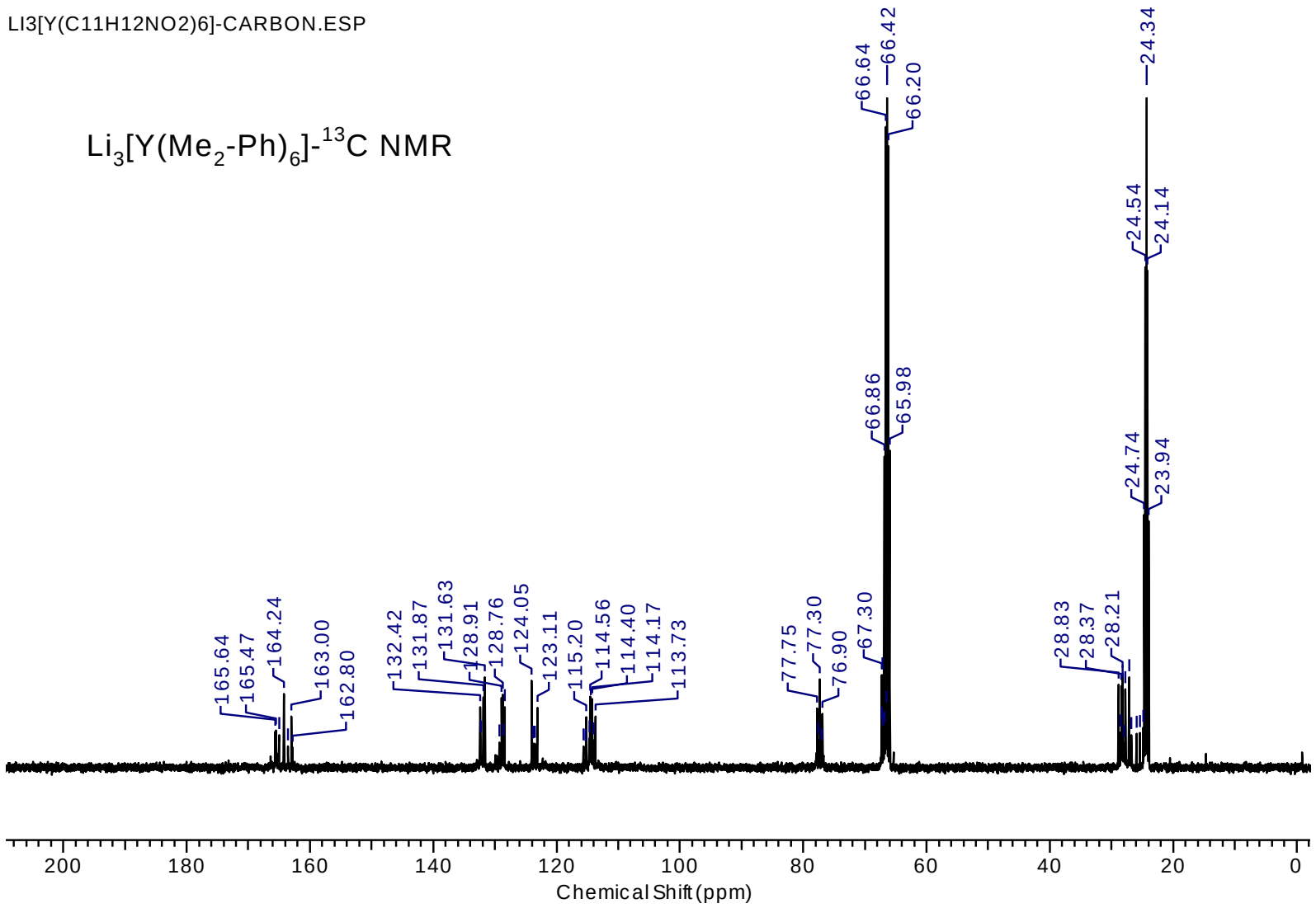
LI3[Y(C11H12NO2)6]-CARBON.ESP
Li3[Y(Me2-Ph)6]-13C NMR
66.64
66.42
66.20
24.34
24.54
24.14
66.86
65.98
24.74
23.94
165.64
165.47
164.24
163.00
162.80
132.42
131.87
131.63
128.91
128.76
124.05
123.11
115.20
114.56
114.40
114.17
113.73
77.75
77.30
76.90
67.30
28.83
28.37
28.21
200
180
160
140
120
100
80
60
40
20
0
Chemical Shift (ppm)

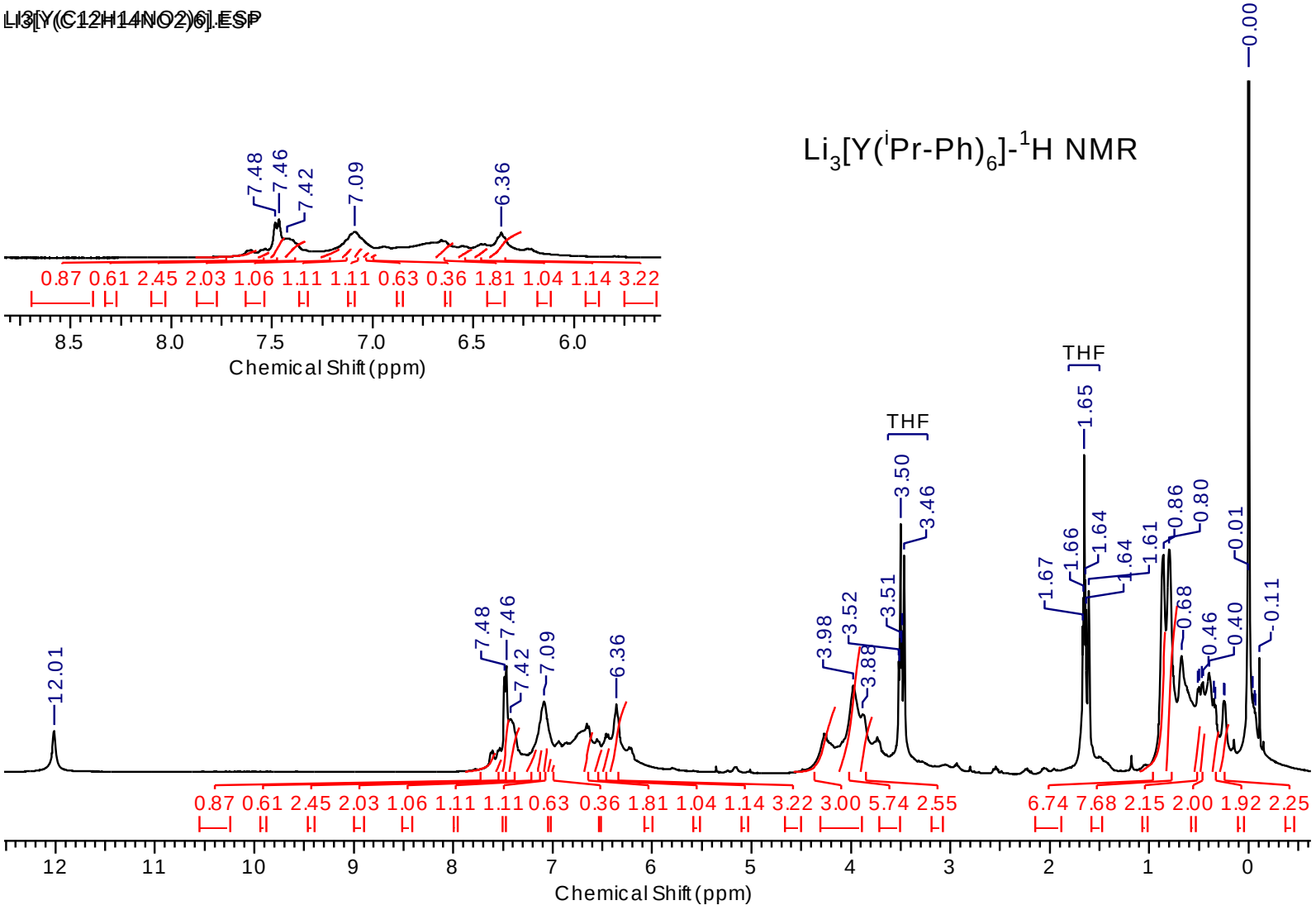
Li3[Y(C12H14NO2)6].ESP
Li3[Y(C12H14NO2)6].ESP
Li3[Y(iPr-Ph)6]-1H NMR
12.01
7.48
7.46
7.42
7.09
6.36
3.98
3.52
3.51
3.50
3.46
3.88
THF
THF
1.67
1.66
1.65
1.64
1.64
1.61
0.86
0.80
0.68
0.46
0.40
0.01
0.00
-0.11
0.87 0.61 2.45 2.03 1.06 1.11 1.11 0.63 0.36 1.81 1.04 1.14 3.22 3.00 5.74 2.55
6.74 7.68 2.15 2.00 1.92 2.25
Chemical Shift (ppm)
0.87 0.61 2.45 2.03 1.06 1.11 1.11 0.63 0.36 1.81 1.04 1.14 3.22
Chemical Shift (ppm)

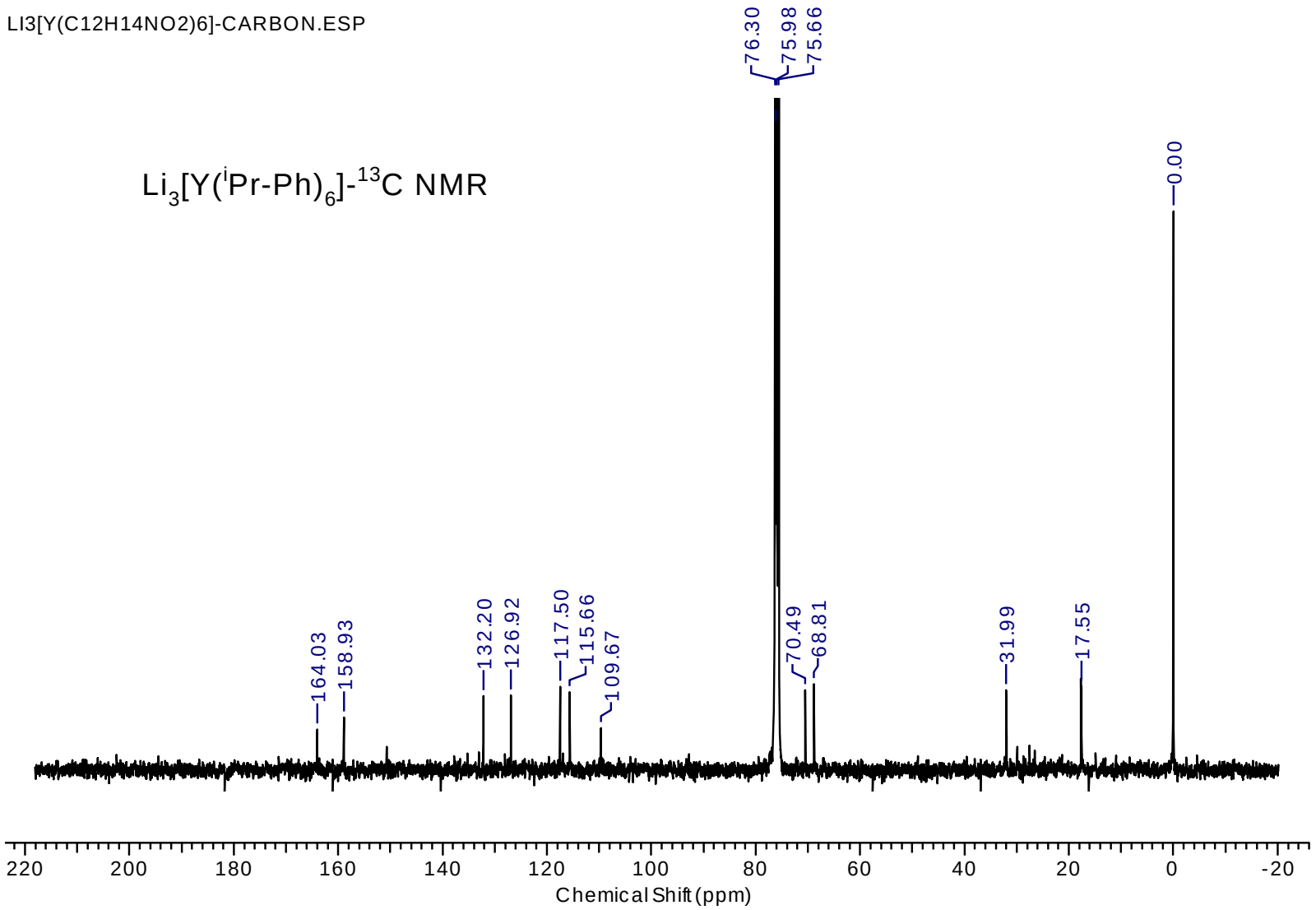
LI3[Y(C12H14NO2)6]-CARBON.ESP
Li3[Y(iPr-Ph)6]-13C NMR
76.30
75.98
75.66
0.00
164.03
158.93
132.20
126.92
117.50
115.66
109.67
70.49
68.81
31.99
17.55
220
200
180
160
140
120
100
80
60
40
20
0
-20
Chemical Shift (ppm)

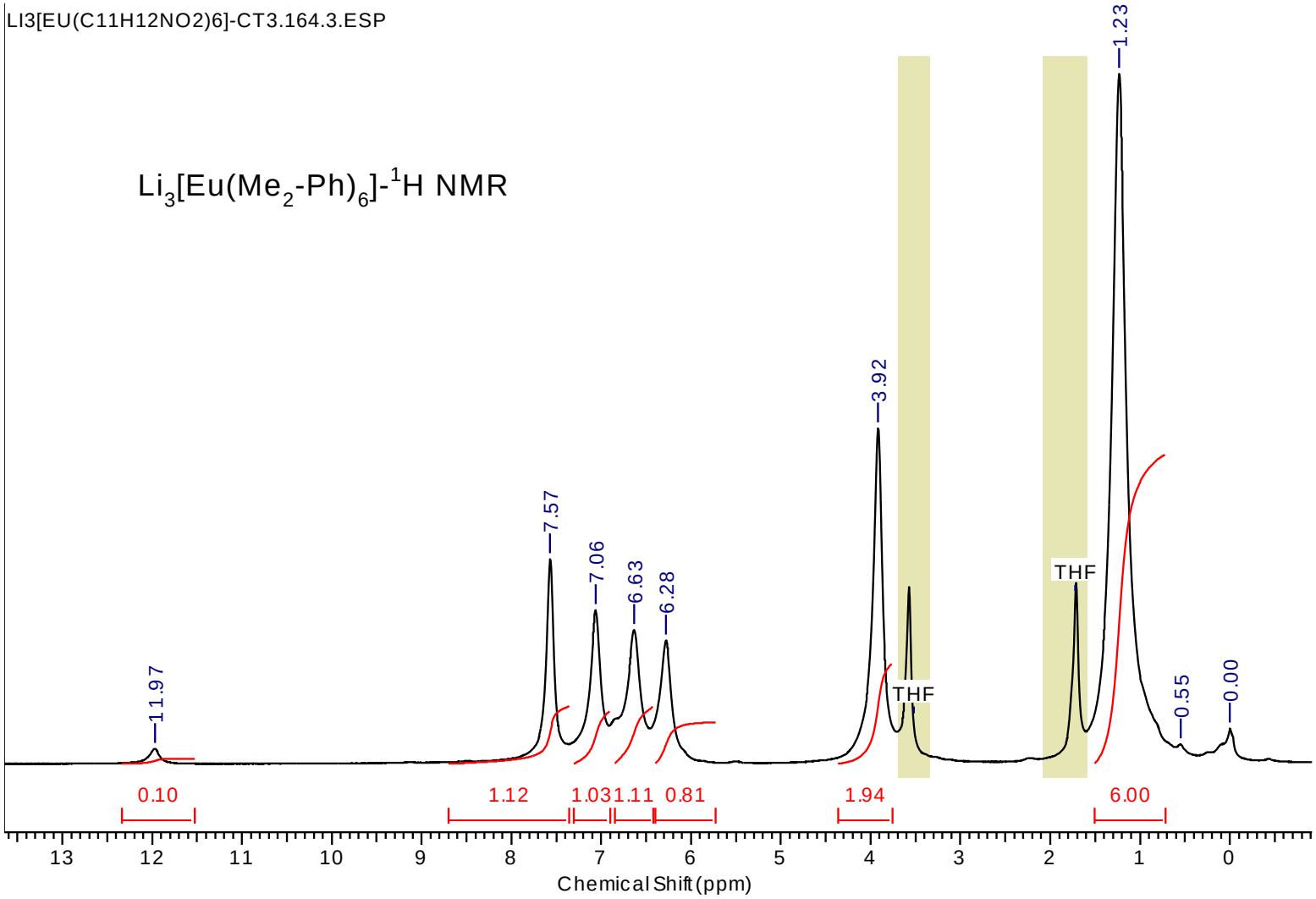
LI3[EU(C11H12NO2)6]-CT3.164.3.ESP
Li3[Eu(Me2-Ph)6]-1H NMR
11.97
7.57
7.06
6.63
6.28
3.92
THF
THF
1.23
0.55
0.00
0.10
1.12
1.03
1.11
0.81
1.94
6.00
13
12
11
10
9
8
7
6
5
4
3
2
1
0
Chemical Shift (ppm)

LI3[EU(C11H12NO2)6]-CARBON.ESP

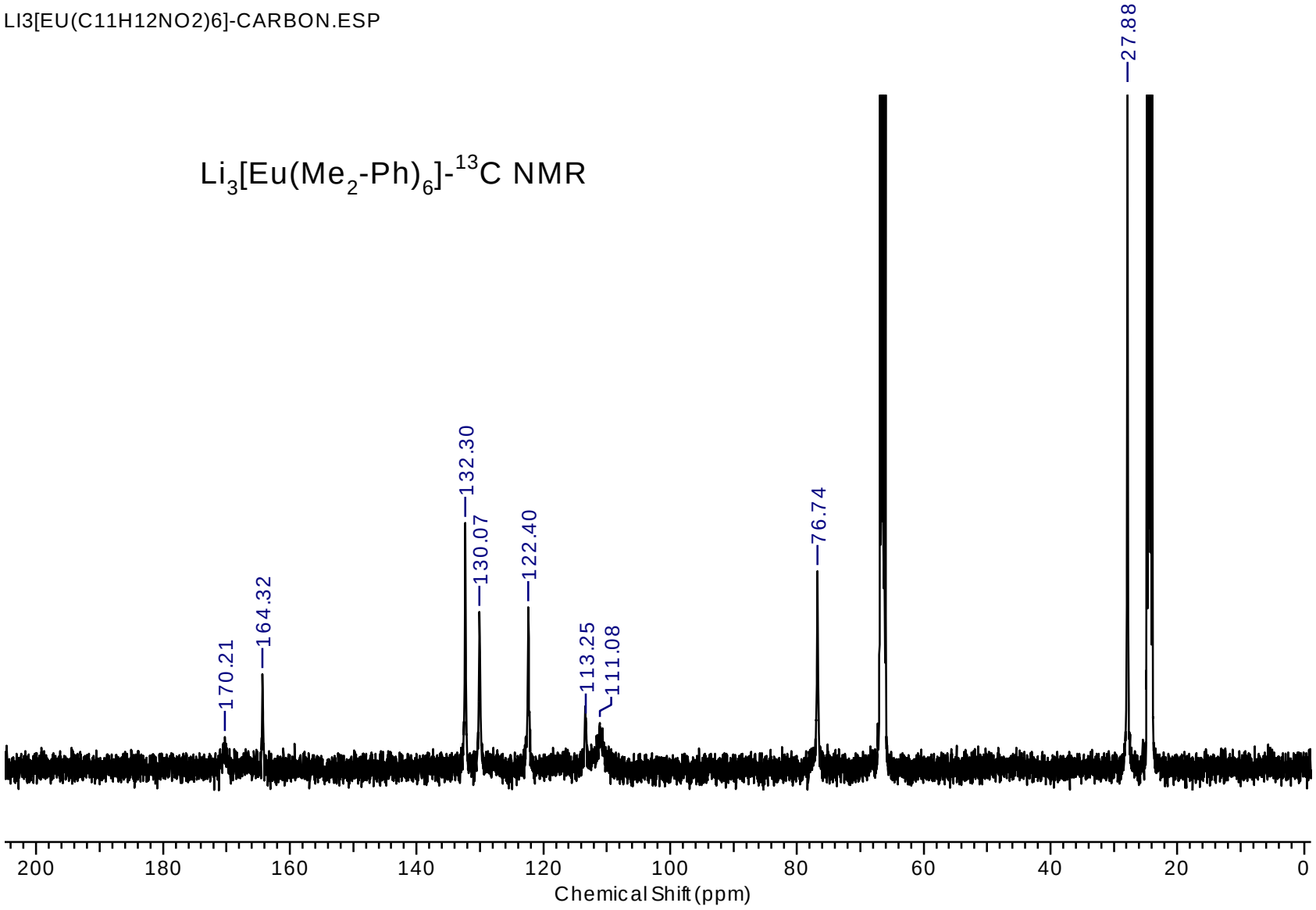

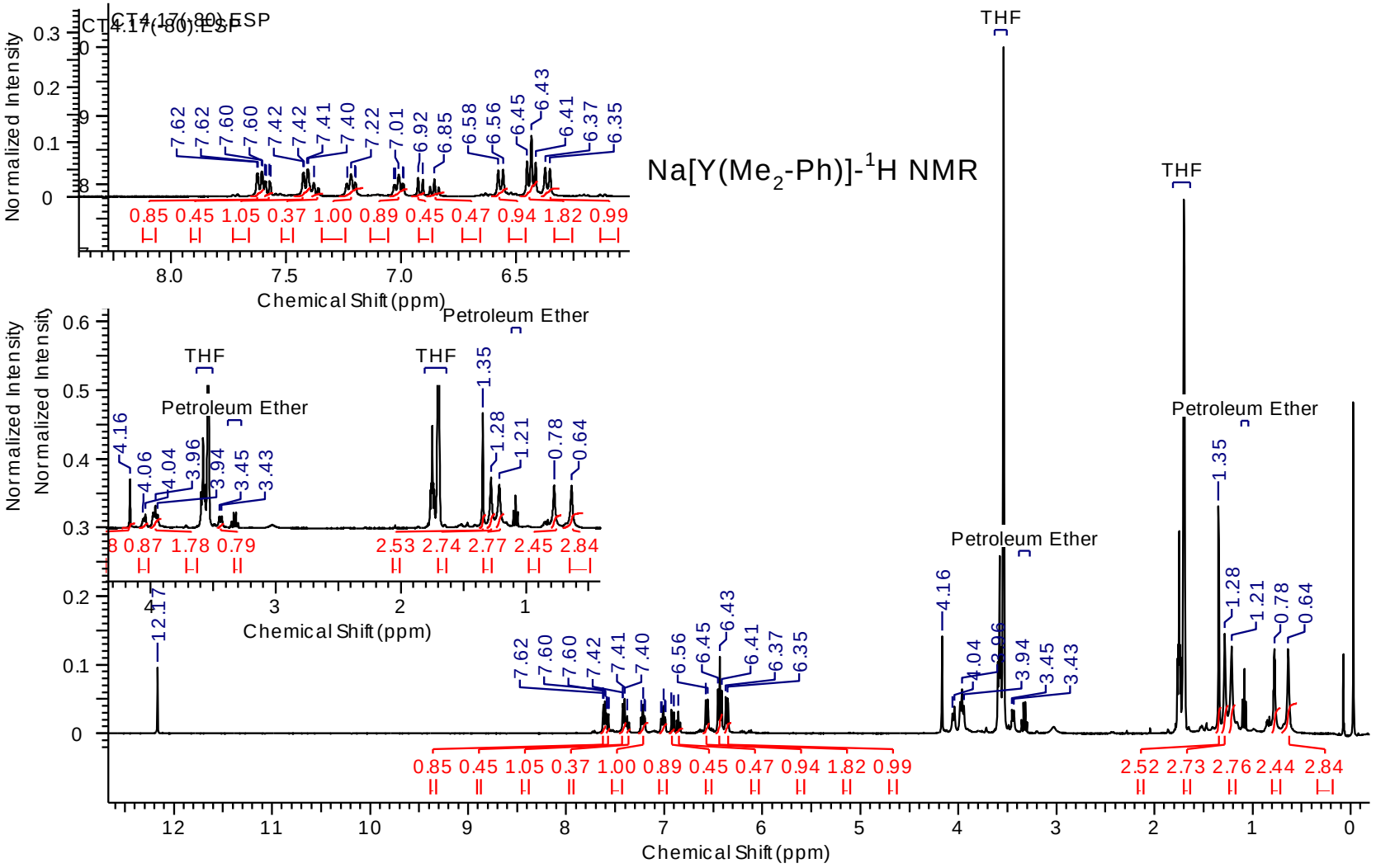
Na[Y(Me2-Ph)]-1H NMR
CT4.17(-80).ESP
Normalized Intensity
Chemical Shift (ppm)
THF
Petroleum Ether
7.62 7.62 7.60 7.60 7.42 7.42 7.41 7.40 7.22 7.01 6.92 6.85 6.58 6.56 6.45 6.43 6.41 6.37 6.35
0.85 0.45 1.05 0.37 1.00 0.89 0.45 0.47 0.94 1.82 0.99
4.16 4.06 4.04 3.96 3.94 3.45 3.43
1.35 1.28 1.21 0.78 0.64
0.87 1.78 0.79
2.53 2.74 2.77 2.45 2.84
12.17
4.16 4.04 3.96 3.94 3.45 3.43
1.35 1.28 1.21 0.78 0.64
2.52 2.73 2.76 2.44 2.84

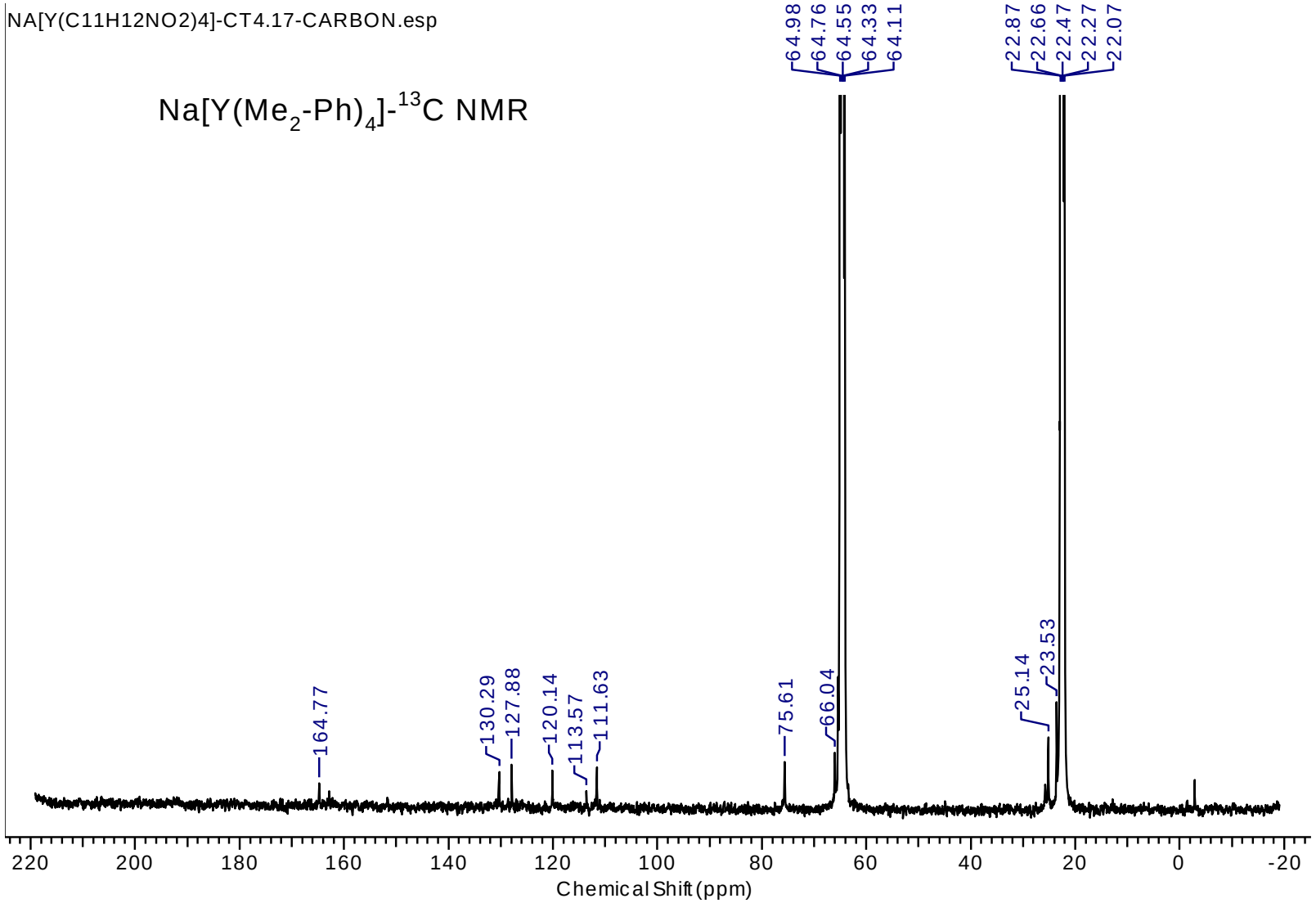
NA[Y(C11H12NO2)4]-CT4.17-CARBON.esp
Na[Y(Me2-Ph)4]-13C NMR
64.98
64.76
64.55
64.33
64.11
22.87
22.66
22.47
22.27
22.07
164.77
130.29
127.88
120.14
113.57
111.63
75.61
66.04
25.14
23.53
220
200
180
160
140
120
100
80
60
40
20
0
-20
Chemical Shift (ppm)

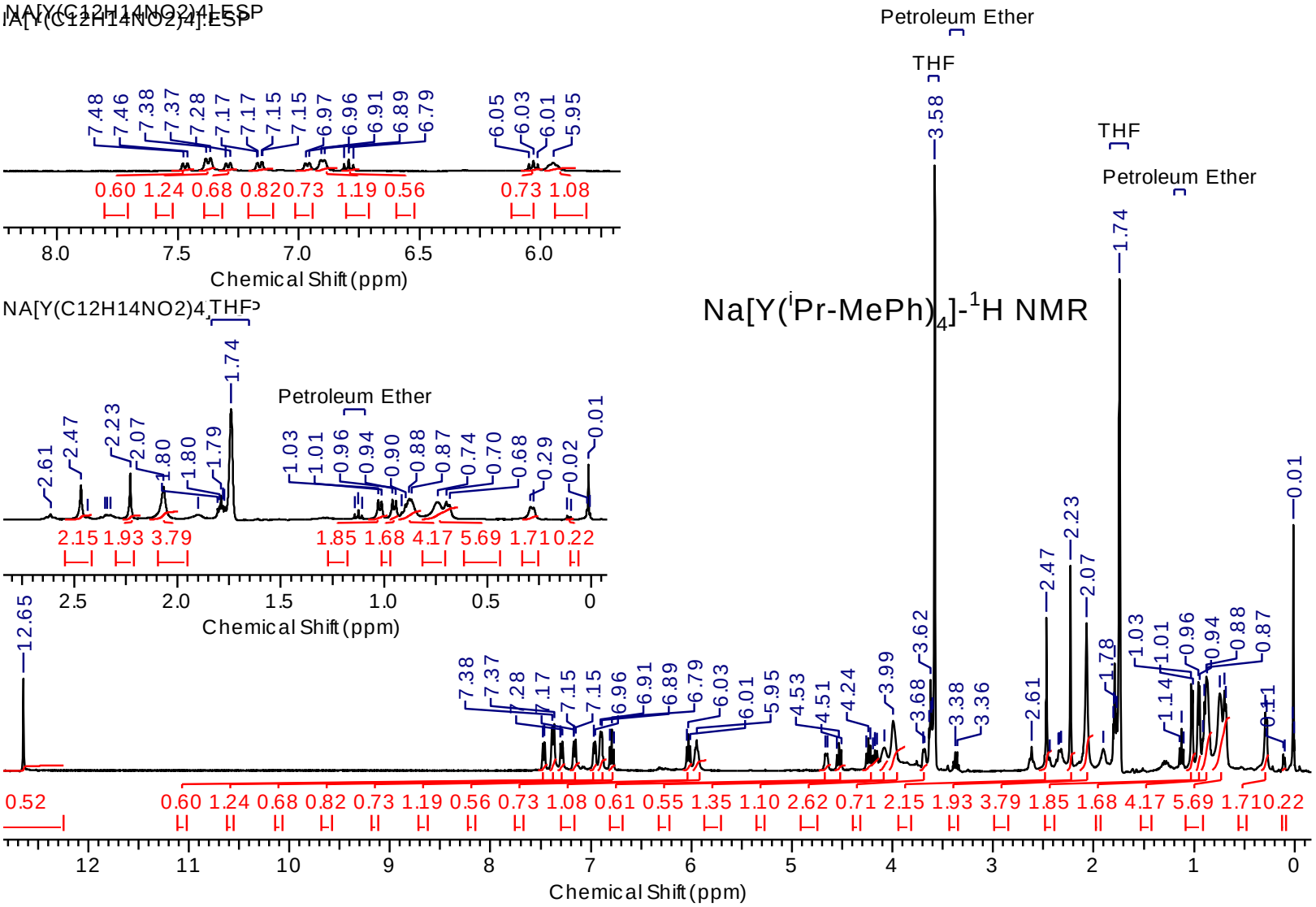
NA[Y(C12H14NO2)4].ESP
Petroleum Ether
THF
Na[Y(iPr-MePh)4]-1H NMR
Chemical Shift (ppm)

14. Crystal structure data tables.

14.1: $Li_3[Y(Me\text{-}Ph)_6]$

Crystal data and structure refinement for $Li_3[YMe\text{-}Ph)_6]$

Empirical formula	C66H72Li3N6O12Y
Formula weight	856.71
Temperature/K	101.26
Crystal system	monoclinic
Space group	C2/c
a/Å	41.288(6)
b/Å	12.5834(19)
c/Å	29.092(7)
α/°	90
β/°	105.267(6)
γ/°	90
Volume/Å3	14581(4)
Z	16
ρcalcg/cm3	1.561
μ/mm-1	1.665
F(000)	7136.0
Crystal size/mm3	0.9 × 0.9 × 0.19
Radiation	MoKα (λ = 0.71073)
2Θ range for data collection/°	4.432 to 52.874
Index ranges	-45 ≤ h ≤ 24, -15 ≤ k ≤ 6, -20 ≤ l ≤ 16
Reflections collected	7788
Independent reflections	5966 [Rint = 0.0365, Rsigma = 0.0822]
Data/restraints/parameters	5966/0/394

Goodness-of-fit on F2	1.099
Final R indexes [I>=2σ (I)]	R1 = 0.1239, wR2 = 0.3539
Final R indexes [all data]	R1 = 0.1602, wR2 = 0.3760
Largest diff. peak/hole / e Å-3	1.90/-0.70

Table 2 Fractional Atomic Coordinates (×104) and Equivalent Isotropic Displacement Parameters (Å2×103) for mo_CT3_139_green_cap_0m_a. Ueq is defined as 1/3 of of the trace of the orthogonalised UIJ tensor.

Atom	x	y	z	U(eq)
Y001	1254.1(3)	-98.1(7)	3787.1(8)	13.1(4)
O002	1555(2)	723(6)	4465(6)	19(2)
O003	1322(2)	1301(6)	3345(6)	22(2)
O004	1115(2)	-728(6)	3032(6)	22(2)
O005	1775(2)	-788(5)	3961(5)	15(2)
O006	1045(2)	-1534(6)	4071(5)	18(2)
O007	741(2)	414(6)	3834(5)	17(2)
O008	334(3)	-3992(6)	3662(6)	26(2)
O009	1657(3)	-1606(7)	2053(7)	35(3)
O00A	450(3)	1145(7)	5084(6)	29(2)
O00B	722(3)	3454(7)	2358(7)	38(3)
N00C	2070(3)	-214(8)	5202(7)	23(3)
N00D	1496(3)	-171(8)	2394(7)	24(3)
C00E	1494(3)	1301(8)	4811(8)	14(3)
O00F	1998(3)	152(8)	5934(8)	44(3)
C00G	1655(4)	1155(8)	5300(9)	18(3)
N00H	901(3)	1747(8)	2424(8)	30(3)
N00I	365(3)	-2246(8)	3832(7)	25(3)

N00J	2380(3)	426(8)	4209(8)	28(3)
O00K	2710(4)	44(9)	3733(9)	60(4)
C00L	2240(4)	-2662(10)	3143(9)	30(4)
C00M	2403(4)	-1758(9)	3359(9)	27(3)
C00N	1370(4)	2356(9)	3375(8)	21(3)
C00O	578(4)	1311(9)	3897(9)	19(3)
C00P	1247(3)	2118(8)	4697(8)	16(3)
C00Q	1163(4)	2709(9)	5050(9)	20(3)
C00R	589(4)	1768(11)	1992(10)	35(4)
C00S	1780(4)	-2327(8)	3472(8)	18(3)
C00T	279(4)	3286(9)	3959(9)	23(3)
C00U	957(4)	-4385(9)	4294(9)	25(3)
C00V	1936(4)	-1383(9)	3704(8)	20(3)
C00W	865(4)	-3352(8)	4131(8)	18(3)
C00X	1046(4)	-1633(9)	2789(9)	22(3)
C00Y	1517(4)	-3827(9)	4653(8)	22(3)
C00Z	834(4)	-2379(9)	2909(8)	22(3)
C010	2269(4)	-990(10)	5572(9)	29(4)
N011	559(3)	-241(7)	4654(7)	21(3)
C012	1934(4)	-2939(9)	3196(9)	23(3)
C013	1125(4)	-2820(9)	2153(9)	25(3)
C014	1315(4)	2523(10)	5529(9)	29(4)
C015	2254(4)	-1124(9)	3659(9)	26(3)
C016	1640(4)	3883(10)	3823(10)	31(4)
C017	2647(4)	1296(11)	4265(10)	32(4)
C018	1198(4)	-1858(9)	2410(9)	21(3)

C019	907(4)	-3551(9)	2268(9)	24(3)
C01A	9(4)	-2430(10)	3525(9)	26(3)
C01B	1598(4)	2799(9)	3774(9)	24(3)
C01C	945(4)	2690(10)	2604(9)	27(3)
C01D	289(4)	2495(9)	4322(9)	23(3)
C01E	517(4)	-3117(9)	3875(9)	24(3)
C01F	1105(3)	-2523(8)	4224(8)	14(3)
C01G	1457(4)	4573(10)	3501(9)	26(3)
C01H	1275(4)	-4626(10)	4552(9)	27(3)
C01I	991(4)	-810(11)	5367(11)	35(4)
C01J	1559(4)	1744(10)	5661(10)	31(4)
C01K	442(4)	1512(9)	4270(9)	19(3)
C01L	1184(4)	3057(9)	3030(9)	24(3)
C01M	1455(4)	-1162(9)	2297(9)	24(3)
C01N	1433(4)	-2805(9)	4489(9)	24(3)
C01O	437(4)	-1719(10)	5144(10)	30(4)
C01P	759(4)	-3329(9)	2652(9)	23(3)
C01Q	2439(5)	-172(11)	3914(11)	32(4)
C01R	415(4)	3090(9)	3587(9)	20(3)
C01S	5(4)	-3590(10)	3419(10)	34(4)
C01T	1914(4)	323(10)	5443(10)	29(4)
C01U	2637(5)	-983(14)	5479(12)	58(6)
C01V	563(4)	2123(9)	3536(8)	21(3)
C01W	1625(5)	908(12)	1777(10)	45(5)
C01X	1771(4)	224(10)	2220(10)	32(4)
C01Y	1231(4)	4175(10)	3100(10)	33(4)

C01Z	2118(5)	-2046(11)	5471(10)	38(4)
C020	2821(6)	1323(14)	4813(12)	58(6)
C021	613(4)	-672(10)	5146(9)	28(3)
C022	1914(5)	-834(11)	2081(10)	39(4)
C023	518(6)	2924(14)	1947(12)	59(6)
C024	484(4)	742(9)	4674(9)	22(3)
C025	330(6)	1149(14)	2153(12)	58(6)
C026	2304(6)	-506(15)	6034(12)	57(6)
O027	2230(5)	-4996(13)	2686(11)	94(6)
C028	-79(7)	-1670(15)	3147(13)	69(7)
C029	483(5)	235(10)	5409(10)	35(4)
C02A	2019(5)	837(12)	2597(10)	42(4)
C02B	2486(5)	2288(13)	4107(11)	49(5)
C02C	646(7)	1156(18)	1580(15)	83(8)
C02D	-208(9)	-2300(20)	3940(18)	123(12)
C02E	1706(7)	-5221(17)	2160(15)	84(8)
Li2F	1996(6)	64(14)	4488(15)	20(5)
C02G	1828(8)	-6259(19)	2343(15)	93(9)
C02H	2889(7)	910(20)	4045(15)	91(9)
C02I	2099(7)	-6005(17)	2727(14)	81(8)
C02J	2023(8)	-4590(20)	2273(17)	105(10)
Li2M	615(6)	-904(15)	4093(15)	22(5)
Li2	1208(7)	574(17)	2746(16)	30(6)
O1	991(14)	5090(30)	3510(30)	-1(18)

Table 3 Bond Lengths for mo_CT3_139_green_cap_0m_a.

Atom	Atom	Length/Å	Atom	Atom	Length/Å
Y001	O002	2.283(12)	C00O	C01V	1.46(3)
Y001	O003	2.240(13)	C00P	C00Q	1.38(3)
Y001	O004	2.264(15)	C00Q	C014	1.39(3)
Y001	O005	2.249(9)	C00R	C023	1.48(2)
Y001	O006	2.252(11)	C00R	C025	1.49(4)
Y001	O007	2.252(11)	C00R	C02C	1.49(5)
Y001	Li2F	3.21(2)	C00S	C00V	1.434(17)
Y001	Li2M	3.16(4)	C00S	C012	1.38(3)
Y001	Li2	3.10(5)	C00T	C01D	1.44(3)
O002	C00E	1.32(3)	C00T	C01R	1.37(3)
O002	Li2F	1.98(3)	C00U	C00W	1.401(17)
O003	C00N	1.342(14)	C00U	C01H	1.36(2)
O003	Li2	1.91(4)	C00V	C015	1.39(3)
O004	C00X	1.331(19)	C00W	C01E	1.46(2)
O004	Li2	1.92(3)	C00W	C01F	1.415(16)
O005	C00V	1.35(3)	C00X	C00Z	1.39(3)
O005	Li2F	1.90(3)	C00X	C018	1.43(3)
O006	C01F	1.323(14)	C00Y	C01H	1.394(19)
O006	Li2M	1.96(3)	C00Y	C01N	1.384(17)
O007	C00O	1.352(18)	C00Z	C01P	1.40(2)
O007	Li2M	1.95(3)	C010	C01U	1.61(3)
O008	C01E	1.387(16)	C010	C01Z	1.464(18)
O008	C01S	1.445(18)	C010	C026	1.45(4)
O009	C01M	1.35(3)	N011	C021	1.49(3)

O009	C022	1.42(2)	N011	C024	1.280(16)
O00A	C024	1.34(3)	N011	Li2M	1.90(5)
O00A	C029	1.47(3)	C013	C018	1.41(2)
O00B	C01C	1.393(17)	C013	C019	1.39(3)
O00B	C023	1.43(3)	C014	C01J	1.385(19)
N00C	C010	1.52(2)	C015	C01Q	1.51(2)
N00C	C01T	1.26(3)	C016	C01B	1.376(17)
N00C	Li2F	2.05(5)	C016	C01G	1.35(2)
N00D	C01M	1.279(16)	C017	C020	1.57(4)
N00D	C01X	1.45(3)	C017	C02B	1.43(2)
N00D	Li2	2.00(5)	C017	C02H	1.41(5)
C00E	C00G	1.41(3)	C018	C01M	1.48(3)
C00E	C00P	1.425(16)	C019	C01P	1.44(3)
O00F	C01T	1.40(3)	C01A	C01S	1.492(18)
O00F	C026	1.47(2)	C01A	C028	1.43(3)
C00G	C01J	1.42(4)	C01A	C02D	1.69(5)
C00G	C01T	1.475(18)	C01C	C01L	1.44(3)
N00H	C00R	1.54(2)	C01D	C01K	1.42(2)
N00H	C01C	1.291(19)	C01F	C01N	1.416(19)
N00H	Li2	2.01(3)	C01G	C01Y	1.38(3)
N00I	C01A	1.522(19)	C01I	C021	1.53(2)
N00I	C01E	1.254(16)	C01K	C024	1.50(3)
N00I	Li2M	2.02(2)	C01L	C01Y	1.428(17)
N00J	C017	1.53(2)	C01O	C021	1.504(19)
N00J	C01Q	1.21(3)	C01R	C01V	1.39(2)
N00J	Li2F	2.02(4)	C01W	C01X	1.53(3)

O00K	C01Q	1.38(3)	C01X	C022	1.55(3)
O00K	C02H	1.49(3)	C01X	C02A	1.50(3)
C00L	C00M	1.39(2)	C021	C029	1.55(3)
C00L	C012	1.36(3)	O027	C02I	1.40(3)
C00M	C015	1.43(4)	O027	C02J	1.38(4)
C00N	C01B	1.41(2)	C02E	C02G	1.45(3)
C00N	C01L	1.40(2)	C02E	C02J	1.49(4)
C00O	C01K	1.37(3)	C02G	C02I	1.39(4)

Table 4 Bond Angles for mo_CT3_139_green_cap_0m_a.

Atom	Atom	Atom	Angle/˚	Atom	Atom	Atom	Angle/˚
O002	Y001	Li2F	37.8(7)	C021	N011	Li2M	130.1(12)
O002	Y001	Li2M	102.0(7)	C024	N011	C021	106.6(19)
O002	Y001	Li2	126.8(6)	C024	N011	Li2M	123.2(19)
O003	Y001	O002	91.0(4)	C00L	C012	C00S	120.5(14)
O003	Y001	O004	75.9(4)	C019	C013	C018	120(2)
O003	Y001	O005	100.2(4)	C01J	C014	C00Q	120(2)
O003	Y001	O006	163.5(4)	C00M	C015	C01Q	119.9(19)
O003	Y001	O007	94.1(4)	C00V	C015	C00M	119.5(14)
O003	Y001	Li2F	94.2(6)	C00V	C015	C01Q	121(2)
O003	Y001	Li2M	130.7(5)	C01G	C016	C01B	122.3(18)
O003	Y001	Li2	37.8(5)	N00J	C017	C020	104(2)
O004	Y001	O002	159.8(5)	C02B	C017	N00J	109.3(14)
O004	Y001	Li2F	126.6(8)	C02B	C017	C020	110.9(19)
O004	Y001	Li2M	98.2(7)	C02H	C017	N00J	106.4(17)

O004	Y001	Li2	38.1(5)	C02H	C017	C020	106.2(19)
O005	Y001	O002	73.1(4)	C02H	C017	C02B	119(3)
O005	Y001	O004	93.9(4)	C00X	C018	C01M	122.7(15)
O005	Y001	O006	92.5(4)	C013	C018	C00X	120.0(17)
O005	Y001	O007	162.8(6)	C013	C018	C01M	117(2)
O005	Y001	Li2F	35.5(6)	C013	C019	C01P	119.7(16)
O005	Y001	Li2M	129.1(5)	N00I	C01A	C02D	100(2)
O005	Y001	Li2	97.7(7)	C01S	C01A	N00I	103.1(11)
O006	Y001	O002	102.7(5)	C01S	C01A	C02D	105.1(18)
O006	Y001	O004	92.9(5)	C028	C01A	N00I	111.2(16)
O006	Y001	O007	75.5(4)	C028	C01A	C01S	121(2)
O006	Y001	Li2F	102.2(6)	C028	C01A	C02D	114(2)
O006	Y001	Li2M	37.9(4)	C016	C01B	C00N	121.0(15)
O006	Y001	Li2	130.3(6)	O00B	C01C	C01L	115.6(12)
O007	Y001	O002	97.2(5)	N00H	C01C	O00B	115.0(16)
O007	Y001	O004	99.0(4)	N00H	C01C	C01L	129.5(13)
O007	Y001	Li2F	134.3(8)	C01K	C01D	C00T	117(2)
O007	Y001	Li2M	37.6(4)	O008	C01E	C00W	114.5(10)
O007	Y001	Li2	99.4(7)	N00I	C01E	O008	116.7(13)
Li2M	Y001	Li2F	124.6(10)	N00I	C01E	C00W	128.8(13)
Li2	Y001	Li2F	114.0(9)	O006	C01F	C00W	124.7(11)
Li2	Y001	Li2M	121.4(8)	O006	C01F	C01N	119.1(11)
C00E	O002	Y001	137.5(9)	C00W	C01F	C01N	116.1(11)
C00E	O002	Li2F	124.3(14)	C016	C01G	C01Y	118.8(13)
Li2F	O002	Y001	97.3(11)	C00U	C01H	C00Y	119.3(13)
C00N	O003	Y001	141.2(15)	C014	C01J	C00G	119(2)

C00N	O003	Li2	121.9(16)	C00O	C01K	C01D	122.3(19)
Li2	O003	Y001	96.2(10)	C00O	C01K	C024	121.0(13)
C00X	O004	Y001	141.2(13)	C01D	C01K	C024	116(2)
C00X	O004	Li2	123(2)	C00N	C01L	C01C	122.3(12)
Li2	O004	Y001	95.3(13)	C00N	C01L	C01Y	119.3(16)
C00V	O005	Y001	132.1(10)	C01Y	C01L	C01C	118.4(15)
C00V	O005	Li2F	123.9(13)	O009	C01M	C018	116.8(12)
Li2F	O005	Y001	101.1(9)	N00D	C01M	O009	117.1(19)
C01F	O006	Y001	145.3(10)	N00D	C01M	C018	126(2)
C01F	O006	Li2M	117.5(14)	C00Y	C01N	C01F	122.6(12)
Li2M	O006	Y001	97.2(9)	C00Z	C01P	C019	120.1(17)
C00O	O007	Y001	139.3(9)	N00J	C01Q	O00K	118.7(16)
C00O	O007	Li2M	117.7(17)	N00J	C01Q	C015	132(2)
Li2M	O007	Y001	97.5(9)	O00K	C01Q	C015	109(2)
C01E	O008	C01S	105.8(10)	C00T	C01R	C01V	122(2)
C01M	O009	C022	103.9(14)	O008	C01S	C01A	106.5(12)
C024	O00A	C029	105.3(13)	N00C	C01T	O00F	117.3(15)
C01C	O00B	C023	105.8(13)	N00C	C01T	C00G	131(2)
C010	N00C	Li2F	137.2(17)	O00F	C01T	C00G	111(2)
C01T	N00C	C010	102(2)	C01R	C01V	C00O	118(2)
C01T	N00C	Li2F	120.6(15)	N00D	C01X	C01W	108.5(15)
C01M	N00D	C01X	109.1(18)	N00D	C01X	C022	100.5(13)
C01M	N00D	Li2	120.6(18)	N00D	C01X	C02A	112(2)
C01X	N00D	Li2	130.2(12)	C01W	C01X	C022	111(2)
O002	C00E	C00G	124.1(12)	C02A	C01X	C01W	111.5(14)
O002	C00E	C00P	119.2(19)	C02A	C01X	C022	113.4(14)

C00G	C00E	C00P	116.6(18)	C01G	C01Y	C01L	121.0(16)
C01T	O00F	C026	105(2)	N011	C021	C01I	109(2)
C00E	C00G	C01J	121.6(13)	N011	C021	C01O	111.4(16)
C00E	C00G	C01T	119.4(19)	N011	C021	C029	102.9(13)
C01J	C00G	C01T	119(2)	C01I	C021	C029	109.0(16)
C00R	N00H	Li2	132.9(12)	C01O	C021	C01I	109.9(12)
C01C	N00H	C00R	108.3(12)	C01O	C021	C029	115(2)
C01C	N00H	Li2	118.7(15)	O009	C022	C01X	105.9(18)
C01A	N00I	Li2M	131.8(10)	O00B	C023	C00R	108.9(18)
C01E	N00I	C01A	107.9(11)	O00A	C024	C01K	115.9(13)
C01E	N00I	Li2M	120.0(12)	N011	C024	O00A	119(2)
C017	N00J	Li2F	137.6(18)	N011	C024	C01K	125(2)
C01Q	N00J	C017	104(2)	C010	C026	O00F	100.4(18)
C01Q	N00J	Li2F	118.1(15)	C02J	O027	C02I	104(2)
C01Q	O00K	C02H	104(2)	O00A	C029	C021	104(2)
C012	C00L	C00M	121(2)	C02G	C02E	C02J	101(2)
C00L	C00M	C015	120(2)	O002	Li2F	Y001	44.9(6)
O003	C00N	C01B	120.1(14)	O002	Li2F	N00C	89.8(18)
O003	C00N	C01L	122.1(14)	O002	Li2F	N00J	134.7(15)
C01B	C00N	C01L	117.6(11)	O005	Li2F	Y001	43.5(6)
O007	C00O	C01K	125.8(18)	O005	Li2F	O002	88.1(11)
O007	C00O	C01V	115(2)	O005	Li2F	N00C	129.4(14)
C01K	C00O	C01V	119.6(14)	O005	Li2F	N00J	94(2)
C00Q	C00P	C00E	121(2)	N00C	Li2F	Y001	119.7(14)
C00P	C00Q	C014	121.3(14)	N00J	Li2F	Y001	118.6(17)
C023	C00R	N00H	101.1(14)	N00J	Li2F	N00C	121.7(13)

C023	C00R	C025	113(2)
C023	C00R	C02C	120(3)
C025	C00R	N00H	104(2)
C02C	C00R	N00H	111.7(18)
C02C	C00R	C025	105.0(19)
C012	C00S	C00V	121.0(17)
C01R	C00T	C01D	121.1(14)
C01H	C00U	C00W	121.9(13)
O005	C00V	C00S	119.5(16)
O005	C00V	C015	122.5(13)
C015	C00V	C00S	117.9(19)
C00U	C00W	C01E	120.1(12)
C00U	C00W	C01F	120.3(12)
C01F	C00W	C01E	119.5(10)
O004	C00X	C00Z	120(2)
O004	C00X	C018	120.1(16)
C00Z	C00X	C018	119.6(15)
C01N	C00Y	C01H	119.7(13)
C00X	C00Z	C01P	120(2)
N00C	C010	C01U	103.7(19)
C01Z	C010	N00C	108.6(14)
C01Z	C010	C01U	109.8(17)
C026	C010	N00C	106.9(15)
C026	C010	C01U	106.5(17)
C026	C010	C01Z	120(2)
C02I	C02G	C02E	102(2)
C017	C02H	O00K	103(2)
C02G	C02I	O027	113(3)
O027	C02J	C02E	108(3)
O006	Li2M	Y001	44.9(8)
O006	Li2M	N00I	91.6(12)
O007	Li2M	Y001	44.9(8)
O007	Li2M	O006	89.7(16)
O007	Li2M	N00I	137(2)
N00I	Li2M	Y001	123.0(18)
N011	Li2M	Y001	113.5(10)
N011	Li2M	O006	121.3(16)
N011	Li2M	O007	93.7(11)
N011	Li2M	N00I	122(2)
O003	Li2	Y001	45.9(10)
O003	Li2	O004	93(2)
O003	Li2	N00D	131.0(14)
O003	Li2	N00H	92.7(14)
O004	Li2	Y001	46.6(11)
O004	Li2	N00D	92.0(12)
O004	Li2	N00H	130.9(18)
N00D	Li2	Y001	118.8(12)
N00D	Li2	N00H	120(3)
N00H	Li2	Y001	122(2)

Table 5 Torsion Angles for mo_CT3_139_green_cap_0m_a.

A	B	C	D	Angle/˚	A	B	C	D	Angle/˚
Y001	O002	C00E	C00G	135.9(13)	C01E	N00I	C01A	C01S	1(3)
Y001	O002	C00E	C00P	-43(2)	C01E	N00I	C01A	C028	-130(3)
Y001	O003	C00N	C01B	43(3)	C01E	N00I	C01A	C02D	109(2)
Y001	O003	C00N	C01L	-133(2)	C01E	C00W	C01F	O006	-4(4)
Y001	O004	C00X	C00Z	45(2)	C01E	C00W	C01F	C01N	178(2)
Y001	O004	C00X	C018	-133.5(18)	C01F	C00W	C01E	O008	159(2)
Y001	O005	C00V	C00S	-51(2)	C01F	C00W	C01E	N00I	-22(4)
Y001	O005	C00V	C015	129.5(15)	C01G	C016	C01B	C00N	2(4)
Y001	O005	Li2F	O002	5.6(13)	C01H	C00U	C00W	C01E	-177(3)
Y001	O005	Li2F	N00C	93.8(17)	C01H	C00U	C00W	C01F	1(4)
Y001	O005	Li2F	N00J	-129.0(8)	C01H	C00Y	C01N	C01F	1(4)
Y001	O006	C01F	C00W	-142.3(19)	C01I	C021	C029	O00A	102.0(18)
Y001	O006	C01F	C01N	36(3)	C01J	C00G	C01T	N00C	-170.4(18)
Y001	O007	C00O	C01K	-117.5(19)	C01J	C00G	C01T	O00F	8(2)
Y001	O007	C00O	C01V	60(2)	C01K	C00O	C01V	C01R	1(2)
O002	C00E	C00G	C01J	-174.8(16)	C01L	C00N	C01B	C016	0(3)
O002	C00E	C00G	C01T	1(2)	C01M	O009	C022	C01X	-18(2)
O002	C00E	C00P	C00Q	176.9(15)	C01M	N00D	C01X	C01W	106.8(18)
O003	C00N	C01B	C016	-177(2)	C01M	N00D	C01X	C022	-9(2)
O003	C00N	C01L	C01C	-4(4)	C01M	N00D	C01X	C02A	-129.9(16)
O003	C00N	C01L	C01Y	176(2)	C01N	C00Y	C01H	C00U	-1(4)
O004	C00X	C00Z	C01P	179.6(13)	C01O	C021	C029	O00A	-134.4(16)
O004	C00X	C018	C013	179.9(13)	C01Q	N00J	C017	C020	-126(2)

O004	C00X	C018	C01M	5(2)	C01Q	N00J	C017	C02B	116(2)
O005	C00V	C015	C00M	-176.6(18)	C01Q	N00J	C017	C02H	-14(3)
O005	C00V	C015	C01Q	2(3)	C01Q	O00K	C02H	C017	-17(3)
O006	C01F	C01N	C00Y	-179(2)	C01R	C00T	C01D	C01K	-1(2)
O007	C00O	C01K	C01D	176.9(12)	C01S	O008	C01E	N00I	3(3)
O007	C00O	C01K	C024	4(2)	C01S	O008	C01E	C00W	-178(2)
O007	C00O	C01V	C01R	-176.8(11)	C01T	N00C	C010	C01U	-135.7(16)
O00B	C01C	C01L	C00N	164(2)	C01T	N00C	C010	C01Z	107(2)
O00B	C01C	C01L	C01Y	-15(3)	C01T	N00C	C010	C026	-23(2)
N00C	C010	C026	O00F	29(2)	C01T	O00F	C026	C010	-24(2)
N00D	C01X	C022	O009	17(2)	C01T	C00G	C01J	C014	-179.6(14)
C00E	C00G	C01J	C014	-4(3)	C01U	C010	C026	O00F	138.9(15)
C00E	C00G	C01T	N00C	14(3)	C01V	C00O	C01K	C01D	-1(2)
C00E	C00G	C01T	O00F	-168.4(14)	C01V	C00O	C01K	C024	-173.6(12)
C00E	C00P	C00Q	C014	0(3)	C01W	C01X	C022	O009	-98(2)
C00G	C00E	C00P	C00Q	-2(2)	C01X	N00D	C01M	O009	-2(2)
N00H	C00R	C023	O00B	-10(3)	C01X	N00D	C01M	C018	-179.3(19)
N00H	C01C	C01L	C00N	-13(4)	C01Z	C010	C026	O00F	-95.6(19)
N00H	C01C	C01L	C01Y	167(2)	C020	C017	C02H	O00K	129.5(19)
N00I	C01A	C01S	O008	1(3)	C021	N011	C024	O00A	-3.9(19)
N00J	C017	C02H	O00K	19(3)	C021	N011	C024	C01K	173.7(14)
C00L	C00M	C015	C00V	-4(3)	C022	O009	C01M	N00D	14(2)
C00L	C00M	C015	C01Q	177.0(17)	C022	O009	C01M	C018	-168.8(16)
C00M	C00L	C012	C00S	-1(3)	C023	O00B	C01C	N00H	-4(3)
C00M	C015	C01Q	N00J	-173(2)	C023	O00B	C01C	C01L	178(2)
C00M	C015	C01Q	O00K	11(3)	C024	O00A	C029	C021	11.4(16)

C00N	C01L	C01Y	C01G	0(4)	C024	N011	C021	C01I	-104.7(16)
C00O	C01K	C024	O00A	157.7(14)	C024	N011	C021	C01O	134.0(15)
C00O	C01K	C024	N011	-20(2)	C024	N011	C021	C029	10.7(17)
C00P	C00E	C00G	C01J	4(2)	C025	C00R	C023	O00B	101(3)
C00P	C00E	C00G	C01T	-180.0(15)	C026	O00F	C01T	N00C	10(2)
C00P	C00Q	C014	C01J	1(3)	C026	O00F	C01T	C00G	-167.8(13)
C00Q	C014	C01J	C00G	1(3)	C028	C01A	C01S	O008	126(2)
C00R	N00H	C01C	O00B	-3(3)	C029	O00A	C024	N011	-5.3(19)
C00R	N00H	C01C	C01L	175(3)	C029	O00A	C024	C01K	176.9(12)
C00S	C00V	C015	C00M	4(3)	C02A	C01X	C022	O009	136(2)
C00S	C00V	C015	C01Q	-177.0(17)	C02B	C017	C02H	O00K	-105(2)
C00T	C01D	C01K	C00O	0(2)	C02C	C00R	C023	O00B	-134(3)
C00T	C01D	C01K	C024	173.7(12)	C02D	C01A	C01S	O008	-104(2)
C00T	C01R	C01V	C00O	-1(2)	C02E	C02G	C02I	O027	-23(4)
C00U	C00W	C01E	O008	-23(3)	Li2F	O002	C00E	C00G	-30(2)
C00U	C00W	C01E	N00I	156(3)	Li2F	O002	C00E	C00P	150.6(15)
C00U	C00W	C01F	O006	178(2)	Li2F	O005	C00V	C00S	151.6(17)
C00U	C00W	C01F	C01N	-1(3)	Li2F	O005	C00V	C015	-27(3)
C00V	O005	Li2F	Y001	162.7(18)	Li2F	N00C	C010	C01U	47(2)
C00V	O005	Li2F	O002	168.4(15)	Li2F	N00C	C010	C01Z	-70(3)
C00V	O005	Li2F	N00C	-103(2)	Li2F	N00C	C010	C026	159.5(18)
C00V	O005	Li2F	N00J	33.7(18)	Li2F	N00C	C01T	O00F	-174.6(12)
C00V	C00S	C012	C00L	1(3)	Li2F	N00C	C01T	C00G	3(2)
C00V	C015	C01Q	N00J	8(4)	Li2F	N00J	C017	C020	53(2)
C00V	C015	C01Q	O00K	-167.2(18)	Li2F	N00J	C017	C02B	-65(3)
C00W	C00U	C01H	C00Y	0(4)	Li2F	N00J	C017	C02H	165(2)

C00W	C01F	C01N	C00Y	0(4)	Li2F	N00J	C01Q	O00K	-177.5(16)
C00X	C00Z	C01P	C019	1(2)	Li2F	N00J	C01Q	C015	8(3)
C00X	C018	C01M	O009	158.6(17)	C02G	C02E	C02J	O027	-32(4)
C00X	C018	C01M	N00D	-24(3)	C02H	O00K	C01Q	N00J	10(3)
C00Z	C00X	C018	C013	2(2)	C02H	O00K	C01Q	C015	-174.1(17)
C00Z	C00X	C018	C01M	-173.0(13)	C02I	O027	C02J	C02E	19(4)
C010	N00C	C01T	O00F	7.7(18)	C02J	O027	C02I	C02G	3(4)
C010	N00C	C01T	C00G	-174.5(15)	C02J	C02E	C02G	C02I	32(4)
N011	C021	C029	O00A	-13.3(15)	Li2M	O006	C01F	C00W	41(3)
C012	C00L	C00M	C015	3(3)	Li2M	O006	C01F	C01N	-141(2)
C012	C00S	C00V	O005	178.3(17)	Li2M	O007	C00O	C01K	29(2)
C012	C00S	C00V	C015	-3(3)	Li2M	O007	C00O	C01V	-153.2(14)
C013	C018	C01M	O009	-16(2)	Li2M	N00I	C01A	C01S	174(3)
C013	C018	C01M	N00D	160.9(18)	Li2M	N00I	C01A	C028	43(4)
C013	C019	C01P	C00Z	0(2)	Li2M	N00I	C01A	C02D	-78(3)
C016	C01G	C01Y	C01L	2(4)	Li2M	N00I	C01E	O008	-176(2)
C017	N00J	C01Q	O00K	2(3)	Li2M	N00I	C01E	C00W	5(4)
C017	N00J	C01Q	C015	-173(2)	Li2M	N011	C021	C01I	71.0(18)
C018	C00X	C00Z	C01P	-2(2)	Li2M	N011	C021	C01O	-50(2)
C018	C013	C019	C01P	-1(2)	Li2M	N011	C021	C029	-173.6(15)
C019	C013	C018	C00X	0(2)	Li2M	N011	C024	O00A	-180.0(15)
C019	C013	C018	C01M	174.7(14)	Li2M	N011	C024	C01K	-2(2)
C01A	N00I	C01E	O008	-2(3)	Li2	O003	C00N	C01B	-149(2)
C01A	N00I	C01E	C00W	179(3)	Li2	O003	C00N	C01L	35(3)
C01B	C00N	C01L	C01C	180(2)	Li2	O004	C00X	C00Z	-149.1(16)
C01B	C00N	C01L	C01Y	-1(3)	Li2	O004	C00X	C018	33(2)

C01B	C016	C01G	C01Y	-3(4)	Li2	N00D	C01M	O009	179.3(18)
C01C	O00B	C023	C00R	9(3)	Li2	N00D	C01M	C018	2(3)
C01C	N00H	C00R	C023	8(3)	Li2	N00D	C01X	C01W	-75(3)
C01C	N00H	C00R	C025	-110(2)	Li2	N00D	C01X	C022	169.0(19)
C01C	N00H	C00R	C02C	137(2)	Li2	N00D	C01X	C02A	48(2)
C01C	C01L	C01Y	C01G	180(2)	Li2	N00H	C00R	C023	-175(3)
C01D	C00T	C01R	C01V	1(2)	Li2	N00H	C00R	C025	67(3)
C01D	C01K	C024	O00A	-15.6(19)	Li2	N00H	C00R	C02C	-46(4)
C01D	C01K	C024	N011	166.6(14)	Li2	N00H	C01C	O00B	180(2)
C01E	O008	C01S	C01A	-2(3)	Li2	N00H	C01C	C01L	-2(4)

Table 6 Hydrogen Atom Coordinates (Å×104) and Isotropic Displacement Parameters (Å2×103) for mo_CT3_139_green_cap_0m_a. Atomx y z U(eq)

H00L	2344	-3095	2955	36
H00M	2613	-1558	3309	32
H00P	1137	2260	4372	19
H00Q	999	3252	4964	24
H00S	1567	-2537	3509	22
H00T	176	3954	3979	28
H00U	793	-4933	4223	30
H00Y	1739	-3983	4835	27
H00Z	739	-2243	3167	26
H012	1825	-3557	3042	27
H013	1225	-2967	1901	30
H014	1252	2930	5766	34

H016	1802	4155	4092	37
H019	856	-4194	2094	29
H01B	1726	2344	4015	29
H01D	197	2628	4584	28
H01G	1483	5317	3550	31
H01H	1331	-5332	4661	33
H01A	1084	-1272	5163	53
H01C	1028	-1131	5683	53
H01E	1101	-114	5395	53
H01J	1661	1605	5988	38
H01N	1602	-2272	4556	28
H01F	194	-1617	5021	44
H01I	487	-1999	5469	44
H01K	516	-2223	4940	44
H01P	609	-3827	2732	28
H01R	408	3632	3358	24
H01L	-170	-3952	3537	40
H01M	-41	-3711	3072	40
H01O	2616	-1072	5138	87
H01Q	2770	-1568	5656	87
H01S	2748	-306	5588	87
H01V	652	1995	3271	26
H01T	1485	465	1524	67
H01U	1809	1217	1666	67
H01W	1489	1480	1858	67
H01Y	1106	4653	2868	39

H01X	1882	-2016	5475	57
H01Z	2239	-2548	5714	57
H	2134	-2282	5157	57
H02A	2666	1628	4981	86
H02B	3024	1760	4872	86
H02C	2881	599	4927	86
H02D	1967	-763	1770	47
H02E	2120	-1039	2325	47
H02F	569	3202	1655	71
H02G	278	3055	1922	71
H02H	411	422	2232	87
H02I	121	1131	1897	87
H02J	288	1489	2435	87
H02K	2510	-66	6132	68
H02L	2306	-1045	6283	68
H02M	-31	-952	3278	103
H02N	-319	-1731	2987	103
H02O	51	-1806	2917	103
H02P	263	48	5465	42
H02Q	644	391	5719	42
H02R	1903	1405	2720	63
H02S	2190	1149	2459	63
H02T	2127	358	2858	63
H02U	2336	2202	3786	74
H02V	2656	2825	4099	74
H02W	2355	2515	4326	74

H02X	778	1587	1414	125
H02Y	429	978	1359	125
HA	769	500	1696	125
H02Z	-140	-2865	4179	185
HB	-449	-2366	3786	185
HC	-161	-1608	4094	185
H0AA	1543	-4932	2324	101
HD	1600	-5244	1812	101
H1AA	1654	-6659	2449	111
HE	1900	-6682	2101	111
H02	3089	636	4284	109
HF	2961	1474	3855	109
H2AA	2278	-6542	2750	97
HG	2026	-6037	3025	97
H3AA	2133	-4653	2009	126
HH	1975	-3835	2315	126
H1	780(30)	5080(70)	3240(70)	0(30)

Table 7 Atomic Occupancy for mo_CT3_139_green_cap_0m_a. Atom Occupancy Atom Occupancy Atom Occupancy

O1	0.14(3)

Experimental

Single crystals of C66H72Li3N6O12Y [mo_CT3_139_green_cap_0m_a] were []. A suitable crystal was selected and [] on a 'Bruker APEX-II CCD' diffractometer. The crystal was kept at

101.26 K during data collection. Using Olex2 [1], the structure was solved with the XS [2] structure solution program using Direct Methods and refined with the XL [3] refinement package using Least Squares minimisation.

Dolomanov, O.V., Bourhis, L.J., Gildea, R.J, Howard, J.A.K. & Puschmann, H. (2009), J. Appl. Cryst. 42, 339-341.

Sheldrick, G.M. (2008). Acta Cryst. A64, 112-122.

Sheldrick, G.M. (2008). Acta Cryst. A64, 112-122.

Crystal structure determination of [mo_CT3_139_green_cap_0m_a]

Crystal Data for C66H72Li3N6O12Y (M =856.71 g/mol): monoclinic, space group C2/c (no. 15), a = 41.288(6) Å, b = 12.5834(19) Å, c = 29.092(7) Å, β = 105.267(6)°, V = 14581(4) Å3, Z = 16, T = 101.26 K, μ(MoKα) = 1.665 mm-1, Dcalc = 1.561 g/cm3, 7788 reflections measured (4.432° ≤ 2Θ ≤ 52.874°), 5966 unique (Rint = 0.0365, Rsigma = 0.0822) which were used in all calculations. The final R1 was 0.1239 (I > 2σ(I)) and wR2 was 0.3760 (all data).

Refinement model description

Number of restraints - 0, number of constraints - unknown.

14.2: $Li_3[Y(^iPr\text{-}Ph)_6]$

Crystal data and structure refinement for $Li_3[Y(^iPr\text{-}Ph)_6]$

Empirical formula	C72H84N6O12Li3Y
Formula weight	872.76
Temperature/K	108.54
Crystal system	orthorhombic
Space group	Pna21
a/Å	25.1288(15)

b/Å 14.7708(9)

c/Å 21.8302(13)

α/° 90

β/° 90

γ/° 90

Volume/Å3 8102.8(8)

Z 8

ρcalcg/cm3 1.431

μ/mm-1 1.510

F(000) 3632.0

Crystal size/mm3 0.21 × 0.124 × 0.09

Radiation MoKα (λ = 0.71073)

2Θ range for data collection/° 4.648 to 41.76

Index ranges -25 ≤ h ≤ 25, -14 ≤ k ≤ 14, -21 ≤ l ≤ 21

Reflections collected 25672

Independent reflections 8099 [Rint = 0.0335, Rsigma = 0.0562]

Data/restraints/parameters 8099/342/891

Goodness-of-fit on F2 1.034

Final R indexes [I>=2σ (I)] R1 = 0.0450, wR2 = 0.1173

Final R indexes [all data] R1 = 0.0518, wR2 = 0.1231

Largest diff. peak/hole / e Å-3 0.63/-0.41

Flack parameter 0.013(4)

Table 2 Fractional Atomic Coordinates (×104) and Equivalent Isotropic Displacement Parameters (Å2×103) for pna21_a. Ueq is defined as 1/3 of of the trace of the orthogonalised UIJ tensor. Atom x y z U(eq)

Y001	3442.3(4)	6207.1(7)	1527.2(5)	27.3(3)
Y002	2396.0(4)	7069.0(7)	396.4(5)	26.4(3)
Y003	3712.2(4)	6095.6(7)	-160.0(5)	27.6(3)
Li04	3320.0(17)	8663(3)	518(2)	37.9(11)
O05	3132(3)	7304(5)	-195(3)	29.6(16)
O06	1935(3)	5816(5)	367(4)	35.8(17)
O07	3029(3)	5956(5)	574(3)	26.3(16)
O08	4338(3)	7111(5)	-357(3)	35.9(19)
O09	3142(3)	4814(5)	1606(4)	39.3(18)
O0A	4058(3)	6224(5)	771(3)	32.0(18)
O00B	1545(3)	6352(5)	-1470(3)	36.7(19)
O00	4186(3)	8251(6)	811(4)	43(2)
O00D	3929(3)	7325(5)	1941(4)	36.7(19)
O1	2900(3)	7386(5)	1255(3)	30.8(16)
O00F	5052(3)	5349(7)	2488(4)	50(2)
O00G	2372(3)	8596(5)	315(4)	33.4(17)
O00H	3303(3)	4836(6)	-385(4)	46(2)
N00I	4243(4)	5474(7)	2048(4)	37(2)
N00J	2863(4)	6113(7)	2481(5)	40(2)
O00K	1045(3)	8575(7)	1519(5)	62(2)
N00L	1922(3)	6990(6)	-631(4)	27(2)
O00M	3664(3)	9641(5)	-259(5)	51(2)
N00N	3751(4)	6253(7)	-1315(5)	37(2)
N00O	1610(4)	7613(7)	1030(4)	36(2)
O00P	4744(4)	3424(5)	-229(4)	54(2)
O00Q	3996(3)	6744(6)	-2257(3)	46(2)

O00R	2226(4)	5583(8)	3123(5)	67(3)
N00S	4413(3)	4832(6)	-244(4)	31(2)
C00T	1730(4)	5203(8)	2(5)	32(3)
C00U	4313(5)	7475(9)	2345(5)	40(3)
O00V	3270(4)	9714(8)	1345(6)	89(4)
C00W	4320(5)	3986(8)	-224(6)	39(3)
C00X	1605(5)	4342(8)	243(6)	44(3)
C00Y	5125(4)	5201(9)	-962(5)	38(3)
C00Z	4621(4)	5883(9)	2341(5)	37(3)
C010	4467(5)	7401(9)	-1432(6)	38(3)
C011	4051(5)	6776(8)	-1624(5)	35(3)
C012	4662(5)	6797(9)	2559(5)	40(3)
C013	2721(5)	4371(9)	1775(6)	42(3)
C014	1634(4)	5365(8)	-626(5)	30(2)
C015	1661(5)	7264(8)	-1661(5)	42(3)
C016	4588(4)	7525(8)	-802(6)	34(3)
C017	1375(5)	8334(8)	-813(6)	41(3)
C018	5056(5)	7031(10)	2991(5)	48(3)
C019	2328(5)	8308(8)	-1175(5)	38(3)
C01A	1720(4)	6270(8)	-890(5)	28(3)
C01B	2866(6)	6734(11)	3038(6)	55(3)
C01C	1830(4)	7751(8)	-1070(5)	33(3)
C01D	2516(5)	5477(10)	2601(6)	45(3)
C01E	3315(6)	3975(10)	-308(7)	57(4)
C01F	3804(6)	3523(8)	-205(7)	52(3)
C01G	2580(6)	3542(9)	1492(9)	63(4)

C01H	1419(5)	4691(9)	-984(6)	44(3)
C01I	5009(4)	4949(8)	-308(6)	38(3)
C01J	5008(4)	8132(8)	-653(6)	39(3)
C01K	5235(5)	5638(9)	127(6)	42(3)
C01L	4757(6)	7898(9)	-1874(7)	52(3)
C01M	2092(5)	9294(8)	451(6)	41(3)
C01N	1217(5)	7025(10)	1344(6)	52(3)
C01O	5204(5)	3975(8)	-174(7)	52(3)
C01P	1287(6)	3856(9)	-758(7)	56(4)
C01Q	2858(5)	5637(10)	-1600(7)	55(4)
C01R	3693(5)	4737(9)	-1815(6)	44(3)
C01S	1466(4)	8452(10)	1121(5)	42(3)
C01T	2856(6)	7732(10)	2822(7)	64(4)
C01U	4386(6)	8355(10)	2561(7)	56(3)
C01V	2118(7)	3090(10)	1675(9)	81(6)
C01W	5131(6)	7870(11)	3196(6)	59(4)
C01X	3450(5)	5681(9)	-1771(5)	39(3)
C01Y	1379(5)	3683(8)	-145(8)	48(3)
C01Z	1494(6)	6240(11)	1681(7)	65(4)
C020	5285(5)	8580(9)	-1103(7)	50(3)
C021	4789(7)	8525(12)	2988(7)	69(4)
C022	5164(6)	8485(9)	-1712(7)	55(3)
C023	1656(4)	9274(8)	854(6)	41(3)
C024	4393(5)	4475(9)	1994(6)	43(3)
C025	811(5)	6692(10)	892(7)	61(4)
C026	4989(5)	4494(10)	2154(7)	57(3)

C027 1935(6) 4178(12) 2416(8) 70(4)

C028 2834(7) 3498(10) -348(9)83(6)

C029 2396(4) 4663(9) 2268(6) 45(3)

C02A 960(6) 7715(13) 1809(8) 75(4)

C02B 4295(6) 4104(9) 1356(6) 49(3)

C02C 3345(6) 6496(12) 3435(6) 66(4)

C02D 4084(5) 3968(9) 2480(6) 45(3)

C02E 3787(7) 2593(12) -108(10) 87(5)

C02F 4186(6) 10012(10) -121(8)67(4)

C02G 2218(7) 10135(11) 181(8) 76(5)

C02H 1800(8) 3411(13) 2128(9) 84(5)

C02I 3529(6) 6189(11) -2369(6) 56(4)

C02J 2335(7) 6469(14) 3349(8) 83(5)

C02K 1380(6) 10101(10) 993(7) 58(4)

C02L 2892(10) 9987(16) 1755(11) 118(8)

C02M 4376(6) 10427(10) -723(7)60(4)

C02N 1526(8) 10893(14) 756(10) 94(6)

C02O 3998(7) 10159(15) -1175(8) 96(7)

C02P 3612(6) 9536(12) -898(7)69(4)

C02Q 2826(9) 2611(16) -269(11) 111(7)

C02R 1922(8) 10913(15) 308(11) 104(6)

O02S 400(9) 2686(16) 904(12) 183(8)

C02T 3274(10) 2149(17) -98(12)123(8)

C02U 3712(10) 10264(17) 1472(13) 128(8)

C02V 3012(9) 10970(14) 1888(10) 95(6)

C7 323(17) 4110(30) 1600(20) 223(17)

C8	259(12)	4300(20)	956(14)	144(9)
C9	66(13)	3483(19)	620(16)	161(11)
C10	3531(15)	11110(20)	1753(18)	182(14)
C11	421(18)	3110(30)	1470(30)	233(19)

Table 3 Anisotropic Displacement Parameters (Å2×103) for pna21_a. The Anisotropic displacement factor exponent takes the form: -2π2[h2a*2U11+2hka*b*U12+…]. Atom

	U11	U22	U33	U23	U13	U12
Y001	23.3(6)	35.5(6)	23.2(6)	-1.9(6)	0.9(5)	-5.9(5)
Y002	19.8(5)	33.5(6)	25.7(5)	-5.3(6)	1.6(5)	-3.5(5)
Y003	20.9(6)	36.9(7)	24.8(6)	-6.1(6)	2.7(5)	-1.7(5)
Li04	31(2)	36(2)	47(3)	-6(2)	1(2)	-5.1(19)
O05	19(4)	38(4)	31(4)	-3(3)	9(3)	0(3)
O06	33(4)	43(4)	32(4)	6(4)	-6(4)	-12(3)
O07	19(4)	37(4)	24(4)	-4(3)	1(3)	0(3)
O08	21(4)	47(5)	40(4)	10(4)	-1(3)	-2(3)
O09	44(5)	36(4)	38(4)	1(4)	2(4)	-9(3)
O0A	29(4)	42(5)	25(4)	0(3)	3(3)	-4(3)
O00B	46(5)	36(5)	27(4)	-8(4)	-12(4)	-3(4)
O00	30(4)	42(5)	57(6)	2(4)	1(4)	-10(4)
O00D	35(4)	39(5)	36(5)	-4(4)	-3(3)	-11(3)
O1	24(4)	38(4)	30(4)	-4(3)	0(3)	-4(3)
O00F	32(5)	76(6)	42(5)	14(5)	-12(4)	-4(4)
O00G	29(4)	32(4)	39(5)	-5(4)	4(3)	0(3)
O00H	28(4)	55(5)	56(5)	-23(4)	13(4)	-13(4)
N00I	28(5)	51(5)	33(5)	3(4)	-2(4)	-2(4)

N00J	30(5)	52(6)	38(5)	2(4)	5(4)	-13(4)
O00K	39(5)	96(7)	53(5)	-10(5)	11(5)	23(5)
O00M	50(5)	39(5)	64(6)	15(4)	5(4)	-11(4)
N00N	21(5)	55(6)	35(4)	-8(4)	3(4)	6(4)
N00O	25(4)	57(6)	26(5)	-4(5)	0(4)	-2(4)
O00P	70(6)	29(4)	61(6)	0(5)	10(5)	4(4)
O00Q	47(5)	64(6)	28(4)	5(4)	4(4)	13(4)
O00R	42(5)	102(8)	57(6)	14(6)	22(5)	-15(5)
N00S	30(4)	38(5)	26(5)	-4(4)	6(4)	-3(3)
C00T	19(6)	34(6)	44(7)	-1(5)	-1(5)	-3(5)
C00U	40(7)	55(7)	24(6)	-5(6)	-5(5)	-21(5)
O00V	73(7)	82(7)	112(9)	-73(7)	45(6)	-26(6)
C00W	55(6)	27(6)	36(7)	-5(6)	4(6)	3(5)
C00X	41(7)	37(7)	53(8)	2(6)	-2(6)	-1(6)
C00Y	22(6)	52(8)	40(6)	2(6)	3(5)	12(6)
C00Z	20(6)	68(7)	24(6)	7(6)	-4(5)	-9(5)
C010	26(6)	44(7)	44(6)	11(6)	6(5)	17(5)
C011	29(6)	43(7)	32(6)	4(5)	3(5)	19(5)
C012	31(7)	67(7)	21(6)	4(6)	3(5)	-18(5)
C013	28(7)	44(7)	53(8)	17(6)	-18(5)	-9(5)
C014	22(6)	31(6)	37(6)	-12(5)	1(5)	-2(5)
C015	53(8)	43(7)	30(7)	-3(5)	-12(6)	10(6)
C016	15(6)	37(7)	51(6)	16(6)	0(5)	5(4)
C017	34(7)	36(7)	54(8)	-12(6)	-9(6)	5(5)
C018	43(8)	76(8)	26(7)	-8(7)	-5(5)	-16(7)
C019	41(7)	42(8)	29(7)	11(6)	4(5)	7(5)

C01A 26(6) 37(6) 20(6) -14(5) 1(5) 8(5)

C01B 57(8) 87(9) 22(6) -4(6) 10(5) -13(7)

C01C 30(6) 39(7) 31(6) -12(5) -1(5) 2(5)

C01D 33(7) 66(8) 35(7) 18(5) 4(5) -14(6)

C01E 51(7) 44(7) 75(11) -23(8) 34(7) -25(6)

C01F 74(7) 27(6) 55(8) -9(7) 16(8) -15(5)

C01G 55(9) 39(8) 94(11) 2(8) -28(8) -11(6)

C01H 51(8) 40(7) 39(7) -15(6) -3(6) 0(6)

C01I 30(6) 39(6) 44(7) 1(6) 3(5) 9(5)

C01J 27(7) 37(7) 54(7) 21(6) -3(5) 6(5)

C01K 29(6) 59(8) 37(6) 3(6) 5(5) -1(6)

C01L 50(8) 55(9) 51(7) 13(7) 17(6) 12(6)

C01M 40(6) 28(6) 56(8) -9(6) -7(6) -3(5)

C01N 26(7) 93(8) 37(7) 7(6) 18(5) 3(6)

C01O 50(7) 46(7) 59(8) 16(7) 16(7) 10(6)

C01P 68(10) 37(7) 63(8) -16(7) 2(7) -13(7)

C01Q 30(6) 76(10) 58(9) -18(8) -13(6) 6(6)

C01R 39(7) 65(7) 27(7) -17(6) 1(6) 2(6)

C01S 20(6) 76(8) 29(7) -10(6) -7(5) 7(6)

C01T 66(10) 76(8) 50(9) -30(7) 17(7) 1(7)

C01U 59(9) 54(7) 57(9) -6(7) -4(6) -22(7)

C01V 79(11) 32(8) 132(17) 20(10) -49(11)-26(7)

C01W 53(9) 90(10) 35(8) -14(7) 1(6) -29(7)

C01X 36(6) 57(7) 24(6) -17(6) 6(5) 4(5)

C01Y 41(7) 25(6) 77(8) 2(7) 5(7) -7(5)

C01Z 47(9) 83(10) 65(11) 24(8) 9(7) 1(7)

C020	28(7)	41(8)	81(9)	25(7)	8(6)	3(5)	
C021	86(12)	62(9)	58(10)	-26(8)	-8(8)	-26(8)	
C022	50(8)	46(8)	69(8)	22(8)	30(7)	0(6)	
C023	22(6)	39(6)	61(8)	-29(6)	-7(5)	8(5)	
C024	40(7)	48(7)	40(7)	6(6)	-2(6)	3(5)	
C025	34(8)	63(9)	86(10)	18(7)	4(7)	-10(6)	
C026	41(7)	76(9)	54(8)	8(7)	-2(6)	3(6)	
C028	67(8)	43(8)	138(17)		-45(10)	40(10)	-28(7)
C029	22(6)	45(7)	68(9)	16(6)	-3(5)	-11(5)	
C02A	56(10)	107(11)		63(10)	4(8)	33(7)	15(8)
C02B	54(8)	45(8)	48(7)	-5(6)	-6(6)	11(6)	
C02C	68(9)	97(12)	34(8)	-5(8)	6(6)	-17(8)	
C02D	48(7)	49(8)	39(6)	3(6)	-1(6)	-6(6)	
C02F	63(9)	61(9)	77(8)	30(9)	-7(8)	-21(7)	
C02I	55(8)	90(11)	22(7)	-5(6)	-10(6)	10(7)	
C02J	61(9)	132(13)		56(10)	-18(9)	27(7)	-20(10)
C02M	60(9)	47(9)	73(9)	14(8)	7(7)	-4(6)	
C02O	72(12)	148(18)		69(9)	41(11)	-8(8)	-51(11)
C02P	65(10)	84(12)	60(8)	21(8)	-1(7)	-5(7)	

Table 4 Bond Lengths for pna21_a.

Atom	Atom	Length/Å	Atom	Atom	Length/Å
Y001	Y002	3.8246(15)	O00V	C02U	1.40(2)
Y001	Y003	3.7487(15)	C00W	C01F	1.467(18)
Y001	O07	2.356(7)	C00X	C01Y	1.409(18)

Y001	O09	2.199(7)	C00Y	C01I	1.504(17)
Y001	O0A	2.263(7)	C00Z	C012	1.434(19)
Y001	O00D	2.244(8)	C010	C011	1.456(18)
Y001	O1	2.290(8)	C010	C016	1.420(18)
Y001	N00I	2.552(9)	C010	C01L	1.415(18)
Y001	N00J	2.545(10)	C012	C018	1.410(17)
Y002	Y003	3.8055(14)	C013	C01G	1.417(19)
Y002	Li04	3.317(4)	C013	C029	1.417(19)
Y002	O05	2.282(7)	C014	C01A	1.472(17)
Y002	O06	2.185(7)	C014	C01H	1.376(17)
Y002	O07	2.321(7)	C015	C01C	1.538(16)
Y002	O1	2.309(7)	C016	C01J	1.421(17)
Y002	O00G	2.263(7)	C017	C01C	1.537(16)
Y002	N00L	2.542(9)	C018	C01W	1.33(2)
Y002	N00O	2.542(9)	C019	C01C	1.514(16)
Y003	O05	2.306(7)	C01B	C01T	1.55(2)
Y003	O07	2.357(7)	C01B	C02C	1.53(2)
Y003	O08	2.215(7)	C01B	C02J	1.55(2)
Y003	O0A	2.219(7)	C01D	C029	1.44(2)
Y003	O00H	2.181(8)	C01E	C01F	1.42(2)
Y003	N00N	2.534(10)	C01E	C028	1.40(2)
Y003	N00S	2.573(9)	C01F	C02E	1.39(2)
Li04	O05	2.583(8)	C01G	C01V	1.40(2)
Li04	O00	2.349(9)	C01H	C01P	1.370(19)
Li04	O1	2.695(9)	C01I	C01K	1.504(17)
Li04	O00G	2.424(8)	C01I	C01O	1.547(16)

Li04	O00M	2.388(10)	C01J	C020	1.374(18)
Li04	O00V	2.385(10)	C01L	C022	1.39(2)
O06	C00T	1.311(13)	C01M	C023	1.408(17)
O08	C016	1.308(13)	C01M	C02G	1.41(2)
O09	C013	1.297(14)	C01N	C01Z	1.54(2)
O00B	C015	1.440(15)	C01N	C025	1.50(2)
O00B	C01A	1.346(14)	C01N	C02A	1.58(2)
O00D	C00U	1.327(14)	C01P	C01Y	1.38(2)
O00F	C00Z	1.378(15)	C01Q	C01X	1.536(17)
O00F	C026	1.467(17)	C01R	C01X	1.524(18)
O00G	C01M	1.284(14)	C01S	C023	1.428(19)
O00H	C01E	1.283(16)	C01U	C021	1.40(2)
N00I	C00Z	1.296(15)	C01V	C02H	1.36(3)
N00I	C024	1.527(16)	C01W	C021	1.37(2)
N00J	C01B	1.523(17)	C01X	C02I	1.520(19)
N00J	C01D	1.307(16)	C020	C022	1.37(2)
O00K	C01S	1.382(15)	C023	C02K	1.435(18)
O00K	C02A	1.43(2)	C024	C026	1.540(18)
N00L	C01A	1.307(14)	C024	C02B	1.517(18)
N00L	C01C	1.495(15)	C024	C02D	1.514(18)
O00M	C02F	1.453(16)	C027	C029	1.40(2)
O00M	C02P	1.410(18)	C027	C02H	1.34(2)
N00N	C011	1.273(15)	C028	C02Q	1.32(3)
N00N	C01X	1.508(15)	C02E	C02T	1.45(3)
N00O	C01N	1.483(16)	C02F	C02M	1.53(2)
N00O	C01S	1.307(17)	C02G	C02R	1.40(3)

O00P	C00W	1.350(15)	C02K	C02N	1.33(2)
O00P	C01O	1.418(16)	C02L	C02V	1.51(3)
O00Q	C011	1.390(14)	C02M	C02O	1.42(2)
O00Q	C02I	1.453(17)	C02N	C02R	1.39(3)
O00R	C01D	1.361(16)	C02O	C02P	1.47(2)
O00R	C02J	1.42(2)	C02Q	C02T	1.37(3)
N00S	C00W	1.272(14)	O02S	C9	1.57(3)
N00S	C01I	1.514(14)	O02S	C11	1.39(5)
C00T	C00X	1.411(17)	C02U	C10	1.47(4)
C00T	C014	1.412(17)	C02V	C10	1.35(4)
C00U	C012	1.411(19)	C7	C8	1.45(5)
C00U	C01U	1.39(2)	C7	C11	1.52(5)
O00V	C02L	1.37(3)	C8	C9	1.49(3)

Table 5 Bond Angles for pna21_a.

Atom	Atom	Atom	Angle/˚	Atom	Atom	Atom	Angle/˚
Y003	Y001	Y002	60.32(3)	C024	N00I	Y001	124.7(7)
O07	Y001	Y002	34.83(17)	C01B	N00J	Y001	128.1(7)
O07	Y001	Y003	37.32(17)	C01D	N00J	Y001	125.8(9)
O07	Y001	N00I	132.4(3)	C01D	N00J	C01B	106.1(10)
O07	Y001	N00J	117.5(3)	C01S	O00K	C02A	106.0(10)
O09	Y001	Y002	97.2(2)	C01A	N00L	Y002	126.9(7)
O09	Y001	Y003	95.6(2)	C01A	N00L	C01C	105.9(9)
O09	Y001	O07	76.7(3)	C01C	N00L	Y002	127.1(6)
O09	Y001	O0A	107.6(3)	C02F	O00M	Na04	114.0(8)

O09	Y001	O00D	147.6(3)	C02P	O00M	Na04	127.1(8)
O09	Y001	O1	121.8(3)	C02P	O00M	C02F	109.2(11)
O09	Y001	N00I	80.7(3)	C011	N00N	Y003	127.3(8)
O09	Y001	N00J	71.9(3)	C011	N00N	C01X	106.7(10)
O0A	Y001	Y002	89.8(2)	C01X	N00N	Y003	125.9(7)
O0A	Y001	Y003	32.88(19)	C01N	N00O	Y002	125.7(8)
O0A	Y001	O07	70.1(3)	C01S	N00O	Y002	126.7(8)
O0A	Y001	O1	102.1(3)	C01S	N00O	C01N	107.5(10)
O0A	Y001	N00I	77.9(3)	C00W	O00P	C01O	106.8(9)
O0A	Y001	N00J	171.4(3)	C011	O00Q	C02I	105.4(9)
O00D	Y001	Y002	112.9(2)	C01D	O00R	C02J	107.1(10)
O00D	Y001	Y003	109.2(2)	C00W	N00S	Y003	125.8(8)
O00D	Y001	O07	135.4(3)	C00W	N00S	C01I	107.2(9)
O00D	Y001	O0A	85.0(3)	C01I	N00S	Y003	127.0(7)
O00D	Y001	O1	82.5(3)	O06	C00T	C00X	118.9(10)
O00D	Y001	N00I	72.8(3)	O06	C00T	C014	122.7(10)
O00D	Y001	N00J	91.3(3)	C00X	C00T	C014	118.4(11)
O1	Y001	Y002	33.88(18)	O00D	C00U	C012	123.6(12)
O1	Y001	Y003	83.44(18)	O00D	C00U	C01U	118.5(13)
O1	Y001	O07	68.1(2)	C01U	C00U	C012	117.9(12)
O1	Y001	N00I	155.2(3)	C02L	O00V	Na04	136.5(12)
O1	Y001	N00J	85.1(3)	C02L	O00V	C02U	104.4(17)
N00I	Y001	Y002	166.1(2)	C02U	O00V	Na04	119.0(13)
N00I	Y001	Y003	106.0(2)	O00P	C00W	C01F	114.2(11)
N00J	Y001	Y002	98.8(2)	N00S	C00W	O00P	117.4(11)
N00J	Y001	Y003	154.8(2)	N00S	C00W	C01F	128.4(11)

N00J	Y001	N00I	93.6(3)	C00T	C00X	C01Y	119.3(12)
Y003	Y002	Y001	58.85(3)	O00F	C00Z	C012	113.9(10)
Na04	Y002	Y001	72.76(8)	N00I	C00Z	O00F	115.1(12)
Na04	Y002	Y003	71.66(8)	N00I	C00Z	C012	130.9(12)
O05	Y002	Y001	81.89(19)	C016	C010	C011	121.0(11)
O05	Y002	Y003	34.16(18)	C01L	C010	C011	120.1(12)
O05	Y002	Li04	51.0(2)	C01L	C010	C016	118.9(12)
O05	Y002	O07	69.3(3)	N00N	C011	O00Q	116.6(11)
O05	Y002	O1	89.1(3)	N00N	C011	C010	131.1(11)
O05	Y002	N00L	83.5(3)	O00Q	C011	C010	112.3(11)
O05	Y002	N00O	152.8(3)	C00U	C012	C00Z	120.9(11)
O06	Y002	Y001	95.8(2)	C018	C012	C00U	118.9(13)
O06	Y002	Y003	97.6(2)	C018	C012	C00Z	120.2(13)
O06	Y002	Li04	167.1(2)	O09	C013	C01G	121.0(13)
O06	Y002	O05	122.8(3)	O09	C013	C029	122.2(12)
O06	Y002	O07	76.6(3)	C01G	C013	C029	116.7(12)
O06	Y002	O1	119.1(3)	C00T	C014	C01A	120.5(10)
O06	Y002	O00G	145.9(3)	C01H	C014	C00T	119.8(11)
O06	Y002	N00L	71.7(3)	C01H	C014	C01A	119.5(11)
O06	Y002	N00O	82.6(3)	O00B	C015	C01C	104.5(9)
O07	Y002	Y001	35.43(17)	O08	C016	C010	123.7(11)
O07	Y002	Y003	35.88(17)	O08	C016	C01J	118.8(11)
O07	Y002	Li04	90.57(19)	C01J	C016	C010	117.5(11)
O07	Y002	N00L	115.8(3)	C01W	C018	C012	123.6(15)
O07	Y002	N00O	131.8(3)	O00B	C01A	C014	113.7(9)
O1	Y002	Y001	33.58(19)	N00L	C01A	O00B	117.4(10)

O1	Y002	Y003	81.90(18)	N00L	C01A	C014	128.8(10)
O1	Y002	Li04	53.7(2)	N00J	C01B	C01T	109.3(10)
O1	Y002	O07	68.4(3)	N00J	C01B	C02J	101.1(11)
O1	Y002	N00L	169.1(3)	C01T	C01B	C02J	111.1(14)
O1	Y002	N00O	85.4(3)	C02C	C01B	N00J	108.5(12)
O00G	Y002	Y001	113.6(2)	C02C	C01B	C01T	113.9(13)
O00G	Y002	Y003	111.98(19)	C02C	C01B	C02J	111.9(13)
O00G	Y002	Li04	46.9(2)	N00L	C01C	C015	103.2(9)
O00G	Y002	O05	79.9(3)	N00L	C01C	C017	107.6(9)
O00G	Y002	O07	137.5(2)	N00L	C01C	C019	112.2(9)
O00G	Y002	O1	82.9(3)	C017	C01C	C015	111.2(10)
O00G	Y002	N00L	88.0(3)	C019	C01C	C015	110.8(10)
O00G	Y002	N00O	73.0(3)	C019	C01C	C017	111.5(10)
N00L	Y002	Y001	151.2(2)	N00J	C01D	O00R	116.2(13)
N00L	Y002	Y003	96.2(2)	N00J	C01D	C029	129.7(12)
N00L	Y002	Li04	115.5(2)	O00R	C01D	C029	114.1(11)
N00O	Y002	Y001	106.8(2)	O00H	C01E	C01F	120.5(11)
N00O	Y002	Y003	165.6(2)	O00H	C01E	C028	118.1(15)
N00O	Y002	Li04	106.0(2)	C028	C01E	C01F	121.4(14)
N00O	Y002	N00L	97.5(3)	C01E	C01F	C00W	122.9(12)
Y001	Y003	Y002	60.83(3)	C02E	C01F	C00W	119.5(14)
O05	Y003	Y001	83.35(19)	C02E	C01F	C01E	117.6(13)
O05	Y003	Y002	33.75(17)	C01V	C01G	C013	119.8(16)
O05	Y003	O07	68.3(2)	C01P	C01H	C014	122.7(13)
O05	Y003	N00N	85.4(3)	N00S	C01I	C01O	100.9(9)
O05	Y003	N00S	172.8(3)	C00Y	C01I	N00S	107.9(9)

O07	Y003	Y001	37.29(17)	C00Y	C01I	C01O	110.4(10)
O07	Y003	Y002	35.24(17)	C01K	C01I	N00S	113.1(9)
O07	Y003	N00N	135.4(3)	C01K	C01I	C00Y	111.0(10)
O07	Y003	N00S	118.9(3)	C01K	C01I	C01O	113.0(11)
O08	Y003	Y001	106.8(2)	C020	C01J	C016	121.1(13)
O08	Y003	Y002	115.0(2)	C022	C01L	C010	122.0(14)
O08	Y003	O05	85.3(3)	O00G	C01M	C023	123.7(11)
O08	Y003	O07	135.1(3)	O00G	C01M	C02G	119.3(13)
O08	Y003	O0A	80.9(3)	C023	C01M	C02G	117.0(12)
O08	Y003	N00N	73.6(3)	N00O	C01N	C01Z	111.1(10)
O08	Y003	N00S	89.5(3)	N00O	C01N	C025	109.9(10)
O0A	Y003	Y001	33.6(2)	N00O	C01N	C02A	101.0(12)
O0A	Y003	Y002	90.9(2)	C01Z	C01N	C02A	111.3(12)
O0A	Y003	O05	102.2(3)	C025	C01N	C01Z	112.0(13)
O0A	Y003	O07	70.8(3)	C025	C01N	C02A	110.9(11)
O0A	Y003	N00N	152.7(3)	O00P	C01O	C01I	105.1(10)
O0A	Y003	N00S	81.9(3)	C01H	C01P	C01Y	118.4(12)
O00H	Y003	Y001	100.0(2)	O00K	C01S	C023	113.6(12)
O00H	Y003	Y002	89.1(2)	N00O	C01S	O00K	115.6(12)
O00H	Y003	O05	110.8(3)	N00O	C01S	C023	130.8(11)
O00H	Y003	O07	74.6(3)	C00U	C01U	C021	119.2(15)
O00H	Y003	O08	150.2(3)	C02H	C01V	C01G	122.0(16)
O00H	Y003	O0A	117.7(3)	C018	C01W	C021	117.1(14)
O00H	Y003	N00N	82.7(3)	N00N	C01X	C01Q	110.4(9)
O00H	Y003	N00S	71.8(3)	N00N	C01X	C01R	110.7(10)
N00N	Y003	Y001	168.7(2)	N00N	C01X	C02I	103.0(10)

N00N	Y003	Y002	108.4(2)	C01R	C01X	C01Q	111.4(11)
N00N	Y003	N00S	88.2(3)	C02I	C01X	C01Q	110.8(11)
N00S	Y003	Y001	103.0(2)	C02I	C01X	C01R	110.2(10)
N00S	Y003	Y002	153.1(2)	C01P	C01Y	C00X	121.4(12)
O05	Li04	Y002	43.31(16)	C01J	C020	C022	122.1(13)
O05	Li04	O1	75.2(3)	C01W	C021	C01U	123.2(15)
O00	Li04	Y002	119.1(3)	C020	C022	C01L	118.3(12)
O00	Li04	O05	97.6(3)	C01M	C023	C01S	122.2(11)
O00	Li04	O1	91.1(3)	C01M	C023	C02K	119.3(12)
O00	Li04	O00G	161.7(3)	C01S	C023	C02K	118.5(12)
O00	Li04	O00M	90.9(3)	N00I	C024	C026	101.8(10)
O00	Li04	O00V	90.6(4)	C02B	C024	N00I	112.4(10)
O1	Li04	Y002	43.65(16)	C02B	C024	C026	112.0(11)
O00G	Li04	Y002	43.01(18)	C02D	C024	N00I	107.3(10)
O00G	Li04	O05	71.2(3)	C02D	C024	C026	110.4(11)
O00G	Li04	O1	72.2(3)	C02D	C024	C02B	112.5(11)
O00M	Li04	Y002	128.8(3)	O00F	C026	C024	103.5(10)
O00M	Li04	O05	96.3(3)	C02H	C027	C029	122.3(17)
O00M	Li04	O1	171.4(3)	C02Q	C028	C01E	120.3(19)
O00M	Li04	O00G	104.5(3)	C013	C029	C01D	121.2(10)
O00V	Li04	Y002	119.1(3)	C027	C029	C013	119.7(13)
O00V	Li04	O05	162.2(4)	C027	C029	C01D	119.0(13)
O00V	Li04	O1	89.0(4)	O00K	C02A	C01N	103.1(11)
O00V	Li04	O00G	96.5(4)	C01F	C02E	C02T	118.6(17)
O00V	Li04	O00M	99.3(4)	O00M	C02F	C02M	104.8(12)
Y002	O05	Y003	112.1(3)	C02R	C02G	C01M	121.5(17)

Y002	O05	Li04	85.7(2)	C027	C02H	C01V	119.2(18)
Y003	O05	Li04	117.7(3)	O00Q	C02I	C01X	103.8(9)
C00T	O06	Y002	144.2(7)	O00R	C02J	C01B	104.2(12)
Y001	O07	Y003	105.4(3)	C02N	C02K	C023	122.2(16)
Y002	O07	Y001	109.7(3)	O00V	C02L	C02V	106(2)
Y002	O07	Y003	108.9(3)	C02O	C02M	C02F	106.0(12)
C016	O08	Y003	143.3(7)	C02K	C02N	C02R	119(2)
C013	O09	Y001	140.7(8)	C02M	C02O	C02P	109.2(14)
Y003	O0A	Y001	113.5(3)	O00M	C02P	C02O	106.2(13)
C01A	O00B	C015	106.9(8)	C028	C02Q	C02T	121(2)
C00U	O00D	Y001	141.9(8)	C02G	C02R	C02N	120(2)
Y001	O1	Y002	112.5(3)	C11	O02S	C9	92(3)
Y001	O1	Li04	117.0(3)	C02Q	C02T	C02E	120(2)
Y002	O1	Li04	82.7(2)	O00V	C02U	C10	109(2)
C00Z	O00F	C026	107.0(9)	C10	C02V	C02L	107(2)
Y002	O00G	Li04	90.0(3)	C8	C7	C11	92(3)
C01M	O00G	Y002	142.9(7)	C7	C8	C9	111(3)
C01M	O00G	Li04	117.6(7)	C8	C9	O02S	104(2)
C01E	O00H	Y003	143.6(9)	C02V	C10	C02U	105(3)
C00Z	N00I	Y001	126.9(8)	O02S	C11	C7	126(4)
C00Z	N00I	C024	108.0(10)				

Table 6 Torsion Angles for pna21_a.

A	B	C	D	Angle/˚	A	B	C	D	Angle/˚
Y001	O09	C013	C01G	148.3(10)	C010	C016	C01J	C020	0.0(17)

Y001	O09	C013	C029	-34.7(19)
Y001	O00D	C00U	C012	18.6(19)
Y001	O00D	C00U	C01U	-162.8(9)
Y001	N00I	C00Z	O00F	-169.3(7)
Y001	N00I	C00Z	C012	13.0(17)
Y001	N00I	C024	C026	157.8(8)
Y001	N00I	C024	C02B	37.8(13)
Y001	N00I	C024	C02D	-86.3(10)
Y001	N00J	C01B	C01T	48.0(15)
Y001	N00J	C01B	C02C	-76.8(13)
Y001	N00J	C01B	C02J	165.3(10)
Y001	N00J	C01D	O00R	-176.4(8)
Y001	N00J	C01D	C029	5(2)
Y002	O06	C00T	C00X	159.2(9)
Y002	O06	C00T	C014	-20.2(18)
Y002	O00G	C01M	C023	11(2)
Y002	O00G	C01M	C02G	-167.9(10)
Y002	N00L	C01A	O00B	-171.9(7)
Y002	N00L	C01A	C014	10.8(16)
Y002	N00L	C01C	C015	166.1(7)
Y002	N00L	C01C	C017	-76.2(10)
Y002	N00L	C01C	C019	46.8(12)
Y002	N00O	C01N	C01Z	44.6(14)
Y002	N00O	C01N	C025	-80.0(12)
Y002	N00O	C01N	C02A	162.7(8)
Y002	N00O	C01S	O00K	-175.7(7)
C010	C01L	C022	C020	0(2)
C011	N00N	C01X	C01Q	-134.4(11)
C011	N00N	C01X	C01R	101.8(11)
C011	N00N	C01X	C02I	-16.0(12)
C011	O00Q	C02I	C01X	-18.2(12)
C011	C010	C016	O08	-1.1(17)
C011	C010	C016	C01J	178.6(10)
C011	C010	C01L	C022	-178.5(12)
C012	C00U	C01U	C021	-1.3(19)
C012	C018	C01W	C021	2(2)
C013	C01G	C01V	C02H	-1(2)
C014	C00T	C00X	C01Y	-1.3(16)
C014	C01H	C01P	C01Y	-1(2)
C015	O00B	C01A	N00L	2.7(13)
C015	O00B	C01A	C014	-179.5(9)
C016	C010	C011	N00N	-1.7(19)
C016	C010	C011	O00Q	-179.4(10)
C016	C010	C01L	C022	1.6(18)
C016	C01J	C020	C022	1.6(19)
C018	C01W	C021	C01U	-2(2)
C01A	O00B	C015	C01C	-10.6(12)
C01A	N00L	C01C	C015	-12.5(11)
C01A	N00L	C01C	C017	105.1(10)
C01A	N00L	C01C	C019	-131.8(10)
C01A	C014	C01H	C01P	-174.5(12)
C01B	N00J	C01D	O00R	6.7(15)

Y002	N00O	C01S	C023	7.7(17)
Y003	O08	C016	C010	3.0(18)
Y003	O08	C016	C01J	-176.7(8)
Y003	O00H	C01E	C01F	-28(2)
Y003	O00H	C01E	C028	153.9(12)
Y003	N00N	C011	O00Q	-179.6(7)
Y003	N00N	C011	C010	2.7(17)
Y003	N00N	C01X	C01Q	50.2(13)
Y003	N00N	C01X	C01R	-73.7(11)
Y003	N00N	C01X	C02I	168.5(8)
Y003	N00S	C00W	O00P	-175.1(8)
Y003	N00S	C00W	C01F	6.0(19)
Y003	N00S	C01I	C00Y	-77.5(11)
Y003	N00S	C01I	C01K	45.7(12)
Y003	N00S	C01I	C01O	166.7(8)
Na04	O00G	C01M	C023	-122.5(10)
Na04	O00G	C01M	C02G	58.3(15)
Na04	O00M	C02F	C02M	167.7(9)
Na04	O00M	C02P	C02O	-165.7(11)
Na04	O00V	C02L	C02V	-148.3(15)
Na04	O00V	C02U	C10	152(2)
O06	C00T	C00X	C01Y	179.3(10)
O06	C00T	C014	C01A	-5.2(16)
O06	C00T	C014	C01H	179.8(10)
O08	C016	C01J	C020	179.7(10)
O09	C013	C01G	C01V	-178.6(12)
C01B	N00J	C01D	C029	-172.4(13)
C01C	N00L	C01A	O00B	6.8(12)
C01C	N00L	C01A	C014	-170.6(10)
C01D	N00J	C01B	C01T	-135.1(12)
C01D	N00J	C01B	C02C	100.0(13)
C01D	N00J	C01B	C02J	-17.8(15)
C01D	O00R	C02J	C01B	-19.9(17)
C01E	C01F	C02E	C02T	-2(3)
C01E	C028	C02Q	C02T	6(3)
C01F	C01E	C028	C02Q	2(3)
C01F	C02E	C02T	C02Q	9(4)
C01G	C013	C029	C01D	177.6(12)
C01G	C013	C029	C027	-5.4(19)
C01G	C01V	C02H	C027	-1(3)
C01H	C014	C01A	O00B	3.4(14)
C01H	C014	C01A	N00L	-179.1(11)
C01H	C01P	C01Y	C00X	0(2)
C01I	N00S	C00W	O00P	3.3(15)
C01I	N00S	C00W	C01F	-175.5(13)
C01J	C020	C022	C01L	-2(2)
C01K	C01I	C01O	O00P	136.8(11)
C01L	C010	C011	N00N	178.4(12)
C01L	C010	C011	O00Q	0.6(15)
C01L	C010	C016	O08	178.8(11)
C01L	C010	C016	C01J	-1.5(16)
C01M	C023	C02K	C02N	-1(2)

O09	C013	C029	C01D	0.6(19)
O09	C013	C029	C027	177.6(12)
O00B	C015	C01C	N00L	13.9(11)
O00B	C015	C01C	C017	-101.2(11)
O00B	C015	C01C	C019	134.1(10)
O00D	C00U	C012	C00Z	0.6(17)
O00D	C00U	C012	C018	-179.9(11)
O00D	C00U	C01U	C021	180.0(12)
O00F	C00Z	C012	C00U	166.8(10)
O00F	C00Z	C012	C018	-12.7(15)
O00G	C01M	C023	C01S	-3.9(19)
O00G	C01M	C023	C02K	177.7(12)
O00G	C01M	C02G	C02R	179.3(15)
O00H	C01E	C01F	C00W	-5(2)
O00H	C01E	C01F	C02E	178.2(15)
O00H	C01E	C028	C02Q	-179.7(17)
N00I	C00Z	C012	C00U	-15.5(19)
N00I	C00Z	C012	C018	165.0(12)
N00I	C024	C026	O00F	20.5(12)
N00J	C01B	C02J	O00R	22.6(16)
N00J	C01D	C029	C013	10(2)
N00J	C01D	C029	C027	-167.0(14)
O00K	C01S	C023	C01M	178.1(11)
O00K	C01S	C023	C02K	-3.5(16)
O00M	C02F	C02M	C02O	-8.2(18)
N00N	C01X	C02I	O00Q	20.6(12)
C01M	C02G	C02R	C02N	7(3)
C01N	N00O	C01S	O00K	6.6(13)
C01N	N00O	C01S	C023	-170.0(12)
C01O	O00P	C00W	N00S	7.8(16)
C01O	O00P	C00W	C01F	-173.2(12)
C01Q	C01X	C02I	O00Q	138.6(11)
C01R	C01X	C02I	O00Q	-97.6(12)
C01S	O00K	C02A	C01N	-22.3(14)
C01S	N00O	C01N	C01Z	-137.7(12)
C01S	N00O	C01N	C025	97.7(12)
C01S	N00O	C01N	C02A	-19.5(13)
C01S	C023	C02K	C02N	-179.0(15)
C01T	C01B	C02J	O00R	138.5(13)
C01U	C00U	C012	C00Z	-178.0(11)
C01U	C00U	C012	C018	1.5(17)
C01X	N00N	C011	O00Q	5.0(13)
C01X	N00N	C011	C010	-172.7(11)
C01Z	C01N	C02A	O00K	143.3(12)
C023	C01M	C02G	C02R	0(2)
C023	C02K	C02N	C02R	7(3)
C024	N00I	C00Z	O00F	3.5(13)
C024	N00I	C00Z	C012	-174.1(11)
C025	C01N	C02A	O00K	-91.2(14)
C026	O00F	C00Z	N00I	10.7(13)
C026	O00F	C00Z	C012	-171.2(10)
C028	C01E	C01F	C00W	173.5(15)

N00O	C01N	C02A	O00K	25.2(13)
N00O	C01S	C023	C01M	-5(2)
N00O	C01S	C023	C02K	173.1(12)
O00P	C00W	C01F	C01E	-168.2(13)
O00P	C00W	C01F	C02E	9(2)
O00R	C01D	C029	C013	-169.1(11)
O00R	C01D	C029	C027	13.9(18)
N00S	C00W	C01F	C01E	11(2)
N00S	C00W	C01F	C02E	-172.1(15)
N00S	C01I	C01O	O00P	15.8(13)
C00T	C00X	C01Y	C01P	1.3(19)
C00T	C014	C01A	O00B	-171.6(9)
C00T	C014	C01A	N00L	5.9(17)
C00T	C014	C01H	C01P	0.5(18)
C00U	C012	C018	C01W	-2.2(19)
C00U	C01U	C021	C01W	2(2)
O00V	C02L	C02V	C10	-23(3)
O00V	C02U	C10	C02V	11(3)
C00W	O00P	C01O	C01I	-14.7(14)
C00W	N00S	C01I	C00Y	104.1(11)
C00W	N00S	C01I	C01K	-132.7(11)
C00W	N00S	C01I	C01O	-11.7(13)
C00W	C01F	C02E	C02T	-179.3(18)
C00X	C00T	C014	C01A	175.5(10)
C00X	C00T	C014	C01H	0.5(16)
C00Y	C01I	C01O	O00P	-98.2(12)
C028	C01E	C01F	C02E	-4(2)
C028	C02Q	C02T	C02E	-11(4)
C029	C013	C01G	C01V	4(2)
C029	C027	C02H	C01V	0(3)
C02A	O00K	C01S	N00O	11.2(15)
C02A	O00K	C01S	C023	-171.6(11)
C02B	C024	C026	O00F	140.7(11)
C02C	C01B	C02J	O00R	-92.8(16)
C02D	C024	C026	O00F	-93.2(12)
C02F	O00M	C02P	C02O	-22.3(18)
C02F	C02M	C02O	C02P	-5(2)
C02G	C01M	C023	C01S	175.4(12)
C02G	C01M	C023	C02K	-3.0(18)
C02H	C027	C029	C013	4(2)
C02H	C027	C029	C01D	-179.5(16)
C02I	O00Q	C011	N00N	8.9(13)
C02I	O00Q	C011	C010	-173.0(10)
C02J	O00R	C01D	N00J	9.0(17)
C02J	O00R	C01D	C029	-171.8(12)
C02K	C02N	C02R	C02G	-10(3)
C02L	O00V	C02U	C10	-26(3)
C02L	C02V	C10	C02U	7(3)
C02M	C02O	C02P	O00M	17(2)
C02P	O00M	C02F	C02M	19.1(16)
C02U	O00V	C02L	C02V	29(2)
C7	C8	C9	O02S	-42(4)

C00Z	O00F	C026	C024	-19.5(12)	C8	C7	C11	O02S	-3(6)
C00Z	N00I	C024	C026	-15.3(12)	C9	O02S	C11	C7	-19(5)
C00Z	N00I	C024	C02B	-135.2(11)	C11	O02S	C9	C8	32(3)
C00Z	N00I	C024	C02D	100.6(11)	C11	C7	C8	C9	27(4)
C00Z	C012	C018	C01W	177.3(12)					

Table 7 Hydrogen Atom Coordinates (Å×104) and Isotropic Displacement Parameters (Å2×103) for pna21_a.

Atom	x	y	z	U(eq)
H00A	4407	8696	733	65
H00B	4287	7769	606	65
H00X	1672	4209	661	52
H00C	4966	4752	-1236	57
H00D	5511	5216	-1026	57
H00E	4975	5799	-1049	57
H01A	1343	7554	-1842	50
H01B	1952	7271	-1967	50
H01C	1044	7982	-815	62
H01D	1331	8874	-1069	62
H01E	1460	8516	-393	62
H018	5280	6565	3143	58
H01F	2455	8550	-783	57
H01G	2248	8809	-1454	57
H01H	2605	7924	-1356	57
H01I	2798	3295	1179	75
H01J	1360	4810	-1407	52

H01K	5098	8229	-236	47
H01L	5074	6230	46	63
H01M	5621	5678	70	63
H01N	5157	5456	550	63
H01O	4670	7827	-2295	62
H01P	5479	3789	-472	62
H01Q	5354	3932	244	62
H01R	1136	3406	-1016	67
H01S	2810	5226	-1253	82
H01T	2653	5416	-1951	82
H01U	2733	6244	-1488	82
H01V	4055	4782	-1978	66
H01W	3476	4361	-2088	66
H01X	3704	4462	-1406	66
H01Y	3190	7875	2612	96
H	2814	8131	3178	96
HA	2557	7822	2540	96
H01Z	4164	8832	2421	68
H01	2024	2540	1476	97
H0AA	5409	8009	3475	71
H1AA	1288	3108	19	57
H2AA	1653	5827	1381	98
HB	1232	5912	1929	98
HC	1773	6483	1948	98
H020	5569	8968	-989	60
H021	4828	9123	3141	83

H022	5355	8812	-2016	66
H02A	625	7210	712	91
H02B	555	6301	1102	91
H02C	990	6349	568	91
H02D	5088	3971	2415	68
H02E	5211	4487	1779	68
H027	1710	4400	2732	84
H028	2513	3813	-431	99
H02F	791	7592	2189	90
H02G	3912	4006	1297	73
H02H	4484	3528	1308	73
H02I	4425	4537	1051	73
H02J	3332	5852	3542	100
H02K	3339	6861	3810	100
H02L	3674	6621	3207	100
H02M	4207	4158	2887	67
H02N	4142	3316	2431	67
H02O	3704	4104	2439	67
H02P	3964	2468	288	105
H02Q	4004	2302	-431	105
H02R	4432	9529	17	81
H02S	4162	10478	204	81
H02T	2510	10172	-93	91
H02U	1485	3096	2240	101
H02V	3591	5764	-2713	67
H02W	3215	6570	-2465	67

H02X	2372	6464	3800	100
H02Y	2047	6895	3234	100
H02Z	1084	10081	1263	69
H02	2613	9632	1923	142
H3AA	4390	11096	-691	72
HD	4735	10201	-830	72
H4AA	1363	11438	891	113
H5AA	4183	9856	-1519	116
HE	3812	10698	-1337	116
H6AA	3247	9689	-1031	83
HF	3691	8904	-1019	83
H7AA	2503	2289	-333	133
H8AA	1990	11457	89	124
H9AA	3248	1534	28	147
H0BA	3908	10397	1089	154
HG	3957	9945	1755	154
H1BA	2768	11409	2038	114
H7A	-2	4224	1845	268
H7B	633	4419	1787	268
H8A	604	4498	782	173
H8B	1	4801	903	173
H9A	134	3540	174	194
H9B	-319	3389	687	194
H10	3734	11643	1825	218

Experimental

Single crystals of C72H84N6O12Li3Y [pna21_a] were []. A suitable crystal was selected and [] on a 'Bruker APEX-II CCD' diffractometer. The crystal was kept at 108.54 K during data collection. Using Olex2 [1], the structure was solved with the XS [2] structure solution program using Direct Methods and refined with the XL [3] refinement package using Least Squares minimisation.

Dolomanov, O.V., Bourhis, L.J., Gildea, R.J, Howard, J.A.K. & Puschmann, H. (2009), J. Appl. Cryst. 42, 339-341.

Sheldrick, G.M. (2008). Acta Cryst. A64, 112-122.

Sheldrick, G.M. (2008). Acta Cryst. A64, 112-122.

Crystal structure determination of [pna21_a]

Crystal Data for C72H84N6O12Li3Y (M =872.76 g/mol): orthorhombic, space group Pna21 (no. 33), a = 25.1288(15) Å, b = 14.7708(9) Å, c = 21.8302(13) Å, V = 8102.8(8) Å3, Z = 8, T = 108.54 K, μ(MoKα) = 1.510 mm-1, Dcalc = 1.431 g/cm3, 25672 reflections measured (4.648° ≤ 2Θ ≤ 41.76°), 8099 unique (Rint = 0.0335, Rsigma = 0.0562) which were used in all calculations. The final R1 was 0.0450 (I > 2σ(I)) and wR2 was 0.1231 (all data).

Refinement model description

Number of restraints - 342, number of constraints - unknown.